

Experimental and numerical studies on forming and failure of woven thermoplastic composites

Nima Akhavan Zanjani

August 2019

A thesis submitted for the degree of Doctor of Philosophy of the
Australian National University



**Australian
National
University**

To my loves

Maryam, Ryan and Rodwin

Declaration

This thesis is an account of part-time research undertaken between March 2011 and December 2017 at The Research School of Engineering, College of Engineering and Computer Science, Australian National University, Canberra, Australia.

I certify that this thesis does not incorporate without acknowledgement any material previously submitted for a degree or diploma in any university, and that, to the best of my knowledge, it does not contain any material previously published or written by another person except where due reference is made in the text. The work in this thesis is my own, except for the contributions made by others as described in the acknowledgements. The thesis is a compilation of 6 manuscripts which are listed as follows:

- Manuscript 1 is presented in Chapter 3 in this thesis.

Statement of Contribution

This thesis is submitted as a Thesis by Compilation in accordance with https://policies.anu.edu.au/ppl/document/ANUP_003405

I declare that the research presented in this Thesis represents original work that I carried out during my candidature at the Australian National University, except for contributions to multi-author papers incorporated in the Thesis where my contributions are specified in this Statement of Contribution.

Title: Induced Forming Modes in a Pre-Consolidated Woven Polypropylene Composite During Stretch Forming Process at Room Temperature: I. Experimental Studies

Authors: Nima A. Zanjani, Anthony Sexton, Shankar Kalyanasundaram

Publication outlet: Composites Part A: Applied Science and Manufacturing, vol. 68, pp. 251-263, 2015

Current status of paper: Not Yet Submitted/Submitted/Under Revision/Accepted/**Published**

Contribution to paper: Project management, Experimental set-up, calibration of equipment, design of experiment, conducting tests, data acquisition and analysis, constructing failure envelope, extracting failure criteria, writing the paper.

Senior author or collaborating authors endorsement:



- Manuscript 2 is presented in Chapter 4 in this thesis.

Statement of Contribution

This thesis is submitted as a Thesis by Compilation in accordance with https://policies.anu.edu.au/ppl/document/ANUP_003405

I declare that the research presented in this Thesis represents original work that I carried out during my candidature at the Australian National University, except for contributions to multi-author papers incorporated in the Thesis where my contributions are specified in this Statement of Contribution.

Title: The Effect of fibre Orientation on the Formability and Failure Behaviour of a Woven Self-Reinforced Composite.

Authors: Nima A. Zanjani, Wentian Wang, Shankar Kalyanasundaram

Publication outlet: ASME-Journal of Manufacturing Science and Engineering, vol. 137(5), pp. 0510121-0510129, 2015

Current status of paper: Not Yet Submitted/Submitted/Under Revision/Accepted/**Published**

Contribution to paper: Project management, set-up and calibration of experiment apparatus, design of experiment, conducting tests, optical microscopy, analysis of results, morphological failure investigation, writing the paper.

Senior author or collaborating authors endorsement:



- Manuscript 3 is presented in Chapter 5 in this thesis.

Statement of Contribution

This thesis is submitted as a Thesis by Compilation in accordance with https://policies.anu.edu.au/ppl/document/ANUP_003405

I declare that the research presented in this Thesis represents original work that I carried out during my candidature at the Australian National University, except for contributions to multi-author papers incorporated in the Thesis where my contributions are specified in this Statement of Contribution.

Title: A Comparison between Forming Behaviours of Two Pre-Consolidated Woven Thermoplastic Composites.

Authors: Nima A. Zanjani, Shankar Kalyanasundaram

Publication outlet: Journal of Materials Science and Chemical Engineering, vol. 3(07), pp.180-189, 2015.

Current status of paper: Not Yet Submitted/Submitted/Under Revision/Accepted/**Published**

Contribution to paper: Managing the project, experimental set-up and calibration, design of experiment, preparation of specimens, formability tests, optical microscopy examination, analysis of results, morphological failure studies, writing the paper.

Senior author or collaborating authors endorsement:



- Manuscript 4 is presented in Chapter 6 in this thesis.

Statement of Contribution

This thesis is submitted as a Thesis by Compilation in accordance with https://policies.anu.edu.au/pp/document/ANUP_003405

I declare that the research presented in this Thesis represents original work that I carried out during my candidature at the Australian National University, except for contributions to multi-author papers incorporated in the Thesis where my contributions are specified in this Statement of Contribution.

Title: Stretch Forming Simulation of Woven Composites Based on an orthotropic non-linear material model.

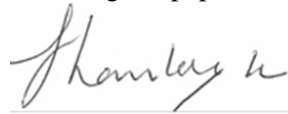
Authors: Nima A. Zanjani, Shankar Kalyanasundaram

Publication outlet: Journal of Materials Science and Chemical Engineering, vol. 3(07), pp. 168-179, 2015.

Current status of paper: Not Yet Submitted/Submitted/Under Revision/Accepted/**Published**

Contribution to paper: conducting characterisation experiments, analysis of results, establishing constitutive equations, development of an orthotropic material model, Developing User Defined material Subroutines, Implementing user defined subroutine into FEA, finite element simulations, analysis of FEA results, writing the paper.

Senior author or collaborating authors endorsement:



- Manuscript 5 is presented in Chapter 7 in this thesis.

Statement of Contribution

This thesis is submitted as a Thesis by Compilation in accordance with https://policies.anu.edu.au/pp/document/ANUP_003405

I declare that the research presented in this Thesis represents original work that I carried out during my candidature at the Australian National University, except for contributions to multi-author papers incorporated in the Thesis where my contributions are specified in this Statement of Contribution.

Title: Experimental and numerical studies on forming and failure behaviours of a woven self-reinforced polypropylene composite.

Authors: Nima A. Zanjani, Shankar Kalyanasundaram

Publication outlet: Advanced Composite Materials (ACM), in press (2020).

Current status of paper: Not Yet Submitted/Submitted/Under Revision/**Accepted**/Published

Contribution to paper: Project management, Development of a numerical model to simulate forming and failure process of composites, writing a user defined material subroutine (UMAT), implementing user define material and failure subroutines into FEA simulation, benchmarking FEA predictions with experimental outcome, writing the paper.

Senior author or collaborating authors endorsement:



- Manuscript 6 is presented in Chapter 8 in this thesis.

Statement of Contribution

This thesis is submitted as a Thesis by Compilation in accordance with https://policies.anu.edu.au/ppl/document/ANUP_003405

I declare that the research presented in this Thesis represents original work that I carried out during my candidature at the Australian National University, except for contributions to multi-author papers incorporated in the Thesis where my contributions are specified in this Statement of Contribution.

Title: Wrinkling Phenomenon during uniaxial extension of a woven thermoplastic composite.

Authors: Nima A. Zanjani, Shankar Kalyanasundaram

Publication outlet: Journal of Advanced Composite Letters (ACL), vol. 24(5), pp. 98-106, 2015

Current status of paper: Not Yet Submitted/Submitted/Under Revision/Accepted/**Published**

Contribution to paper: Managing the project, Design of novel geometries, set-up and calibration of equipment, preparation of samples, conducting modified yoshida buckling test, analysis of results, writing the report.

Senior author or collaborating authors endorsement:



Candidate: Nima Akhavan Zanjani

Signature:



Date: 06/08/2019

Endorsed

Primary Supervisor: Professor Shankar Kalyanasundaram

Signature:



Date: 06/08/2019

Conferences

1. **Nima A. Zanjani**, S. Kalyanasundaram, '*The effect of fibre orientation on the forming behaviour of a self-reinforced polypropylene composite*', Proceedings of ICNMMCS, Torino, Italy, 2012.
2. **Nima A. Zanjani**, S. Kalyanasundaram, '*An Investigation on the effect of aspect ratio variations on induced deformation modes of self-reinforced polypropylene composite at room temperature*', Proceedings of ECCM-12, Venice, Italy, 2012.
3. **Nima A. Zanjani**, S. Kalyanasundaram, '*Investigation on the wrinkling limit diagram of self-reinforced polypropylene woven composite at room temperature*', Proceedings of ACAM-7, Adelaide, Australia, 2012.
4. **Nima A. Zanjani**, S. Kalyanasundaram, '*Effect of aspect ratio variations on forming limit diagram of glass-fibre reinforced polypropylene composite at room temperature*', Proceedings of ACAM-7, Adelaide, Australia, 2012.
5. S. Kalyanasundaram, **Nima A. Zanjani**, W. Wang, '*Rapid forming of composite materials*', Composites damage workshop 6, September, Girona, Spain, 2014.
6. S. Kalyanasundaram, **Nima A. Zanjani**, W. Wang, '*Forming and failure in composite materials*', Composites damage workshop 7, September, Venice, Italy, 2015.
7. S. Kalyanasundaram, **Nima A. Zanjani**, J. Liang, D. Rahiminejad, W. Wang, '*Failure behaviour of thermoplastic composites*', Proceedings of ACAM-9, Sydney, Australia, 2017.
8. D. Rahiminejad, **Nima A. Zanjani**, S. Kalyanasundaram, '*A failure examination of metal/Composite material systems*', Proceedings of ACAM-9, Sydney, Australia, 2017.

Publications

9. **Nima A. Zanjani**, S. Kalyanasundaram, '*Induced forming modes in a self-reinforced polypropylene sheet during stretch forming process at room temperature: I-Experimental Studies*', Composites Part A: Applied Science and Manufacturing, Vol.68, pp.251-263, 2015, <https://doi.org/10.1016/j.compositesa.2014.09.023>.
10. **Nima A. Zanjani**, W. Wang, S. Kalyanasundaram, '*The effect of fibre orientation on the formability and failure behaviour of a woven self-reinforced composite during stamp forming*', ASME – J. Manuf. Sci. Eng.,137(5):051012-19, 2015, <https://doi.org/10.1115/1.4030894>.
11. W. Wang, A. Lowe, S. Davey, **Nima A. Zanjani**, S. Kalyanasundaram, '*Establishing a new forming limit curve for a flax fibre reinforced polypropylene composite through stretch forming experiments*', Composites Part A: Applied Science and Manufacturing, Vol.77, pp.114-123, 2015, <https://doi.org/10.1016/j.compositesa.2015.06.021>.
12. **Nima A. Zanjani**, A. Dervaric, S. Kalyanasundaram, '*A novel buckling indicator using the correlation between in-plane and out-of-plane displacements*', International Journal of Engineering Research & Technology, Vol.3(10), 2014.
13. **Nima A. Zanjani**, S. Kalyanasundaram, '*Wrinkling phenomenon during uniaxial extension of a woven thermoplastic composite*', Journal of Advanced Composite Letters (ACL), Vol.24 (5), pp.89-97, 2015, <https://doi.org/10.1177/096369351502400501>.
14. **Nima A. Zanjani**, S. Kalyanasundaram, '*Stretch Forming Simulation of Woven Composites Based on an Orthotropic Non-linear Material Model*', Journal of Materials Science and Chemical Engineering, Vol.3, pp.168-179, 2015,

<http://dx.doi.org/10.4236/msce.2015.37023>.

15. **Nima A. Zanjani**, S. Kalyanasundaram, '*A Comparison Between Forming Behaviours of Two Pre-consolidated Woven Thermoplastic Composites*', Journal of Materials Science and Chemical Engineering, Vol3., pp.180-189, 2015, <http://dx.doi.org/10.4236/msce.2015.37024>.
16. **Nima A. Zanjani**, S. Kalyanasundaram, '*Experimental and numerical studies on forming and failure behaviours of a woven self-reinforced polypropylene composite*', Advanced Composite Materials (ACM), in press (2020).

Acknowledgements

I would like to thank my principal supervisor Professor Shankar Kalyanasundaram for providing guidance and support, and sharing his thoughtful insights throughout the project. Thanks for offering me the opportunity to be a part of this exciting research program. I would also like to extend my gratitude to Professor Zbigniew Stachurski, Professor Paul Compston, Dr. Adrian Lowe, Dr. Mathew Doolan, and Professor Daniel MacDonald for their support and assistance.

A special thanks goes to my colleagues, Dr. Anthony Sexton, Sebastian Davey, Dr. Sudharshan Venkatesan, Jae Nam, Dr. Wentian Wang, and Davood Rahiminejad. This project would not have been successful without the advice, knowledge, and support provided by you.

Many thanks to the staff working in IT, workshop, and admin areas for providing ongoing support during all stages of my PhD candidature. My special thanks goes to Kylee Robinson and Andrew Wilkinson who were always there to solve problems as quickly as possible.

I am very grateful and indebted to my parents for lifetime encouragement to follow my dreams and realise my own potentials. All the unconditional support and love you have offered me over the years was the greatest gift anyone has ever given me.

Finally, I would like to express my highest appreciations to my wife, Maryam, for her ongoing supports, patience, and love. Thank you for listening, understanding and taking care of our beloved Ryan and Rodwin while I was working on this project.

Abstract

Fuel efficiency, weight reduction, and sustainability are major global challenges fuelling research into advanced material systems. There is an urgent necessity to reduce weight of products using durable, recyclable, and lightweight materials. Woven thermoplastic composites are attractive candidates for the replacement of metals in a wide range of industries from automotive to aerospace. They offer attractive benefits such as high specific strength, balanced thermomechanical properties, improved fatigue and wear resistance, and recyclability. However, there are major concerns regarding adaptability of woven thermoplastic composites into the mainstream of high-volume manufacturing industries. Addressing these concerns necessitates understanding forming and failure behaviours of this class of composite under high strain forming conditions.

A survey of literature highlights shortcomings of existing failure criteria of composite materials. Most of these failure theories are based on failure in a single layer lamina and as such their accuracy drops significantly in multilayered composite materials. Residual stress induced by the manufacturing processes is neglected in most failure models. Most importantly existing failure theories have been developed on fibre reinforced thermoset composites. This invalidates application of existing failure theories on woven thermoplastic composites due to complex interlacing structure of textile reinforcement and fundamental differences between forming and failure behaviours of thermosets and thermoplastics.

This thesis investigates formability and failure behaviour of a woven self-reinforced polypropylene composite (SRPP) using a custom-built press, an open die system, and a real time three-dimensional photogrammetry measurement equipment (ARAMIS). Specimens with novel geometries with different aspect ratios and fibre orientations were formed until

catastrophic failure event. Deformations and strains were measured and a forming-mode dependent failure envelope was constructed. Failed samples were examined using optical microscopy technique to reveal the correlation between failure mechanisms and deformation modes of the woven composite. Forming behaviour of SRPP were benchmarked against a woven glass-fibre reinforced polypropylene composite (GRPP) and the effect of reinforcements in formability and failure of woven composites was elucidated.

Mechanical characterisation experiments were conducted on SRPP using a universal testing machine and a non-contact in-situ strain measurement system to characterise mechanical behaviour of the composite at room temperature. The highly nonlinear behaviour of SRPP necessitated adopting an incremental deformation theory to develop constitutive stress-strain relations and construct an orthotropic material model. Material and failure models were implemented into a finite element analysis software (Abaqus) using FORTRAN. A finite element model with nonlinear contact conditions was developed to predict formability and failure behaviours of the SRPP during stamp forming process. Strain path, strain distribution and failure loci in SRPP specimens were predicted using finite element analysis with a high accuracy. Results, verified by experiments, demonstrated the high potential of the proposed numerical model in predicting forming and failure behaviours of woven thermoplastic composites under a wide range of deformation modes.

Wrinkling behaviour of the SRPP composite was investigated through a novel Modified Yoshida Buckling Test (MYBT). Specimens with unique geometries were uniaxially stretched to initiate out-of-plane deformations. Strains and their evolutions were studied before and after wrinkling initiation. Effect of specimens' aspect ratio on onset of wrinkling was investigated. It was shown that the severity and height of wrinkles are dependent to specimens' aspect ratio. Experimental results were employed to construct a Wrinkling Limit Diagram (WLD) for a composite for the first time. Some of the limitations

of existing wrinkling measures to predict onset of compressive instability in woven composites was demonstrated.

Table of contents

Experimental and numerical studies on forming and failure of woven thermoplastic composites	1
Chapter 1	1
Introduction	1
1.1 Background to the Study	1
1.2 Research Objectives	5
1.3 Thesis Structure.....	7
Chapter 2.....	9
Failure and wrinkling in composites.....	9
2.1 Introduction.....	9
2.2 Failure in unidirectional fibre-reinforced composites	12
2.2.1 Advanced failure theories of thermoset composites.....	23
2.2.2 Failure of woven composites.....	26
2.2.3 Failure of thermoplastic composites.....	29
2.2.4 Summary	36
2.3 Buckling and Wrinkling	37
2.3.1 Fundamentals	37
2.3.2 Analytical methods.....	39
2.3.3 Experimental methods.....	43
2.3.4 Wrinkling Limit Curve (WLC)	46
2.3.5 Summary	49
Chapter 3.....	51
Forming and failure of a consolidated self-reinforced polypropylene composite	51
Chapter 4.....	69
The effect of fibre orientation on formability and failure behaviour of SRPP composite	69
.....	71
Chapter 5.....	80
A comparison between forming behaviours of two woven thermoplastic composites	80
Chapter 6.....	93

Development of a nonlinear material model for woven composites	93
Chapter 7	107
FEA predictions on forming and failure behaviours of a woven composite	107
Chapter 8	125
Wrinkling behaviour of a woven composite	125
Chapter 9	136
Summary and future work.....	136
9.1 Introduction.....	136
9.2 Contributions.....	137
9.3 Summary of findings.....	139
9.4 Future work.....	141
Bibliography	142
Appendix A	154

Introduction

1.1 Background to the Study

In recent decades, increased usage of fossil fuels has caused major environmental issues such as shortages of non-renewable energy resources, air pollution, and anthropological climate changes. Studies [1-5] predict that under current consumption rates most of fossil energy resources will be depleted in near future. According to other studies [6, 7], the annual emission of CO₂ and other Green House Gases (GHGs) have increased significantly over the last few decades. The total GHG emission increased by 41% from 1990 to 2009, and the annual emission rate rose by 3.4% between 2000 and 2008. The global average temperature has risen by 0.6°C over the last three decades and 0.8°C since last century [8]. These figures indicate an accelerating trend of fuel consumption and GHGs emission. Table 1.1 demonstrates data on energy consumption since 1971 and predicted energy usage in future.

According to statistics published by the International Energy Agency (IEA), the automotive industry is responsible for nearly 23% of total CO₂ emissions worldwide [9]. It was revealed that among several contributing factors, weight of the automobile is one of the most critical parameter influencing CO₂ emission and fuel consumption. It has been demonstrated that every 100 kg decrease in the weight of an automobile results in a 12% reduction in fuel consumption of diesel engines and 15% for gasoline engines [10]. A 100 kg reduction in the weight of an automobile yields 8.4 g/km decrease in CO₂ emissions.

Table 1.1: World energy consumption (Mtoe) [11]

Energy source	1971	2000	2010	2030	Annual increase
Coal	530	554	592	664	0.6%
Oil	1,890	2,943	3,545	4,956	1.8%
Gas	604	1,112	1,333	1,790	1.6%
Electricity	377	1,088	1,419	2,235	2.4%
Heat	68	247	260	285	0.5%
Renewables	66	86	106	150	1.8%
Total	3,634	6,032	7,254	10,080	1.7%

The aforementioned facts and figures necessitate finding appropriate substitutes for current high-density material systems (e.g. metals) utilised in mass production industries. Several reports [12, 13] confirm that the total contribution of the transport industry in fuel consumption is equal to 20%, 28%, and 24% in Europe, the US, and Australia, respectively [14]. Currently, metals such as steel (HSS and HSLA) and aluminium alloys (Al–Si alloys) are extensively adopted for the manufacture of components used in transportation vehicles. An underlying factor of this high level usage is the superior mechanical properties of metals, such as excellent formability, high strength, and recyclability. However, high density of metals results in heavy products that contribute to preceding environmental problems. Achieving weight reduction targets to satisfy tight regulatory reinforcements in transport industry necessitates substituting metals with light material systems such as composites. The substitute materials need to satisfy design, manufacturing and production requirements including strength, toughness, cycle time and cost.

Advanced composite material systems could be found in different industrial applications due to a wide range of attractive properties including high specific strength,

improved wear resistance and design adaptability. It has been shown that polymer matrix composites (PMCs) offer additional advantages over other classes of composite including relatively low manufacturing cost and improved impact energy absorption.

PMCs are categorised based on the type of polymer used in their structure namely thermosetting (thermoset) and thermoplastic composites. Thermosets, composed of monomeric polymer resins with a quite low viscosity, penetrate easily between reinforcements and impregnate fibres. Applying sufficient pressure and temperature over a period of time on thermoset prepregs cross-links them through covalent-bonds and produce high strength products. However, manufacturing process of thermosets is complex, labour-intensive and time-consuming and the final product cannot be recycled. Components are made from thermoset-based composites using different techniques such as hands lay-up, compression moulding, and resin transfer moulding (RTM). Thermoset composites are mainly used in the aerospace industries due to their high specific strength, adaptability to design criteria and high resistance against corrosion.

Thermoplastics are polymeric materials with long molecular chains that are not cross linked. They soften if heated and flow like a highly viscous fluid. They can be reshaped after initial consolidation. Thermoplastic composites are manufactured through similar processes as thermosets; however, heating and cooling period is different and curing process is not required. Thermoplastic composites offer advantages over thermosets include higher ductility, shorter manufacturing cycle time, and recyclability. These properties make them attractive alternatives to thermoset-based composites in high volume industries where environmental concerns are a priority.

Thermosets and thermoplastics are both classified as polymers, yet possess distinct structural, chemical, and physical attributes. As a result, the composites made from these polymers exhibit different response to external loadings which contribute to a completely different forming behaviour and failure mechanism. These differences are accentuated by

a different bond strength between fibre and matrix in the two polymer composites.

In the aerospace industry, thermoplastic composites have gained an increasing popularity in high performance applications. The airbus A340-600 and A380, introduced to the market in 2002 and 2007 respectively, utilise some of the largest thermoplastic components in their structures [15]. These components include thermoplastic skins reinforced with welded ribs, angle brackets and panels. Substituting original components made of aluminium and titanium with thermoplastic composites have resulted in weight savings between 20% and 50%. Gulfstream G650 is another example of aircrafts using thermoplastic composites in their floor panels[16]. As a result of a welded thermoplastic component used in rubber and elevator rail sections, a 10% weight reduction was achieved compared to the original component made of a thermoset composite. The usage of thermoplastic composites in aerospace industry has increased by approximately 400% since 2005 [15].

Woven Thermo-Plastic Composite Materials (WTPCMs) are a new class of composite materials in which woven fibres are used as structural reinforcements. Application of woven composites in manufacture of components eliminates the inherent shortcomings of fibre-reinforced composites (FRCs) and offer superior mechanical properties including improved resistance to crack propagation and balanced thermomechanical properties [17]. High volume production capability is an essential element for the introduction of WTPCMs into high-volume industries such as the automotive. Stamp-forming has long been used to rapidly produce metal components. A number of studies [18-21] have examined the potential of stamp forming of composite prepregs. However, no effort has been made to investigate formability and failure behaviour of WTPCMs under consolidated forming conditions. Wide spread application of composites could be realized if existing complex, labour intensive manufacturing methods are substituted with rapid forming techniques such as stamping. Stamp forming of consolidated composites not only yields cost-effective

products but also facilitates a smooth transition from metals to composites by integrating with existing production technologies.

Another limitation to the wide spread application of woven thermoplastic composites is the lack of efficient models to predict failure of WTPCMs under complex loading conditions. There are myriads of failure models originally developed on unidirectional fibre-reinforced thermosetting composites. However, failure of thermoset-based composites is substantially different to failure of thermoplastic composites. Thermosetting composite are very brittle and experience localised failure at a very early stage of deformation, while thermoplastics are ductile and can sustain large deformations before failure. These differences invalidate application of existing failure models on thermoplastic composites.

Woven thermoplastic composites possess very different reinforcing and polymeric structures to thermoset-based FRCs, and as such exhibit different failure behaviours due to the following reasons: First, interactions between warp and weft yarns makes failure phenomena very complex compared to fibre reinforced composites. Second, deformation and failure of thermoplastics and thermosets are inherently different. These fundamental differences necessitate studying forming and failure behaviours of woven thermoplastic composites by a combined experimental-numerical approach adopted in the current research project.

1.2 Research Objectives

High volume production of WTPCMs requires adopting suitable criteria for predicting failure under high strain forming conditions. Conventional failure models are not robust enough to predict failure during rapid forming of composites. Moreover, existing failure models originally developed for unidirectional thermosetting composites are not applicable

to WTPCMs. The current study investigates forming and failure behaviours of WTPCMs using an innovative technique inspired from metal industry. Using a combination of different fibre orientations and aspect ratios, formability of WTPCMs under a wide range of deformation modes is studied. A strain based failure envelope is constructed. The effect of process parameters on forming behaviour of a SRPP composite is investigated and benchmarked against formability of a GRPP composite.

The current research project aims at establishing foundations of a scientifically sound and reliable predictive model applicable to rapid forming of woven thermoplastic composites. Achieving these objectives necessitates characterising mechanical response of WTPCMs and developing constitutive stress-strain relations under rapid forming conditions. Material and failure models are incorporated into a finite element simulation to predict forming and failure behaviours of woven thermoplastic composites. FEA results are benchmarked against experimental forming outcomes to assess the validity and reliability of the proposed model.

Finally, wrinkling behaviour of WTPCMs is studied. By introducing novel geometries, a Modified Yoshida Buckling Test (MYBT) method is designed and implemented to measure wrinkling tendency of SRPP. The effect of specimens' geometry on initiation and severity of wrinkling is investigated, and a novel wrinkling indicator based on the evolution of surface strains is proposed. Understanding fundamental mechanisms involved in initiation of instabilities under tension and compression is essential in developing an effective tool for predicting failure and wrinkling onset under high strain conditions. The predictive tool has the potential to assist designer, engineers and researchers to establish a refined and comprehensive framework applicable to mass production of woven thermoplastic composites.

1.3 Thesis Structure

The current thesis is mainly structured around research findings published in a collection of journal papers. First chapter highlights the significance of the current research program in the context of addressing current environmental and sustainability issues by adopting woven thermoplastic composites in mass production industries. The second chapter reviews failure studies conducted on composite materials through a comprehensive literature survey. In this chapter, existing failure criteria of composites is reviewed and the necessity to develop a robust and novel failure criterion for woven thermoplastic composites is emphasized. This chapter includes a detailed survey of literature on existing failure criteria of composites and a summary on their shortcomings as highlighted through the outcomes of the World Wide Failure Exercise (WWFE) program. Finally, Fundamentals of buckling and wrinkling, as the most common type of compressive instability in manufacturing are summarised and common analytical and experimental techniques for the analysis of buckling/wrinkling problems are discussed.

Outcomes of the current research project conducted on forming and failure behaviours of WTPCMs are presented in chapters 3 to 8 through a series of published journal articles. Chapter three investigates formability and failure of a consolidated SRPP composite through a customised test set up designed to stamp specimens with novel geometries into an open die using a hemispherical punch. Deformations and strains on the surface of samples were measured and a novel strain-based failure model is proposed. Experimental outcomes highlight the suitability of pre-consolidated SRPP for forming into complex double curvature geometries using stamp forming technique. In chapter four, the effect of fibre orientation on forming and failure behaviours of the composite is studied. It is concluded that if a proper combination of fibre orientation, aspect ratio and boundary conditions are selected, the formability of the SRPP can be greatly improved. Chapter five

compares forming and failure behaviours of two different woven thermoplastic composites using a real time non-contact strain measurement system and optical microscopy technique. These differences are highlighted by studying strain paths variations of the composites under similar loading conditions and dissimilar failure mechanisms caused by different type of reinforcements. In chapter six, results of characterisation experiments conducted on SRPP composite are presented. Constitutive stress-strain equations are constructed and a nonlinear orthotropic material model is developed to predict forming behaviour of woven composites under complex loading conditions. Finally, the effect of process parameters on the formability of SRPP composite is discussed using finite element analysis. In chapter seven, material and failure models are implemented into a finite element simulation to predict strains and their evolution, strain path at different locations and onset of failure in SRPP composites under different deformation modes. Comparison with experimental outcomes demonstrates high accuracy and reliability of the numerical model in predicting forming and failure behaviours of woven thermoplastic composites. Chapter eight investigates onset of compressive instabilities in woven thermoplastic composites using a modified Yoshida buckling test. Wrinkling initiation and propagation in novel geometries with different aspect ratios are studied under uniaxial extension conditions. A wrinkling limit diagram is established and its predictability on wrinkling of woven composites is studied. Chapter nine summarises findings of the current research project, highlights original contributions made in this research program, and discusses possibilities for expanding the scope of this research in future.

Failure and wrinkling in composites

2.1 Introduction

Mass production of components made of woven thermoplastic composites requires fundamental knowledge on failure behaviour of this class of materials. Understanding failure in composites allows engineers to optimise designs and achieve a balance between strength, quality, and cost objectives. Preliminary studies on failure behaviour of composites were performed on parts used in the aerospace industry. The failure phenomenon was investigated during long service life of components made of unidirectional fibre-reinforced thermoset composites. These studies showed that microscopic scale damage started early at low strains, gradually accumulated and evolved into larger cracks until leading to catastrophic failure events such as delamination. Due to progressive nature of failure in these case studies, proposed models are not suitable for predicting damage under rapid forming conditions.

A survey in literature shows that the existing body of knowledge on failure of composites is not applicable to woven thermoplastic composites. First, conventional manufacturing methods of composites are not designed for high volume production. Mass production of composite materials requires application of rapid manufacturing techniques to reduce cycle time and costs. Second, Mechanical behaviour of woven composites is more intricate than unidirectional fibre-reinforced composites due to complex interactions between interlacing yarns. Third, failure onset and propagation mechanisms are fundamentally different in thermoset and thermoplastic composites. Failure in

thermosetting polymers initiates at a very low strain, leading to stress concentration in the fibre-matrix interface, transverse crack propagation, de-bonding between fibres and matrix, and delamination; however, thermoplastic composites possess a much higher failure strain compared to thermosets [15], and matrix cracks are not precursors to failure. *In summary, failure mechanisms, initiation and propagation are completely different in these two classes of polymer composites due to their structural and polymeric bond differences.* In figures 2.1 to 2.3 typical examples of damage progression leading to failure in composites are demonstrated. These failure phenomena include fibre cracking, fibre bundle fracture, matrix cracking and transverse cracks in laminated composites.

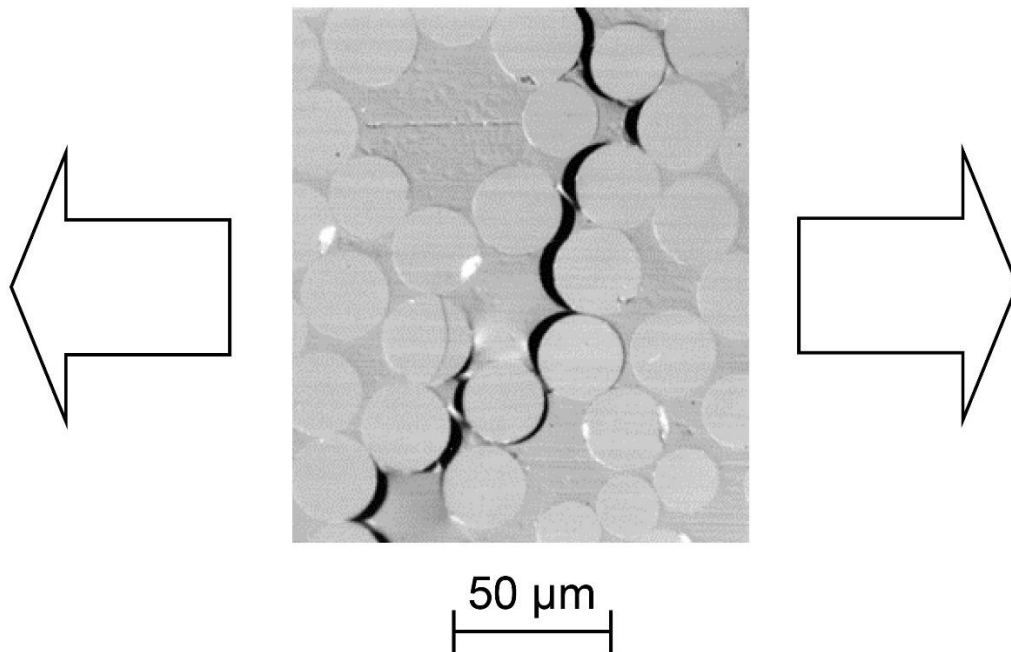


Figure 2.1: Microscopic image of the coalescence of cracks caused by fibre-matrix de-bonding during transverse loading of a fibre reinforced composite [22]

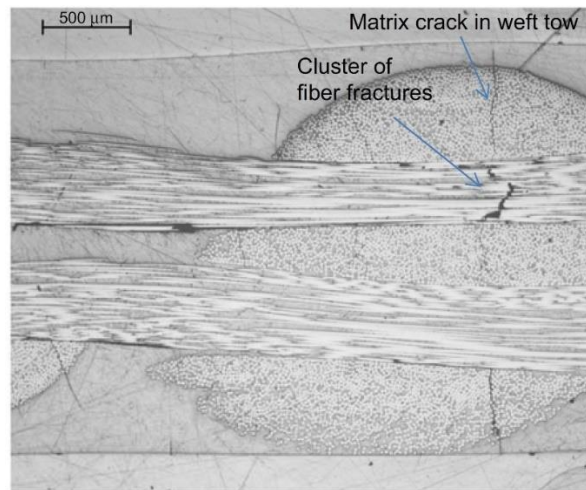


Figure 2.2: Warp bundle fibre fracture adjacent to a matrix crack in a non-crimp woven composite [23]

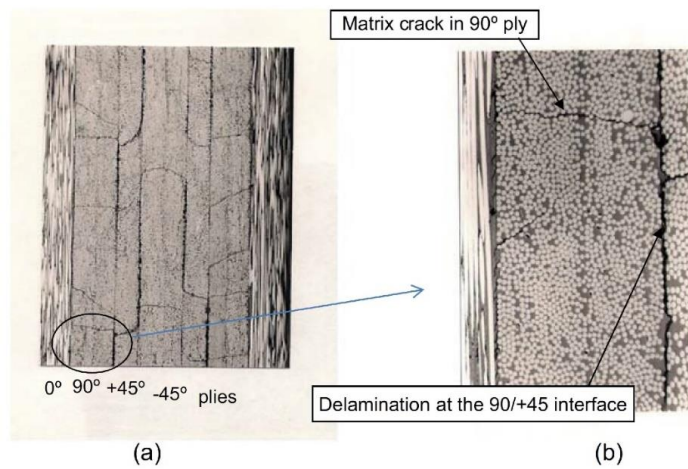


Figure 2.3: (a) Section view of a CFRP laminated composite after fatigue loading demonstrates matrix cracking in 0 ° and 45° plies (b) Higher magnification of matrix cracks shown in (a) [24]

This chapter reviews the literature on failure of composite materials. First, conventional failure theories developed on unidirectional fibre reinforced thermoset composites are discussed. Shortcomings of these models outlined through the well-known World-Wide Failure Exercise (WWFE) are summarised. This is followed by a discussion on failure and damage progression theories developed on thermoset composites. Analysis of failure in thermoplastic composites with an emphasis on woven thermoplastic composites is presented in subsequent sections. The first part of the literature survey is concluded with a discussion on the applicability and limitations of existing failure models on woven thermoplastic composites. Second part of literature survey investigates wrinkling and buckling phenomena in composites by drawing a distinct boundary between these two compressive modes of failure. Different methodologies for the analysis of compressive instabilities are discussed. Finally, a critical survey of the most commonly used wrinkling indicator examining its shortcomings and applicability to composites is given.

2.2 Failure in unidirectional fibre-reinforced composites

Failure is the inability of a component or structure to maintain its functionality under working conditions. In the context of composite materials engineering, unlike to crystalline structures such as metals, failure is a complicated phenomenon due to complex interactions between micro- and macro-level structures of constituents. In composites, failure is highly phenomenological and application-oriented. For example, in a composite member under tension, failure could be defined as rupture of the fibres (Fig. 2.4); In a pipe under internal pressure it could be defined as penetration of fluid through micro-cracks caused by fibre fracture (Fig. 2.5); For a vehicle suspension system failure is defined as the onset of delamination, leading to an abrupt decrease in the member's bending stiffness; And in an

aircraft skin it could be the instability initiated through the delamination of plies at a free edge (Fig. 2.6).

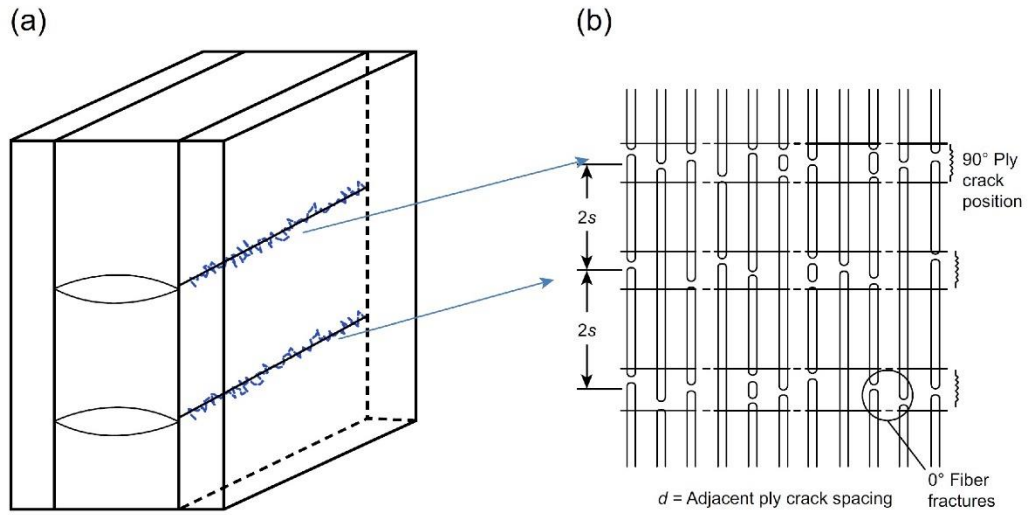


Figure 2.4: (a) fibres fracture in a 0° ply adjacent to matrix cracks in a 90° ply; (b) 0° fibres fracture in the adjacent ply [25]

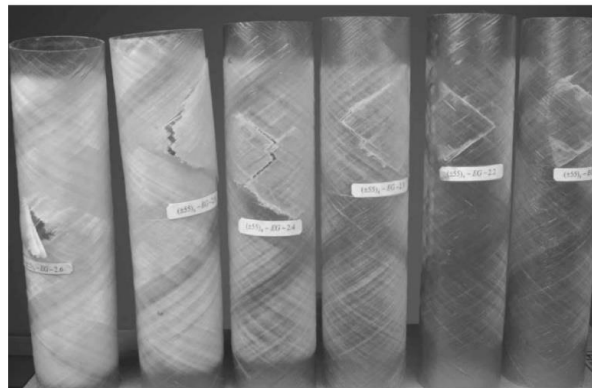


Figure 2.5: Progression of failure in a glass/epoxy composite pipe due to internal loading (low to high loads from right to left) [26]



Figure 2.6: Delamination at the free edge of an aircraft wing [27]

Composite materials are generally made of stacked layers with different fibre orientations. These layers are attached together by adhesives to produce a multidirectional laminate. If a specific loading scenario is applied to the composite laminate, stress and strain states within each layer are different. This results in the progressive failure of the assembly, from one ply to the next, until catastrophic failure event. Therefore, a thorough study of failure in composites encompasses: (1) Initiation of failure or First Ply Failure (FPF), (2) Ultimate Laminate Failure (ULF) or Last Ply Failure (LPF), and (3) Failure of the adhesive layers or Inter-laminar failure. Determination of failure progress from FPF to LPF introduces more complexities into the subject, due to complex damage accumulation mechanisms which are addressed under crack initiation and damage progression studies.

There are two general classes of failure theories established for composite materials: micromechanics and continuum mechanics based failure theories. Micromechanical studies focus on failure of the composite's constituents, including reinforcement, matrix, and their

interphase. Continuum-based macroscopic failure theories investigate failure in the multidirectional laminate, treating the composite as a homogenous material without differentiating between its constituents. Both of these methods have some advantages and shortcomings: micro mechanistic failure theories are accurate as they investigate failure at the level of the constituents; however, they seem to be just an approximation of macro-scale failure, and cannot accurately capture global failure in composites. Macro mechanical failure theories consider composite material as a homogenous material; therefore, failure occurrence is studied at the global level, and failure initiation and propagation at the constituent level is not investigated. This treatment is incapable of recognising and tracking initial failure event within a composite's constituents. Furthermore, studies based on macro-mechanical failure theories do not represent a complete picture of the material's response after failure onset. *In general, an extensive experimental data which can be used to build a sound and trustworthy failure theory for composites and to validate their predictions for multidirectional composites, do not exist* [28-30]. Most of available experimental data on failure mechanisms are obtained through in-plane loading experiments on lamina, or extracted from maintenance information on aerospace structures over their long service lives. The stress state and failure in each lamina is influenced by adjacent layers which makes failure determination in a multidirectional composite a challenging and formidable task.

Failure in composites is generally expressed by a set of equations which are based on different failure modes of constituents. From this perspective, failure criteria can be classified into three major groups: The first group, **Interactive failure models**, uses a combination of different failure modes in a single polynomial or tensor equation to predict failure in a composite. The most well-known interactive failure criteria in this group are Tsai–Hill and Tsai–Wu. The second group, **Non-interactive (superimposed or independent) failure models**, uses an individual criterion for the occurrence of failure for

each mode of deformation, such as failure in tension, compression, and shear. Maximum stress and strain criteria are the most widely used non-interactive failure theories. The third group, **Failure-mode models**, such as Hashin–Rotem and Puck failure theories are among the most widely adopted failure criteria for composites. These theories consider a different criterion for each mode of failure in each constituent of the composite, including failure of the matrix under tension/compression, failure of the fibres in tension, and fibre kinking under compression.

To assess the maturity of composite’s failure models, a “World Wide Failure Exercise” (WWFE) was organised by the science and engineering council of the UK in three stages over a 12-year period. The three main motives for conducting a comprehensive evaluation on the efficiency of failure models included: lack of a universal definition of failure in composites, inefficiency of existing failure theories in practical engineering applications, and the necessity to benchmark failure theories under a consistent experimental framework.

The results of the WWFE with a conclusive recommendation on predictability of participating failure models were published in four special editions of the *Composite Science and Technology* journal [28, 29, 31, 32]. The first stage of WWFE involved benchmarking of 19 different models by predicting failure in composites through 14 different in-plane loading scenarios. The purpose of this stage was to benchmark the status, accuracy and limitations of existing failure models through a round-robin blind test. In the second stage of WWFE, participants were offered opportunities to refine their theories based on the outcomes of the first stage. This stage involved verification of modified theories with experimental outcomes for two and three dimensional loaded components, encompassing 11 case studies. The third phase of WWFE involved assessment of failure theories in predicting damage initiation and development in unidirectional fibre-reinforced thermoset composites.

Several observations can be made on the outcomes of three stages of WWFE: First,

most failure models are based on the failure of a single layer composite and hence their accuracy drops dramatically in multilayered composite components. Effects of ply thickness, lay-up sequence, and interaction between cracks in differently oriented adjacent layers are overlooked issues in these models. Second, most existing theories do not consider effects of unloading and reloading conditions on failure of composites. Residual stress created in the composite laminate during manufacturing requires thorough investigations, and micromechanical analysis is critical in predicting failure initiation in composites.

Integrating failure theories into a finite element analysis is another important concern which needs to be addressed. After developing a reliable failure model based on extensive experimental data, conducting a finite element analysis facilitates studying effect of process parameters on failure onset in composites. Further refinement of the model such as integrating micro and macro level simulations can achieve a more profound understanding on failure initiation and propagation in composites. Further investigation is still required to investigate failure in other classes of composites not covered in WWFE, such as thermoplastic composites and woven reinforced composites. *As a summary to WWFE findings, it should be concluded that although predictability of some theories are better than others, none of them are capable of predicting failure in composites experiencing complicated loading conditions.*

A summary of classic failure theories of unidirectional thermoset composites examined in the first two stages of WWFE is given below.

One of the earliest failure theories for fibre-reinforced composites was proposed by Tsai and Wu. They developed a failure criterion for anisotropic materials based on stress components. This failure theory can be expressed as a function of two strength tensors. In this theory, interactions among stress components are independent from material properties, making it invariant from coordinate transformations. This failure theory also takes into account the difference in strength due to positive and negative stresses, but it

cannot distinguish failure events in the composite constituents. The Tsai-Wu theory is a non-phenomenological failure model which was originally developed for unidirectional composites and as such cannot be directly applied to woven composites. This model adopts a quadratic polynomial function of stresses with tensorial coefficients to predict failure in a composite. Determination of interactive coefficients used in this model is challenging as it requires conducting biaxial tests on samples to determine failure limits of the material under different stress ratios. The assumptions used in this model restricts its application to materials with a closed failure envelope. Finally, the ellipsoidal representation of strength in unidirectional composites under plane stress conditions is a postulate not supported by any physical evidence.

The Zinoviev failure theory [33, 34] is a revised version of the maximum stress theory which predicts failure in a composite once any component of the stress tensor exceeds the strength of a lamina in a specific direction. The locus of failure is defined by the lamina's normal strength in principal directions. As long as the stress state lies within the given boundaries, the composite does not fail. Zinoviev developed the maximum stress failure theory to consider different factors in the failure of composites such as the unloading behaviour of cracked laminates and geometrical nonlinearity in composites caused by a change in the ply angle during loading. The Zinoviev theory is a structural-phenomenological model that considers coupling between different deformation and failure modes. Shortcomings of this model include inability of handling large deformations, nonlinear material behaviour and residual stress during manufacturing.

The Hart-Smith I failure theory [35] is a generalised version of Tresca failure theory adopted for composite materials. This theory is developed on a strain plane and assumes three possible fibre-failure mechanisms among which the dominant mode is fibre fracture in shear, but no attempt was made to characterise failure of the matrix. The reason behind this approach was to establish simplified design rules for carbon-reinforced epoxy

composites in which the fibres carried most of the load and the role of the matrix was merely binding the fibre. It was assumed plane sections remain plane during deformation, which is a reasonable assumption for carbon/epoxy laminates but can become a conservative design guideline for composites such as glass fibre reinforced polymers. Hart-Smith developed his second failure theory (Hart-Smith II) [36] based on a truncated maximum strain failure theory to determine the maximum shear stress in composite constituents. This theory predicts the lamina failure by superimposing failure envelopes of fibre and matrix. Hart-Smith assumed that in situ strength of a lamina within a multilayered laminate is much higher than the strength of the same individual lamina alone. Therefore, the lower bounds of his failure criterion specifies the strength limit of an individual unidirectional lamina, and as such is not applicable to a lamina within a multi-ply composite. Hart-smith developed his second theory to overcome shortcomings of his first theory as it yielded non conservative failure predictions for composites reinforced by isotropic fibres. His second theory still is incapable of addressing intra-laminar matrix cracking between fibres in each ply.

Rotem-Hashin theory [37] employs separate criteria for failure of fibres and matrix. This failure criterion is essentially a non-interactive, mode-dependent failure criterion which is based on the following fundamental assumptions: (1) Failure in fibre and matrix is a completely localised phenomenon, the laminate is free of any discontinuity, and there is no interlaminar shear, (2) The state of stress in the laminate is plane-stress, and (3) Matrix is softer than fibres and more susceptible to onset of failure. In this theory, no distinction between matrix and fibre-matrix interface failures is made. The stress interaction between laminas and its effects on degradation of composite properties is not considered. The authors recognised some limitations and incoherent consequences resulting from the choice of a polynomial to represent failure in the matrix. This model predicts that failure in a composite occurs in the maximum transverse shear plane which is difficult to accept as a

general rule. This theory lacks the capability of predicting response of the composite after failure initiation event as it does not consider the effect of matrix degradation on the strength of composite. The WWFE outcome showed that this failure model is extremely conservative for some loading combinations as compared to test results, and hence yielding oversized products.

Puck-Schurmann failure theory [38] assumes nonlinear stress-strain behaviour in the lamina. The model predicts an initial fracture in a composite and computes the degraded material's behaviour through implementation of a progressive damage model. This theory establishes a physically-based failure model for typical engineering problems. In this theory, two main failure modes in a composite are assumed: failure of fibres and inter-face failure of fibre and matrix. No interactions between different components of transverse stress are considered which makes this theory unsuitable for woven composites due to their interlaced structure. Another drawback of this theory includes its incapability of predicting failure under compressive state of stress.

Edge failure theory [39] is a stress based failure theory developed by E.C. Edge at British Aerospace defence based on the Grant-Sanders method. This theory is capable of predicting modes and loci of failure under FPF and LPF events, and calculating properties degradation due to progressive failure phenomena. This theory assumes that the failed ply will be unloaded gradually. The Edge failure theory, designed for predicting failure in aircraft structures, investigates failure based on a discrete ply-by-ply method while assuming nonlinear behaviour of the matrix. In this methodology, only two interactions are considered: shear-tension for matrix failure and shear-compression for fibre failure. In this model, in-plane shear failure is considered to be the final failure mode due to associated low-stiffness and large distortion in the composite. Transverse tension and compression failures are considered as the initial failure modes, causing gradual decrease in the composite's ply stiffness. WWFE exercise found significant discrepancies between

predictions made by this theory and experimental results in some regions of stress space. In some quadrants, this theory was exceedingly conservative while in other regions was non-conservative. The Edge model also exhibited fundamental weaknesses in post failure analysis of composites.

C.C. Chamis [40] developed a failure model based on the micromechanics of composites at NASA. He implemented a progressive fracture scheme to predict first ply failure and fracture of epoxy composites under combined loading conditions. The micromechanical model was calibrated against unidirectional properties of the composite obtained from experiments. Two computer codes were developed to generate failure envelopes and integrated with a finite element commercial package to allow failure analysis of fibre reinforced composites using Chamis model. The theoretical model used to predict damage initiation is based on a Modified Distortion Energy (MDE) criterion. Outcome of WWFE showed that this theory under-predicts failure initiation in regions with at least one component of compressive stress.

The failure theory developed by G. C. Eckold [41] is a simplified approach for predicting failure in FRCs. This criterion was developed as a part of a British design code (BS4994) to avoid resin cracking and resin/fibre de-bonding in tanks and pressure vessels made of glass-fibre reinforced thermoset composites used in chemical process plants. This research project was developed as a response to wide demand for a pragmatic and auditable design approach for FRCs in a wide range of industrial applications. In this model, material nonlinearities under tensile and compressive state of stress are ignored. A short coming of this theory includes the assumption of equal strength in composites under tension and compression. This theory was originally developed for unidirectional fibre reinforced composites and as such is not applicable to woven structures which demonstrate a complex failure phenomenon due to interactions between interlacing yarns. The differences between failure in FRC and woven composites will be highlighted more in depth in section 2-2-2 of

this thesis.

Wolfe failure theory [42] is based on a theoretical model primarily introduced by Sandhu [31]. They initially developed a model to predict failure of FRCs under biaxial loading [32] which was later extended to contain triaxial loading conditions [33]. In this model, an iterative incremental constitutive law based on the laminated plate theory is combined with a strain-energy based failure criterion. This model captures nonlinear response, failure onset, and failure propagation in FRCs under biaxial loading. Wolfe theory is designed to cover a variety of ply-unloading mechanisms. Calibrating Wolfe model is intensive as it requires data from five different mechanical characterisation experiments: longitudinal tension/compression, transverse tension/compression, and shear tests. The nonlinear response of the composite laminate is modelled using a piecewise cubic spline interpolation function. This model facilitates calculating composite properties as a function of stress and strain. The Wolfe failure model assumes that the strain energy of an orthotropic material model under uniaxial tension/compression, transverse tension/compression, and shear are independent.

In conclusion, outcomes of WWFE exercise on classic failure theories demonstrated discrepancies of 300% between these theories and experimental outcomes. Almost all theories were accurate in predicting laminate properties under very low strains; however, none of them were capable of capturing nonlinear behaviour of composites at high strains dominated by the matrix behaviour which is typical in thermoplastic composites. These models are based on failure in a lamina, and as such are not suitable for predicting failure in multilayered composites. To highlight the importance of finding or constructing an accurate and scientific failure model for multidirectional laminate composites, it suffices to quote professor Hashin's reasoning for declining to participate in WWFE exercise: "My only work on this subject relates to failure criteria of unidirectional fibre composites, not to laminates... I must say to you that I personally do not know how to predict the failure of

a laminate. (And furthermore, I do not believe that anybody else does! [25])”.

WWFE outcomes demonstrated that the divergence between theories and experimental results was greater in triaxial than biaxial loading conditions. Ignoring the complex interactions between different layers of the composite, as well as non-existence of standard experimental procedures for triaxial loading scenarios are among drawbacks of these failure theories. Damage development and initiation of delamination are among overlooked areas of these theories. Finally, these theories are incapable of predicting failure in composites having complex reinforcement structures and different matrix materials such as woven and thermoplastic composites.

2.2.1 Advanced failure theories of thermoset composites

The third stage of WWFE was designed to measure and validate performance of failure models in handling damage development in thermoset composites. Design of composites requires dealing with damage initiation and propagation until ultimate failure. One of the most common form of damage is initiation and accumulation of multiple cracks in the matrix leading to delamination and failure at the fibre-matrix interface in a thermoset composite. Following a discussion on failure theories originally developed to predict failure initiation in composites, this section reviews failure models capable of predicting damage accumulation and progression in unidirectional thermoset composites.

Kashtalyan and Soutis developed an analytical model [43] to predict the effect of intra- and inter- laminar damage (matrix cracking, splitting, and delamination) on the residual stiffness of a composite laminate to be used in post-initial failure analysis. This model is based on a two-dimensional shear lag stress analysis model and the Equivalent Constraint Model (ECM) of the damaged laminate. The results of this model was compared with experimental outcomes and it was advised that the damage modelling of the composite was still immature and requires more development before being used by the design community.

Drawbacks of this model include its limitation to thermoset composites and calculating damage parameters based on matrix cracking as the main degradation mechanism and neglects damage in the composite cause by fiber fracture. Finally, this study attempted to present a general methodology to calculate degraded properties rather than predicting ultimate failure of the composite.

Pinho et al. developed a failure model [44] based on plasticity theory and incorporated a new yield function in conjunction with a kinematic strain hardening law to predict failure in composites. The model is capable of distinguishing between matrix and fibre failure and fibre kinking modes. Failure propagation is predicted by employing the fracture energy method associated with each failure mode. The failure index of the matrix is a modified Mohr-Coulomb criterion adopted for unidirectional composites. A damage model based on a saturation crack density function is employed to calculate degraded matrix properties. After failure of a ply, the effective modulus of the composite is calculated using the classical laminate theory. The thermal effects and residual stresses in the composite due to manufacturing processes are among disregarded areas in this model.

C. Soutis introduced a failure theory based on a cohesive zone model to predict damage initiation from notches in members under tension [45]. This model, initially developed for an IM7/8552 carbon fibre/epoxy quasi-isotropic multidirectional laminate, is capable of determining the growth of micro-wrinkles originating from a hole in a composite laminate under compression. A plastic fibre kinking analysis is conducted in conjunction with implementing a linearly softening model to predict the un-notched and open-hole compressive strengths of the composite.

R. Talreja combined micromechanics and Continuum Damage Mechanics (CDM) into a single Synergistic Damage Mechanics (SDM) model to predict the mechanical response of a composite laminate experiencing multidirectional ply cracking conditions [46]. The material constants required for the model are obtained from stiffness property changes in a

reference laminate. This model reproduces the stress-strain response of the composite by combining degraded stiffness properties and evolution of the crack density.

P. Camanho et al. developed two different failure theories for different classes of thermoset-based woven composites. In the first model, based on the plastic deformation theory, mechanical nonlinearities arising from permanent deformation and damage were considered [47]. This model uses the Ramberg–Osgood equation in conjunction with a user-defined subroutine to define loading curves of the composite. Failure is predicted using either a maximum stress failure theory or a Tsai–Wu failure model. The model has been assessed based on experimental outcomes on plain-weave and twill-weave carbon fibre composites. In the second model [48], developed for a fibre reinforced composite with highly cross-linked epoxy resins (RTM6), a micromechanical pressure-dependent failure model was adopted to calculate the maximum principal stresses at the tip of small internal defects. Microscopic defects were incorporated into a unit cell to predict fracture under compressive and tensile loadings using finite element analysis. The Camanho model was constructed on the existing failure models and lacked originality in proposing a theory to predict failure in composite materials under different loading conditions.

Barbero et al. [49, 50] investigated local damage effects and the resultant degraded material properties using Discrete Damage Mechanics (DDM) framework augmented with a fibre damage model. They incorporated micromechanical damage mechanics constitutive models into finite element analysis to predict initiation and evolution of intra-laminar transverse and shear damage until fracture. The DDM model was calibrated for carbon epoxy laminates based on data obtained from characterisation tests.

Tsai proposed an invariant-based failure approach [51-53] to predict elastic properties and failure limits of composite laminates based on the trace of the plane stress stiffness matrix. An invariant omni-strain LPF envelope, normalised based on failure limits of the composite in uniaxial tension and compression, was constructed to specify the inner failure

limits of a composite under all possible ply orientations. The applicability of the normalised unit circle in identifying failure limits of a carbon-fibre composite was justified by anchoring the uniaxial test data. However, in a glass-fibre reinforced composite, an omni-strain LPF failure envelope was recommended. The proposed model was implemented into a numerical simulation to predict failure in carbon/epoxy composites.

The failure theories studied in this section were developed to model damage accumulation and propagation in fibre-reinforced thermoset composites. These models predict degradation of composite material properties due to development of localised damage events starting at very low strains in a thermoset matrix. This phenomenon is common in components made of thermoset composites experiencing progressive failure during their long service life and substantially different to failure of composites under high strain forming rate such as stamping. Moreover, damage in thermoset composites is substantially different to thermoplastics due to dissimilar molecular structure and bonding strength between their constituents. These differences invalidate application of progressive failure theories developed for thermosets on thermoplastic composites.

2.2.2 Failure of woven composites

Woven composites exhibit an improved damage tolerance owing to their interlacing structure. They are becoming increasingly important class of high performance materials in high-end applications. Since woven composites possess the same local morphologies as their cross-ply unidirectional counterparts, failure initiation and progression have certain similarities. However, owing to their distinct structural features, new failure patterns have been found in woven composites. In this section, some recent attempts to study failure in woven composites are highlighted. *It should be emphasized that none of these studies have yet resulted in a model that can predict failure in woven composites under different deformation modes.*

Lomov et al. investigated failure onset, damage accumulation, and damage progression in woven composites in a series of published articles [52-56]. They investigated failure onset and progression in a wide range of woven composites at different scales using quasi-static uniaxial extension, tetrahedron and double dome-forming experiments. Post-mortem CT and X-ray scanning methodologies were used to identify fracture sites and reveal damage progression patterns in composites. Optical microscopy and SEM methods were employed to study local damage modes. A three-dimensional photogrammetry system was adopted to study evolution of strains, before and after damage onset. In some test cases, an Acoustic Emission (AE) system was employed to determine corresponding damage modes in composites during deformation. They developed a standard test procedure to monitor damage initiation and accumulation at different length scales in textile composites.

A distinct feature in textile composites is the presence of yarns. The locations of transverse matrix cracks can be controlled by the architecture of the textile reinforcement. In a woven reinforced composite, it is possible to observe fibre-matrix de-bonding on yarn boundaries earlier than de-bonding inside yarns. De Greef et al. [54] observed this phenomenon while studying failure in a carbon fibre/epoxy composite. Analysis of results from quasi-static tensile loading tests and acoustic emission investigations demonstrated that fibre-matrix de-bonds first appeared at yarn boundaries, which did not develop into large cracks. A similar phenomenon was observed in a carbon-epoxy three dimensional woven composite [55]. Fibre-matrix debonds at yarn boundaries were also found under bias loading condition [56]. In this case, damage development was similar to longitudinal loading condition. The experiment results revealed that the composite material would exhibit fracture caused by high shear deformation in the matrix.

Yarn crimp is a special structural feature in textiles and has an important influence on damage initiation and development in woven composites. This influence is commonly attributed to the complicated state of stress in yarns caused by their structural features. The

complex state of stress introduces a non-negligible shear component due to the presence of yarn crimps, even when the yarns are oriented at the same direction with loading [57]. Comparative studies were conducted on three dimensional non-crimp orthogonal weave and two dimensional plain weave glass/epoxy composites using tensile loading tests [49, 50]. The composite material systems examined in these studies had a very similar reinforcements and fibre volume fractions. The main difference between these two types of composites was the yarn crimp. The two dimensional composite was reinforced with four plies of conventional plain weave having substantial crimps. The three dimensional orthogonal weave composites, on the other hand, had negligible crimp. Outcome of these studies showed that the three dimensional woven composites have considerably higher in-plane strengths and ultimate failure strains compared to the two dimensional laminated counterpart. Once both were loaded in fibre direction, the three dimensional composite showed higher damage initiation threshold than the composite with two dimensional reinforcements. However, when the loading was in the 45° bias direction, the damage initiation threshold was lower in three dimensional composite. In a two dimensional weave laminate with substantial crimps, the dominant failure was extensive delamination caused by transverse cracks. In three dimensional non-crimp composite, the growth of transverse cracks was delayed and these transverse cracks were less susceptible to the formation of yarn-matrix interfacial cracks.

In textile composites, geometry of matrix cracks are affected by the yarn crimps. At early stage of loading, cracks occur in different locations and the crack length is usually limited by the crimp intervals. Once loading is increased, cracks propagate into the structure of yarns leading to catastrophic failure event in the composite. Ivanov et al. [58] investigated development of cracks in a triaxial braided carbon-epoxy composite. This composite had high crimp with intensive interlacing yarns. They found that although matrix cracks occurred in different locations, they normally were confined inside unit cells of the

textile composite in the early stage of loading. The matrix cracks were also initiated at different locations in the yarn depending on the textile structure [59, 60]. In conclusion, yarn crimp influences stress distribution, and as such generates different types of failure in the weave structure of the composite.

2.2.3 Failure of thermoplastic composites

Failure studies discussed earlier were dedicated to initiation and progression of failure in thermoset composites as the first composites used extensively in industrial applications. It is just recently that thermoplastics have gathered worldwide attention as the matrix of polymer composites. There are major differences between failure behaviours of these polymers caused by distinct molecular structure and polymeric bond of thermosets and thermoplastics. *These differences necessitate developing new failure criteria for thermoplastic composites, as the existing criteria cannot correctly capture failure event in this class of composites due to fundamentally different behaviour of thermoset and thermoplastic composites at micro and macro levels.* In this section, recent failure studies on thermoplastic composites are investigated. It should be highlighted that these studies shed light into failure initiation and propagation mechanisms in thermoplastic composites; however, no model has been proposed to predict failure in this class of composites yet.

Yurgratis and Sternstein [61] conducted experimental failure studies on carbon fibre thermoplastic composites. They manufactured composite laminates from carbon fibre prepregs with different volume fractions embedded in five different thermoplastic resins. They conducted a four-point bending test on composite specimens until failure. They employed a carbon-fibre epoxy composite for benchmarking with thermoplastic composites. Mechanical characterisation results showed that yield stress of all thermoplastic composites were equal or higher than of the epoxy resin. Failure strain of thermoplastic composites showed an increase of 200% to 500% compared to epoxy. They

found out that all thermoplastic composites failed by an abrupt longitudinal compression buckling of the outer ply. Micrographs revealed micro-kinking in thermoplastic composites have led to other types of damage such as ply splitting, transverse ply shear failure, fibre tensile failure, and transverse ply cracking. However, fibres were failed in bending rather than in direct compression. The thermoplastic composites were successful in suppressing delamination compared to epoxy-based composite. Another difference was noticeable effect of residual thermal stress caused during manufacturing on mechanical properties of thermoplastics. However, authors could not justify the weak compression strength of thermoplastic composites as compared to thermosets.

Couque et al. [62] conducted studies on failure mechanisms of thermoplastic FRCs under uniaxial, in-plane biaxial, and hydrostatically confined compression tests. They conducted experiments on two different thermoplastic carbon-fibre reinforced composites (Poly Ether Ether Ketone (PEEK) and Polyacrylonitrile (PAN)). They found out thermoplastic composites buckle under low stress states caused by out-of-plane compliance of the composites and natural waviness of fibres. Authors did not conduct analytical studies on failure onset in the thermoplastic composite, and as such could not propose a failure model.

Oya and Hamada [63] investigated failure mechanisms of different thermoplastic composites made of carbon fibres embedded in PAN, APA6, and PPS resins. They examined mechanical properties of these materials such as strength, strain to failure, and elastic moduli under tensile and compressive loads. They performed centre cracked plate tensile (CCT) experiments on specimens and examined failure regions using Scanning Electron Microscopy (SEM). They found that interfacial bonding properties highly influenced strength and failure limits of composites. However, they were unsuccessful in proposing a model that can predict failure in thermoplastic composites under different stress states and modes of failure.

Ramirez-Jimenez et al. [64] conducted tensile experiments on glass-fibre reinforced polypropylene composites having different fibre orientations. Variations of fibre orientation resulted in failure under different modes. They captured stress waves emitted during failure by an acoustic piezoelectric sensor. The primary frequency of failure event was plotted as a function of time. The resulting graphs demonstrated clusters around specific frequencies. Using acoustic emission technique and SEM, they proposed a hypothetical theory which stated there was a relation between each micro level failure mode and the released stress wave frequency. However, they could not distinguish between different failure-modes in a mixed mode failure event. Furthermore, the accuracy of the hypothesis was not investigated on composites made of different fibres or resins.

Fritzsche et al. [65] conducted crash simulations on components made of thermoplastic composites to predict failure initiation and propagation. They used softening behaviour of polymer composites to predict strain localisation during impact. They employed fracture energy regulation method to overcome convergence problems during crack initiation and propagation and to obtain mesh-independent results. Scatter in material properties were considered in finite element analysis and stress concentration was estimated through detailed geometrical modelling. The simulation results showed a good agreement with experiments; however, no attempt was made to develop a failure criterion for thermoplastic composites or to predict failure in thermoplastics under different loading conditions.

Izer et al. [66] studied failure mechanisms and fracture behaviours of a woven self-reinforced polypropylene composite during uniaxial extension tests. They made composite sheets through film stacking and compression moulding techniques. The failure behaviours of specimens were assessed by the Acoustic Emission (AE) process. A relation between number of AE events and adhesion between two crystalline phases of the polypropylene was discovered. It was concluded that the quality of consolidation has a major effect on failure response and failure mechanism of the composite.

Reyes and Sharma [67] investigated damage behaviour of woven glass fibre reinforced polypropylene composites during low velocity impact using experiments and analytical techniques. Specimens having different volume fractions and lay up configurations were subjected to impact by a drop weight impact tower and under four-point bending condition. Load-displacement graphs demonstrated high energy absorption capability of woven composites as compared to thermosets. Scanning electron microscopy analysis showed no sign of matrix cracking in the impact zone. An energy balance model was employed to simulate and predict impact response of woven composites. Finally, fractured specimens were repaired through a compression moulding process and an excellent recovery in flexural strength and modulus of thermoplastic composites were observed.

Böhm et al. [68] developed a phenomenological damage model for woven and braided composite materials. Based on experimental observations on a woven hybrid glass fibre-PP composite and within a continuum damage mechanics framework, they developed a failure mode dependent criterion using a stiffness degradation scheme. They did not validate their numerical model against experiments, neither benchmarked their failure theory predictions against existing failure criteria. This study was exclusively focused on glass-fibre reinforced composites and therefore cannot be generalised to other types of composites with a more ductile reinforcement.

Hufenbach et al. [69] investigated temperature effects on mechanical properties and failure behaviours of hybrid woven composites using six different in-plane loading scenarios. The elastic constants and strength of woven composites were obtained from uniaxial tensile and compressive tests data within -40 to +80°C temperature range. Visual observations and optical microscopy techniques showed a brittle to ductile transition in failure around glass transition temperature. Below this temperature, high brittleness of the thermoplastic resin resulted in inter fibre fracture phenomenon perpendicular to the loading direction. At 80°C temperature, cracks and voids formed in the matrix while the interface

bonding strength was improved. They concluded that temperature affects woven composite behaviours through two mechanisms: change in material properties and shift of damage mechanism.

Fedulov et al. [70] proposed a material model to simulate plastic behaviour and damage accumulation in a carbon fibre-reinforced PEEK composite under different stress states. They determined plasticity constants using uniaxial tension and compression tests. They showed that a change in the state of stress in the composite might strengthen the matrix. They employed an existing failure model in the Abaqus software library to predict failure and damage accumulation in the composite. They verified the numerical predictions against transverse tension experiment and interface failure during fibre pull out test. Their work lacked novelty in proposing a failure model for thermoplastic composites.

Wang et al. [71] proposed a novel failure model for a flax fibre reinforced polypropylene composite through analysis of strain evolution on hour glass specimens. It was shown that the conventional forming limit diagram is not able to predict failure in this class of composites. They constructed a failure model based on maximum fibre strain theory. This model was implemented into finite element analysis and successfully verified against experimental results on failure of the natural fibre composite under different deformation modes. In this study, efficiency of their model in predicting failure in other type of composites such as woven composites with different fibre reinforcements was not investigated. The proposed failure model assumed fibre fracture as the main mode of failure in the composite. This assumption makes the model inapplicable to composites exhibiting other types of failure mechanisms such as failure of the matrix and delamination. Composites such as self-reinforced polypropylene composite exhibit a less pronounced mechanical properties difference between fibre and matrix and as such demonstrate different types of failure as highlighted in chapter 3 and 4 of this thesis.

Temperature is a common contributing factor which can influence failure behaviour in

thermoplastic composite materials. Hufenbach et al. [72] studied the mechanical properties and failure behaviour of multi-axially reinforced thermoplastic textile composites under different thermomechanical loading conditions. They employed glass/Polypropylene composite material systems with different reinforcement structures including a 3 dimensional textile composite with weft-knitted reinforcement and a woven reinforcement structure. Uniaxial tension and compression tests were conducted with temperatures ranging from -40 to 80°C. It was revealed that the mechanical properties of both material systems were temperature dependent, including shear properties and compressive strength of composites. The fibre dominated properties, such as modulus of elasticity, were less influenced by the temperature. The mechanical properties of both material systems were largely dependent to the glass transition temperature of the polymer matrix. At temperatures below the glass transition temperature, the matrix became brittle and formation of cracks was intensified. Above the glass transition temperature, the polymer became ductile and less matrix cracks were found.

Recently, a probabilistically based damage model [73] was developed for textile thermoplastic composites. Experimental and numerical studies were conducted to validate the failure models [73]. The failure model was based on continuum damage mechanics where damage was defined as a degradation of material stiffness [74]. In a conventional unidirectional laminate, the failure progression can be described by the progression of discrete damage events. Normally, this sequential damage event is triggered by small matrix cracks, and can be quantified by a crack density parameter. This is followed by delamination, which can be quantified by the delamination length or area. In composites with woven or braided reinforcement, different damage mechanisms can occur simultaneously, making it impossible to separate and quantify all the different damage mechanisms. In order to deal with this complex damage phenomenon in the woven or braided reinforced composites, a probabilistic approach is adopted to provide failure curves

with associated probabilities. In this study, the failure of textile reinforced composites was characterised by different failure modes. The interactions between failure-modes were characterized by the summation of probability functions. Using this approach, different failure curves formed a theoretical probability plot of failure which were employed to predict damage in textile reinforced composites.

S. Kalyanasundaram studied the effect of process parameters on formability and failure behaviour of fibre metal laminates [75-78]. A self-reinforced polypropylene composite and a glass-fibre reinforced polypropylene composite sandwiched between two layers of monolithic aluminium were stamp formed into a channel section. Laminates were pre-heated to 160°C in a heated platen press and deep drawn using a hemispherical punch. Formability of the composite-metal laminates were investigated using three different tool temperatures (80, 100, 120°C) and under three different blank holder forces (1, 3.5, 6 kN). Three different feed rates (4.4, 28 and 53 mm/s) were used to deep draw specimens into the die cavity. Shape error and delamination were used as quality indicators in formed specimens. This study showed the dependence of fibre metal laminate formability to time and temperature parameters and an optimal processing windows were suggested to yield minimum shape errors. Comparisons were made with channel forming of aluminium specimens and it was concluded that geometry variations in both post formed fibre-metal laminates were significantly less than aluminium specimens. It was found that forming rate has a more significant effect on the quality of the post formed channels compared to plain metal forming. This behaviour was attributed to temperature-dependent nature of the polymer's viscosity and the transient temperature profile of the laminate during forming. Strain rate effect was considered as the second underlying reason for this behaviour.

More recent studies on failure of composites can be found in [79-85]. Some of these publications only investigate shortcomings of existing failure theories, while others conduct preliminary studies on failure of composites. These articles do not introduce novel

criteria to predict onset of failure in composites and therefore are not discussed in this thesis.

2.2.4 Summary

Predicting failure in composites has been subject of research for almost half a century. Numerous theories have been proposed, however literature studies show that none of these theories were successful in predicting initiation and propagation of failure in composites under complex loading conditions. The outcomes of WWFE revealed that neither of these theories are capable of predicting failure in all regions of strain or stress space with a reasonable accuracy. These theories were developed on a case-by-case basis during long service life of composites used in aerospace industry. These theories were originally developed to predict failure in thermoset composites under fatigue and creep conditions, and were mainly designed for unidirectional fibre reinforced composites.

There are several factors demonstrating the gap of knowledge in failure of woven self-reinforced thermoplastic composites: failure mechanisms in thermoset and thermoplastic composites are fundamentally different due to their dissimilar properties at micro and macro levels. Interfacial bond strength is dissimilar in two-phase and single-phase composites. Adhesion quality between constituents of a composite plays an important role in load transfer mechanisms and the shear and transverse strengths of composites, and as such has a detrimental factor in failure initiation and propagation mechanisms. Interlacing structure of woven reinforcements adds to the complexity of failure in woven composites by simultaneously introducing different damage mechanisms. These differences necessitate studying failure of a SRPP composite experiencing high strain rate forming conditions.

2.3 Buckling and Wrinkling

2.3.1 Fundamentals

Buckling and wrinkling are two common types of instability caused by the development of compressive stress in materials, leading to catastrophic failure or malfunction of the product. Although similar in nature, these two phenomena have some fundamental differences. Buckling is a global phenomenon, with a wavelength (and amplitude) relatively large compared to dimensions of the part. Buckling occurs as a result of both elastic and plastic deformations in materials. Wrinkling, as a local defect, occurs within small wave lengths and propagates on the surface of specimens in plastic deformation regime. Wrinkling, or localised buckling, might trigger onset of other types of instability, such as puckering. Figures 2.7 and 2.8 depict actual cases of buckling and wrinkling failures in structural and non-structural components. Fig. 2.7 shows a composite column exhibiting a third mode of buckling under compression and Fig. 2.8 illustrates wrinkles developed on the flange of a steel cup during manufacturing.



Figure 2.7: Buckled composite structure [16]

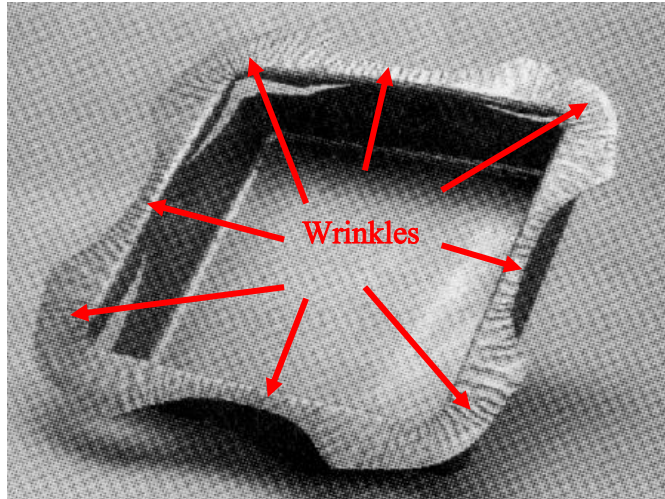


Figure 2.8: Wrinkling in the flange area of a cup formed from a steel sheet [86]

An increasing demand to employ thinner sheets in the manufacture of light-weight products has raised the likelihood of failure due to wrinkling. Wrinkling is undesirable as it causes shape distortion, degradation of mechanical properties, generation of unacceptable tolerances, and difficulties in the assembly process. Wrinkling is one of the main causes of manufacturing problems in industries that require stringent dimensional, geometrical, and surface tolerances. Several parameters affect onset and propagation of wrinkling. These factors include mechanical properties of the material, stress and strain states during manufacturing, geometrical parameters such as aspect ratios and local curvature of specimen, ratio of in-plane to bending stiffness, and contact conditions.

A thorough analysis of wrinkling considering all main parameters is a formidable task as a small change in these parameters causes a wide scatter of data [87-89]. Due to these reasons, wrinkling is generally investigated on a case-by-case basis, using specific indicators. Wrinkling is analysed using analytical, numerical and experimental techniques. The analysis of wrinkling initiation and propagation is a very challenging problem due to

complex interactions between contributing factors. Study of wrinkling necessitates application of a combined methodology applicable to different loading scenarios. Existing criteria for determination of wrinkling is very sensitive to loading, boundary, and contact conditions and as such makes the process complex and time consuming.

In industrial applications, trial-error and die try-out methodologies are often adopted to eliminate or alleviate wrinkling; however, these processes are expensive, intensive and time-consuming. These shortcomings necessitate developing a universal indicator to predict and prevent the onset of wrinkling and to optimise the production of defect free parts due to wrinkling. In the following section, conventional methodologies for the analysis of wrinkling are explained.

2.3.2 Analytical methods

Four different analytical methods are generally used to study wrinkling in materials: static analysis method, initial imperfection technique, bifurcation analysis, and energy method. In the static method, the material is considered to be in equilibrium state while experiencing a small localised imperfection such as geometry or material imperfection. Equilibrium equations are expressed by an incremental formulation. The boundary conditions are applied and the solution of equilibrium equations is calculated. This solution determines the critical load that triggers onset of wrinkling. This method is extensively applied to solve wrinkling problem of parts made of thin sheets and plates having regular geometries and well defined boundary conditions [90-93]. The main advantage of this method is the provision of a global view which determines tendency of parts to wrinkle and elucidates the effect of individual parameters on the wrinkling onset. However, in real-world problems, applied boundary conditions are complex, the shape of the component is irregular, and the stress distributions are uneven. Due to these factors, this method is impractical and ineffective for most engineering applications.

In 1961, Timoshenko and Gere [94] found that real cylinders buckle at loads much lower than loads calculated based on static equilibrium method. This finding led to extensive research on buckling phenomenon in subsequent decades. It was demonstrated that the real cause of this discrepancy was geometrical and material imperfections [95-99]. These findings led to the introduction of an alternative method to solve buckling and wrinkling problems. In the new method, an initial imperfection in the material is assumed. The partial differential equations of equilibrium, based on a stress function, are derived and solved to determine the critical wrinkling loads. The application of this method is restricted to simple problems with regular geometries and well defined boundary conditions [100-102]. There are two main difficulties in treating wrinkling problems using this method: The wrinkling problem is highly complex to formulate and finding a solution to the resultant nonlinear partial differential equations is very challenging. The second problem is related to the nature of imperfections: in reality the nature of manufacturing induced imperfections are random; however, in in this model, a perfect and idealised distribution of imperfections is considered. Therefore, the predictions made by this model deviates from experimental results.

The bifurcation method is based on a functional and criterion proposed by the Hutchinson [103-105]. This criterion was initially employed to study post-bifurcation and imperfection-sensitivity aspects of plastic buckling. However, this method was later adopted to treat some wrinkling problems with success. It was realised that the onset of wrinkling can be determined by the bifurcation point on the load path of the material from the primary to the secondary equilibrium states, as shown in Fig. 2.9. In this figure, variable P is the force and variable u depicts displacement. The material initially follows deformation path of OB (the primary path of deformation). After getting to point B, the energy required to deform the material under the primary path is more than the energy required to follow the secondary path. Therefore, although the primary path shows the

material's intrinsic property, the specimen follows the secondary path or the perturbed solution. In the bifurcation method a functional (F) is defined. The structure or material is considered to be perfect. Functional F determines the total potential energy of the system prior to wrinkling onset. The bifurcation functional defines the system's energy as a function of its current configuration, induced deformations and their derivatives. Constitutive stress-strain relation is incorporated into the flow role of the material expressed by a set of differential equations. The material's yield surface is defined by a yield theory. Then the functional and its derivatives are set to zero to determine the critical condition of wrinkling.

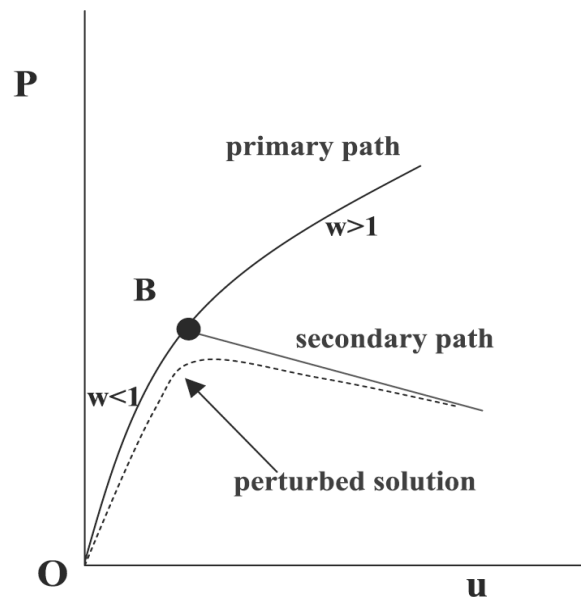


Figure 2.9: Force–displacement path of a specimen prior and after wrinkling

Energy method is an alternative, yet widely applied approach for treating wrinkling problems. In this technique, the incremental deformation energy is calculated using in-plane stress and strain states of the material during forming. Then, incremental bending energy required to initiate localised wrinkling is defined. By equating these two components, the onset of wrinkling can be predicted. The major advantage of this method

is that the set of partial differential equations does not need to be solved. This method has been adopted to solve a wide range of wrinkling problems [106-109]; however, simplified assumptions used in this method, such as idealistic contact conditions, make the energy method inapplicable to problems with complex boundary conditions.

The following section provides historical background as well as more recent advances in using the energy approach as the most efficient and widely adopted method in the analysis of wrinkling. It should be emphasised that the energy method uses a scalar variable to predict wrinkling in metals and as such cannot be effectively applied to composites due to their anisotropic properties.

Geckeler [110] was among the very first pioneers who studied wrinkling phenomenon using an analytical approach. He adopted the energy method to predict critical stress required for onset of wrinkling on the flange region of deep drawn specimens. Geckeler's method was improved by Senior [111] who introduced the blank holder force to the problem. During deep drawing process, the material was drawn into the die cavity by a punch while the flange region was subjected to a radial tensile stress and a compressive circumferential stress. It was assumed that the amplitude of wrinkles, expressed by a sinusoidal wave, is constant over the width of the flange. A rectangular segment on the flange area was selected to represent the unit deflection of the flange and to simplify the analysis. The energy conservation theory states that the critical wrinkling condition is achieved when the strain energy in the rectangular segment equals to the work done by the external load. Initiation of wrinkling in the flange region requires that the sum of bending energy and restraining energy due to lateral restraints should be equal to the external work calculated from the circumferential shortening of the flange segment. The critical wrinkling stress can then be calculated using this equality. An outcome of this study concluded that the overall flange deflection function expressed by the number and amplitude of wrinkle waves is crucial in estimation of critical wrinkling stress. Based on this reasoning, Senior

adopted different deflection functions and boundary conditions to predict critical stress.

Alexander [112] claimed that a good approximation to the Senior's methodology can be achieved only under narrow flange condition attributable to the usage of a one-dimensional buckling model. In a wide flange, the amplitude of wrinkles cannot be assumed constant over the width of the flange, and as such Senior's approach might fail to provide accurate prediction on critical stress conditions. Yu and Johnson [113] improved Senior's approach by refining the deflection function in the flange region. In this study, the wrinkling problem of a flange was simplified to an annular plate simply supported at inner and outer edges, and subjected to a radial tensile stress along the inner edge. A normal constrain was applied to simulate the blank holder effect. An energy criterion was extracted using a new deflection function and the critical stress was calculated.

Morovvati et al. [114] applied an energy method to study the effect of blank holder force on eliminating wrinkles. The critical blank holder force required to suppress wrinkles in single and two-layer circular metal specimens under deep drawing process was calculated. The critical conditions were estimated using Senior's approach. The results of analytical approach showed a good agreement with experimental outcomes. The effects of material properties on wrinkling tendency of circular samples were also investigated and it was concluded that wrinkling can be eliminated by a change of blank holder force, modulus of elasticity and yield strength of the material.

2.3.3 Experimental methods

Different experimental methodologies are adopted to investigate wrinkling behaviour of components under different loading/boundary conditions. Each experimental technique targets a particular feature of the wrinkling problem. These simulative experiments are generally conducted to evaluate the predictability of developed analytical or numerical models of wrinkling. A summary of each method is given below:

- ***Swift cup test***

This method provides a draw-ability measure of sheets by introducing a Limiting Draw Ratio (LDR) parameter. LDR is defined by the ratio of maximum blank diameter, which can be drawn successfully without any failure, to the punch diameter. In this method, a rectangular or circular specimen is drawn into a die, while no or a small blank holder force is applied to the flange area. Excessive hoop compressive stress causes wrinkling on specimen during deformation. It is shown that the flange and side-walls areas are most prone to initiation and growth of wrinkle waves. Several research studies have been conducted on wrinkling behaviour of blanks using this method [115-118]. This method is not suitable to be used in conjunction with a real time photogrammetry measurement system, as the experimental set-up configuration will not allow capturing images of regions susceptible to wrinkling. The swift cup test is suitable to determine effects of individual process parameters on wrinkling behaviour of blanks under no or low blank holder force and therefore is not suitable for studying wrinkling under stretch forming conditions.

- ***Conical (tractrix) dies***

This technique is similar to the swift cup test except for the shape of the die and the absence of a blank holder system. This method is mainly used to investigate wrinkling phenomena during a deep drawing process [119-122]. Blanks are deep drawn into a conical die with a punch having a tapered or cylindrical geometry. This process induces compressive circumferential stress in the specimen which leads to the onset of wrinkling in unsupported regions such as sidewalls. Conical die test offers several advantages over swift cup test. This method facilitates forming of specimens to higher depths. Conical test results in a significant reduction of drawing loads as compared to swift cup test [123]. In a swift cup test, two different failure modes might occur depending on the applied blank holder force and material property, which are rupture and wrinkling. However, specimens

formed by a conical die will always experience wrinkling instability in side walls. Absence of a blank holder system makes this process suitable for three-dimensional photogrammetry measurement; however, due to high level of localised bending strains, this method is not appropriate for specimens made of composite materials, as they experience premature failure due to localised fracture of fibres [114].

- ***Axial compression test***

This method is generally applied to investigate collapse of hollow cylinders under wrinkling, such as off-shore submerged buried pipelines [124-126] and axial members under impact loading [127-129]. In this technique, a uniaxial compressive force is applied to thin or thick wall cylindrical specimens. In materials deforming in elastic regime, the failure would be sudden and catastrophic. If material experiences plastic deformations, failure is preceded by localised wrinkling phenomenon which develops through the length of the member. Increase in the amplitude of the wrinkles reduces the axial rigidity of the member until a limit load is reached. Reaching this limit causes local collapse of the member. Different parameters are used to determine the occurrence of failure under elastic or plastic deformation modes, such as diameter-to-thickness ratio of the member and mechanical properties of the material. Using a compression test setup, the effect of combined loadings, such as bending and torsion, on wrinkling limits of the member can be investigated. This method is not suitable for determination of wrinkling in thin sheets and blanks.

- ***Yoshida experiment***

This test set up, first introduced by K. Yoshida in 1983 [130], was designed to investigate the effect of geometrical and material properties on wrinkling behaviour of samples. In this method, a square sample is stretched along diagonal direction. The tensile

stress in longitudinal direction causes compressive stress state in transverse direction. The accumulated compressive stress leads to wrinkling/plastic buckling at the centre of specimen. It has been found that the Yoshida test was an effective method to study wrinkling of materials [131]; however, due to the fixed length-to-width ratio of the samples, it was not possible to study wrinkling tendency under different stress ratios. For this reason, a modified Yoshida buckling test was developed to overcome this problem [132-134]. The modified Yoshida test is suitable to be used in conjunction with three-dimensional optical strain measurement systems to investigate behaviour of specimens during wrinkling evolution. The current thesis investigates the potential of this method to study wrinkling behaviour of composite materials. Change of fibre orientation and aspect ratio of specimen triggers wrinkling initiation and propagation under a wide range of deformation modes.

- **Uniaxial stretch of thin strips**

Emerge of new technological advancements necessitated using very thin sheet of materials for different applications, such as thin photovoltaic layers. These materials when exposed to high temperatures experience compressive stress. In this method, thin sheets or membranes, possessing very low bending stiffness, are stretched in longitudinal direction. High Poisson's ratio and very low bending rigidity result in onset and propagation of wrinkling waves on the surface of membranes at the early stages of deformation.

2.3.4 Wrinkling Limit Curve (WLC)

WLC is a commonly used measure in industries for predicting onset of wrinkling instability during manufacturing. Induced strains in blanks are specified in the principal strain space. In sheet metal forming practice, it is generally believed that once the ratio of minor to major strain (SR) is lower than -2, the sheet thickens and wrinkling initiates [135]. Constructing a WLC requires some fundamental assumptions during materials behaviour

under compression: First, it is assumed that wrinkling is an intrinsic material property, and as such WLC does not depend on the dimension or shape of specimens. Second, onset of wrinkling can be predicted using the strain state on the surface of specimen and is not affected by through-thickness strains.

There are numerous attempts to predict wrinkling initiation using WLC. One of the earliest attempts was carried out by Hassani and Neal [136]. They realised that under conical cup deep drawing conditions, sheet of metals experience wrinkling when SR decreases below a critical value (-1.17). However, this critical value was dependant to the geometry of punch, shape of the die, and forming parameters, and as such this metric was only valid under the specific test conditions.

The dependence of the wrinkling limit to the strain hardening coefficient, yield stress, sheet thickness, and the anisotropy parameter was investigated by Kim, Son and Park [137]. They analysed the wrinkling problem on three different materials using a combined experimental-numerical methodology. They realised that wrinkling initiates quickly, as hardening coefficient decreases, yield stress increases, thickness decreases, and anisotropy increases. However, they found a discrepancy between experiments and numerical simulation results: Experimental outcomes suggested that the principal strain at wrinkling limits fall into a narrow band regardless of the material thickness. On the other hand, the numerical simulation results demonstrated a dependency between critical wrinkling strain and sheet thickness. This work was focused on three different metals and as such might not be applicable to other type of materials including composites.

Szacinski and Thomson [138] studied existence of WLC by the analysis of strain evolution at the onset of wrinkling in a representative sink bowl forming experiment. Rectangular specimens made of a stainless steel with a uniform thickness of 0.9 mm were formed to three different depths. This study successfully investigated localised strain conditions in the final product, but failed to provide information on the evolution of strains

during forming. Experimental outcomes demonstrated that wrinkling at flange, corners, and mid-part of the walls initiated at strain ratios of -1.0, -0.5, and +0.5, respectively. This study proved that wrinkling limits depend on location and as such predicting wrinkling onset using a single-valued WLD is impractical.

Narayanasamy et al. [116, 139] investigated the effect of mechanical properties on wrinkling initiation using conical and tractrix die forming. Three different metals were used in this study: commercially pure aluminium annealed to different levels, aluminium 5086 alloy annealed at different temperatures, and interstitial-free steels with different thicknesses. Blanks having different diameters were formed in conical and tractrix dies with a flat punch. A grid measurement technique was used to facilitate measuring critical strains on formed parts. To measure strain evolution before and after wrinkling initiation, the blanks were partially drawn to six different depths until wrinkling developed. A WLC was developed to define safe working conditions. The outcomes of this study showed that an increase in the value of Young's modulus, yield stress, strain hardening ratio, anisotropy, and thickness will exhibit a better resistance against wrinkling.

Wrinkling limits of thin-walled tubes with large diameters was studied by Li et al. [140]. They developed an analytical model based on combined energy method and numerical simulation results to predict wrinkling of tubes under different loading paths. A modification function was introduced to make final results closer to experimental outcomes. A limitation of this study is the modification function which is only applicable to thin walled tubular problems. The modification function is dependent to specimen's geometry and boundary conditions which makes it difficult to be applied to other manufacturing and forming processes.

In another study conducted by Djavanroodi and Derogar [141] wrinkling limit of Ti6Al4V alloy and Al6061-T6 alloys were investigated using experiments and numerical simulations. They employed the strain ratio of -2 to specify wrinkling initiation in

experimental and simulative results. They adopted a grid measurement technique to measure strains in initial and final stages of experiment. The outcomes of this study suggested that a strain ratio of -2 can be used to predict wrinkling in this specific case, but might not be applicable to other case studies. Due to limitations of the strain measurement technique, analysis of deformations before wrinkling onset was not conducted.

WLC is extensively used to predict wrinkling onset during manufacturing [116, 134, 142]. However, its effectiveness in predicting wrinkling onset in composite materials has not yet been assessed. Some researchers have questioned the validity and reliability of WLC in predicting wrinkling as a universal indicator [143], since wrinkling limits are dependant to the manufacturing operations and can vary with material properties and geometry. It has recently been shown that the wrinkling limit cannot be defined through single-valued point variables such as stress or strain [144]. Most of current studies on wrinkling were conducted using a grid mark analysis method to measure strains. This method is unable to capture strains during manufacturing operations. Without adequate information on strain distribution and strain evolution prior to onset of wrinkling, the current studies lack the ability to predict wrinkling initiation. These shortcomings necessitate developing an effective and robust wrinkling indicator capable of predicting wrinkling onset during manufacturing of thermoplastic composites [145]. The current study aims at finding an indicator capable of predicting wrinkling in thermoplastic composites by focusing on the evolution of strains before and after wrinkling initiation using an optical strain measurement system.

2.3.5 Summary

This chapter provided a summary of literature related to the failure of fibre reinforced polymer composites due to fracture and wrinkling. First, an overview of existing failure theories developed on unidirectional fibre reinforced thermoset composites is provided and

their shortcomings reflected in the outcomes of the worldwide failure exercise is summarised. It is highlighted that structural features of woven composites introduce distinct type of failure mechanisms in this class of composites. It is also demonstrated that failure initiation and propagation in thermoplastics is fundamentally different to thermosets due to their dissimilar microstructural features. A survey on recent studies conducted on failure in woven thermoplastic composites is presented. Finally, conventional analytical and experimental methodologies for the analysis of wrinkling in materials are examined and their shortcomings in predicting onset of compressive instability in composites are highlighted.

Wide spread application of woven thermoplastic composites necessitates developing cost-effective, rapid manufacturing techniques suitable for high volume industries. This requires access to effective failure and wrinkling criteria for composites under high strain rate conditions. Existing failure measures are originated from studying failure in thermoset fibre-reinforced composites and as such they cannot be effectively employed to predict failure in thermoplastic composites. Extensive literature survey shows that a trustworthy failure criterion capable of predicting failure in woven thermoplastic composites under complex loading conditions does not exist. WLC is the mostly applied wrinkling indicator conventionally used in metal forming industry. The fundamental difficulty with WLC is its dependency to geometry of the part and its sensitivity to initial imperfections. No study has been conducted to assess the efficiency of WLD on woven thermoplastic composites. Outcomes of this survey demonstrate the necessity to study failure in woven thermoplastic composites and develop appropriate models for predicting fracture and wrinkling in this class of composite materials.

Forming and failure of a consolidated self-reinforced polypropylene composite

A Forming Limit Curve (FLC) is a graphical representation of materials formability under different deformation modes. FLC was originally developed to predict failure in monolithic metals. Metals are considered to be homogenous and isotropic, while composites possess heterogeneous, anisotropic properties. Utilising a FLC based failure model diverges from conventional treatment of failure in composites; however, deformation behaviour and failure mechanisms in a SRPP composite diverges from two-phase composites and invalidates application of conventional failure models to this class of composites.

Property mismatch at the matrix and fibre interphase plays an important role in failure behaviour of two-phase composites. In a SRPP composite, both constituents are made from the same material system (e.g. polypropylene) with similar chemical and physical properties. SRPP falls under a class of polymers known as self-reinforced composite, single polymer composites, or homogenous composite. In two phase composites, low surface free energy and bonding imperfections cause fractures to initiate at the interphase of fibre and matrix. In contrast to two-phase composites, single phase composites possess perfect adhesion between fibre and matrix due to mutual diffusion between the two chemically identical components of the composite.

Further to these facts, the woven structure of SRPP reduces anisotropy as compared to unidirectional fibre reinforced composites. As such, failure behaviour of woven SRPP composite is different to two-phase fibre reinforced composites such as polymer composites reinforced with carbon or glass fibres (chapter 5). Considering these

fundamental dissimilarities, SRPP is treated as a homogenous material in the current study and the failure is predicted using an FLC based criteria which is justified by the similar constituents' property. Chapters 6 and 7 provide more evidence on the accuracy of the proposed model in predicting forming and failure of a woven self-reinforced composite material under high strain rate forming condition.

In the current chapter, stretch forming experiments have been conducted on a woven self-reinforced polypropylene composite to investigate its formability and develop a strain-based criterion for predicting failure under a wide range of deformation modes. A deformation mode is defined as the ratio of minor to major strain. Based on the value of strain ratio ($SR = \frac{\epsilon_{minor}}{\epsilon_{major}}$), five different deformation modes are identified: Biaxial stretch mode in $SR = +1$, plane strain mode in $SR = 0$, uniaxial deformation mode in $SR = -0.5$, shear deformation mode in $SR = -1$, and wrinkling mode in $SR \leq -2$. Specimens with different aspect ratios were stretch formed to induce failure under a specific deformation mode. Measured strains at the vicinity of failed region were employed to construct a failure envelope for the composite. Outcomes of these experiments showed that due to a uniform strain distribution, the woven SRPP composite could be formed into complex doubly-curved geometries. Outcome of this study was used to introduce a deformation-mode path dependant failure model for a woven thermoplastic composite.

In this study, a pre-consolidated woven self-reinforced polypropylene composite (SRPP or CURV®) were formed using a 300kN custom built press until catastrophic failure. Specimens with different width-to-length ratios were stretch formed in an open die configuration equipped with a built-in lock ring. The role of the lock ring was to fix the boundary of specimens so they can be stretched into the die cavity. Samples were fixed in the die system and formed by a hemispherical punch to failure as indicated by a 20% drop in the load measured by a load cell. The specific forming set-up forced samples to stretch along longitudinal direction and draw into the die cavity along the transverse direction.

Displacements were captured by a non-contact 3D photogrammetry system (ARAMIS) made of two CCD high speed cameras and strains were calculated using a built-in algorithm. Principal strains on the entire surface of samples were calculated and plotted in a two-dimensional strain space. Principal strains, strain ratio and their evolution were studied at different locations on the surface of specimens. Strain gradient along longitudinal and transverse directions were plotted and compared with the behaviour of a monolithic aluminium. The results of strain measurement indicated a uniform strain distribution on the composite in almost all stages of deformation and the absence of localised thickness thinning prior to failure.

It was shown that the combined effect of enforced boundary condition, and aspect ratio and fibre orientation of specimens resulted in failure of the composite under a wide range of deformation modes. Induced deformation modes ranged from biaxial stretch to shear deformation modes. In specimens with $[0^\circ, 90^\circ]$ fibre orientations, the failure under biaxial stretch mode was observed in the full circular sample, while the narrowest specimen failed under uniaxial extension mode.

Strain field analysis demonstrated that failure occurrence was triggered by exceeding a failure limit dictated by the principal strains and strain ratio. Localised strains caused by the friction between punch and specimens induced failure in SRPP at a specific location in the vicinity of contact region. The uniform distribution of the strain field facilitated forming of the composite to high depths. The results of this experiment confirmed the potential of SRPP to be formed in consolidated state.

Localised principal strains around failed regions were measured to specify failure envelope of the SRPP composite. The principal strains prior to failure were mapped into a two-dimensional strain space to construct a Forming Limit Curve (FLC). The FLC specified failure limits of the SRPP composite as a function of principal strains and strain ratio.

The procedure used to measure strains on the surface of specimens and construct a FLC for the composite includes the following steps:

1. Composite blanks were cut into specific geometries using water jet method,
2. Edge of specimens was deburred after cutting to prevent premature failure during forming,
3. Surface of samples was cleaned by an isopropanol solution and covered with a stochastic pattern of black dots on a white sprayed background,
4. Specimens were placed and fixed in an open die configuration using precise tightening torques,
5. A real time photogrammetry system was mounted beneath the die to capture deformations during forming while strains were calculated using continuum mechanics principals,
6. Samples were formed using a hemispherical punch until catastrophic failure,
7. Principal strains were calculated at the vicinity of cracked region to identify failure envelope at a specific deformation mode, AND
8. A FLC was constructed to differentiate between failed and safe regions of deformation captured by the ARAMIS.

The constructed FLC was used to develop an analytical expression for the failure in the woven SRPP composite. This FLC has the potential to be used in manufacture of SRPP components with complicated geometries. Proposed path-dependent failure envelope offers several advantages to conventional failure models of composites:

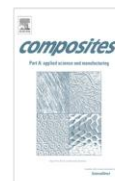
- The proposed failure model is capable of predicting failure in SRPP composite under different deformation modes ranging from biaxial stretch to uniaxial extension mode,
- Effect of residual thermal stress during manufacture of composites could be studied using path dependency of failure criteria,

- The effect of load path on failure of composite can be clearly elucidated,
- The failure limit curve has the potential to be implemented in a numerical simulation to predict failure in a woven SRPP composite under complex loading conditions.



Contents lists available at ScienceDirect

Composites: Part A

journal homepage: www.elsevier.com/locate/compositesa

Induced forming modes in a pre-consolidated woven polypropylene composite during stretch forming process at room temperature: I. Experimental studies



N.A. Zanjani*, A. Sexton, S. Kalyanasundaram

Research School of Engineering, ANU College of Engineering and Computer Science, Australian National University, 31 North Road, Canberra, ACT 0200, Australia

ARTICLE INFO

Article history:

Received 17 July 2014

Received in revised form 2 September 2014

Accepted 28 September 2014

Available online 13 October 2014

Keywords:

A. Fabrics/Textiles

A. Thermoplastic resin

B. Strength

E. Forming

ABSTRACT

In the current study, rectangular specimens of pre-consolidated woven Self-Reinforced Polypropylene (SRPP) possessing different fibre orientations and aspect ratios were stretch formed in an open die. Induced displacements were recorded by an in-situ 3D photogrammetric measurement system. Resultant principal strains were investigated to clarify the role of different deformation modes during stamp forming. The dependency of induced deformation modes to the specimens' geometries was studied. A novel path/deformation dependent failure criterion was established to distinguish between safe and failed regions of SRPP in a stamping process and to elucidate the dependency between failure and induced forming modes in a woven composite. The experimental results highlighted the suitability of consolidated SRPP to be formed into complex doubly curved geometries by the stamp forming process at room temperature. It was found that required forming depths could be achieved if a proper combination of specimen size, boundary condition, and fibre orientation was selected.

© 2014 Elsevier Ltd. All rights reserved.

1. Introduction

In last few decades, shortage of fossil fuel resources, global warming and air pollution have raised worldwide concerns toward excessive energy consumption and its inevitable environmental impacts. According to statistics published by IEA (International Energy Agency) in 2012 [1], the transport industry is responsible for 22% of the total CO₂ emissions worldwide. To address this issue, European Union set mandatory regulations on car manufacturers to reduce CO₂ emissions of automobiles produced after 2015 [2] or they will be penalised for excess emissions. Results of analyses conducted by IFEU (Institute of Energy and Environmental Research) [3] revealed that every 100 kg reduction in the mass of automobiles results in a decrease of 2.2 t in CO₂ emission and 300–800 litre savings in fuel consumption over the lifespan of a vehicle. This provides sufficient incentives for car manufacturers to reduce the weight of their products to reach mandatory targets.

Woven Self-Reinforced Polypropylene (SRPP) composite, manufactured from polypropylene both as the matrix and reinforcements, offers a wide range of superior properties over monolithic materials and conventional fibrous composites. Thermoplastic polymers offer recyclability characteristics due to ability to be

re-moulded and re-shaped after being initially consolidated. Polypropylene, as a typical thermoplastic polymer, offers low fabrications costs, environmental stability and ease of processing [4]. SRPP, constituted from highly drawn polypropylene fibres, benefits from a broad range of attractive properties including light weight, relatively high mechanical strength compared to plain polymers [5] and enhanced energy absorption characteristics. These properties make SRPP an attractive candidate to metals in applications where a combination of structural strength and reduced weight is necessitated. Woven SRPP possesses other attractive properties including higher modulus than polypropylene, internal integrity, balanced in-plane thermomechanical properties and enhanced resistance to crack propagation [6].

Currently, composites are manufactured via time-consuming, complex methods, such as hand lay-up and moulding techniques. High costs associated with these techniques and their incompatibility to current manufacturing procedures in major industries has hitherto restricted their applications to a few limited industries such as aerospace. Benefitting from composites in a broader range of applications is viable only if they are produced via a more effective technique capable of addressing high volume production rates. Stamp forming, as a rapid manufacturing technique, has been extensively applied and studied on prepreg woven composites [7–16]. The procedure includes forming of already impregnated woven fabrics into the desired geometry by a punch (draping)

* Corresponding author. Tel.: +61 (2)61258546.

E-mail address: nima.akhavan@anu.edu.au (N.A. Zanjani).

whilst sufficient pressure and temperature is applied. However, some issues can arise from excessive distortion and re-orientation of the material during forming due to the very low stiffness of the fabric. This can result in reduced mechanical properties of final products. Inefficiencies of current failure criteria in predicting safe deformation margins of a woven composite is another obstacle to be overcome if wide spread applicability of stamping on composites is desired.

To attain low manufacturing cycle times for components made of woven SRPP and to obtain cost-effective products, stamp forming of pre-consolidated composites seems propitious. Several studies have been previously conducted in this area [17–25]. The present study investigates the stretch forming behaviour of pre-consolidated sheets of woven SRPP at room temperature. The current research, inspired from sheet metal industry, aims at presenting a reliable measure to predict failure in woven composites during stamping procedure. This was accomplished by constructing a Forming Limit Curve (FLC), employed extensively in metal forming, based on induced strains in different specimens in the last stage of deformation. The novelty of this approach is demonstrated through predicting failure in composites by a combination of a history dependent failure criterion with induced deformation modes introduced by the ratio of two principal strains. This enabled us to establish an independent set of failure criterion for SRPP composite in particular regions of strain space each representing a different deformation mode. This methodology is analogous to employ an interactive failure criterion to predict failure in composites without imposing restrictions of a constant term on the right hand side of the equation.

This approach offers both simplicity of using an independent failure criterion and precision of considering strain history in the current mechanical state of the composite. Furthermore, the accuracy of predicting failure in a woven SRPP composite, during a typical forming exercise, increases considerably. This is due to the fact that the current failure criterion is established based on the outcomes of an extensive forming practice on the composite rather than simple uniaxial and biaxial characterization tests. Furthermore, outcomes of the current study highlighted substantial differences between stamp forming behaviour of metals and pre-consolidated woven SRPP at room temperature. The current study is the very first of its kind to investigate stretch forming of a pre-consolidated SRPP and to predict failure in a woven composite through an evolving Forming Limit Diagram (FLD).

2. Experimental procedures

2.1. Material

Specimens were made of balanced multilayered 2/2 twill weave SRPP having 0.9 g cm⁻³ volumetric density manufactured by Propex Fabrics GmbH (Germany) (Fig. 1). The material was produced via a hot compaction technique, originally developed at Leeds University. The fibre volume fraction of SRPP was 55% according to manufacturer's datasheet [26]. Some basic mechanical properties of SRPP composite are provided in Table 2.

2.2. Specimens geometry

The specimens were consisted of rectangular cut-outs from a 200 mm diameter circle. The width of the samples varied from 12.5 mm to 200 mm (Table 1). In Table 1, **Re** indicates Rectangular shape of the specimen, as opposed to the specimen possessing an hour-glass geometry commonly used in stretch forming of metallic samples. The number after **Re** indicates the sequence by which the specimen was used in stamp forming experiment and **W** indicates

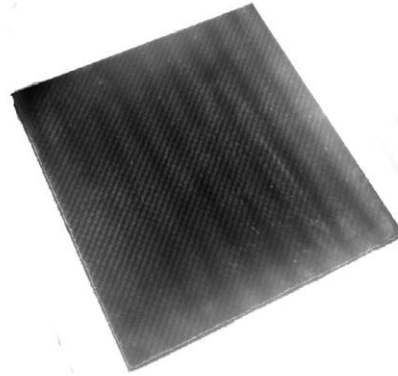


Fig. 1. A sheet of SRPP composite.

Table 1
Specimens employed in the study.

Sample	W (mm)	Sample	W (mm)
Re1W12.5	12.5	Re5W100	100
Re2W25	25	Re6W125	125
Re3W50	50	Re7W150	150
Re4W75	75	Re8W200	200

Table 2
Mechanical properties of SRPP composite.

Technical properties	Test method	Value	Unit
Density	ISO 1183	0.92	g/cm ³
Initial tensile modulus	DIN EN ISO 527	4200	N/mm ²
Tensile strength	DIN EN ISO 527	120	N/mm ²
Tensile strain to failure	DIN EN ISO 527	20	%
Flexural modulus	DIN EN ISO 178	3500	N/mm ²
Compression strength	EN ISO 604	300	Mpa
Tensile impact strength	EN ISO 8256	1000	kJ/m ²

the width of the specimen. Thickness of all samples was 1 mm. To elucidate different forming behaviour in stretch forming, each specimen was employed with two different fibre orientations. Specimens possessing [0°, 90°] fibre orientation were used to reveal forming behaviour ranging from uniaxial extension to biaxial stretch. To reveal intra-ply shear behaviour of SRPP, samples possessing [45°, 45°] fibre orientations were stretch formed. To investigate failure in SRPP, two concepts extensively employed in metal fabrication was applied: The Forming Limit Diagram and the Forming Limit Curve. The Forming Limit Diagram (FLD) is a graphical representation of strain state at different material points determined by induced minor and major strains. The FLD could be constructed at any single deformation stage and therefore it demonstrates an evolving behaviour due to the evolution of the material's strain state during a forming process. The FLD is used to investigate induced deformation modes in different regions of specimens and to evaluate the contribution of different strain states in a typical deformation practice. To determine safe and failed deformation margins of SRPP, a Forming Limit Curve (FLC) was employed. A FLC is a curve tangent to the FLD at the last stage of deformation and is obtained via forming specimens beyond their failure limits. This curve distinguishes between failed and safe deformation margins of a typical material during any forming practice.

Incorporated failure modes in a forming exercise are depicted by a strain ratio parameter (SR or β = minor strain/major strain). Each deformation mode is characterised by a constant value

depicting a different strain ratio: $\beta = 1$ for biaxial extension, $\beta = 0$ and $\beta = -0.5$ for plane strain and uniaxial extension respectively, $\beta = -1$ for shear deformation and $\beta = -2$ indicating initiation of wrinkling on the surface of specimens; henceforth described as the wrinkling mode. The wrinkling mode depicts initiation of out-of-plane deformations on the surface of specimens experiencing in-plane loadings due to onset of compressive instabilities in the material. Each deformation mode determines the ratio of contributed forming modes in a typical forming practice including stretch, draw and compression. Consolidation of data obtained from these two sets of experiments into a unified FLC results in determination of full-field failure threshold for a woven SRPP composite at room temperature.

2.3. Experimental equipment

In the current study, strains were measured by an in-situ non-contact measurement system (ARAMIS). The ARAMIS is composed of two high speed, high resolution CCD cameras capable of capturing images during deformation of a specimen. This facilitated tracking of strain evolutions through every single stage of deformation process by comparing current positions of surface points to their undeformed or initial positions. This process was automatically done by the ARAMIS system through an automated point tracking system or a 3D mapping procedure [27]. Stretch forming experiments were captured by the ARAMIS with the rate of 20 fps (frames-per-second). Analysis of results started with

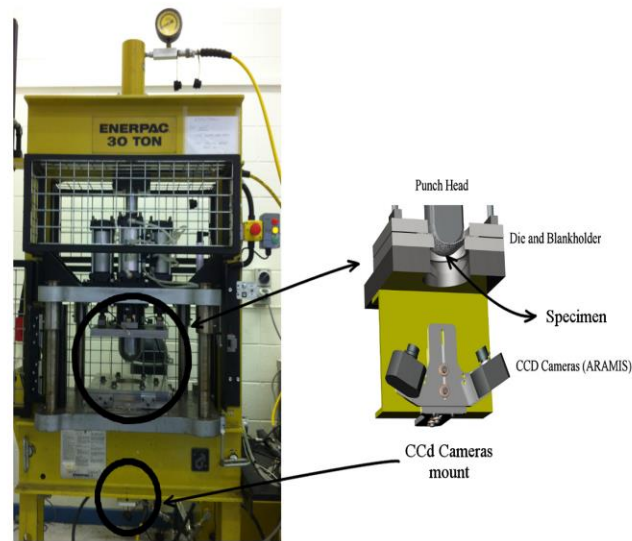


Fig. 2. Stamp forming equipment and measurement system set-up. (For interpretation of the references to colour in this figure legend, the reader is referred to the web version of this article.)

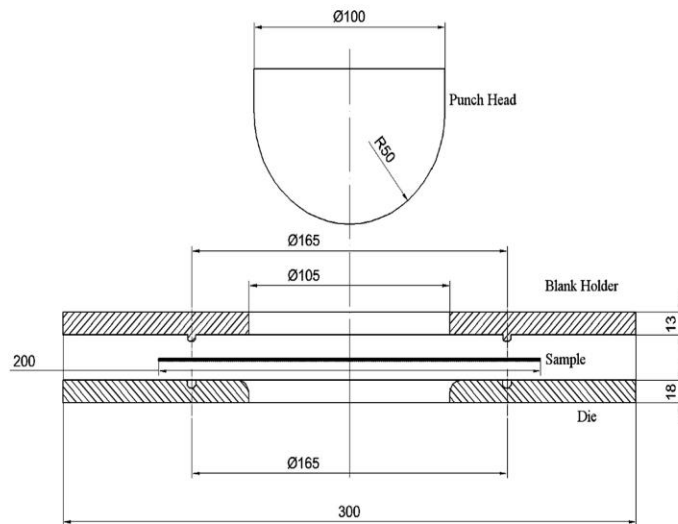


Fig. 3. Dimensions of stamping equipment and fixtures.

decomposition of images into various virtual squares and rectangles (facets). Computation of displacements was done by comparing initial and final positions of every single facet, followed by the calculation of induced strains using the deformation kinematics. The procedure of calculating strains was automatically done via the built-in algorithm implemented in the ARAMIS by the manufacturer. Forming of samples was accomplished via a custom-built press with a 300 kN load capacity. The press consisted of a 100 mm in-diameter hemispherical punch and an open die, enabling ARAMIS to be located at the bottom of the press and to capture induced strains during all stages of the deformation. The feed rate of the punch was set to 10 mm/s. This resulted in capturing two images of the deformed specimen for each millimetre of downward penetration of the punch (along z axis depicting normal direction to the surface of undeformed specimens). The ARAMIS was mounted beneath the open die via a T-joint adaptor facing toward the painted surface of the specimen (Fig. 2). Dimensions and configuration of the fixture used to clamp the specimen and to impose fixed boundary condition are represented in Fig. 3.

3. Results and discussions

All specimens were deformed up to failure indicated by a 20% drop in the load measured by the load cell. Evolution of principal strains along the 0° and 45° axes were investigated in a strain space to reveal the role of different deformation modes on the forming behaviour of SRPP. The effect of specimens' geometry on induced principal strains was investigated. The deformation modes and their evolutions were studied via a strain ratio parameter (β). Room temperature FLC was constructed and fundamental differences between the forming behaviour of SRPP and AL 5005-O, as a typical metallic alloy, were discussed. Finally, a novel strain-based failure criterion for composites based on induced deformation modes in SRPP was introduced. The originality of this criterion is evident in determination of a failure for a composite by both induced strains and strain ratio as an indicator of induced deformation modes. The significance of adopting the current approach to predict failure is demonstrated through its path-dependent, deformation-mode sensitive behaviour. Stamp forming is a complicated process that incorporates a variety of simultaneous forming modes into a single process to conform the initial blank to the final complex geometry. The analysis of a stamp forming practice becomes more intricate if an inherently heterogeneous material such as a woven composite is employed. This approach offers a straightforward, unambiguous failure criterion applicable to stamping process of a woven SRPP by eliminating the need to tackle with the complicated microstructural behaviour of this class of material. Furthermore, incorporating the proposed criterion in a numerical simulation would result in a direct and cost-effective analysis suitable for most forming processes.

3.1. Evolution of the FLD in various samples

Fig. 4(a–c) represents the evolution of Forming Limit Diagram (FLD) for three typical samples of SRPP having $[0^\circ, 90^\circ]$ orientations at various stages of deformation. In these figures, Z direction is considered as the normal direction to the plane of specimens prior to the deformation. Therefore, Z parameter represents downward displacement of the punch measured from the initial contact point between the punch and the specimen. Although all specimens were fixed in a similar fixture, due to possessing different aspect ratios, the clamped circumferential length and therefore imposed boundary conditions were different from sample to sample. These specimens characterized three important modes of deformation associated with every complex forming exercise including uniaxial extension (4-a), plane strain (4-b), and biaxial stretch (4-c). Collaboration of a wide variety of different forming modes in stamping of composites and the complex interaction between interlacing yarns obscure any clear judgement on failure behaviour of composites based on the existing failure criteria. Therefore, it is of vital importance to comprehend the contribution and evolution of these forming modes during stamping of pre-consolidated composite samples possessing different aspect ratios. Evolution of FLD is depicted from 5 mm downward punch penetration to the maximum punch displacement prior to failure of the specimen, at 10 mm intervals (Depicted by different Z values). Rigorous investigation of these figures reveals fundamental differences between evolutions of FLD in these specimens:

- Induced deformation mode on the surface of the sample is dependent on the specimen's aspect ratio and imposed boundary conditions. The narrowest sample experienced uniaxial extension in all stages of deformation, whereas in Re5W100 deformation modes spread among uniaxial extension and biaxial stretch modes, demonstrating plane strain in some specific areas. Induced deformation modes in the widest sample were located mainly in first quarter of strain space, bounded between plane strain and biaxial stretch.
- In the narrower specimens (4-a and 4-b), the evolution of FLD exhibits more proportionality to the depth of deformation than other specimens. In other words, the depth of deformation and the shape of FLD have a one-to-one dependency. This implies that if FLD of narrow specimens is known at any two stages of deformation, its evolution at any forming depth can be predicted by a linear intra/extrapolation technique. The error induced by the interpolation technique increases as the width of specimens extends.
- In the widest specimen (4-c), an increase in the depth of deformation (or Z) results in a disproportional extension in FLD envelope. This includes an unbalanced shift of FLD along both positive and negative directions. This behaviour caused by an alternating combination of drawing and stretching at different

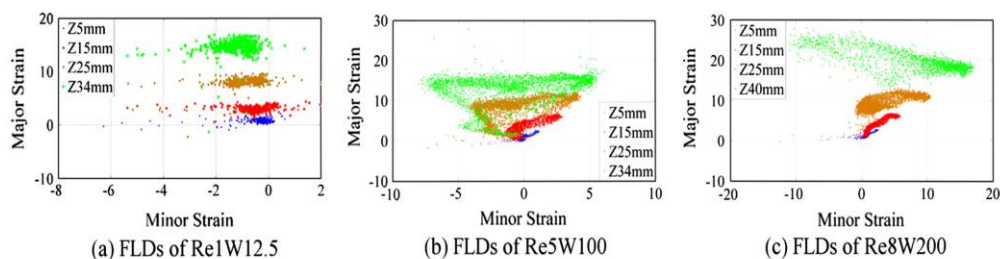


Fig. 4. Evolution of principal strains on the surface of different SRPP specimens. (For interpretation of the references to colour in this figure legend, the reader is referred to the web version of this article.)

stages of deformation is dependent on a variety of parameters including microstructure of the woven SRPP and imposed boundary conditions.

- Extents of the FLD envelope are influenced by the specimen's aspect ratio and applied boundary conditions. However, induced minor strain is more influenced by these parameters than major strain. For instance, minor strain extents in Re5w100 and Re8w200 are 75% and 262% larger than of Re1W12.5 specimen. This also indicates the contribution of a broader range of deformation modes in forming of larger specimens.
- Formability of SRPP is impacted by the combination of deformable material and applied boundary conditions determining induced deformation modes. Therefore, an appropriate selection of initial geometry and applied boundary conditions results in a satisfactory forming practice while prohibiting failure initiation and propagation due to the balance between stretching and drawing. Considering the woven structure of the SRPP, the failure is definitely affected by governing deformation modes induced in specimens. This emphasizes on the necessity of determination of failure in pre-consolidated woven SRPP based on induced deformation modes which is the focus of the current study.

3.2. Deformations and incorporated failure modes in stamp forming

Fig. 5a–e illustrates the evolution of induced deformation modes in aforementioned samples along their meridians and 45°

sections as depicted in Fig. 6. The parameter β (strain ratio or SR) indicates the ratio of minor to major strains at any given stage of deformation. The evolution of strain ratio is visualized in three subsequent stages of forming specified by the punch penetration: 10 mm, 20 mm, and the last stage of deformation. It is noteworthy to mention that the visible length of meridian section to the ARAMIS is less than the actual length of the specimen or 200 mm. This is due to the fact that a considerable proportion of

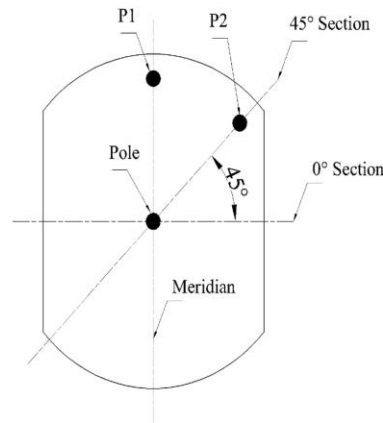


Fig. 6. Position of meridian and 45° sections on the specimens.

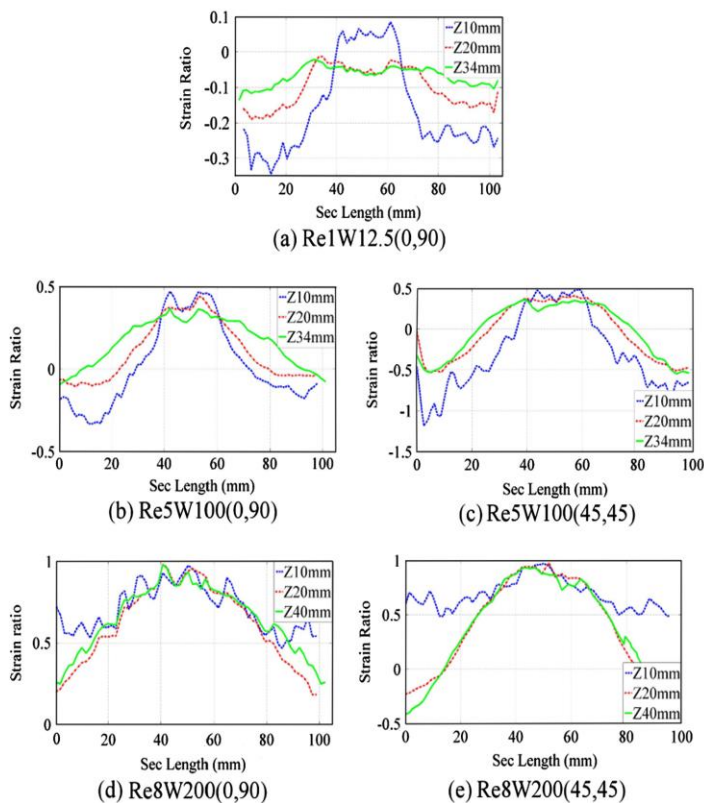


Fig. 5. Evolution of principal strains along meridians of different SRPP specimens. (For interpretation of the references to colour in this figure legend, the reader is referred to the web version of this article.)

specimen length was covered between the die and the blank holder (Fig. 3). This explains why the meridian length in these figures is equal to 100 mm rather than 200 mm which is the actual length of specimens.

During early deformation stages of Re1W12.5, the middle section of the specimen experiences a close to plane strain deformation mode and points near fixed edges roughly experience uniaxial extension. The transition between these two deformation modes occurs too expeditiously, resulting in a sharp localised gradient. This rapid change in behaviour results from the contact (friction) condition between the specimen and the punch in the middle of samples. Friction and imposed boundary conditions at edges of the specimen suppress transverse strains normally caused by Poisson's effect. An increase in forming depth causes the strain ratio to evolve more homogeneously, resulting in a monotonic behaviour and smooth distribution of deformation modes.

In Re5W150, the difference between minimum and maximum strain ratios is more pronounced, and does not stabilise fully even at the last stage of deformation (Fig. 5b and c). This behaviour is caused by the friction condition and a different aspect ratio of the sample. However, the sharp gradient in meridian strain disappears as a result of increase in contact surface between punch and the sample. Generally, the difference between minimum and maximum strain ratios is more evident in a 45° section than in a 0° direction due to the contribution of a different deformation mechanism (Trellising) during forming.

Induced deformation modes in Re8W200 follow an opposite trend. It initially shows a more homogenous pattern of deformation modes and then demonstrates pronounced inconsistencies in different locations at the last stages of deformation (Fig. 5d and e). This is caused by different imposed boundary conditions that do not allow trellising to contribute in formability of this specimen. It should be emphasized although all samples were clamped in the lock-ring, due to variations in their widths, the length of the fixed circumference and therefore imposed boundary condition were different among specimens. In general, the aspect ratio of the specimen was the determinant factor on the length of the fixed circumference and the free edge and therefore changed the imposed boundary condition on specimens. Conclusively, the contact surface, friction and actual boundary conditions are three influential parameters on induced forming modes in a SRPP specimen, although their effect on the forming modes could not be judged easily. This demonstrates the complex and non-linear dependency of induced deformation modes in the SRPP on effective forming parameters including contact.

Substantial differences among forming behaviour of these samples can be summarized as follows.

In wider samples, the gradient of β changes gradually during initial stages of deformation, while it varies more drastically in last stages of deformation. These could be justified by an increase in the contact surface between the specimen and the punch, more even distribution of traction forces and the amount of free material to flow. In the narrower sample the trend is reversed. Variations in the induced deformation modes in Re1W12.5 during last stages of deformation become less severe as a result of a decrease in length of the clamped perimeter and the small amount of material to deform into the die cavity. These behaviours highlight the impact of a hemispherical punch on forming behaviour of SRPP. The hemispherical punch affects a very small central region of samples at early stages of deformation, while the contact surface between punch and the blank gradually increases as forming depth grows (Nakazima effect).

Forming characteristic of SRPP specimens along meridian and 45° axes is completely different to its behaviour along a 90° axis, both in terms of induced deformation modes and variation of β along the section length. This is due to the effect of shear

deformation mode and its dominance along 45° section. This mode of deformation extends limits of β , as the principal forming mode changes from fibre extension and interplay shear to trellising or intra-ply shear in a woven composite.

It is noticeable that as the forming depth of the samples increases, the fluctuation of β (or its spiky behaviour) along 45° section decreases. This could be explained by undulation of fibres during the initial stages of deformation and the influence of fibre extension on shear deformation in the last stages of deformation. Another reason for such forming behaviour could be the dominance of static friction in initial stages of deformation and its evolution to dynamic friction after yarn slippage is initiated. Increase in forming depth produces an even distribution of normal pressure on contact surfaces, leading to a steady state in friction condition. These observations illustrate the complex forming behaviour of SRPP composite due to intricate micro and meso level interactions in a woven composite.

The strain ratio evolution with forming depth is graphically illustrated across the surface of specimens in Fig. 7(a–c). In the pre-stretch stage, which is indicated by fixing specimens between the die and the fixture, the strain state in Re1W12.5 and Re5W100 are mainly consisted of uniaxial extension mode, while bi-axial extension is the dominant forming mode in Re8W200. The initial stochastic distribution of strain ratio is caused by an uncontrolled pre-stretch state imposed by the lock ring (lock-ring effect). The mode of deformation becomes more coherent toward the final stage of deformation for all samples as the lock-ring effect is counteracted by the strain state induced by the punch. Induced deformations in Re1W12.5 finally approaches toward uniaxial extension mode ($-0.1 \leq \beta \leq -0.3$). In Re5W100, biaxial extension mode is induced in the central elliptical region, shifting to plane strain mode in a rhomboid-shaped region across the side walls. In Re8W200, the central rhomboid-shaped region experiences bi-axial strain mode, shifting to plane strain mode in outer regions. The deformation mode along 45° axis and near clamped edges develops into plane strain. The noticeable difference between forming behaviour of Re5W100 and Re8W200 samples near 45° boundaries, is caused by the free rotation between interlacing fibres in the former while in the latter, the imposed fixed boundary conditions prohibits free rotation of interlacing fibres around their crossover joints.

In Fig. 8, evolution of strain ratio is demonstrated at following locations: Pole, P1, and P2 (Fig. 6). These points could not only be differentiated by their position, but by how warp and weft yarns are interacting with each other. After early stages of forming, the strain ratio of poles tends to follow a constant value. However, this constant value varies between samples: strain ratios of -0.1 , $+0.3$, and $+1$ are indicated for Re1W12.5, Re5W100, and Re8W200 samples, respectively. In Re1W12.5 and Re5W100 specimens, the strain ratio at P1 and P2 increases gradually and does not become steady even in the last stages of deformation. In all three samples, the strain ratio changes gradually at the pole while this ratio for P1 and P2 fluctuates rapidly. This could be explained by the combined effect of strain concentration at the fixed edges and simultaneous undulation of the interlacing yarns.

These behaviours clearly indicate that the forming behaviour of pre-consolidated woven SRPP is completely different to metals which maintain a constant strain ratio through all stages of the deformation [28]. These observations illustrate the complicated forming behaviour of woven composites and its dependency to forming parameters including contact and boundary conditions, forming depth and fibre orientation that is specified by the woven structure of the composite. These observations highlight the importance of seeking a novel failure criterion for woven composites as their forming and failure behaviours changes dramatically with variations of deformation mode, while offering

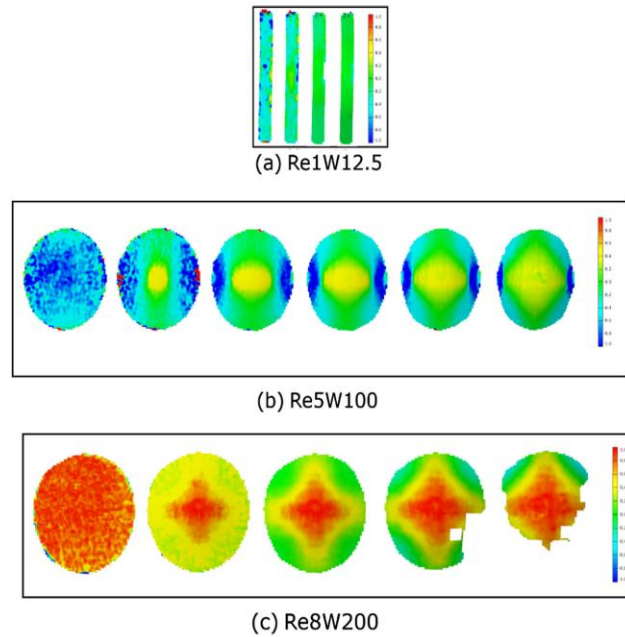


Fig. 7. Evolution of strain ratios on the surface of different specimens (progressing from left to right). (For interpretation of the references to colour in this figure legend, the reader is referred to the web version of this article.)

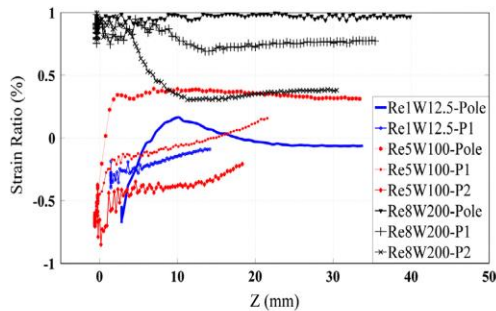


Fig. 8. Strain ratio evolution of different points of interests. (For interpretation of the references to colour in this figure legend, the reader is referred to the web version of this article.)

a non-consistent strain history at different locations during stretch forming practice. Furthermore, constantly evolving strain ratio at each material point necessitates considering the strain ratio parameter as a major factor in developing a suitable failure criterion to predict failure in SRPP during stamping process.

Incorporated failure modes in SRPP samples can be observed from different perspectives (macroscopic or microscopic), while each provides a different insight into failure of SRPP during stamp forming. Microscopic failure modes in Re2W25 and Re6W125, as two typical specimens, are represented in Figs. 9 and 10, respectively. Fig. 9a and b depict localised failures due to compressive stress states within the sample. Fig. 9a shows fibre kinking and yarn rupture while Fig. 9b reveals buckling of the yarns at the edge of the specimen. Fig. 9c and d represents longitudinal cracks and yarn splits due to tensile stresses during stamp forming. Curvilinear shapes of yarns after failure indicate plastic deformation in Re2W25 specimen. Fig. 10 represents different incidences of failure

in Re6W125 specimen, including fibre kinking due to localised compression, Mode II fracture due to in-plane shear (observed via hackles in the specimen), out-of-plane buckling indicated by two adjacent bright and dark surfaces, in addition to longitudinal and transverse cracks. The microscopic failure modes cover a wide range of failure morphologies resulted from in-plane tractions and bending moments.

However, macroscopic observations more clearly elucidate the effect of woven reinforcement and specimen's aspect ratio in morphologies of failure in a woven pre-consolidated SRPP composite. Fig. 11(a–d) represents different failure mechanisms associated with stretch forming of specimens with different aspect ratios. Fig. 11a depicts associated failure modes in Re2W25. The failure surface makes a completely transverse plane to the major strain direction (along weft yarns), indicating yarn rupture. The jagged failure surface shows yarn pull-out which is re-emphasized by the longitudinal fibre pull-out on the surface of the right part (11-a). Delamination is also observed in this figure at the edge of the specimen. Fig. 11b shows ruptured surface of Re4W75. The main failure mechanisms are yarn rupture and fibre pull-out. However, the failure surface is not normal to the major strain direction and is guided along a 45° transverse direction in the middle of the sample. The inclined failure path indicates the support of orthogonal fibres in load bearing capacity of the composite which results in the transfer of load between warp and weft fibres. This phenomenon (bridging effect) delays failure in stretch forming of woven pre-consolidated SRPP specimens possessing specific aspect ratio.

Fig. 11c shows a more pronounced bridging effect in Re7W150 as the propagated crack did not extend completely through the width of the specimen and has been stopped by transverse yarns. The incorporated failure modes are yarn rupture and matrix shearing at the interface of yarns. Fig. 11d depicts a completely different failure phenomenon in Re8W200. The failure surface is constructed from two orthogonally intersecting individual paths in the middle of the specimen making a 45° angle with the yarn direction. It

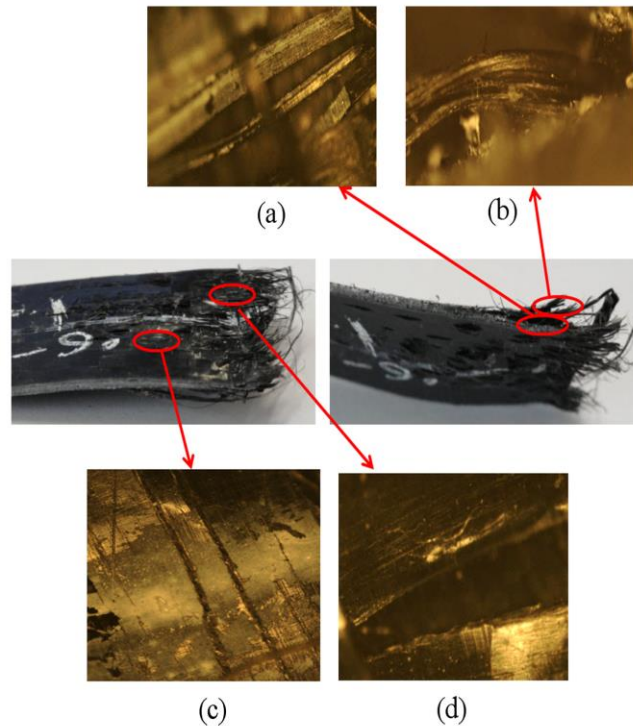


Fig. 9. Microscopic examination on stampformed Re2W25 SRPP specimen (X10). (For interpretation of the references to colour in this figure legend, the reader is referred to the web version of this article.)

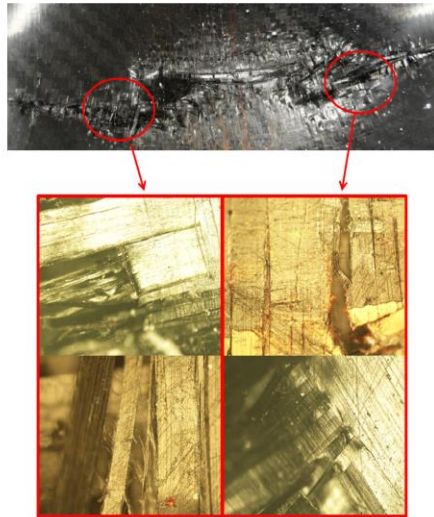


Fig. 10. Microscopic examination on stampformed Re6W125 SRPP specimen (X10). (For interpretation of the references to colour in this figure legend, the reader is referred to the web version of this article.)

shows shear failure and breakage of the yarns. The specific failure behaviour of Re8W200 SRPP composite was resulted from the imposed boundary condition. The full perimeter of Re8W200 was locked in the lock-ring. This prohibited fibres drawing excessively during stamp forming. However, other specimens were able to draw and stretch simultaneously to form into the desired geometry. Besides, some yarns were allowed to trellis during

forming depending on the imposed boundary conditions, while in Re8W200 the only contributing forming mechanism was stretching of warp and weft yarns. Therefore, based on macroscopic failure observations during stretch forming of different specimens, it can be concluded that incorporated failure mechanisms and the geometry of the failure surface is strongly influenced by the induced forming modes. Therefore, incorporated failure mechanism is strongly affected by the specimen's aspect ratio and boundary conditions.

3.3. Major strain evolution

The evolution of major strains along meridian of three typical samples is shown in Fig. 12(a–c). The meridian major strains are depicted at different stages of deformation until failure. The fluctuations are caused by specific twill pattern of SRPP, and the image capturing process employed by ARAMIS. The ARAMIS utilises square meshed facets to measure and calculate strains in different regions of specimens. These facets coincide with warp and weft yarns alternatively, reporting different local major and minor strains due to different local behaviour of warp and weft yarns. These figures indicate highly heterogeneous nature of woven composites, making it extremely difficult to predict their forming and failure behaviours. This explains inefficiency and inapplicability of current failure criteria on woven composites and the necessity to adopt a more appropriate measure to predict failure in this class of material during forming. This also highlights limitations of an optical measurement system in measuring strains in a woven composite and the necessity to follow a rational evaluation procedure during interpretation of such a visually captured data.

Critical observation on major strain evolution of SRPP composite reveals their significantly different behaviour to metals. These differences could be summarized as follows:

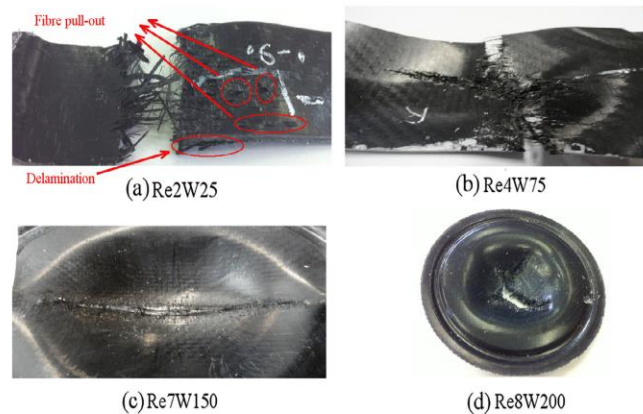


Fig. 11. Failure morphologies in different SRPP specimens after stamp forming. (For interpretation of the references to colour in this figure legend, the reader is referred to the web version of this article.)

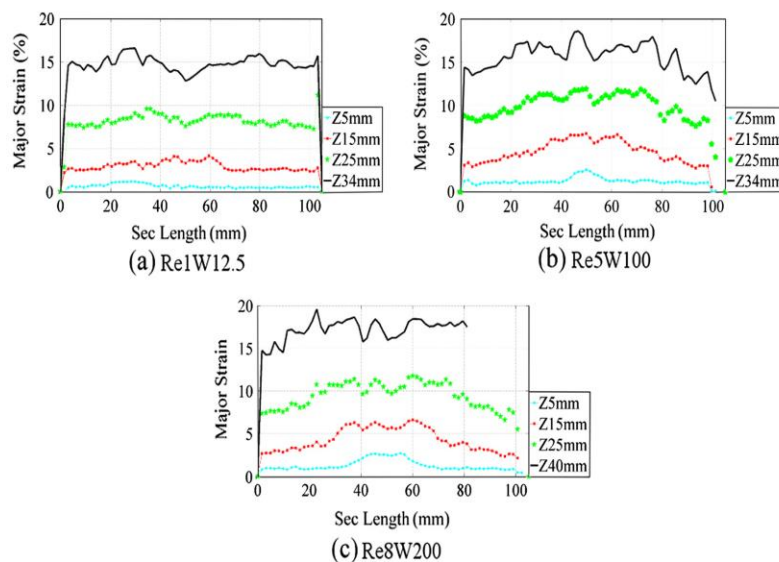


Fig. 12. Meridian strain evolution in different SRPP specimens. (For interpretation of the references to colour in this figure legend, the reader is referred to the web version of this article.)

- Localised necking phenomenon was not observed in major strain evolution of SRPP along their meridian section. This is clearly demonstrated by the absence of any sharp peaks or spiky behaviour in Fig. 12(a–c). In fact, meridian major strain evolution in these specimens represents a uniform behaviour. In the absence of necking, all surface strains increase simultaneously all over the specimen. This process results in greater strain energy stored in the specimen during forming and therefore enhances its energy absorption capability. This specific behaviour results in improved formability of a woven composite, if a proper combination of forming parameters are selected.
- The necking phenomenon in metals is specified by localised strain concentration along their meridians at the last stages of deformation, as observed in Fig. 13. The sharp peaks in meridian strain evolution indicate the occurrence of localised thinning in metallic specimen due to existing imperfections.
- Visual observations of failed SRPP specimens confirmed fundamentally different behaviour of woven composites to metals, as

the thickness thinning was not observed across the failed region in SRPP.

- Heterogeneous mechanical characteristic of SRPP enforced rapid, drastic change of local values of major strain along a typical section. This spiky behaviour was dictated by the complex microstructure of woven composite and intricate intra-layer frictional interactions between embedded yarns.

The contribution of in-plane strains, including normal and shear strains, in the evolution of meridian major strain of SRPP specimens is elucidated in Fig. 14. These in-plane components of strain tensor are depicted at the last stage of deformation. It should be mentioned that y and x directions specify in-plane longitudinal and transverse axes, located along length and width of specimens, respectively. Therefore, due to specimens' fibre orientation, imposed boundary condition, induced tractions and kinematics of stretch forming, the major and minor strains correspond to ϵ_y and ϵ_x axes, respectively.

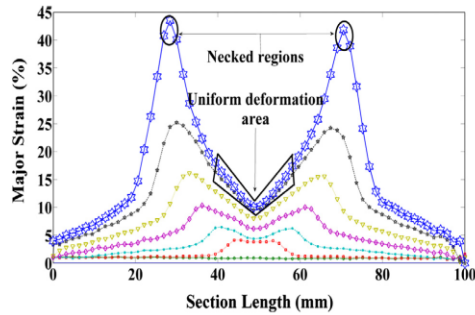


Fig. 13. Evolution of meridian strain in metals. (For interpretation of the references to colour in this figure legend, the reader is referred to the web version of this article.)

Friction between punch and Re1W12.5 suppresses evolution of minor strain along x axis due to Poisson's effect, thus it merely experiences draw in this direction and induced strain would be zero ($\epsilon_x \approx 0$). Re5W100 specimen possesses larger contact surface with the equal amount of friction causing slightly higher minor strain along x direction. Large non-contact surface area of Re8W200 increases meridian minor strains compared to the other specimens. The contribution of shear strain (ϵ_{xy}) is zero due to orientation of fibres and stress state in specimens. Perimeter of Re8W200 is fully clamped in the lock ring, therefore punch penetration into the specimen results in an equal amount of stretch in both x and y directions at the pole ($\epsilon_y \approx \epsilon_x$). The contribution of the real contact surface between punch and specimens and therefore friction effect in evolution of ϵ_y and ϵ_x is clearly highlighted in these figures.

3.4. Construction of Forming Limit Curve (FLC)

A FLC is constructed from induced principal strains near ruptured area at the last stage of deformation. Determination of FLC in metals is straight forward as they experience necking or localised strain concentration in the ruptured area. Following ISO

12004-2 standard, strain states in these locations are determined and then a smooth curve is passed through limiting strains to construct the materials' FLC. However, as mentioned previously, SRPP does not exhibit necking prior to rupture. Therefore, an alternative procedure was sought to construct FLC for this class of material. First, several axis parallel to the length of the specimens were constructed and maximum strains and corresponding deformation modes were determined via the ARAMIS results. These deformation modes were dependent to the specimens' aspect ratios. Then, failure points were specified in strain space and connected via a smooth curve. The resultant curve, distinguishing between failed and safe deformation margins in strain space, is called the FLC of SRPP. Specific behaviour of a woven composite necessitates considering both strain ratio and forming path simultaneously when specifying failure in SRPP via a FLC. This specific behaviour of woven composites and its significance in determination of a safe forming practice for composites is clearly elucidated by the outcomes the current research.

The resultant FLC of SRPP composite is constructed and depicted in Fig. 15. In this figure, the bold curve indicates FLC of SRPP, constructed by previously mentioned procedure. Dashed lines specify prominent paths of deformation intersecting with the FLC at different locations. It is obvious that failure in SRPP could be predicted by a horizontal line specified between biaxial to uniaxial extension modes. This is in complete agreement with maximum strain failure criterion. Data extracted previously from uniaxial extension experiments on rectangular SRPP samples shows that SRPP specimens fail at major strains ranging from 16% to 20% due to variation in mechanical properties. This behaviour is re-validated by the constructed FLC. However, in the region between uniaxial extension and shear mode, the failure limit strain changes drastically. The failure in shear deformation indicates an increase equal to 135% compared to failure in uniaxial extension. This designates a fundamental change in forming mechanism of SRPP in shear deformation at a microstructural level (trellising effect). This also elucidates the effect of fibre orientation on deformation of SRPP and explains how higher forming depth could be achieved by a change in active deformation mechanism.

In Fig. 15, an FLC of Aluminium 5005 is also represented to facilitate comparing forming limits of the self-reinforced

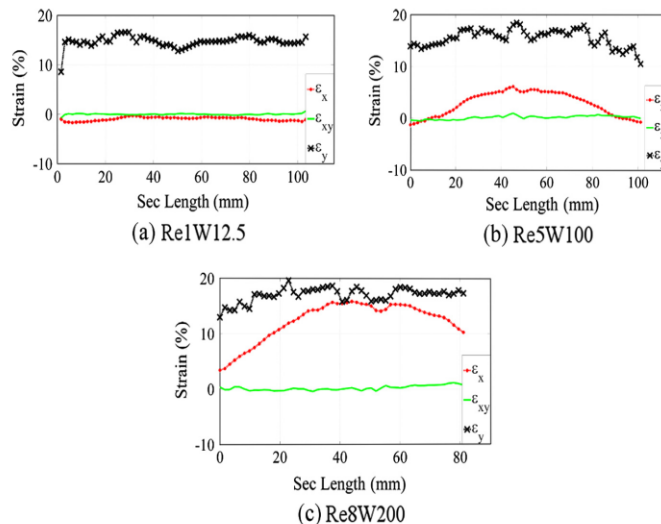


Fig. 14. Normal and shear strains along meridian of different SRPP specimens prior to rupture. (For interpretation of the references to colour in this figure legend, the reader is referred to the web version of this article.)

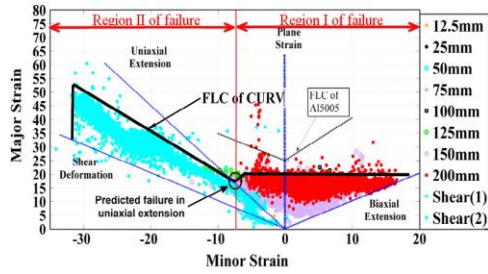


Fig. 15. FLC of SRPP. (For interpretation of the references to colour in this figure legend, the reader is referred to the web version of this article.)

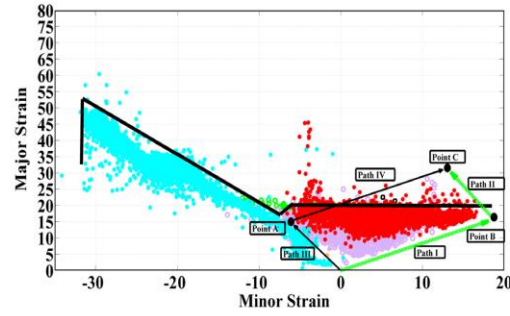


Fig. 16. Path/history dependency of the constructed FLC for SRPP composite. (For interpretation of the references to colour in this figure legend, the reader is referred to the web version of this article.)

polypropylene and a common metallic alloy used in the industry. Although the forming limit of the Aluminium is slightly higher than of SRPP, the extents of resultant FLC for the latter is much greater than of the former. This implies the contribution of considerably more deformation modes in formability of SRPP compared to the Aluminium. Besides, in shear region, deformation envelope of SRPP is greatly enlarged. These results promise potential applications for a woven SRPP composite in primary and secondary structures if a proper deformation mechanism (trellising) is enforced. Applying a proper deformation mechanism greatly increases uniformly-distributed strains in SRPP specimens, as observed in experimental results [29].

The resultant FLC could be employed to predict failure of SRPP during any forming process. Initially, the strain space is divided into different sub-regions, each bounded between two specific minor strains. Then, limits of fracture criterion can be determined by the combination of induced minor strain and strain ratio (deformation mode). For example, the resultant strain space for the given SRPP composite was divided into two separate regions: Region (I) indicated by minor strain greater than -8% and region (II) depicted by minor strains less than -8% (Fig. 15). Then, the maximum permissible major strain, prior the fracture of the composite, could be extracted from the FLC. The analytical expressions for the proposed failure criterion, based on experimental outcomes on SRPP, are as follows:

$$\begin{cases} \epsilon_{Minor} \geq -8\% \\ -0.5 < d(SR) \leq +1 \end{cases} \Rightarrow (\epsilon_{Major})_{failure} \geq 18\% \quad (I)$$

$$\begin{cases} \epsilon_{Minor} < -8\% \\ -2 < d(SR) \leq -0.5 \end{cases} \Rightarrow (\epsilon_{Major})_{failure} \geq \alpha \cdot (\epsilon_{Minor}) + \beta \quad (II)$$

In these equations, $d(SR)$ depicts instantaneous strain ratio and shows the path-dependency of the proposed failure criterion. If the current strain state of a point and its deformation history satisfies one of these limits, then the failure could be predicted by the relevant major strain. Equation (I) states that if minor strain at a material point is larger than -8% and induced deformation mode is located between biaxial-stretch to uniaxial extension modes, then the failure in the SRPP composite initiates when the major strain becomes greater than 18% . The equation (II) indicates that if minor strain is less than -8% and induced deformation mode is between shear and wrinkling, then failure in the composite initiates when induced major strains satisfy the given linear equation. Parameters α and β are determined experimentally. Base on the experimental outcomes, these values have been obtained as: $\alpha = -1.5$ and $\beta = 0.05$. If the strain path during a forming practice does not satisfy either of these equations, the composite does not fail. The path dependency of the proposed failure criterion is explained more clearly in Fig. 16 [30]. Consider the deformation path indicated by Path I and Path II by which a point located initially at the origin goes through point B to get to point C. Point C

satisfies boundaries of region (I) and therefore failure criterion (I) should be employed for the occurrence of failure. However, the instantaneous strain ratio prior to point C, depicted by gradient of path II, does not satisfy limits indicated by criterion (I). Therefore, the point C does not exhibit failure although the induced major strain is already greater than 18% . However, if Point C follows Path III and IV (travels through point A), it fails as both deformation path and instantaneous strain state satisfies failure criterion and the final major strain is greater than the major strain calculated by equation (I).

This reveals a significant contribution achieved by the outcomes of the current research: constructing a FLC for a woven composite is determinant in achieving flawless products as it clearly illustrates the safe deformation paths in shaping them into complex geometries. Experimental outcomes suggest that to form a SRPP into a desired geometry, the forming processes should be modified to encourage contribution of other effective forming mechanisms, such as trellising. This provides a suitable, effective tool for design and manufacturing engineers to modify their tooling to achieve successful products by improving material formability and hampering failure mechanisms in woven composites.

Employing an FLC in determination of failure in composites offers numerous advantages over conventional failure models, including:

- All deformation paths, ranging from biaxial stretch to shear modes, have a specific intersection with FLC. Therefore, the failure limits for each deformation mode is uniquely determined.
- Constructed failure criteria is both path and deformation mode dependent. Therefore, the effect of each deformation mode on the failure limits of the composites could be clearly and separately evaluated. Furthermore, the effect of fabrication induced stresses on the current state of the composite and its safe failure threshold could be evaluated directly.
- This failure criterion could be easily implemented in a numerical simulation to predict failure in any SRPP composite when subjected to specific forming conditions. This reduces the required time to complete the cumbersome die try out and therefore decreases manufacturing associated prices significantly in producing flawless products.

A comparison between FLCs of SRPP and Al5005-O reveals fundamental difference between forming behaviour of SRPP and metals. The room temperature FLC of Al5005-O is represented individually in Fig. 17. The minimum failure limit for Al samples is located in plane strain region, while the minimum major strain for SRPP samples lies in uniaxial region. These behaviours, resulted from different microstructures, elucidate clearly the influence of

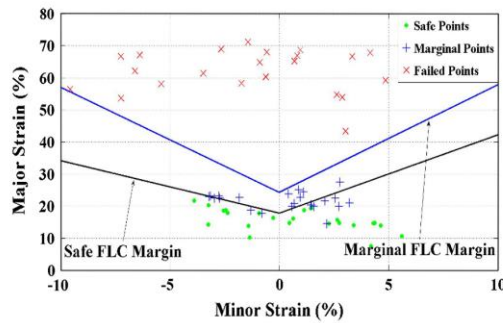


Fig. 17. FLCs of Al5005-O. (For interpretation of the references to colour in this figure legend, the reader is referred to the web version of this article.)

micro-level structure on macro-level forming behaviour in two materials. In former, the dislocations of crystalline structure is the driving force shaping sheets into desired geometries, while in the latter, interactions between interlacing yarns acts as the forming mechanism. These interactions include friction, slippage, trellising and shear. To predict forming and failure behaviours of woven composites in industrial applications, it is reasonable to apply a simple, yet rational method to facilitate manufacturing of complex components. This justifies application of current approach to predict failure in this class of materials by implementing a FLC. Adopting the current methodology results in flawless products without incurring high costs associated with complex computer simulations.

Further investigations reveal other fundamental differences between FLC of these two materials:

Maximum limits of induced major strain in Al and SRPP specimens in the first (positive) quarter of strain space is equal. However, the induced minor strain threshold is much larger in SRPP than Al specimens for the same deformation mode. In the second quarter of strain space, both major and minor strains induced in SRPP specimens increase significantly compared to Al specimens. Once more this indicates the dominance of a different microstructural forming mechanism in SRPP (trellising) compared to metals (crystalline dislocation). It was not feasible to induced 100% biaxial deformation in Al samples, as a result of friction between specimens and the punch. Therefore, data extrapolation was employed to predict failure limits of Aluminium in this region. A more conservative procedure was followed to predict failure of SRPP specimens in this region based on curve fitting on acquired test data.

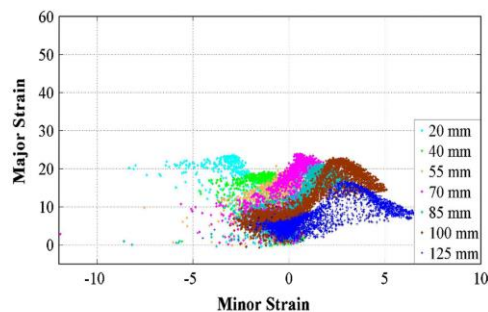


Fig. 18. FLD of Al5005-O prior to necking. (For interpretation of the references to colour in this figure legend, the reader is referred to the web version of this article.)

To construct a full field FLD for aluminium, specimens' width changed from 20 mm to 125 mm. To obtain the same results for SRPP, specimens possessing 12.5 mm–200 mm widths were employed. This depicts the greater sensitivity of SRPP to variations in width than Al specimens. Furthermore, FLD of Al samples having different aspect ratios made separate, distinguishable boundaries with each other, while FLD of different SRPP specimens were more mixed together, showing less distinct boundaries (Fig. 18).

4. Conclusions

Eight pre-consolidated woven SRPP, having different aspect ratios, were stretch formed up to the failure at room temperature. Displacements and strains were measured and calculated by an in-situ 3D photogrammetric technique, capable of capturing evolution of deformation on specimens continuously. The experimental outcomes of the current study are summarized as follows:

- Formability of SRPP is associated with a more uniform strain distribution compared to metals. This specific behaviour observed in the current study, extends SRPP forming envelope as it prohibits failure due to necking or highly localised strain which is commonly observed in stretching of metals. Elimination of necking in SRPP delays failure due to a more uniform strain distribution and an increase in the energy absorption capability of the material.
- A novel history/path dependent failure criterion, inspired from metal forming, was constructed based on outcomes of extensive stamp forming on SRPP specimens.
- The proposed failure criterion indicates failure limits of SRPP composite as a combination of maximum principal strain and induced deformation mode depicted by the ratio of minor to major strain.
- It was shown that an appropriate selection of forming parameters, such as boundary condition, aspect ratio and fibre orientation, greatly influence the formability of pre-consolidated SRPP composite by changing the forming path. For instance, a change in forming mode from uniaxial extension to shear mode increased forming limits of SRPP composite by 135%.

References

- [1] International Energy Agency. www.iea.org.
- [2] European Commission of Energy. <http://ec.europa.eu>.
- [3] Helms H, Lambrecht U. Energy savings by light weighting. IFEU – Institut für Energie- und Umweltforschung Heidelberg GmbH 2003.
- [4] Cabrera NO, Alcock B, Peijs T. Design and manufacture of all-PP sandwich panels based on co-extruded polypropylene tapes. *Compos B Eng* 2008;39:1183–95.
- [5] Alcock B, Cabrera NO, Barkoula N-M, Loos J, Peijs T. The mechanical properties of unidirectional all-polypropylene composites. *Compos A Appl Sci Manuf* 2006;37:716–26.
- [6] Abot JL, Gabbai RD, Harsley K. Effect of woven fabric architecture on interlaminar mechanical response of composite materials: an experimental study. *J Reinf Plast Compos* 2011;30:2003–14.
- [7] Suemasu H, Friedrich K, Hou M. On deformation of woven fabric-reinforced thermoplastic composites during stamp-forming. *Compos Manuf* 1994;5:31–9.
- [8] Lussier DS, Chen J. Material characterization of woven fabrics for thermoforming of composites. *J Thermoplast Compos Mater* 2002;15:497–509.
- [9] Launay J, Hivet G, Duong AV, Boisse P. Experimental analysis of the influence of tensions on in plane shear behaviour of woven composite reinforcements. *Compos Sci Technol* 2008;68:506–15.
- [10] Zhu B, Yu TX, Zhang H, Tao XM. Experimental investigation of formability of commingled woven composite preform in stamping operation. *Compos B Eng* 2011;42:289–95.
- [11] Wolthuisen DJ, Schuurman J, Akkerman R. Forming limits of thermoplastic composites. *Key Eng Mater* 2014;611:407–14.
- [12] Haanappel SP, Thijse ten RHW, Sachs U, Rietman B, Akkerman R. Formability analyses of uni-directional and textile reinforced thermoplastics. *Compos A Appl Sci Manuf* 2014;56:80–92.

- [13] Harrison P, Gomes R, Curado-Correia N. Press forming a 0/90 cross-ply advanced thermoplastic composite using the double-dome benchmark geometry. *Compos A Appl Sci Manuf* 2013;54:56–69.
- [14] Chen Q, Boisse P, Park CH, Saouab A, Bréard J. Intra/inter-ply shear behaviors of continuous fiber reinforced thermoplastic composites in thermoforming processes. *Compos Struct* 2011;93:1692–703.
- [15] Ma CM, Wang TH, Yu CT, Cheng BW. Two-dimensional stamp forming analysis for thermoplastic composites. *J Appl Sci* 2013;13:1461–6.
- [16] Wang P, Hamila N, Boisse P, Chaudet P, Lesueur D. Thermo-mechanical behavior of stretch-broken carbon fiber and thermoplastic resin composites during manufacturing. *Polym Compos* 2014;20:14–20 (on-line). <http://onlinelibrary.wiley.com/doi/10.1002/pc.22988/full>.
- [17] Sexton A, Cantwell WJ, Kalyanasundaram S. Stretch forming studies on a fibre metal laminate based on a self-reinforcing polypropylene composite. *Compos Struct* 2012;94:431–7.
- [18] Kalyanasundaram S, Dharmalingam S, Venkatesan S, Sexton A. Effect of process parameters during forming of self reinforced - PP based fiber metal laminate. *Compos Struct* 2013;97:332–7.
- [19] Mosse L, Cantwell WJ, Cardew-Hall MJ, Compston P, Kalyanasundaram S. A study of the effect of process variables on the stamp forming of rectangular cups using fibre-metal laminate systems. *Adv Mater Res* 2005;68:649–56.
- [20] Mosse L, Cantwell WJ, Cardew-Hall MJ, Compston P, Kalyanasundaram S. The effect of process temperature on the formability of fibre-metal laminates. *Compos A Appl Sci Manuf* 2005;36:1158–66.
- [21] Davey S, Das R, Cantwell WJ. Forming studies of carbon fibre composite sheets in dome forming processes. *J Compos Struct* 2013;97:310–6.
- [22] Gresham J, Cantwell W, Cardew-Hall MJ, Compston P, Kalyanasundaram S. Drawing behaviour of metal-composite sandwich structures. *Compos Struct* 2006;75:305–12.
- [23] Mosse L, Compston P, Cantwell WJ, Cardew-Hall MJ, Kalyanasundaram S. Stamp forming of polypropylene based fibre-metal laminates: the effect of process variables on formability. *J Mater Process Technol* 2006;172:163–8.
- [24] Compston P, Cantwell WJ, Cardew-Hall MJ, Kalyanasundaram S, Mosse L. Comparison of surface strain for stamp formed aluminium and aluminium-propylene laminate. *J Mater Sci* 2004;39:6087–8.
- [25] Kalyanasundaram S, Dharmalingam S, Venkatesan S, Sexton A. Effect of process parameters during forming of self-reinforced PP-based fibre metal laminates. *Compos Struct* 2012;97:332–7.
- [26] CURV-self-reinforced thermoplastic composite data sheet. Propex fabrics; 2003. www.curvonline.com.
- [27] ARAMIS v6.3. User manual. The basics of strains; 2011 [chapter K]. <http://www.Gom.com>.
- [28] Hu J, Marciniak Z, Duncan J. *Mechanics of sheet metal forming*. 2nd ed. Butterworth-Heinemann; 2002.
- [29] Zanjani NA, Kalyanasundaram S. The effect of fibre orientation on the forming behaviour of a self-reinforced polypropylene composite. In: *Proceedings of mechanics of nano, micro and macro composite structures conference*, Torino; 2012.
- [30] Stoughton TB, Zhu X. Review of theoretical models of the strain-based FLD and their relevance to the stress-based FLD. *Int J Plast* 2004;20:1463–86.

The effect of fibre orientation on formability and failure behaviour of SRPP composite

The previous chapter mainly dealt with formability and failure of a SRPP composite with $[0^\circ, 90^\circ]$ fibre orientations. The resultant modes of failure in specimens with different aspect ratios included biaxial stretch to uniaxial deformation modes. This chapter deals with forming and failure of SRPP composite possessing $[-45^\circ, +45^\circ]$ fibre orientations to characterise composite behaviour under shear deformation mode.

In the current chapter, the effect of fibre orientation on forming and failure behaviours of a consolidated woven composite is investigated. Off axis specimens were stretch formed until failure and strain at the vicinity of failed regions were captured to construct a forming limit envelope in shear deformation region. Induced deformation modes and failure mechanisms in on-axis and off-axis specimens were compared. Failure morphologies in two sets of samples with different fibre orientations were studied using an optical microscope. It was revealed that delamination and intra-laminar shear were the main causes of failure in off-axis specimens.

A conclusion from this study showed that changing fibre orientation facilitates forming of woven composites in regions prone to failure due to fibre breakage. The reason for this behaviour is a change in the forming mode which facilitates forming through trellising and shearing of the matrix as opposed to stretching the fibres. It was shown that using a combination of on- and off-axis laminates facilitates manufacture of flawless products and yields cost savings in mass production of woven composite.

18 different specimens made of a balanced twill-weave SRPP composite with different aspect ratios and fibre orientations were employed in this experimental study. First stage

of this study involved unidirectional extension of on-axis and off-axis specimens using a universal testing machine. Strains and their evolution were captured using a non-contact two-dimensional photogrammetry measurement system. The second stage of experimentation included stretch forming of semi-rectangular SRPP samples by a 300 mm diameter hemispherical punch in an open die configuration. A real-time three-dimensional strain measurement system, comprised of two high speed cameras mounted beneath the die, were used to measure strains and strain evolution on the outer surface of specimens. Specimens were stretch formed until failure and Phenomenological failure studies were conducted using an optical microscopy system.

It was shown that failure mechanism in SRPP composite drastically changed by varying fibre orientation and aspect ratio of specimens. Optical microscopy examination of failed specimens demonstrated that that yarn splitting and fibre fracture were the main causes of failure in on-axis samples. Failure in off-axis specimens was more complex and a combination of different failure mechanisms were observed.

A modified failure envelope was constructed to reveal failure mechanisms in off-axis samples and explain higher formability of off-axis specimens compared to on-axis samples. Normal and shear strains were measured during deformation of off-axis samples and a rotation tensor was defined. Using tensor transformation laws, rotation of fibres at each increment of deformation was measured and strains along fibres and perpendicular to fibre directions were calculated. It was proved that fibre strain did not exceeded the maximum permissible strains and as such fibre fracture was not the dominant failure mode in off-axis samples. This finding revealed that formability of the composite is dominated by the failure of the thermoplastic matrix. Finally, results were compared with maximum strain failure theory predictions and it was shown that the proposed FLC-based failure model can better predict failure in woven SRPP composites.

The Effect of Fiber Orientation on the Formability and Failure Behavior of a Woven Self-Reinforced Composite

Nima A. Zanjani¹

Research School of Engineering,
The Australian National University,
31 North Road,
Canberra 2601, Australia
e-mail: nima.akhavan@anu.edu.au

Wentian Wang

Research School of Engineering,
The Australian National University,
31 North Road,
Canberra 2601, Australia

Shankar Kalyanasundaram

Research School of Engineering,
The Australian National University,
31 North Road,
Canberra 2601, Australia

This article investigates the effect of fiber orientation on forming and failure behaviors of a preconsolidated woven self-reinforced polypropylene (SRPP) composite during the stamp-forming process. Specimens with different aspect ratios were employed to study their formability during forming through a hemispherical punch in an open die configuration. The strain evolution in specimens was captured using a real-time strain measurement system (the ARAMIS). A forming limit diagram (FLD), inspired from metal forming, was constructed to investigate the failure onset in the woven composite. The FLD revealed dominant failure mechanisms in [0 deg,90 deg] specimens were yarn splitting and fiber fracture as depicted by optical microscopy. A modified FLD was proposed to investigate failure mechanisms in [45 deg,-45 deg] samples. It was shown that delamination and intralaminar shear are the main causes of failure in this set of specimens. The outcomes of this study suggest that by changing forming parameters, such as fiber orientation, boundary condition, and aspect ratio, the formability of a preconsolidated SRPP can be improved. These results show the possibility of producing cost-effective, flawless, and fully recyclable products from consolidated woven composites. The proposed criterion can accurately predict failure in a woven composite by considering the combined strain interactions. This is reflected in the implementation of induced deformation modes and strain history into the failure criterion, making it a practical measure for rapid manufacturing techniques, such as stamping. The novel path-dependent failure criterion, introduced in this study, attempts to fill the gap for a reliable and accurate failure measure for woven composites. [DOI: 10.1115/1.4030894]

Keywords: woven thermoplastic composite, failure, fiber orientation, forming

1 Introduction

Air pollution, global warming, and shortage of fossil fuels are some of major issues relevant to the well-being of the society. The transport industry is solely responsible for a quarter of the greenhouse emissions in Europe, 16% in Australia, and 23% in the U.S. [1–3]. Weight reduction in vehicles can substantially reduce fuel consumptions and emitted pollutants [4] and therefore is regarded as one of the major priorities in the automotive industry. A directive issued by the European Commission of Energy enacted policies to reduce emissions from the cars by 2020. Furthermore, to alleviate the adverse effect of end-life vehicles on the environment, a policy was set in place to force manufacturers to make 95% of cars (by weight) from recyclable materials [5]. These directives have made the automotive industry to seek alternative material systems to replace current metallic components.

Fiber-reinforced polymers are attractive candidates to be used in vehicles [6,7]. These materials can reduce the weight of automobiles significantly, providing improved wear resistance and high-energy absorption capacity. A typical application is the BMW i3 outer skin made completely from a thermoplastic polymer through the injection molding technique [8].

Woven thermoplastic composite materials (WTPCMs) offer the advantage of a different polymeric configuration, eliminating the necessity for debonding and restructuring procedures common in thermoset polymers. They can be regarded as potentially suitable

candidates to be employed in several industries including aerospace and automotive applications. This is due to recyclability, improved resistance to crack propagation, excellent impact toughness, and significantly decreased processing time compared to thermoset-based composite materials [9–12]. Employing woven composites in different industries eliminates the shortcomings of fiber-reinforced composites, such as through-thickness strength and fiber placement accuracy [13]. Furthermore, they can be used in fiber-metal-laminate (FML) systems, consisting of a composite layer sandwiched between two sheets of metal. FMLs offer advantages over monolithic materials, such as weight reduction while providing the required strength. Furthermore, they do not suffer from necking as the polymer core distributes the strains more evenly on the surface of the metal.

Components made of composite materials are generally manufactured through labor intensive, time-consuming techniques resulting in expensive products. Therefore, they are mainly employed in applications where the production rates are low and the price is not a major factor. To facilitate the wide spread application of WTPCMs and FMLs in mass-production applications, the conventional techniques in fabricating composites should be replaced with a more cost-effective, rapid manufacturing method.

Stamp forming is often considered as the preferred manufacturing technique for mass production of metallic alloys. This method of production results in high-quality, cost-effective products. Stamp-forming behavior of preconsolidated WTPCMs is a recent research initiative. Mosse et al. [14–17] studied stamp forming of a FML both experimentally and numerically. In these studies, the effect of the blank holder force, punch feed rate, and tool radius on the quality of channels and domes was investigated. Sexton et al. [18] studied stretch forming of FMLs possessing different

¹Corresponding author.

Contributed by the Manufacturing Engineering Division of ASME for publication in the JOURNAL OF MANUFACTURING SCIENCE AND ENGINEERING. Manuscript received November 27, 2014; final manuscript received June 18, 2015; published online September 4, 2015. Assoc. Editor: Jingjing Li.

geometries. A 3D photogrammetry system (ARAMIS) was employed to record strain evolutions in sheets during forming. Based on experimental results, FLD of the material was constructed. It was concluded that FMLs exhibited better formability than aluminum owing to a wider forming envelope. Zanjani et al. [19] investigated stretch-forming behavior of a preconsolidated thermoplastic composite at room temperature. It was found out that SRPP composites offer excellent formability due to the capacity to sustain a larger minor strain for a given major strain. Davey et al. [20] investigated forming behavior of a carbon/poly ether ether ketone composite through the finite-element method. The numerical predictions were evaluated based on draw forming outcomes through a varying blank holder force.

The present study aims at investigating the room temperature stretch-forming behavior of a preconsolidated woven SRPP composite, as a fully recyclable, low-density composite material [21]. In this study, various SRPP specimens were stretch formed by a hemispherical punch and the induced strains and deformation modes were calculated by a digital image correlation technique. A FLD, inspired from metal forming [22,23], was constructed to reveal safe and failed deformation margins and to introduce a novel strain-based path-dependent failure criterion for the composite. Finally, a modified FLD was introduced to reveal the effect of fiber orientation on the incorporated failure mechanism.

The proposed criterion offers some benefits in evaluating failure in a woven composite over independent failure criteria, such as maximum strain theory: It is a history/path-dependent failure criterion and therefore the effects of process-induced strains and the forming history on failure limits of the composite can be evaluated directly. It covers all possible forming modes incorporating to failure onset in the woven composite and is applicable to a wide range of manufacturing processes. Furthermore, safe margins of a deformation process can be evaluated easily without the necessity to incorporate the highly complex structure of a woven composite in micro/meso-scales. The proposed FLD is suitable for rapid fabrication processes and mass-production manufacturing environments. Finally, the proposed failure measure can be easily implemented into a finite-element simulation to elucidate the failure envelope of the woven composite in the stretch-forming process. The forming limit curve (FLC)-based failure criterion is introduced in the current research paper to bridge the gap on the shortcomings of the current failure criteria for composites [24,25].

2 Experimental Procedure

2.1 Specimens Properties. Specimens were made of SRPP woven composite, CURVTM, produced by Propex Fabrics of Germany. A balanced twill-weave prepreg fabric of polypropylene (PP) was processed by a heat compaction technique to produce consolidated SRPP sheets with 0.9 g/cm³ density. Reinforcements and the matrix of SRPP were made of a semicrystalline PP. The thickness of consolidated SRPP blanks was 1 mm. The tensile strength and strain to failure of SRPP were 120 MPa and 20%, respectively [26]. Flexural modulus of the material was reported to be 3500 MPa by the manufacturer.

2.2 Experimental Setup. To clearly reveal the effect of fiber orientation on the formability and incorporated failure mechanisms in SRPP composite, two different sets of experiment were conducted. Initially, uniaxial extension on [0 deg,90 deg] and [45 deg,-45 deg] rectangular samples was carried out. This was accomplished by uniaxially stretching specimens by an INSTRON machine. The test procedure and specimens' specifications conformed to ASTM D3039 standard for polymer matrix composite materials. Prior to the test, samples were painted by a stochastic pattern of black dots on a white background required for the 3D photogrammetry measurements through the ARAMIS system. The ARAMIS system was made of two high-speed CCD cameras

capturing images from specimen during deformation. By employing a built-in 3D mapping algorithm [27], the ARAMIS system calculated displacements and induced strains in specimens. After painting, specimens were fixed between the INSTRON grippers, facing toward the CCD cameras. After initiation of extension by the INSTRON machine, the ARAMIS system continuously captured deformations on samples, resulting in calculation of different components of strain tensor (normal and shear) during uniaxial extension. The test setup for uniaxial extension is shown in Fig. 1. The specifications of the ARAMIS system are represented in Table 1. The load cell of the INSTRON measured the applied load until the catastrophic failure of the specimen depicted by 20% drop of the load.

Second set of experiment was conducted by stretch forming of [0 deg,90 deg] and [45 deg,-45 deg] specimens. This experiment was designed to elucidate the effect of fiber orientation on the formability and induced deformation modes in SRPP composite. The rectangular specimens employed in stamp-forming process were cut out from initially circular blanks. The geometry and dimensions of these specimens are depicted in Fig. 2 and Table 1, respectively. The stretch-forming process was accomplished by a 300 kN custom-build stamping press equipped with a 100 mm in diameter hemispherical punch and a 105 mm open die. The configuration of the press, the die, the specimen, and the ARAMIS system during stretch forming is shown in Fig. 3. Data acquisition and press parameters control (feed rate and punch displacement) were accomplished through a local personal computer. A load cell was also employed to measure the punch force versus displacement of the punch. Six M12 bolts were used to completely fix rectangular specimens in the fixture, enforcing a fixed boundary condition on the two opposite edges of the sample, while the other two were free. The full circumference of the circular specimen (W200) was completely clamped in the lock ring.

The forming procedure was initiated by locating the specimen and the blank under the press and forming specimens by the hemispherical punch with a 10 mm/s feed rate up to the failure. Occurrence of failure was specified by a sudden drop in the punch load. The shutter speed of CCD cameras was selected to 20 frames per second resulted in taking approximately ten pictures of the deformed specimen for each 5 mm depth of punch downward displacement. Setup parameters used to capture images with the ARAMIS system are depicted in Table 2.

2.3 FLD and FLC. The FLD is a graphical illustration of forming behavior of sheets. It commonly consists of major and minor strains induced in specimens during various stages of deformation. Generally, a forming process is facilitated through

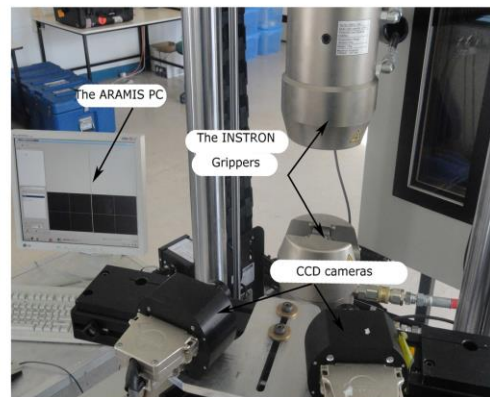


Fig. 1 Test setup of uniaxial extension of [0 deg,90 deg] and [45 deg,-45 deg] SRPP specimens

Table 1 Width of SRPP samples employed in this study

Specimen	W (mm)
W12.5	12.5
W25	25
W50	50
W75	75
W100	100
W125	125
W150	150
W200	200

different deformation modes. Each deformation mode is highlighted by a different strain ratio (SR), calculated by the ratio of minor to major strains induced in the specimen during forming (Table 3 and Fig. 4).

A FLC is a curve established on the FLD of specimens prior to failure (Fig. 4). The FLC distinguishes between safe and failed regions during deformation by specifying major and minor strains prior to failure. To construct a full-field FLD and to develop the FLC for the material under investigation, the effective forming parameters were changed to induce different deformation modes. In this article, the change of specimen's aspect ratio induced deformation mode ranging from biaxial stretch to uniaxial extension. To exhibit forming behavior of SRPP between shear and wrinkling modes, [45 deg, -45 deg] specimens were employed. Outcomes of forming experiments on [0 deg, 90 deg] and [45 deg, -45 deg] SRPP samples revealed the full-field forming behavior of a PP-based WTPCM ranging from SR = +1 to SR = -2, constructing its full-field FLC.

3 Results and Discussion

To understand clearly the effect of fiber orientation and different deformation modes on the forming behavior of a WTPCM, initially results of uniaxial extension on [0 deg, 90 deg] and [45 deg, -45 deg] woven SRPP specimens are introduced. The failure morphologies in these specimens are studied and the effect of induced deformation modes and fiber orientation on failure onset is discussed. Afterward, forming response of SRPP specimens possessing different aspect ratios is investigated and the effect of a woven microstructure on SRPP formability is

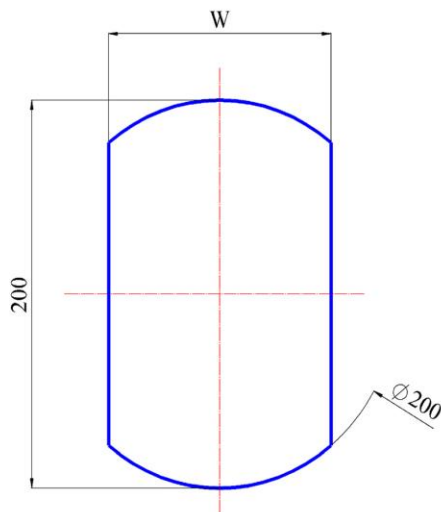


Fig. 2 Geometry of SRPP specimens employed in stretch forming

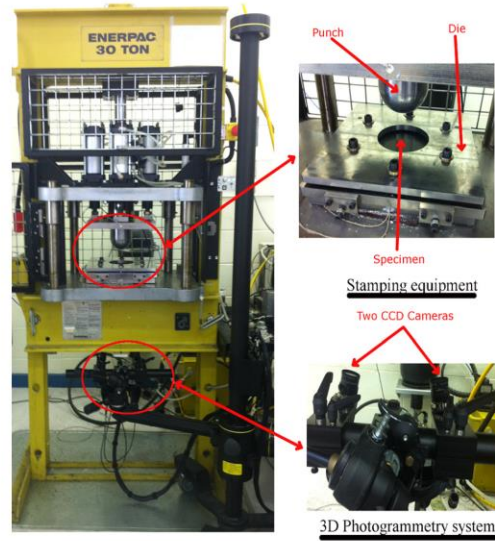


Fig. 3 Test setup for stretch forming of SRPP

Table 2 Specifications of the ARAMIS

Parameter	Specification
Camera resolution	1280 × 1024 pixels
Maximum frame rate	24 Hz
Shutter time	[0.1 ms, 2s]
Strain range	0.05–100%
Strain accuracy	0.02%

elucidated. The strain evolutions in different specimen are compared. Finally, a FLD, inspired from metal forming, is constructed to reveal the failure limits of SRPP and the dependency of failure mechanism to the induced forming modes.

3.1 Failure of Preconsolidated SRPP During Uniaxial Extension. Studying uniaxial and bias extension tests plays an important role in revealing the effect of different deformation modes in the forming and failure behaviors of SRPP composite during a stamp-forming process. This is due to the elimination of highly complicated contact phenomenon in a uniaxial extension experiment. There are substantial differences between mechanical responses and failure morphologies of [0 deg, 90 deg] and [45 deg, -45 deg] specimens, signifying the contribution of different mechanisms in deformation of preconsolidated SRPP samples.

The numerous mechanisms contributing in forming and failure behaviors of the preconsolidated SRPP can be better understood by versatility of failure morphologies depicted in Figs. 5 and 6. Specimens possessing [0 deg, 90 deg] fiber orientations mainly failed due to fiber rupture and debonding between fibers and the matrix exhibited by the jagged surface of fractured area.

Table 3 Induced deformation modes during forming

Deformation mode	SR
Biaxial stretch	+1
Plane strain	0
Uniaxial extension	-0.5
Shear	-1
Wrinkling	-2

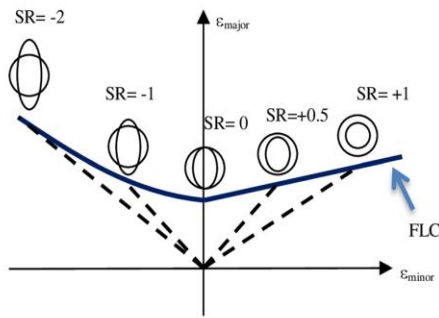


Fig. 4 Induced deformation modes in forming

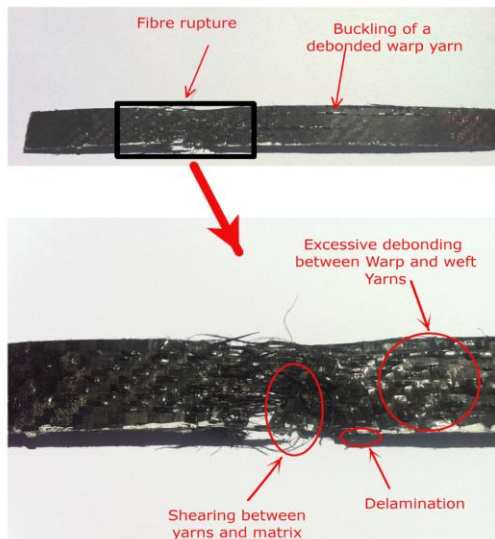


Fig. 5 Incorporated failure mechanisms in uniaxial extension of [0 deg, 90 deg] SRPP specimens

Disentanglement between warp and weft yarns can also be observed. Furthermore, the failure has propagated across the surface of the specimen, affecting areas far away from fracture site. This can be observed by the pull-out and buckling of warp yarns after catastrophic failure of highly drawn PP fibers in the woven structure.

Figure 6 represents failure mechanisms observed in the [45 deg, -45 deg] specimen, signifying the fundamental differences between [0 deg, 90 deg] and [45 deg, -45 deg] specimens: The failure is concentrated over a very small region around the fractured area, without affecting other regions. The fractured site is

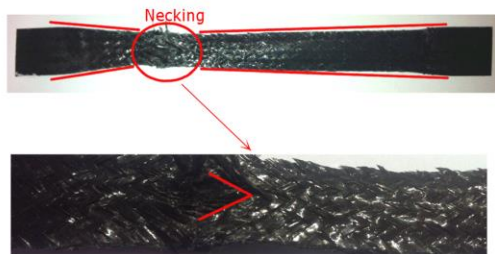


Fig. 6 Incorporated failure mechanisms in uniaxial extension of [45 deg, -45 deg] SRPP specimens (bias test)

depicted by the gradual decrease in the specimen's width from both ends toward the ruptured area. It is a resemblance of necking phenomenon in metals, although the underlying mechanism is completely different. This is caused by a different forming and failure mechanism: Formability of preconsolidated woven [45 deg, -45 deg] SRPP specimen is facilitated by trellising and shear phenomena, resulting in the large amount of extension in the composite without considerable stretching of fibers.

Interestingly, the necking phenomenon observed in [45 deg, -45 deg] specimens is completely different to the forming behavior observed in woven textiles and prepreg woven composites during a bias test [28,29]. The prepregs and textiles show an extended region in the middle of the [45 deg, -45 deg] samples, experiencing pure shear deformation without any localized high strain. This is due to the significant difference between shear stiffness of the unconsolidated and consolidated polymer resins. Consolidation of the polymeric matrix in a woven composite causes a significant increase in the shear stiffness of the resin compared to low shear stiffness of the woven fabric. Therefore, in a prepreg woven composite the bias behavior is dominated by shear behavior of the fabric. However, in a preconsolidated woven composite it is dominated by the shear behavior of the matrix. This is in complete agreement with previous studies on [45 deg, -45 deg] woven composites during bias extension [30].

The shear strength of the matrix restricts the extension of the [45 deg, -45 deg] coupon test, resulting in the rupture of the sample due to shear failure in the matrix. This is clearly observed by the excessive disentanglement between warp and weft yarns near the failure region, elucidated through the portion of unaffected longitudinal yarns which remained intact after failure of the specimen (Fig. 6).

Microscopic failure morphologies, as shown in Fig. 7, exhibit a fundamentally different failure mechanisms incorporated in extension of [45 deg, -45 deg] specimens. These morphologies include multiple transverse and longitudinal cracks and shear of the matrix as the main failure modes. In contrast to extensive fiber rupture in on-axis specimens, branching of yarns was dominantly observed in textile reinforcement during the bias test. Figure 7(a) exhibits failure in longitudinal yarns due to bending effects caused by the undulation of yarns during extension. This phenomenon has resulted from interactions between interlacing yarns and excessive distortion of reinforcement due to trellising effect. Figure 7(b) represents multiple parallel longitudinal and transverse cracks, resulting in branching of yarns. The fiber kinking is

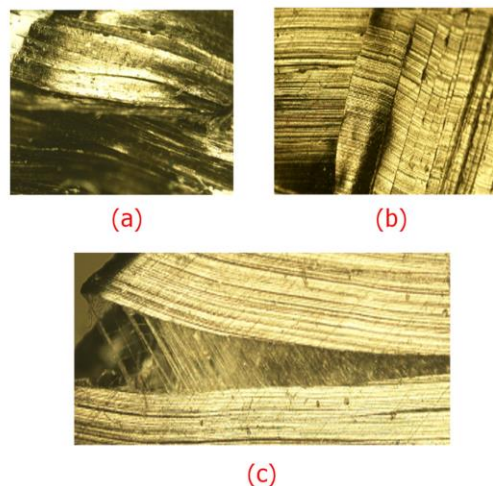


Fig. 7 Microscopic failure modes during bias extension test (x10)

also visible in this image. Figure 7(c) shows the appearance of hackles between split sections of a yarn due to mode (I) of fracture.

3.2 Force–Displacement Evolution During Forming.

Figure 8 illustrates the force–displacement of typical SRPP specimens during forming possessing different fiber orientations. These diagrams indicate a nearly linear relation between force and displacement in narrow [0 deg,90 deg] samples shifting toward a parabolic dependency in wider samples. This is due to different imposed boundary conditions resulting in a combination of stretching and drawing modes. Another significant behavior of SRPP composites is related to the sudden change of force–displacement diagrams between [0 deg,90 deg] and [45 deg,–45 deg] specimens. Forming depth of [45 deg,–45 deg] samples was increased extremely, showing highly increased formability of the material due to a change in fiber orientation. This shows the superior capacity of SRPP to absorb the energy prior to rupture. This specific behavior demonstrates the potential application of [45 deg,–45 deg] SRPP where high-energy absorption capability is required, such as bumper of cars, as depicted in Ref. [31]. Furthermore, in producing components from SRPP a huge amount of energy can be preserved if proper boundary conditions are applied to restrict fiber extension prior to failure and to allow forming by trellising. This saves the energy up to 50%, as depicted by the surface area under force–displacement graphs of [0 deg,90 deg] and [45 deg,–45 deg] samples.

The experimental forming outcomes elucidated the great potential of a preconsolidated woven composite to achieve high-forming depths while conserving the energy required for stamping, yet providing a balance between formability and strength. This represents the significance of process design during stamping of a woven composite and proper orientation of the fabricated component. This can essentially affect the quality, strength, and cost-effectiveness of the final product made from preconsolidated composites, specifically in mass-production industries, such as the automotive industry.

3.3 The Evolution of Principal Strains at the Pole.

The SR, defined as the ratio of minor to major strain, is a measure of formability through characterizing the induced deformation modes in specimens during the stamp forming. The evolution of SR at the pole of a specimen (midpoint of the sample), as a typical surface point establishing the initial contact with the punch, elucidates the effect of forming parameters on the formability of the material. It also reveals the effect of fiber orientation in induced deformation modes. Figure 9 elucidates the strain path of the pole in [0 deg,90 deg] and [45 deg,–45 deg] specimens through the variation of SR parameter. The induced deformation modes, varied by specimens' aspect ratios, included biaxial strain, plain strain, and uniaxial strain in [0 deg,90 deg] specimens and mainly shear deformation in [45 deg,–45 deg] samples. The effect of different stages of

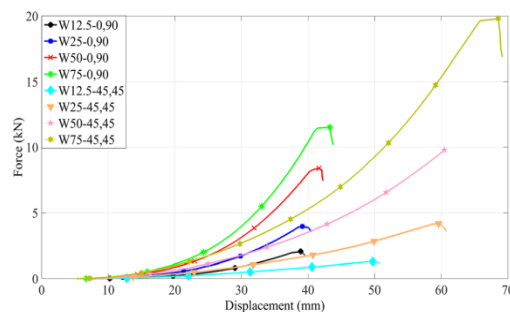


Fig. 8 Force–displacement of [0 deg,90 deg] and [45 deg,–45 deg] specimens

deformation, from clamping of specimens in the die to different contact conditions between the punch and the blank, is clearly reflected in the strain path history of the pole.

The strain path in most specimens consists of three different stages: (1) Initial stretch due to clamping in the die (lock ring effect), inducing uniaxial stretch mode in specimens, (2) subsequent biaxial stretch (Nakazima effect) as a result of initial contact between blanks and the hemispherical punch, and (3) main path of deformation due to imposed boundary conditions, interaction between orthogonal yarns, evolution in contact and the aspect ratio of specimens. The effect of fiber orientation on the SR is clearly reflected in these figures. In [0 deg,90 deg] samples, principal directions coincide with fiber orientations and thus the mode of deformation changes with specimens' width. This includes biaxial mode for full circular sample where the circumference is fully clamped in the die and uniaxial extension associated with the thinnest sample. Other deformation modes are located between these two extremes. However, in [45 deg,–45 deg] specimens, only two modes of deformation dominate forming behavior of SRPP: shear mode and biaxial mode. The imposed boundary condition enforces the two largest specimens, W150 and W200, to exhibit biaxial stretch during all stages of deformation. The shear deformation mode is the dominant deformation mode in other specimens resulted from a large number of free yarns. This deformation mode causes unclamped yarns to freely trellis over their pin joints.

The effect of fiber orientation and imposed boundary conditions on forming of SRPP is distinctly reflected in the evolution of the SR depicted in Fig. 9. Some conclusions can be drawn from this figure: First, the maximum permissible major and minor strains in [45 deg,–45 deg] specimens are vastly expanded. Considering the low extensibility of PP fibers, the underlying mechanism of the extended formability should be intra-ply shear. Furthermore, [0 deg,90 deg] specimens exhibited a wavy strain path while [45,–45 deg] specimens followed a monotonic, yet smoother strain path. To explain this behavior, the applied boundary condition on both ends of orthogonal yarns passing through the pole of [45 deg,–45 deg] specimen should be considered. Both ends of these yarns in [45 deg,–45 deg] samples are free and do not experience undulation during forming. Reduced internal friction

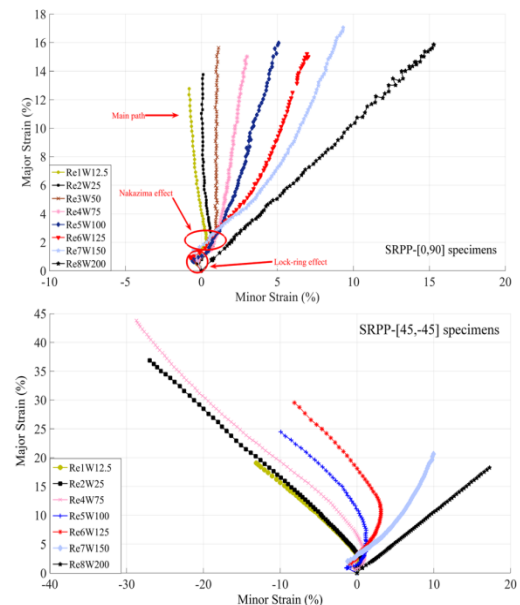


Fig. 9 Strain evolution at pole during stretch forming of SRPP specimens

between warp and weft yarns in [45 deg, -45 deg] samples is another effective parameter.

Yarns oriented along a 45 deg axis do not stretch during stamping; therefore the slippage between yarns does not occur. On the other hand, both ends of longitudinal yarns in [0 deg, 90 deg] samples are fixed in the lock ring. During stretch of the specimens, they tend to undulate excessively, resulting in the large increase of contact pressure between interlacing yarns. This causes the roll-over of fibers within a yarn bundle and slippage of yarn bundles over each other, exhibiting a wavy path of deformation revealed by the high sensitivity of the ARAMIS system. The high-contact pressure also changes the cross section of elliptical yarns by affecting their eccentricity (or flattening) ratio and therefore changes the bending stiffness of the preconsolidated composite during forming. The effect of forming parameters in failure mechanism of [0 deg, 90 deg] and [45 deg, -45 deg] specimens will be discussed later.

3.4 Construction of the FLD. FLD was employed to determine the induced deformation modes in specimens during different stages of deformation. To construct a FLD, the blanks were deformed through different forming modes up to fracture. Variations in applied boundary conditions and specimens' aspect ratios resulted in different deformation modes, affecting the formability of the material. The last stage FLD for [0 deg, 90 deg] SRPP specimens is shown in Fig. 10.

FLD at the last stage of deformation exhibits the ultimate permissible strain of SRPP in different regions of strain space. Figure 10 demonstrates explicitly the range of induced deformation modes, located between biaxial stretch and uniaxial deformation modes. The failure strain of SRPP predicted by the proposed method maintains a constant value throughout the aforementioned deformation modes and is validated by the maximum strain criterion of fibrous composite. This value corresponds to the maximum permissible strain of [0 deg, 90 deg] specimens ($18 \pm 2\%$) during uniaxial extension. Hence, for the region between biaxial stretch and uniaxial extension, a primary failure limit can be established based on limiting strain of fibers:

$$\text{If } -0.5 \leq \text{ISR} \leq +1 \text{ and } \epsilon_{\text{minor}} \geq -8\% \Rightarrow \frac{\epsilon_{\text{ff}}}{\epsilon_f} = 1 \quad (1)$$

where ϵ_{ff} depicts the maximum permissible strain in highly drawn PP fibers ($=18 \pm 2\%$), and ϵ_f represents induced strain in fibers during forming. ISR is the abbreviation of instantaneous strain ratio. The failure criterion depicted by Eq. (1) states that the SRPP woven composite fails if the three following conditions are fulfilled simultaneously:

- (1) instantaneous strain ratio lies between -0.5 and $+1$
- (2) minor strain is greater than -8%
- (3) induced strain in the fiber is greater than the failure strain of highly drawn PP fibers (18%)

The main difference between the proposed failure criterion and the maximum strain theory is that the former considers the combined effects of fiber strain, deformation mode, and strain history in determination of failure in the composite. The path/history dependency of this criterion is depicted in instantaneous strain ratio condition (ISR). The proposed procedure is an accurate measure for predicting failure in a woven composite as it considers the combined strain interactions in complex forming procedures through the induced SR. Based on calculated FLC, it is rational to conclude that the main failure mechanism of preconsolidated [0 deg, 90 deg] SRPP specimens during stretch forming is fiber fracture. The validity of this prediction is validated by the visual observations of a typical failed specimen (W200) as depicted in Fig. 11.

Different locations on the ruptured surface of W200-[0 deg, 90 deg] SRPP specimen are chosen to consider all possibilities of failure mechanisms. Figures 11(a) and 11(b) exhibit yarn breakage and multiple cracking of yarns resulted from excessive extension of fibers, respectively. Figure 11(c) shows failure in bending and splitting of yarns as the sample conformed to the punch curvature. Figure 11(d) represents forming of hackles during yarn disentanglement. All these evidences validate the previous conclusions drawn on the main failure mechanism in [0 deg, 90 deg] specimens. This is also in complete agreement with failure morphologies observed during uniaxial extension of [0 deg, 90 deg] specimens (Fig. 6). It should be emphasized that the appearance of some points over the proposed failure limits of [0 deg, 90 deg] SRPP, as depicted by the FLD in Fig. 11, is caused by two reasons: (1) change in the path of deformation (Fig. 9). This behavior also emphasizes on the path/history dependency of the proposed failure criterion. (2) High sensitivity of the ARAMIS system in capturing localized strains in resin-rich regions. This phenomenon demonstrates heterogeneous nature of the woven composite.

Figure 12 exhibits last stage FLD of different [45 deg, -45 deg] specimens. It is clearly evident that the majority of surface points follow the shear deformation mode. Furthermore, major strains along positive direction and minor strains along negative directions are much larger in magnitude compared to [0 deg, 90 deg] specimens. Some significant discussions can be made on the FLD of [45 deg, -45 deg] specimens:

- Completely fixed boundaries of wider specimens enforced fibers to be stretched in both directions, leading to fiber fracture as the dominant mode of failure (more specifically observed in [0 deg, 90 deg] specimens).
- Decreasing the width of specimens shifted the FLD toward more negative minor strains. This was caused by the change of boundary conditions due to the change of specimens' aspect ratios. This allowed transverse yarns to rotate freely around their pin joints, producing high-compressive stresses between adjacent yarns and thus results in an increase of induced minor strain.
- Capability of thinner specimens for trellising and therefore sustaining large shear strains without failure resulted in higher minor strains prior to failure. This caused the FLD of

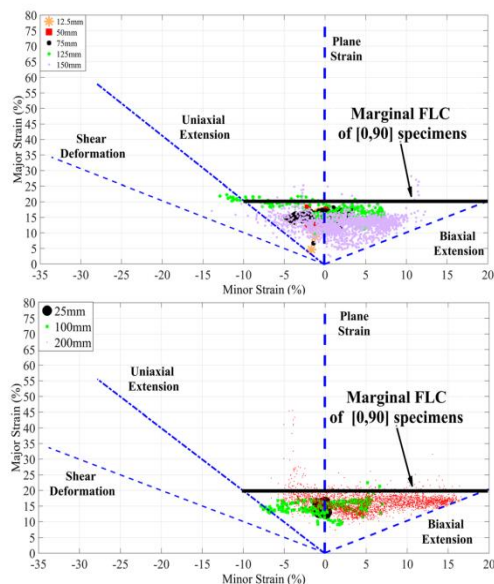


Fig. 10 FLD and marginal FLC of [0 deg, 90 deg] SRPP specimens prior to rupture

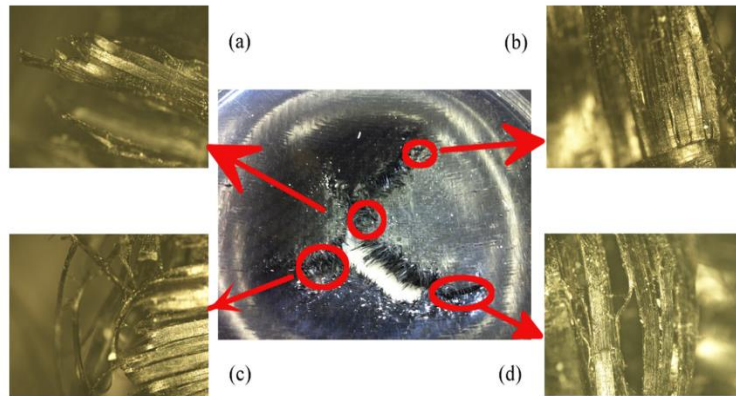


Fig. 11 Failure in W200-[0 deg,90 deg] SRPP specimen during stamp forming

thinner specimens to be located mainly around shear deformation modes, experiencing large major and minor strains.

- By allowing the preconsolidated woven composites to experience shear deformation during forming, its formability can be largely extended.

It is interesting to mention that the maximum major strains induced in the majority of [45 deg,-45 deg] specimens are well beyond the failure strain of PP fibers. This insists on the fact that the fiber rupture, in contrast to [0 deg,90 deg] specimens, is not the main cause of failure in [45 deg,-45 deg] specimens. To investigate the validity of this assumption, two different methodologies are adopted:

- (1) a modified FLC to determine the induced strains in fibers versus induced deformation modes in the composite during forming
- (2) microscopic observations of failure in [45 deg,-45 deg] specimens

To measure the induced strains in reinforcements of [45 deg,-45 deg] specimens, the current FLD should be modified accordingly. In the modified FLD, proposed for the first time in this article for the composite materials, induced strains in fibers are plotted against the induced deformation modes. This procedure captures the actual strains of reinforcements as a function of induced deformation modes. The outcomes of this investigation reveal the effect of SR on the maximum induced strain along fibers prior to the rupture of the composite.

To calculate the induced strain in warp and weft reinforcements accurately, initially the strains along X and Y directions were calculated (Off axis to fibers and along length and width of specimens as depicted in Fig. 13). A tensor transformation was applied

to calculate strains along ± 45 deg angles, corresponding to the initial position of reinforcements. According to the calculated shear strain, the angle of rotation and therefore the new orientation of fibers were calculated in each stage of forming process. In the next stage, the same procedure was followed and incremental strains in fibers were calculated based on the updated configuration of the composite. Finally, the total strains in fibers at the last stage of deformation were calculated based on incremental deformations. The deformation modes at each stage of forming process were calculated by dividing minor to major strains. After determination of fiber's strain and induced deformation mode, they were plotted against each other to obtain the new FLC for [45 deg,-45 deg] SRPP specimens.

The results of applying an incremental procedure in capturing the actual strains in [45 deg,-45 deg] woven specimens are represented in Fig. 15. Two horizontal bold lines in this figure depict failure limits of the preconsolidated SRPP based on uniaxial extension outcomes. The maximum strain in fibers exhibits highest value in biaxial stretch region ($0.5 < SR < 1$) indicating the initiation of fiber rupture. The decrease in SR causes a significant drop in the maximum strain induced in fibers prior to failure of SRPP. Figures 12 and 14 clearly demonstrate that by moving from SR of +1 toward SR of -1, the maximum major strain and therefore the formability of the composite is increased significantly

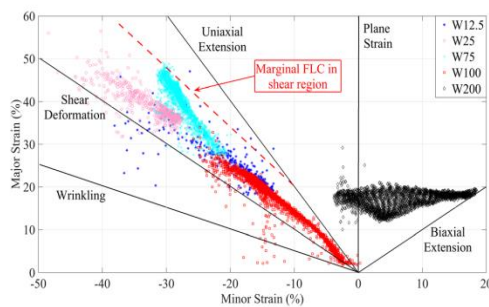


Fig. 12 FLC of [45 deg,-45 deg] SRPP specimens

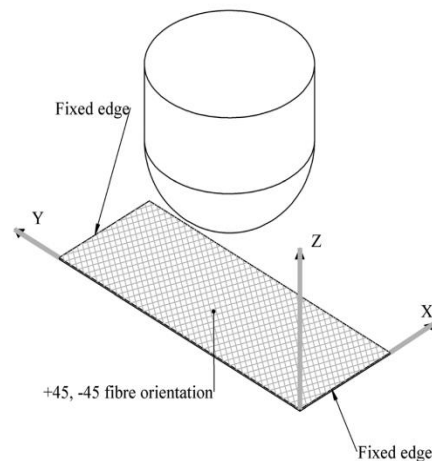


Fig. 13 Convective coordinate attached to [45 deg,-45 deg] specimens during forming for calculation of strains in the fibers based on incremental deformation

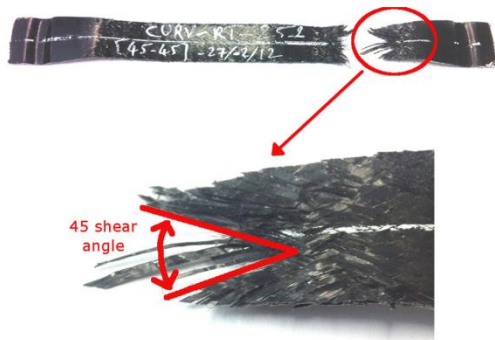


Fig. 15 Failed W25-[45 deg, -45 deg] SRPP specimen during stamp forming

without fibers being stretched further. This behavior elucidates the underlying reason for the increased formability of [45 deg, -45 deg] SRPP specimens compared to [0 deg, 90 deg] samples as observed in Fig. 8. It also shows that fiber fracture is not the dominant failure mode of SRPP during some deformation modes, mainly in the second quarter of strain space.

In Fig. 14, failure region predicted by maximum strain criterion is compared with the failure indicator proposed in this study. The predicted failure limits predicted by maximum strain is specified by the horizontal red bold line intersecting with vertical axis at 18% strain. It shows that the maximum strain criterion can accurately predict failure of SRPP between SRs of -0.2 and +1. However, it overpredicts the failure limits for the SRs less than -0.2. The proposed failure criteria in this study can more accurately predict failure in SRPP specimens due to considering both the SR and fiber strains in specifying failure limits. In other words, the proposed FLC considers the effect of both principal strains in maximum fiber strains prior to failure.

Microscopic and macroscopic images of failure in [45 deg, -45 deg] specimens more clearly demonstrate a different failure morphologies compared to [0 deg, 90 deg] samples (Figs. 15 and 16). The observed ruptured surface of W25-[45 deg, -45 deg] clearly demonstrates occurrence of failure in the specimen. However, unlike [0 deg, 90 deg] samples, no brushy surface is observed and yarns are not disentangled. The 45 deg angle of the failed surface highlights the shear failure between yarns and the matrix.



Fig. 16 Failure in [+45 deg, -45 deg] W75 SRPP specimen during stamp forming

There are also some evidences of delamination at the edge of the specimen, exhibiting interlaminar shear between different composite laminates. These failure incidences show a different failure morphology in [45 deg, -45 deg] specimens compared to [0 deg, 90 deg] samples during stamp forming.

Interestingly, no clear failure phenomena can be observed in macroscopic image of stamp formed W75-[45 deg, -45 deg] specimen (Fig. 16). However, the significant drop of the force observed during the last forming stage (Fig. 9) explicitly indicates the onset of failure in this sample. Delamination at the edge caused by interlaminar shear seems to be the dominant cause of failure. Disentanglement between warp and weft yarns is also evident on the surface of the sample. These evidences imply the occurrence of shear failure between the textile and the matrix. However, no evidence of yarn rupture, leading to catastrophic failure, can be observed. These observations support the previous predictions made by the modified FLC. These evidences prove that failure in [0 deg, 90 deg] and [45 deg, -45 deg] preconsolidated SRPP specimens is driven by two fundamentally different mechanisms.

Finally, due to specific behavior of [45 deg, -45 deg] SRPP specimens, the failure criterion for the deformation modes between uniaxial extension and shear mode can be expressed as (Fig. 13)

$$\text{If } -1 \leq \text{ISR} \leq -0.5 \text{ and } \epsilon_{\text{minor}} \leq -8\% \Rightarrow \epsilon_{\text{major}} = -1.5 \times \epsilon_{\text{minor}} + 0.05 \quad (2)$$

Equation (2) explicitly determines the failure limits of SRPP in shear region as a function of principal strains, the instantaneous

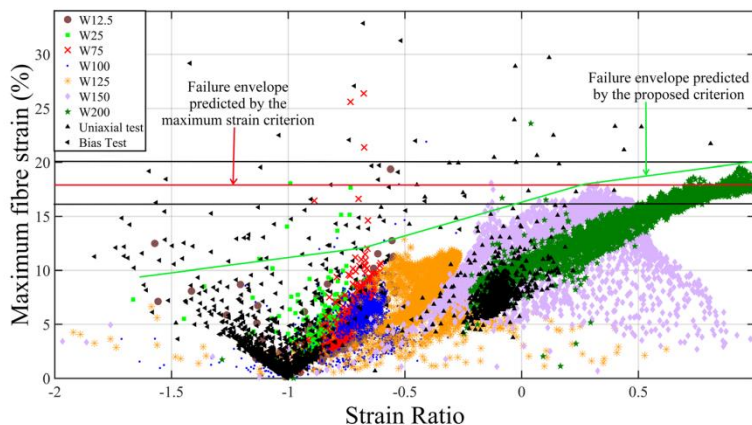


Fig. 14 Modified FLC for [45 deg, -45 deg] SRPP specimens

deformation mode prior to failure and deformation history. Therefore, the second introduced failure criterion states that the preconsolidated woven SRPP composite fails if the three following conditions are simultaneously satisfied:

- (i) Instantaneous strain ratio is located between -1 and -0.5
- (ii) Minor strain is less than -8%
- (iii) Major strain reaches the critical value of $(-1.5 \times \epsilon_{\text{minor}} + 0.05)$

By employing the two resultant failure criteria (Eqs. (1) and (2)), the failure limits of the preconsolidated woven SRPP through a wide range of deformation modes can be calculated.

4 Conclusions

The experimental work undertaken in the current research comprised of uniaxial extension and stretch forming of $[0 \text{ deg}, 90 \text{ deg}]$ and $[45 \text{ deg}, -45 \text{ deg}]$ preconsolidated SRPP specimens possessing different aspect ratios. The characterization results and failure morphologies in $[0 \text{ deg}, 90 \text{ deg}]$ and $[45 \text{ deg}, -45 \text{ deg}]$ specimens during uniaxial extension revealed different deformation mechanisms and failure morphologies in SRPP composites, influenced by the fiber orientation. The macroscopic and microscopic failure observations in these samples highlighted the interaction effects between the two orthogonal interlacing yarns of the preconsolidated woven composite.

Stretch-forming studies revealed the capability of preconsolidated SRPP to be formed into complex geometries. The effective change in deformation path, by a proper combination of boundary condition, aspect ratio, and fiber orientation, results in extensive forming depths and flawless products. The results of 3D photogrammetry technique on stretch forming of SRPP elucidated the safe deformation margins of the preconsolidated SRPP during different deformation modes through constructing a FLD. Based on the results of stretch-forming experiments on $[0 \text{ deg}, 90 \text{ deg}]$ specimens, it was shown that failure of SRPP can be accurately predicted in the region located between biaxial stretch and uniaxial extension modes by the maximum induced strain along the fibers. The failure of the composite specimens between these regions was characterized by a modified maximum strain theory, presented in this article, considering the mutual effects of deformation path and SR.

Forming experiments on $[45 \text{ deg}, -45 \text{ deg}]$ samples demonstrated that shear deformation enhances formability of the material considerably by expanding its failure limits up to 100%. It was concluded that the increase in failure limits of the preconsolidated SRPP is dependent to the induced deformation mode in the composite. To calculate failure limits of SRPP in shear region, a criterion incorporating principal strains and strain path was proposed. These path/history-dependent failure criteria are proposed for the first time to fill the gap for the lack of an accurate and trustworthy failure measure on woven composites. To elucidate the different failure mechanisms during stretch forming of $[0 \text{ deg}, 90 \text{ deg}]$ and $[45 \text{ deg}, -45 \text{ deg}]$ specimens, a new FLD applicable to $[45 \text{ deg}, -45 \text{ deg}]$ composite specimens was proposed and constructed. The outcomes showed that interlaminar shear between the plies of the composite and shear between the matrix and the woven structure are the main mechanisms of failure in $[45 \text{ deg}, -45 \text{ deg}]$ samples.

References

[1] European Commission of Energy, 2014, "Progress Towards Achieving the KYOTO and UE 2020 Objectives," Technical Report No. 1-2014-689.
 [2] Australian Government, Climate Change Authority, 2014, "Reducing Australia's Greenhouse Gas Emissions-Target and Progressive Review."
 [3] United States Environmental Protection Agency, 2015, "Inventory of U.S. Greenhouse Gas Emissions and Sinks," Report No. EPA 430-R-15-004.

[4] National Research Council, 2010, *Technologies and Approaches to Reducing the Fuel Consumption of Medium-and Heavy-Duty Vehicles*, National Academies Press, Washington, DC, Chap. 2.
 [5] EU-Directive, 2000, "Directive 2000/2053/EC," <http://eur-lex.europa.eu>
 [6] Pihliti, H., and Tosun, N., 2002, "Investigation of the Wear Behaviour of a Glass-Fibre-Reinforced Composite and Plain Polyester Resin," *Compos. Sci. Technol.*, **62**(3), pp. 367–370.
 [7] Radvan, B., and Till, A., 1987, "Fibre Reinforced Composite Plastics Material," U.S. Patent No. 4690860.
 [8] "BMW Co.," <http://www.bmwgroup.com>
 [9] Abot, J. L., Gabbai, R. D., and Harsley, K., 2001, "Effect of Woven Fabric Architecture on Interlaminar Mechanical Response of Composite Materials: An Experimental Study," *J. Reinf. Plast. Compos.*, **30**(24), pp. 2003–2014.
 [10] Fokker Co., "New Evolution: Progress in Thermoplastic Composites," <http://www.fokker.com>
 [11] Biron, M., 2007, *Thermoplastics and Thermoplastic Composites*, Elsevier Publication, New York, Chap. 6.
 [12] Ashby, F. A., and Jones, D. R. H., 2006, *Engineering Materials 2: An Introduction to Microstructure, Processing and Design*, 3rd ed., Pergamon Press, New York, Chap. 28.
 [13] Tan, H., and Yao, Y. L., 2013, "Laser Joining of Continuous Glass Fiber Composite Preforms," *ASME J. Manuf. Sci. Eng.*, **135**(1), p. 011010.
 [14] Mosse, L., Cantwell, W. J., Cardew-Hall, M. J., Compston, P., and Kalyanasundaram, S., 2005, "The Effect of Process Temperature on the Formability of Fibre-Metal Laminates," *Composites, Part A*, **36**(8), pp. 1158–1166.
 [15] Mosse, L., Cantwell, W. J., Cardew-Hall, M. J., Compston, P., and Kalyanasundaram, S., 2005, "A Study of the Effect of Process Variables on the Stamp Forming of Rectangular Cups Using Fibre-Metal Laminate Systems," *J. Adv. Mater.*, **6–8**, pp. 649–656.
 [16] Mosse, L., Cantwell, W. J., Cardew-Hall, M. J., Compston, P., and Kalyanasundaram, S., 2006, "The Development of a Finite Element Model for Simulating the Stamp Forming of Fibre-Metal Laminates," *Compos. Struct.*, **75**(1–4), pp. 298–304.
 [17] Mosse, L., Cantwell, W. J., Cardew-Hall, M. J., Compston, P., and Kalyanasundaram, S., 2006, "Stamp Forming of Polypropylene Based Fibre-Metal Laminates: The Effect of Process Variables on Formability," *J. Mater. Process. Technol.*, **172**(2), pp. 163–168.
 [18] Sexton, A., Cantwell, W. J., and Kalyanasundaram, S., 2012, "Stretch Forming Studies on a Fibre Metal Laminate Based on a Self-Reinforcing Polypropylene Composite," *Compos. Struct.*, **94**(2), pp. 431–437.
 [19] Zanjani, N. A., Sexton, A., and Kalyanasundaram, S., 2015, "Induced Forming Modes in a Pre-Consolidated Woven Polypropylene Composite During Stretch Forming Process at Room Temperature. I—Experimental Studies," *Composites, Part A*, **68**, pp. 251–263.
 [20] Davey, S., Das, R., Cantwell, W. J., and Kalyanasundaram, S., 2013, "Forming Studies of Carbon Fibre Composite Sheets in Dome Forming Processes," *Compos. Struct.*, **97**, pp. 310–316.
 [21] Romhányi, G., Bányai, T., Czizgány, T., and Kocsis, J. K., 2007, "Fracture and Failure Behavior of Fabric-Reinforced All-Poly(Propylene) Composite (Cur[®])," *Polym. Adv. Technol.*, **18**(2), pp. 90–96.
 [22] Li, S., He, J., Xia, C., Zeng, D., and Hou, B., 2014, "Bifurcation Analysis of Forming Limits for an Orthotropic Sheet Metal," *ASME J. Manuf. Sci. Eng.*, **136**(5), p. 051005.
 [23] He, J., Xia, C., Li, S., and Zeng, D., 2013, "M-K Analysis of Forming Limit Diagram Under Stretch-Bending," *ASME J. Manuf. Sci. Eng.*, **135**(4), p. 041017.
 [24] Hinton, M. J., Kaddour, A. S., and Soden, P. D., 2004, *Failure Criteria in Fibre-Reinforced-Polymer Composites*, Elsevier Publications, Oxford, UK, Chap. 6.1.
 [25] Kaddour, A. S., Hinton, M. J., Smith, P. A., and Li, S., 2013, "A Comparison Between the Predictive Capability of Matrix Cracking, Damage and Failure Criteria for Fibre Reinforced Composite Laminates: Part A of the Third World-Wide Failure Exercise," *J. Compos. Mater.*, **47**(20–21), pp. 2749–2779.
 [26] Propex Fabrics Co., "Cur—What Will You Make of It," <http://www.curvonline.com>
 [27] Gom Co., "Gom," <http://www.gom.com>
 [28] Launay, J., Hivet, G., Duong, A. V., and Boisse, P., 2008, "Experimental Analysis of the Influence of Tensions on in Plane Shear Behaviour of Woven Composite Reinforcements," *Compos. Sci. Technol.*, **68**(2), pp. 506–515.
 [29] Dridi, S., Dogui, A., and Boisse, P., 2010, "Finite Element Analysis of Bias Extension Test Using an Orthotropic Hyperelastic Continuum Model for Woven Fabric," *J. Text. Inst.*, **102**(9), pp. 781–789.
 [30] Selezneva, M., Montesano, J., Fawaz, Z., Behdinan, K., and Poon, C., 2011, "Microscale Experimental Investigation of Failure Mechanisms in Off-Axis Woven Laminates at Elevated Temperatures," *Composites, Part A*, **42**(11), pp. 1756–1763.
 [31] Hosseinzadeh, R., Shokrieh, M. M., and Lessard, L. B., 2005, "Parametric Study of Automotive Composite Bumper Beams Subjected to Low-Velocity Impacts," *Compos. Struct.*, **68**(4), pp. 419–427.

A comparison between forming behaviours of two woven thermoplastic composites

In previous chapters formability of a pre-consolidated self-reinforced polypropylene composite was investigated. SRPP specimens with different fibre orientations and aspect ratios were stretch formed to study failure of the composite under a wide range of deformation modes. In the current chapter, a benchmarking study was conducted to compare formability and failure of woven composites reinforced with different textile materials.

For the purpose of the comparison, two woven thermoplastic composites were selected: a self-reinforced polypropylene composite (SRPP) and a glass-fibre reinforced polypropylene composite (GRPP), both with a 55% fibre volume fraction. Composite specimens with different aspect ratios were stretch formed in a die equipped with a built-in lock ring system using a 100 mm diameter hemispherical punch head. Loads and displacements of the punch head was measured using a load cell and a linear transducer, respectively. Deformations were recorded by an in-situ three-dimensional photogrammetry system using a Digital Image Correlation (DIC) technique (ARAMIS). Strains and their evolutions on the surface of specimens were calculated using built-in algorithm of the ARAMIS. Varying dimensions and the imposed boundary conditions caused specimens to fail under different deformation modes. Distinct properties of reinforcements used in the two composites induced different failure mechanisms in GRPP and SRPP composites under similar forming conditions.

For this study, 16 different pre-consolidated specimens of each composite were formed into a double curved surface by a hemispherical punch. The strain evolutions at three

different locations on surface of specimens were recorded and compared: Pole (intersection of symmetry axes of samples), a point along the horizontal axis with 30 mm distance from the pole and a point on an orthogonal 45° axis 30 mm away from the pole. Evolution of strains revealed three different stages of deformation based on contact conditions between samples and the punch: (1) lock-ring stage caused by fixing specimens in the lock ring which induced a deformation mode as a function of the width and Poisson's ratio of materials. In narrow samples, the induced deformation mode was close to uniaxial extension while by increasing the width, deformation mode moved toward biaxial stretch, (2) Initial contact stage caused slightly different deformation modes in samples due to localised deformation in samples. The deformation mode was a function of aspect ratio and stiffness of the materials, and (3) Final contact induced distinctly different deformation modes dictated by the aspect ratio of samples, boundary conditions and the punch geometry. Differences between strain paths at the pole of SRPP and GRPP composites were associated to their dissimilar material properties.

The experimental results revealed that mechanical properties of reinforcements have pronounced effects on formability and failure behaviour of woven composites. The site of fracture was studied using an optical microscope to elucidate the different failure mechanisms between the two woven composites. It was found that the main mode of failure in a GRPP composite is fibre fracture while failure in SRPP is a complex phenomenon involving different failure mechanisms.

Major findings of this manuscript can be summarised as:

- GRPP composite is highly sensitive to the strain path and as such its formability can be greatly increased by a drastic change in the strain path,
- SRPP composite is less sensitive to strain path and its formability can be enhanced by a change in the deformation mode,

- Major forming mechanism resulting in higher forming depth in GRPP is trellising of the woven reinforcement as opposed to matrix shearing in SRPP,
- SRPP composite can sustain large deformation before catastrophic failure event while GRPP composite experience gradual fracture of fibres during deformation leading to total failure of the composite at the last stage of deformation,
- A combination of aspect ratio, fibre orientation and boundary condition can be used to enhance formability of woven composites in pre-consolidated state by hampering premature failure event due to fibre fracture.

A Comparison between Forming Behaviours of Two Pre-Consolidated Woven Thermoplastic Composites

N. A. Zanjani, S. Kalyanasundaram

Research School of Engineering, ANU College of Engineering and Computer Science, Australian National University, Canberra, Australia
Email: nima.akhavan@anu.edu.au

Received 26 June 2015; accepted 9 July 2015; published 16 July 2015

Abstract

This paper presents the results of an investigation on stretch forming behaviour of two consolidated woven thermoplastic composites: a self-reinforced polypropylene (SRPP) and a glass-fibre reinforced polypropylene (GRPP) composite. A custom-built press with a hemispherical punch was employed to deform composites' specimens possessing different aspect ratios into an open die. The induced strains on the outer surface of specimens were measured continuously through two high speed, high resolution CCD cameras by employing a Digital Image Correlation (DIC) technique. The strain paths at three different locations on the surface of specimens were compared to elucidate the effect of fibre and matrix on the formability of a woven composite. The fractured surface of specimens was investigated to reveal the effect of fibre mechanical properties on failure morphologies in woven composites. It was found out that the main mode of failure in GRPP is fibre fracture while observed failure morphologies in SRPP were a complex combination of different failure mechanisms. It was revealed that the combination of applied boundary conditions and specimen's width determines the effective forming mechanisms.

Keywords

Woven Composite, Stamp Forming, Self-Reinforced Polypropylene, Glass-Fibre Reinforced Polypropylene, Failure

1. Introduction

Anthropological climate changes, excessive exploitation of fossil fuels and weight reduction of products are main drivers behind extensive research on finding new material systems. Automotive industry has been continuously cited as one of the major contributors of the human interventions on the environment [1]. The global automotive market, already passed 1 billion fleets in service with an annual increase of 77 million cars, accounts for 40% of fuel consumptions and 27% of CO₂ emissions worldwide [1] [2]. On average, each car consumes 7 l/km petrol and emits 136 g/km CO₂. A weight reduction of 100 kg results in 5% saving in fuel consumption and

How to cite this paper: Zanjani, N.A. and Kalyanasundaram, S. (2015) A Comparison between Forming Behaviours of Two Pre-Consolidated Woven Thermoplastic Composites. *Journal of Materials Science and Chemical Engineering*, 3, 180-189. <http://dx.doi.org/10.4236/msce.2015.37024>

4.5% reduction in CO₂ emissions for every 100 km of transportation [3]. These figures necessitate reducing weight of vehicles by employing lighter material systems to address environmental footprint issues while achieving higher efficiency and cost reduction targets.

Woven Thermoplastic Composite Materials (WTPCMs) offer attractive properties including very low specific density, improved impact resistance, higher fatigue durability and ease of manufacturing [4] [5]. Moreover, they benefit from a unique polymeric structure that allows them to be re-melted and re-shaped after initially consolidated. These properties make them suitable candidates to be employed in the automotive industry to address sustainability and recyclability issues. However, the current manufacturing techniques applied to composites, such as moulding and hand lay-up, has suppressed their widespread application due to the complex and labour-intensive nature of manufacturing processes. Substitution of the current manufacturing techniques with more efficient methods encourages adopting woven composites in mass production industries to address environmental issues and achieve weight reduction targets.

Stamp forming has been extensively studied and applied on metals [6]-[8]. This manufacturing method employs a press equipped with a punch, a die and a blank holder system to deform sheets into desired geometries. Advantages of stamp forming in manufacturing parts include cost-effectiveness, high production rate and precision manufacturing. Although stamp forming of woven prepreps has been studied in numerous works [9]-[11], formability of pre-consolidated WTPCMs, as a current research initiative [12]-[18], still requires extensive investigations. The current article studies stamp forming of two pre-consolidated woven thermoplastic composites: a self-reinforced polypropylene composite and a glass-fibre reinforced polypropylene composite. Specimens possessing different geometries were stamp formed via a hemispherical punch in an open die. Evolution of principal strains and their distributions on the surface of samples were measured through an optical strain measurement system. The strain paths at three different locations were studied to reveal the effect of fibres and the matrix on the forming behaviour of a woven composite. Finally, different fracture morphologies in the two WTPCMs were compared and the underlying causes for this behaviour was discussed and then validated based on force-displacement curves of different specimens.

2. Experimental Procedures

2.1. Materials Systems and Specimen's Geometries

The two WTPCMs employed in the current study were constituted of an identical matrix reinforced by two different textile materials: a self-reinforced polypropylene composite (SRPP) and a glass-fibre reinforced polypropylene composite (GRPP). **Figure 1** illustrates a closed-up view from the structure of the two consolidated blanks made of these two material systems. The textile pattern of both composites was 2×2 twill weave structure. Both warp and weft yarns in the SRPP structure were straight, however one of the two orthogonal yarns in GRPP composite was curved. The SRPP composite was made by OCV reinforcements Co. [19] from multi-layered sheets of two structurally different polypropylene (PP) polymers stacked up together and consolidated via a hot compaction technique developed initially at Leeds University [20]. The GRPP composite, constituted from a single layer fabric of comingled glass fibre (GF) and PP fibre, was manufactured by Owens Corning Co. [21]. The manufacturing process of GRPP included heating up the commingled GF/PP fabric well beyond melting point of the PP fibres followed by cooling down process under low pressure to manufacture consolidated GRPP. A comparison between typical properties of the two woven composites is made in **Table 1**.

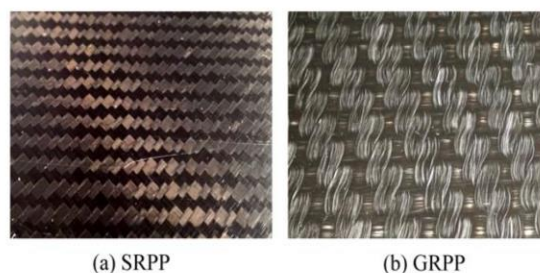


Figure 1. SRPP and GRPP specimens.

Table 1. Comparison between mechanical properties of the two woven composites [16] [18].

Mechanical properties	SRPP	GRPP
Density (g/cm ³)	0.92	1.5
Tensile modulus (GPa)	4	14
Tensile strength (MPa)	120	300
Flexural modulus (GPa)	3.5	12.5
Fibre volume fraction (%)	-	55%

2.2. Geometry of Specimens

The specimens were cut-out from initially circular 200 mm in-diameter blanks. The samples' widths (W in **Figure 2**) varied between 25 mm to 150 mm in 25mm increments. An additional full circular specimen with 200 mm diameter was made to reveal forming behaviours of the two composites under biaxial stretch. The thickness of all samples was 1 mm. General dimensions of specimens are shown in **Figure 2**. Each specimen is specified by a CWN parameter in which C specifies the type of WTPCM (S for SRPP and G for GRPP), W is an abbreviation of the Width and N is a number specifying the width of the sample. For instance, SW50 and GW100 represent a SRPP sample with 50mm width and a GRPP specimen with 100 mm width, respectively.

2.3. Experimental Equipment and Procedures

The samples were initially painted by a stochastic pattern of black dot spray on a white paint background to provide sufficient contrast required for strain measurements. After specimens were dried, they were fixed in an open die system. The die system was composed of upper and lower blank-holders by which the specimens were fully clamped along their circular circumferences through a built-in lock-ring. Then they were deformed until failure by a built-in press with 300 kN capacity equipped with a hemispherical punch. The applied force was measured by a load cell. Dimensions and configuration of the forming equipment are shown in **Figure 3**.

The displacements and induced strains were continuously measured by two CCD cameras installed beneath the open die (The ARAMIS) [22]. The strain measurement was started from the very early stages of the experiment to capture the effect of lock-ring on the blanks and to measure the induced strains during deformation of samples by the punch until failure. Fractured regions of specimens were examined through an optical microscopy system to elucidate different failure morphologies between SRPP and GRPP woven composites.

2.4. Deformation Modes in Forming

In a typical sheet forming practice different forming modes at different locations on the blank are induced. These deformation modes facilitate forming of raw material into desired geometry by incorporating different mechanisms during forming of the samples. It is a common practice to characterise induced deformation modes by the ratio of minor to major strains. Typical forming modes in a stamping process include: 1-Biaxial stretch (SR = +1) 2-Plane strain (SR = 0) 3-Uniaxial extension (SR = -0.5) 4-Shear deformation (SR = -1) 5-Wrinkling (SR = -2). The graphical representation of different strain paths in a strain space is depicted in **Figure 4**, in which vertical axis represents major strain and horizontal axis depicts minor strain. Generally, the forming path in metals is constant and considered as proportional as it does not experience abrupt changes. However, due to complex internal structure of woven composites, this hypothesis needs to be carefully investigated through experimental observations.

3. Results and Discussion

Results of stretch forming experiments on WTPCMs made of different textile reinforcements are discussed in this section. Initially, strain measurements conducted by the 3D photogrammetry system at three points on the surface of [0°, 90°] specimens are presented. The locations of these points are depicted in **Figure 5**. The Pole is located at the intersection of horizontal and vertical symmetry axes of specimens, P1 is located X mm further from the pole on the warp (longitudinal) fibres and P2 is located X mm away from the pole along the 45° orien-

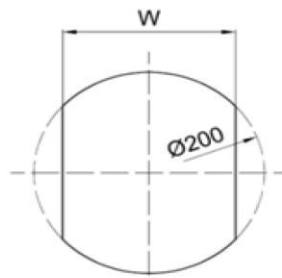


Figure 2. Dimensions of woven composite specimens.

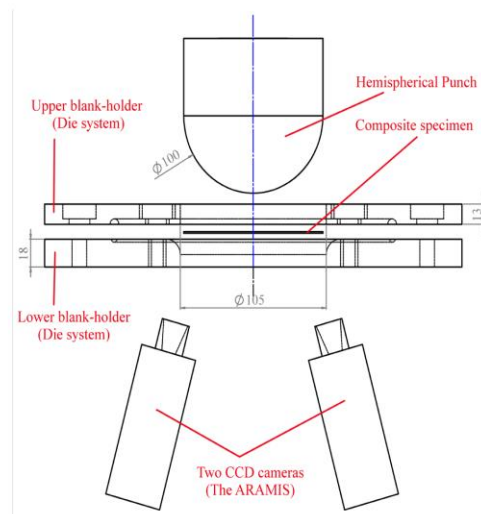


Figure 3. Configuration of stretch forming equipment and measurement system.

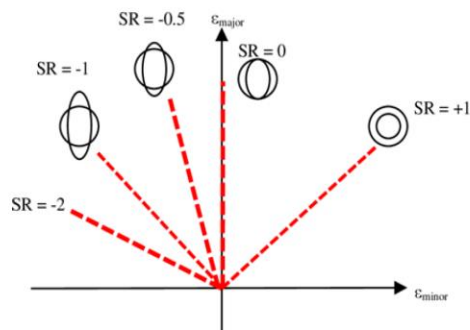


Figure 4. Main deformation modes during sheet forming.

tation. The value of X , dependent to the sample's width, is mentioned later. These points are representative of different forming behaviours of a WTPCM at different regions specified by different contact evolution, fibre extension and shear behaviour and therefore elucidate formability of a pre-consolidated woven composite under different deformation modes.

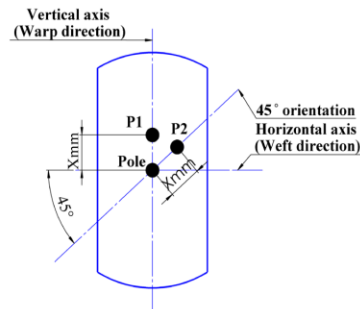


Figure 5. Points of interest on WTPCM specimen.

3.1. Strain Path at Points of Interests

It is beneficial to examine different stages of deformations based on the contact conditions between samples and the punch and to correlate between the evolution of strain path at the pole and the depth of deformation induced by a hemispherical punch. Generally, three stages of deformation during stretch forming of a woven composite can be distinguished (Figure 6).

1-Lock-ring effect (edge-effect): This stage is caused by the lock-ring system during clamping of specimens. The gradient of the strain path and therefore the induced deformation mode is a function of specimen's width and the material's Poisson's ratio. In narrow samples, the induced deformation mode is near to uniaxial extension and in the widest sample it is close to biaxial stretch. The induced principal strains in this stage are very low compared to the total strains induced by the punch due to comparatively low clamping torque applied to specimens. **2-Initial contact:** The mode of deformation induced in this stage is a function of specimen's aspect ratio and the material's stiffness. In a woven composite with a relatively low stiffness (compared to metals), the induced mode of deformation is near to biaxial stretch due to the localised contact between punch and the blank, identical extension of both warp and weft yarns and the highly localised deformation and strain concentration during contact with a hemispherical punch. **3-Final contact:** At this stage, the biaxial stretch mode disappears and the sample's specific deformation mode, determined by the specimen's aspect ratio and the punch geometry, governs its forming behaviour. Due to the enforced boundary condition, the contact surface between the specimen and the punch along warp and weft directions are not identical and therefore friction force along warp is more than of weft direction. However, increase of the forming depths results in a similar contact surface along the two orthogonal directions and therefore causes a gradual shift in the induced deformation mode leading to failure. This point is depicted by point C in Figure 6. Another factor, changing strain path after point C, is the evolution of material properties by the applied strains. Figure 6 illustrates these stages of deformation in the strain path of a typical WTPCM.

To represent different forming behaviours of SRPP and GRPP specimens, three specimens from each group is selected: SW25, SW75, SW150, GW25, GW75 and GW150. It will be shown that a change in specimen's width alters the deformation mode under which the material fails (deformation mode in final stage of deformation). This behaviour is caused by a combination of different phenomena: Larger specimens, possessing bigger mass, have enough material to deform into the die cavity and therefore can potentially sustain larger forming depths. However, increase in the width of samples causes the ratio of clamped length to the total circumference of the sample enlarges and therefore the forming depths decrease due to the enforced boundary condition. The synergy between these two factors makes a balance between draw and stretch behaviours of samples and therefore determines the forming depth at which specimens fracture. Three different points on the surface of each SRPP and GRPP specimens were selected to study behaviour of these materials under different forming mechanisms: Pole, P1 and P2 (Figure 5). In this figure, X is equal to 10mm in W25 samples and 30mm in larger specimens. Pole is located at the intersection of two symmetry axes of the specimens where warp and weft yarns intersect and therefore determines the forming limits of the material under the influence of both orthogonal yarns. The behaviour of specimens at P1 is mainly influenced by the extension of the longitudinal (warp) yarns and P2 exhibits the specimen's formability under combined matrix shearing and fabric trellising mechanisms. Figures 7-9 com-

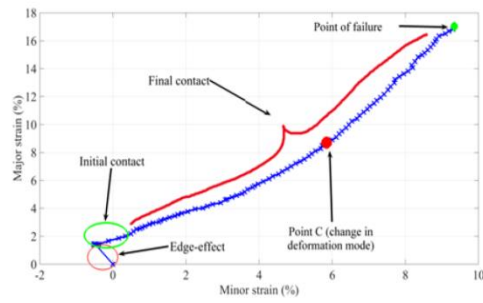


Figure 6. Different stages of deformation during stretch forming of a woven composite (SW150).

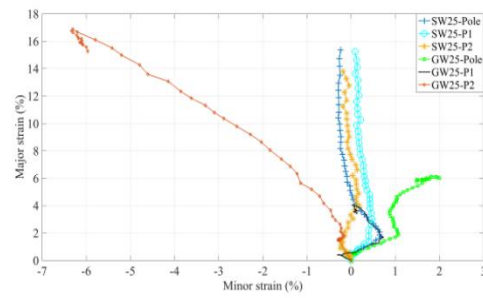


Figure 7. Induced principal strains on SW25 and GW25 specimens.

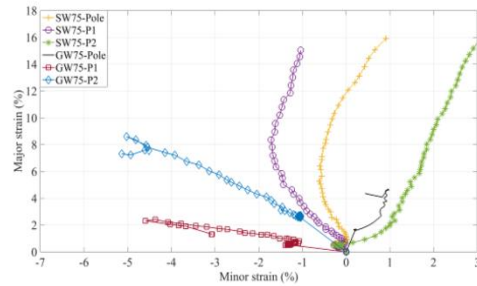


Figure 8. Induced principal strains on SW75 and GW75 specimens.

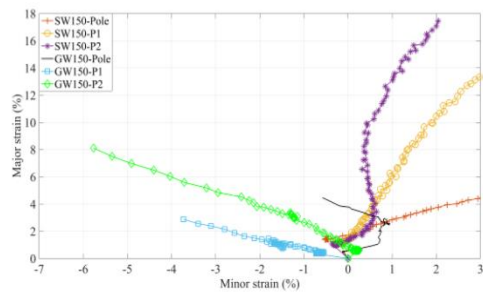


Figure 9. Induced principal strains on SW125 and GW125 specimens.

pare forming behaviours of the two material systems at different depths of deformation in specimens possessing 25 mm, 75 mm and 150 mm widths, respectively.

In **Figure 7**, all three surface points of SW25 exhibit near to uniaxial extension mode, followed up by a near to biaxial stretch mode during the lock-ring and initial contact stages of deformation. The final deformation modes is located between uniaxial extension and plane strain modes, dictated by the contact between punch and the sample counteracting Poisson's effect in inducing negative minor strain along weft (transverse) direction. The similarity between induced strain ratios at these three locations elucidates the insensitivity of the deformation mode in these SRPP specimens to the location. However, in the GRPP composite, the location of the points shows a significant effect on the induced strain path. The final deformation mode at the pole initially follows a uniaxial extension path which is abruptly changed to biaxial stretch. This behaviour is specific to woven composites reinforced with highly inextensible, brittle fibres: increase of punch penetration rises the contact pressure between the blank and the punch leading to sudden localised fracture of glass fibres at the pole which changes the strain path. However, at point P1, this behaviour is not observed due to a decreased contact pressure between the blank and the punch at this location. At point P2, excessive shearing of the fabric (trellising) causes the strain path at GW25-P2 to follow shear deformation mode. The dissimilar strain path at point P2 in SRPP and GRPP specimens profoundly highlights the fundamental differences between manufacturing processes of the two composites and the different interface properties between fibres and the matrix leading to dissimilar mechanical behaviours of the two woven composites.

The W75 specimens show completely different forming behaviours, compared to W25 samples, as a result of having different aspect ratios (**Figure 8**). This is due to a completely different trend in the evolution of contact surface between punch and specimens, resulting in a more distinguished difference between strain path at the pole, P1 and P2. However, the gradient of the strain path at the final stage of deformation for the three points on SW75 specimens is similar, in contrast to GW75 specimens, re-emphasizing the fundamental differences between the structures of the two WTPCMs.

All points on SW150 specimens show a biaxial stretch mode at the final stage of the deformation due to the applied boundary conditions and specimens' widths (**Figure 9**). However, in GW150 sample, the pole shows a near to biaxial stretch mode until onset of localised fracture of glass fibres, while points P1 and P2 depict shear deformation mode. However, point P2 shows much higher strains compared to all other points due to excessive trellising of the glass-fibres, delaying the initiation of fracture in GRPP composite by hampering fibre extension.

3.2. Fracture of SRPP and GRPP Composites during Stretch Forming

Different strain paths and their evolutions in the two WTPCMs depict different formability characteristics of these material systems under stretch forming conditions. This is resulted from different reinforcements, dissimilar matrix-fibre interface and manufacturing processes applied to the two composites. In this section, the effects of these parameters on failure morphologies of the two composites are investigated. **Figure 10** and **Figure 11**

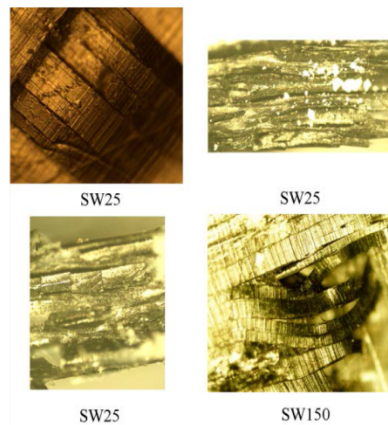


Figure 10. Failure morphologies in SRPP specimens.

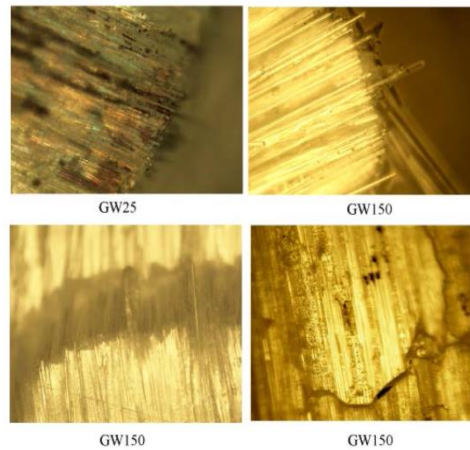


Figure 11. Failure morphologies in GRPP specimens.

reveal optical microscopy results on two typical SRPP and GRPP samples, respectively. Longitudinal crack growths and rupture of the yarns are observed in SRPP specimens. These phenomena show mode I of fracture or tensile opening at the matrix-fibre interface. Delamination is another dominant failure mode in SRPP specimens. Matrix thinning is also observed which can be regarded as a pseudo-plastic behaviour of the material. Transverse cracks are developed through the thickness of the SRPP specimens. At some locations, fibre kinking is also observed due to highly localised compressive strains.

On the other hand, the dominant failure mode in GRPP specimens is fibre fracture. The even fractured surface of these specimens shows that fibre pull-out due to yielding of the material at the fibre-matrix interface has not occurred and the failure sites predominantly exhibit a rough fractured surface on the GRPP composite due to its brittle nature. Fracture is caused by inextensibility of glass fibres and its brittle behaviour. These microscopy images show different failure mechanisms of the two WTPCMs: The SRPP failure is more complex than GRPP as a result of complex interactions between reinforcement and the matrix, their identical mechanical properties and fusion of fibres and the matrix at their interface. However, in a GRPP composite, inextensibility of glass fibres and completely different mechanical properties of the reinforcement and the matrix makes the fibre fracture to be the main reason of the failure. However, the strain path evolution of GRPP specimens reveals the gradual onset of failure during conformity of the samples to the punch.

Studying force-displacement graphs of the two WTPCMs during stamping reveals the fundamental differences between the responses of these material systems to out-of-plane loading and re-emphasizes on the previous assumptions on failure mechanisms of the two composites based on microscopy observations. **Figure 12** represents stamping force (in kN) versus depth of deformation (in mm) of three different SRPP and GRPP specimen until failure. Depth of deformation for SRPP is generally twice as of GRPP composite, resulted from high extensibility PP polymer fibres.

The force-displacement of SRPP shows a smooth, exponentially increasing trend with a gradual increase in the material's resistance to deform further. This behaviour can be related to the woven structure of the composite in which the orthogonal yarns support each other during application of external loadings and the internal friction between these yarns increases as the contact pressure between punch and the blank rises. A sudden drop in force at the final stage of deformation is observed which indicates the catastrophic failure of the SRPP composite. The aspect ratio of the SRPP composite does not affect the final depth of deformation drastically. The GRPP response to external loadings is completely different: the aspect ratio greatly affects the forming depth highlighting the stronger support of orthogonal yarns during stamping. The narrowest sample (GW25) deforms up to the depth 15mm, while the largest GRPP specimen (GW150) deforms twice of GW25. Secondly, the recurrent decrease in the slope of force-displacement curve indicates the gradual fracture of the glass-fibres and re-validates the precious assumption on the main cause of fracture in GRPP composite during stamp forming.

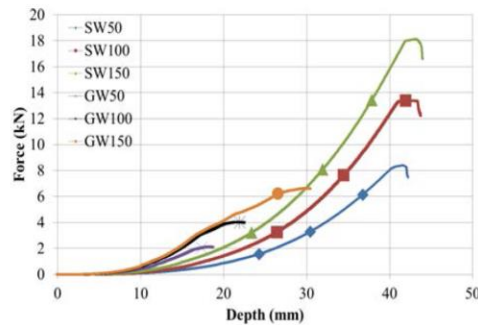


Figure 12. Comparison between force-displacement curve of two WTPCMs during forming.

4. Conclusions

Specimens of two consolidated woven composites possessing different aspect ratios were stretch formed with a hemispherical punch. The induced deformations were measured through a 3D photogrammetry system and the strains were calculated. Comparison between strain paths at different locations on samples revealed the following fundamental differences between stamp-forming behaviours of the two composites:

- Higher sensitivity of strain ratio and therefore induced deformation modes to the location in GRPP composite compared to SRPP composite.
- Significant higher formability of GRPP composite under shear deformation mode.
- Pure trellising of GRPP at $\pm 45^\circ$ directions compared to more matrix shearing in SRPP.
- Catastrophic failure of SRPP compared to gradual and localised fibre fracture of GRPP.
- The combination of specimen's width and applied boundary condition is a determinant factor on the formability of a woven composite.

The optical microscopy examination on the site of failure revealed the main cause of failure in GRPP composite is fibre fracture while failure phenomena in SRPP composite is a complex mixture of different mechanisms including fibre pull-out, shearing of the matrix and delamination. The different failure behaviours of the two WTPCMs were well reflected in their force-displacement curves, re-emphasizing the effect of reinforcements' mechanical properties on the failure mechanism of a woven composite. The investigations on forming of the two consolidated woven composites show their great potential to be formed into different geometries through stamping process and therefore to be employed in producing cost-effective, mass produced components.

References

- [1] Kastensson, G.A. (2014) Developing Lightweight Concepts in the Automotive Industry: Taking on the Environmental Challenge with the SÄNÄtt Project. *Journal of Cleaner Production*, **66**, 337-346. <http://dx.doi.org/10.1016/j.jclepro.2013.11.007>
- [2] Mayyasa, A., Qattawia, A., Omara, M. and Shana, D. (2012) Design for Sustainability in Automotive Industry: A Comprehensive Review. *Renewable and Sustainable Energy Reviews*, **16**, 1845-1862. <http://dx.doi.org/10.1016/j.rser.2012.01.012>
- [3] International Council of Clean Transportation (ICCT) (2013) Reducing CO₂ and Fuel Consumption from New Cars: Assessing the Near-Term Technology Potential in the EU. <http://www.theicct.org>
- [4] Reyes, G. and Sharma, U. (2010) Modeling and Damage Repair of Woven Thermoplastic Composites Subjected to Low Velocity Impact. *Composite Structures*, **92**, 523-531. <http://dx.doi.org/10.1016/j.compstruct.2009.08.038>
- [5] Karakuzua, R., Aslanb, Z. and Okutan, B. (2004) The Effect of Ply Number, Orientation Angle and Bonding Type on Residual Stresses of Woven Steel Fiber Reinforced Thermoplastic Laminated Composite Plates Subjected to Transverse Uniform Load. *Composites Science and Technology*, **64**, 1049-1056. <http://dx.doi.org/10.1016/j.compscitech.2003.09.014>
- [6] Keeler, S.P. (1990) Automotive Sheet Metal Formability. National Steel Corporation, Product Application Center, Technical Report AU 89-1.

- [7] Tekkaya, A.E. (2000) State-of-the-Art of Simulation of Sheet Metal Forming. *Journal of Materials Processing Technology*, **103**, 14-22. [http://dx.doi.org/10.1016/S0924-0136\(00\)00413-1](http://dx.doi.org/10.1016/S0924-0136(00)00413-1)
- [8] Makinouchi, A. (1996) Sheet Metal Forming Simulation in Industry. *Journal of Materials Processing Technology*, **60**, 19-26. [http://dx.doi.org/10.1016/0924-0136\(96\)02303-5](http://dx.doi.org/10.1016/0924-0136(96)02303-5)
- [9] Van West, B.P., Byron Pipes, R., Keefe, M. and Advani, S.G. (1991) The Draping and Consolidation of Commingled Fabrics. *Composites Manufacturing*, **2**.
- [10] Badel, P., Gauthier, S., Vidal-Sallé, E. and Boisse, P. (2009) Rate Constitutive Equations for Computational Analyses of Textile Composite. *Composites: Part A*, **40**, 997-1007. <http://dx.doi.org/10.1016/j.compositesa.2008.04.015>
- [11] Sargent, J., et al. (2010) Benchmark Study of Finite Element Models for Simulating the Thermostamping of Woven-Fabric Reinforced Composites. *International Journal of Material Forming*, **3**, 683-686. <http://dx.doi.org/10.1007/s12289-010-0862-5>
- [12] Zanjani, N.A. and Kalyanasundaram, S. (2015) Induced Forming Modes in a Self-Reinforced Polypropylene Sheet during Stretch Forming Process at Room Temperature: I-Experimental Studies. *Composites Part A*, **68**, 251-263. <http://dx.doi.org/10.1016/j.compositesa.2014.09.023>
- [13] Zanjani, N.A., Wang, W. and Kalyanasundaram, S. (2015) The Effect of Fibre Orientation on the Formability and Failure Behaviour of a Woven Self-Reinforced Composite during Stamp Forming. *ASME Journal of Manufacturing Science and Engineering*, in Press.
- [14] Wang, W., Lowe, A., Davey, S., Zanjani, N.A. and Kalyanasundaram, S. (2015) Establishing a New Forming Limit Curve for a Flax Fibre Reinforced Polypropylene Composite through Stretch Forming Experiments. *Composites Part A*, in Press. <http://dx.doi.org/10.1016/j.compositesa.2015.06.021>
- [15] Davey, S., Das, R., Cantwell, W.J. and Kalyanasundaram, S. (2013) Forming Studies of Carbon Fibre Composite Sheets in Dome Forming Processes. *Journal of Composite Structures*, **97**, 310-316. <http://dx.doi.org/10.1016/j.compstruct.2012.10.026>
- [16] Compston, P., Cantwell, W.J., Cardew-Hall, M.J., Kalyanasundaram, S. and Mosse, L. (2004) Comparison of Surface Strain for Stamp Formed Aluminium and Aluminium-Propylene Laminate. *Journal of Material Science*, **39**, 6087-6088. <http://dx.doi.org/10.1023/B:JMSE.0000041707.68685.72>
- [17] Kalyanasundaram, S., Dhar Malingam, S., Venkatesan, S. and Sexton, A. (2012) Effect of Process Parameters during Forming of Self-Reinforced PP-Based Fibre Metal Laminates. *Composite Structures*, **97**, 332-337. <http://dx.doi.org/10.1016/j.compstruct.2012.08.053>
- [18] Mosse, L., Compston, P., Cantwell, W.J., Cardew-Hall, M.J. and Kalyanasundaram, S. (2006) Stamp Forming of Polypropylene Based Fibre-Metal Laminates: The Effect of Process Variables on Formability. *Journal of Materials Processing Technology*, **172**, 163-168. <http://dx.doi.org/10.1016/j.jmatprotec.2005.09.002>
- [19] CV Reinforcement Co. www.ocvreinforcements.com
- [20] Ward, I.M. and Hine, P.J. (2004) The Science and Technology of Hot Compaction. *Journal of Polymer*, **45**, 1413-1427. <http://dx.doi.org/10.1016/j.polymer.2003.11.050>
- [21] Owens Corning Co <http://fiberglassindustries.com>
- [22] GOM mbH. www.GOM.com

Development of a nonlinear material model for woven composites

In previous chapters, experimental forming studies were carried out to study forming and failure behaviours of a consolidated woven SRPP composite under stretch forming conditions. As a result, a strain-based failure model was developed to elucidate failure envelope of the SRPP composite under a wide range of deformation modes. In this chapter, characterisation experiments on a SRPP composite are conducted and a nonlinear orthotropic material model is developed. Constitutive stress-strain relation is implemented into an implicit numerical scheme to predict formability of the composite using a finite element simulation.

The proposed numerical model is adopted to predict strain evolution of the composite under different deformation modes. After confirming validity of finite element predictions with experimental outcomes, the numerical model was employed to study the effects of friction condition and mechanical property variations on formability and strain path of the composite. It was shown that in narrow samples the Poisson's ratio and friction coefficient have major effects on the strain evolution on the surface of the composite. On the other hand, shear stiffness and Young's modulus have a detrimental impact on formability of wider specimens.

In this chapter, a complete set of mechanical characterisation experiments were conducted on consolidated woven SRPP composite. These tests included uniaxial and bias extension tests using a universal testing machine, dynamic extensometers, and a 3D real time strain measuring system. Characterisation experiments were conducted under ASTM D3039 standard procedure designed for polymer matrix composite materials. Experimental

outcomes were used to define material properties of the composite including Young's modulus, Poisson's ratio and shear stiffness as functions of fibre strain. Due to highly nonlinear behaviour of transverse to longitudinal strain of SRPP, the conventional Poisson's ratio was replaced with a novel definition based on an incremental deformation theory. In the new definition of Poisson's ratio, it is represented as the instantaneous gradient of transverse to longitudinal strains during deformation.

The composite was modelled as an orthotropic, transversely isotropic material and all independent material constants were defined as function of fibre strains. The characterisation experiment results were used to develop constitutive stress-strain relations for the SRPP composite. The material model was incorporated into a finite element software (Abaqus/implicit) to predict stamp forming behaviour of SRPP composite under different deformation modes. Numerical simulation was used to study the effect of material properties and friction condition between punch and specimen on strain path at the pole of specimens. Using numerical simulation results, the evolution of shear strain at different depths of deformation was revealed and a profound understanding on the formability of a woven composite was revealed. It was shown that shear deformation contributes significantly in forming of a thin sheet made of a consolidated woven composite.

Stretch Forming Simulation of Woven Composites Based on an Orthotropic Non-Linear Material Model

N. A. Zanjani, S. Kalyanasundaram

Research School of Engineering, ANU College of Engineering and Computer Science, Australian National University, Canberra, Australia
Email: nima.akhavan@anu.edu.au

Received 26 June 2015; accepted 9 July 2015; published 16 July 2015

Abstract

Characterisation experiments have been conducted on a woven self-reinforced polypropylene composite (SRPP) including uniaxial and bias extension tests. Outcomes of these experiments were employed to develop a non-linear orthotropic material model within an incremental deformation framework. The material model of the woven composite was implemented into a finite element simulation to predict stretch forming behaviour of SRPP specimens. The predicted strain paths at the pole of specimens were verified against experimental outcomes. It was shown that specimens possessing different aspect ratios deform under a wide range of deformation modes from uniaxial extension to biaxial stretch modes. Finally, the effect of different forming parameters on the strain path evolution of the woven composite was elucidated through numerical simulations. It was shown that the aspect ratio of the samples plays an important role in forming behaviour of woven composites. Development of a reliable and accurate numerical model for predicting forming behaviour of woven composites and understanding their main forming mechanisms promote and encourage the extensive application of these materials systems in a wide range of mass producing industries. Adopting woven composites in manufacturing industrial components facilitates addressing environmental concerns such as recyclability and sustainability issues.

Keywords

Woven Composite, Stretch Forming, Finite Element Analysis, Nonlinear Orthotropic Material

1. Introduction

Key criteria in developing new products include sustainability, recyclability and weight reduction. Published data [1] shows that the transportation industry accounts for 27% of the total Green House Gas (GHG) emissions solely in the United States. Results of analyses published by the institute of energy and environmental research [2] reveal that mass reduction of vehicles can substantially decrease CO₂ emission and fuel consumptions. Thus, weight reduction in vehicles is regarded as one of the major priorities in the mass production industries such as

How to cite this paper: Zanjani, N.A. and Kalyanasundaram, S. (2015) Stretch Forming Simulation of Woven Composites Based on an Orthotropic Non-Linear Material Model. *Journal of Materials Science and Chemical Engineering*, 3, 168-179. <http://dx.doi.org/10.4236/msce.2015.37023>

automotive industry [3]-[5].

Woven Thermoplastic Composite Materials (WTPCMs) have shown great potential to be employed in the automotive industry due to their attractive properties including high specific strength, excellent impact energy absorption and balanced in-plane thermomechanical properties [6] [7]. Furthermore, they can be melted and re-shaped after initially consolidated, making them suitable candidates to address recyclability issues. However, the components currently made from these material systems are produced through labour-intensive, complex manufacturing techniques, such as moulding and hands lay-up of prepregs, resulting in very low manufacturing rates and expensive final products, hampering their wide spread applications. These manufacturing processes are not suitable for mass producing industries, where cost-effective products and high production rates are essential. Stamp forming of pre-consolidated woven composites is an efficient method for mass production of this material system. Recent studies show the great potential of producing complex components from woven composites through stamp forming [8]-[13]. However, successful adoption of stamp forming on woven composites necessitates a thorough study on the formability of this class of composite materials.

Formability of unconsolidated woven composites (prepregs) has been studied extensively [14]-[17]. However, forming behaviour of pre-consolidated woven composites through stamp forming is a current research initiative which needs to be addressed properly. To investigate formability of pre-consolidated woven composites under different forming conditions numerical simulation is an effective tool that can substitute cumbersome trial and error method in finding efficient production procedure. In the current study, an orthotropic material model based on the outcomes of characterisation experiments on a woven self-reinforced polypropylene composite (SRPP) is developed within an incremental deformation theory framework. The developed model was implemented into a Finite Element Analysis (FEA) software program (ABAQUS/Implicit solver) through a User-defined Material subroutine (UMAT). The numerical simulation predictions were verified against experimental results on the strain evolution at the pole of different samples. The combined effects of samples' aspect ratios and forming parameters, including in-plane material stiffness and contact conditions, on the formability of a woven composite were elucidated. It was shown that the main forming parameters are dependent to the aspect ratio of a woven composite. The proposed nonlinear material model showed high capacity in predicting formability of a woven composite during rapid manufacturing processes and therefore offers good potential to be employed in the process of manufacturing industrial components.

2. Experimental Procedure

2.1. Material System

The pre-consolidated sheets of a multilayered 2/2 twill weave self-reinforced composite (SRPP) employed in the current study was manufactured by OCV reinforcements Co. [18] with 0.9 gm^3 volumetric density. Both reinforcements and the matrix were manufactured from a highly oriented semi-crystalline polypropylene polymer, making the final product to be completely recyclable. The woven fabric is manufactured from PP copolymers, made of two structurally different concentric cylinders of PP: a core made of α -PP polymer covered by β -PP polymer as the skin, in which the former has significantly higher melting temperature than the latter. Applying sufficient pressure and heat to the composite prepregs melts the skin of PP copolymer and constructs the matrix by embedding the unmelted β -PP reinforcement (selectively melting process). After cooling period, the consolidated multilayered SRPP composite sheets are produced.

2.2. Geometry of Specimens

In the current study, SRPP specimens with different aspect ratios (width-to-length ratios) were employed to characterise the woven composite and to study its forming behaviour at room temperature through two different sets of experiments:

1) Characterisation specimens: rectangular SRPP samples possessing $200 \text{ mm} \times 20 \text{ mm} \times 1 \text{ mm}$ (length, width and thickness) dimensions were employed to characterise the composite material through uniaxial extension and bias extension tests. The test procedure followed ASTM D3039 standard as the standard test procedure for characterisation of polymer matrix composites. Specimens possessing $[0^\circ, 90^\circ]$ fibre orientations were used in uniaxial extension tests to calculate longitudinal stiffness (Young's modulus or E) and Poisson's ratio (PR) of SRPP and samples with $[-45^\circ, +45^\circ]$ fibre orientations were employed to measure the shear stiffness (G) of the

SRPP composite through the bias extension test.

2) Stretch forming specimens: These specimens were cut-out from initially circular specimens of 200 mm in diameter. The samples' widths (W in **Figure 1**) varied between 12.5 mm to 200 mm. The thickness of samples was 1 mm. General dimensions of SRPP specimens are shown in **Figure 1**. Each specimen is depicted by WN parameter in which N exhibits the width of the sample. For example, $W50$ and $W200$ represent a semi-rectangular specimen with 50 mm width and a full circular specimen with 200 mm diameter, respectively.

2.3. Experimental Equipment and Procedures

Two different experiments were conducted to develop a nonlinear material model and to evaluate the accuracy of the numerical model in predicting the stretch forming behaviour of SRPP composite:

1) Characterisation experiments: Two sets of experiments were conducted to characterise the SRPP composite including uniaxial and bias extension tests. The former was employed to characterise composite mechanical response to unidirectional loadings along the fibres, to calculate modulus of elasticity as a function of longitudinal strain and to evaluate Poisson's ratio (PR) of the woven composite. The latter was designed to characterise the shear stiffness of the material by uniaxially extending $[-45^\circ, +45^\circ]$ SRPP specimens in a bias extension test. The equipment included a universal testing machine (INSTRON 8874) to extend SRPP samples and to measure the force by a load cell and a CCD camera for recording deformations and calculating strains during deformations.

2) Stretch forming experiments: This set of experiment was designed and conducted on a variety of $[0^\circ, 90^\circ]$ specimens to study their forming behaviours under different forming paths specified by the ratio of minor to major strains. Forming equipment included: a custom-built press with 300 kN capacity, a hemispherical punch, an open die with a built-in lock ring to enforce boundary conditions, a blank holder system, and two CCD cameras installed beneath the open die to measure strains and their evolutions during forming. The configuration of stretch forming equipment is shown in **Figure 2**. Strains were measured by an in-situ non-contact measurement system (the ARAMIS). The ARAMIS system was constructed of two high speed, high resolution CCD cameras capable of capturing images during deformation of a specimen to facilitate continuous tracking of displacements and calculating strains through deformation kinematics. In both experiments, the ARAMIS was set to capture deformations with the rate of 20 fps (frames-per-second). The cameras were positioned beneath the open die by an adjustable tripod, facing toward the painted surface of the specimen during forming (**Figure 2**). More details of the ARAMIS system and the implemented algorithm for calculation of strains can be found in [19].

3. Results and Discussions

3.1. Development of the Material Model

The characterisation experiments conducted on $[0^\circ, 90^\circ]$ and $[-45^\circ, +45^\circ]$ SRPP specimens revealed the nonlinear response of the woven composite to external loadings. The full characterisation of the woven SRPP required the definition of three different stress and strain dependencies: correlation between longitudinal stress and strain, longitudinal to transverse strains dependency and shear stress-strain behaviour. The outcomes of charac-

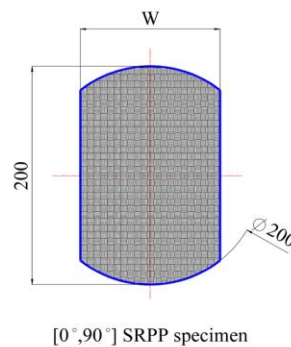


Figure 1. SRPP specimens.

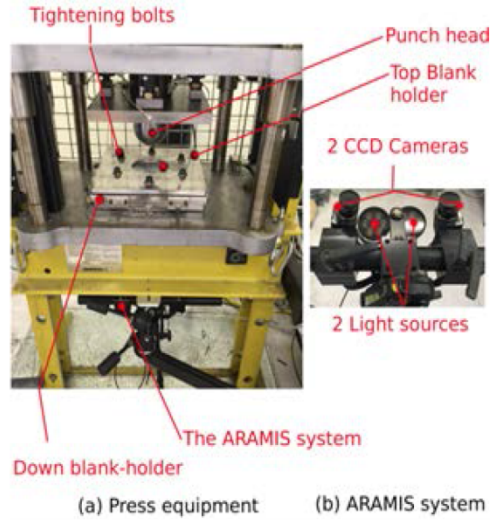


Figure 2. Stretch forming equipment.

terisation experiments are depicted by the following equations:

$$\sigma(\varepsilon) = F + A * \exp\left(-\frac{\varepsilon}{c}\right) + B * \exp\left(-\frac{\varepsilon}{d}\right). \quad (1)$$

$$\varepsilon_2(\varepsilon) = L + M * \exp\left(-\frac{\varepsilon}{p}\right) + N * \exp\left(-\frac{\varepsilon}{q}\right). \quad (2)$$

$$\tau(\gamma) = H + R * \gamma + S * \exp(-t\gamma). \quad (3)$$

In the above equations, the parameters are defined as follows: $A = -18.5E6$, $B = -25.2$, $c = 14188.75$, $d = 0.00841$, $F = 18.5E6$, $M = 0.052$, $N = 0.0043$, $p = 1.08$, $q = 0.009$, $L = -0.056$, $R = 117.8$, $S = -11.6$, $t = 28.35$ and $H = 11.6$. The highly nonlinear nature of these relations necessitates application of an incremental deformation theory to effectively capture complex forming behaviour of SRPP as follows:

$$E_1 = E_2 = \frac{d\sigma}{d\varepsilon}. \quad (4)$$

$$v_{12} = v_{21} = -\frac{d\varepsilon_2}{d\varepsilon_1}. \quad (5)$$

$$G_{12} = \frac{d\tau}{d\gamma}. \quad (6)$$

These equations yield the following material properties for the SRPP woven composite:

$$E(\varepsilon) = 1300 * \exp\left(-\frac{\varepsilon}{c}\right) + 2997 * \exp\left(-\frac{\varepsilon}{d}\right). \quad (7)$$

$$v(\varepsilon) = -(0.05 * \exp\left(-\frac{\varepsilon}{p}\right) + 0.5 * \exp\left(-\frac{\varepsilon}{q}\right)). \quad (8)$$

$$G_{12} = R + 328.7 * \exp(-t\gamma). \quad (9)$$

Subsequently, the stress and strain tensors can be coupled together through the following plane stress orthotropic material model:

$$\begin{pmatrix} \sigma_1 \\ \sigma_2 \\ \sigma_{12} \end{pmatrix} = \begin{pmatrix} \frac{E_1}{1-\nu_{12}\nu_{21}} & \frac{\nu_{21}E_1}{1-\nu_{12}\nu_{21}} & 0 \\ \frac{\nu_{12}E_2}{1-\nu_{12}\nu_{21}} & \frac{E_2}{1-\nu_{12}\nu_{21}} & 0 \\ 0 & 0 & G_{12} \end{pmatrix} \begin{pmatrix} \varepsilon_1 \\ \varepsilon_2 \\ \varepsilon_{12} \end{pmatrix}. \quad (10)$$

In this equation, σ_1 , σ_2 and σ_{12} depict different components of the Cauchy's stress tensor including normal stress along 1 and 2 axes and in-plane shear stress. ε_1 , ε_2 and ε_{12} represent normal strains along 1, 2 and in-plane shear, respectively. E_1 and E_2 depict Young's modulus along 1 and 2 axes, while ν_{12} and ν_{21} are the two Poisson's ratios of the SRPP caused by stretching the specimen along the first axis depicted by the first subscript on the induced strain along the transverse axis, shown by the second subscript. The stiffness matrix of the woven composite was considered asymmetrical based on the following reasons: 1) E and ν are both functions of strain. During each increment, the induced strains in 1 and 2 axes are not necessarily identical (depending on the width of the sample and enforced boundary conditions). Therefore, E and ν along these two directions possess different values during different stages of deformation. 2) Existence of a strain potential function during a linear, small deformation process guarantees symmetrical properties of the material's stiffness matrix. However, during stretch forming of a SRPP composite, large, non-linear deformations occur.

3.2. Stretch-Forming Studies

A total of 16 different SRPP specimens with different aspect ratios were stretch formed by the hemispherical punch until they fractured. The induced strains on the surface of SRPP samples were measured by the ARAMIS system. Principal strains were continuously calculated during each deformation increment. The ratio of minor to major strains (SR) was calculated to determine the induced deformation modes at the pole of specimens (The intersection of the two symmetry axes of the specimen). These deformation modes varied between the following regions: $SR = -0.5$ depicting uniaxial extension mode, $SR = 0$ exhibiting plane stress deformation and $SR = +1$ showing biaxial stretch.

Stretch forming simulations was conducted by the ABAQUS/implicit solver. The developed orthotropic material model was implemented into the ABAQUS by considering the plane stress condition governing stretch forming of thin SRPP blanks. Geometrical modelling of stretch forming experiment was accomplished through the ABAQUS Graphical User Interface. Four main parts were modelled within the ABAQUS/CAE (**Figure 3**): a hemispherical punch, an open die, a blank holder and the SRPP specimen. The first three components were modelled as 3D analytical rigid shells. The SRPP blank was modelled as a deformable 3D surface and was discretised by S4R5 thin shell elements to effectively capture bending phenomenon during stamp forming.

This type of shell element enforces Kirchhoff's thin shells theory during forming of the composite. A total of 5000 to 10000 elements were used to discretise the blanks depending on their size. The numerical simulation was accomplished through three general steps: **1**: The blank was positioned on the die and a normal traction force was applied to the semi-circular edges of specimens (**Figure 1**). This step was incorporated to simulate clamping or initial stretching of the blank due to local bend-unbend deformations applied by the lock ring embedded in the die system on samples **2**: Both semicircular edges of the blank were fixed in the pre-stretch position and a normal pressure was applied on its flange areas through the blank holder **3**: Initially, the punch was moved slowly toward the blank to stabilise the contact between the punch and the blank, prohibiting severe convergence issues due to local instabilities such as chattering. Afterwards, the punch was moved downward with a realistic forming speed (10 mm/s) to deform the blank until depth of failure specified by experimental outcomes.

The friction coefficient between blank holder-blank, die-blank and punch-blank pairs was set between 0.3 - 0.5. The contact between contact pairs was established through the master-slave approach with a surface-to-surface contact reinforcement. A linear penalty method was reinforced to the normal contact condition to prevent penetration of the contact pairs into each other. A general stabilisation procedure was enforced to address convergence issues during contact. To minimise the numerical errors, the ratio of the dissipated energy during contact and the overall energy required for forming was kept below a critical value.

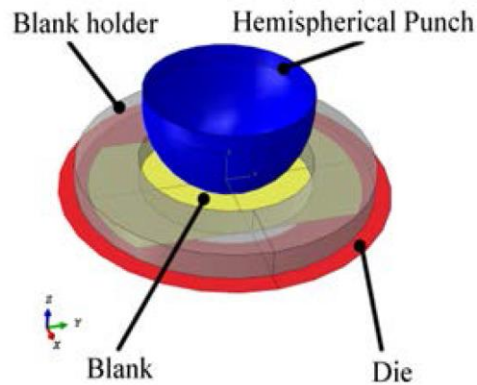


Figure 3. Modelling of Stretch Forming Components Assembly in the ABAQUS.

Figure 4 compares the experimental outcomes and the numerical predictions on the strain path of different specimens at the pole.

The nonlinear strain path, evident in all specimens except for W200, is caused by different phenomena: 1) fixing merely the circular edges of specimens in the lock-ring causes a stretch and a contraction along the length and the width of the specimen due to Poisson's effect, respectively 2) Establishment of initial contact between punch and the blank causes a local biaxial stretch in the pole of samples 3) Increase of forming depth changes biaxial stretch mode to another deformation mode governed by the aspect ratio of the sample 4) Gradual conformation of the blank to the punch geometry causes evolution of friction condition by variation of normal pressure and an asymmetrical contact surface along warp and weft directions (or along principal directions).

The FEA predictions demonstrate a similar trend with experimental outcomes during all stages of deformation. These results prove the high accuracy and reliability of the implemented numerical model for a woven composite during stretch forming condition. Both experiment and numerical simulations show the dependency of strain path to the aspect ratio of specimens: W25 and W50 demonstrate uniaxial and plain strain deformation modes, respectively. Increase of the specimens' widths causes the deformation mode to shift toward biaxial stretch until W200 which exhibits SR of +0.95. The small deviation of W200 strain ratio from a complete biaxial stretch is due to the friction between the sample and the punch.

3.3. Effects of Different Parameters on the Strain Path

Experimental and analytical investigation on stamp forming of woven composites is complicated, time consuming and challenging due to the highly complex nature of contact condition between the punch and the blank, nonlinear mechanical response of woven composites to external loadings and complex coupling between different forming parameters. Employing a macro-mechanical numerical model facilitates analysis of different parameters on the formability of the woven SRPP efficiently by avoiding incorporation of complex interactions within the weave structure of the composite. Three specimens are selected (W25, W100, W150 with $[0^\circ, 90^\circ]$ fibre orientations) and the effect of different mechanical properties and contact conditions on the strain path are studied.

The effect of friction condition on forming behaviour of a woven composite is elucidated in **Figure 5**. High and low friction conditions depict a friction coefficient of 0.1 and 0.9 between punch and the blank. The effect of friction condition on different regions of strain path is not identical. In wider specimens, the strain path does not change noticeably and the friction merely affects the maximum strains induced in the specimen: higher friction results in a more rigid body motion in the region around the pole, resulting in a decrease of induced strains. Lower friction causes a larger strain at the pole, causing more deformation on regions surrounding the pole. In wider specimens, increase in friction coefficient redistributes surface strains and decreases the maximum strain at the pole. In narrower specimens, the change in strain path is more noticeable. Generally, higher friction causes

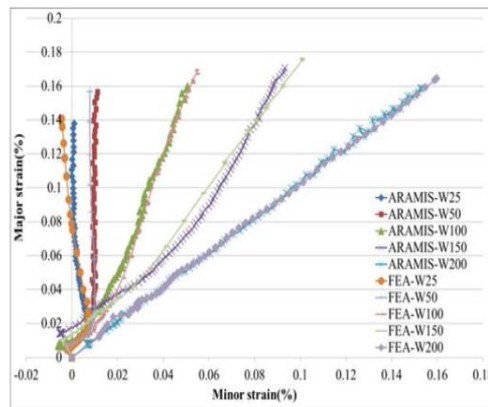
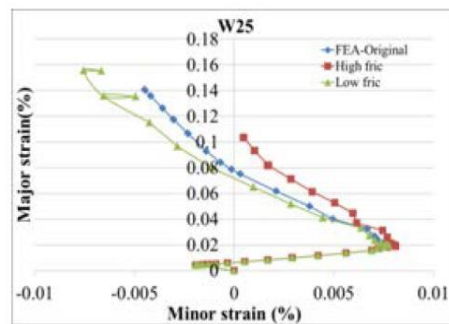
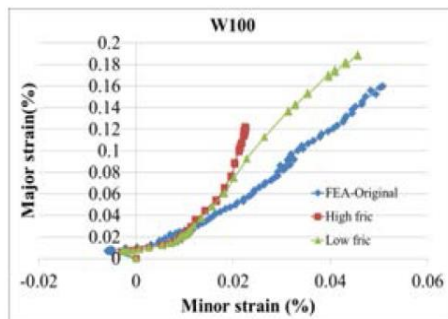


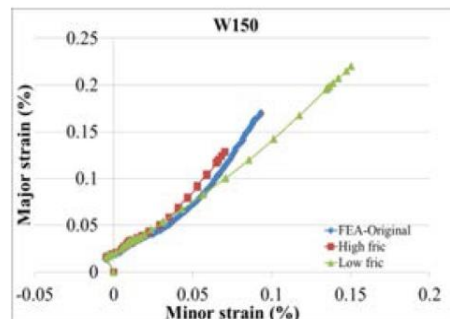
Figure 4. Comparison between predicted strain path at the pole of different specimens by experimental and numerical simulations.



(a)



(b)



(c)

Figure 5. Effect of changing friction coefficient on strain path at the pole.

the strain path to shift toward the plane strain by counteracting Poisson's effect and hampering development of the negative minor strain. Friction condition only affects maximum induced strain during stretch forming of wide specimens but results in a major shift of the strain path in narrower samples due to non-proportional contact surface along warp and weft directions.

Figure 6 illustrates the effect of composite's stiffness on the forming path. High and low stiffness of the

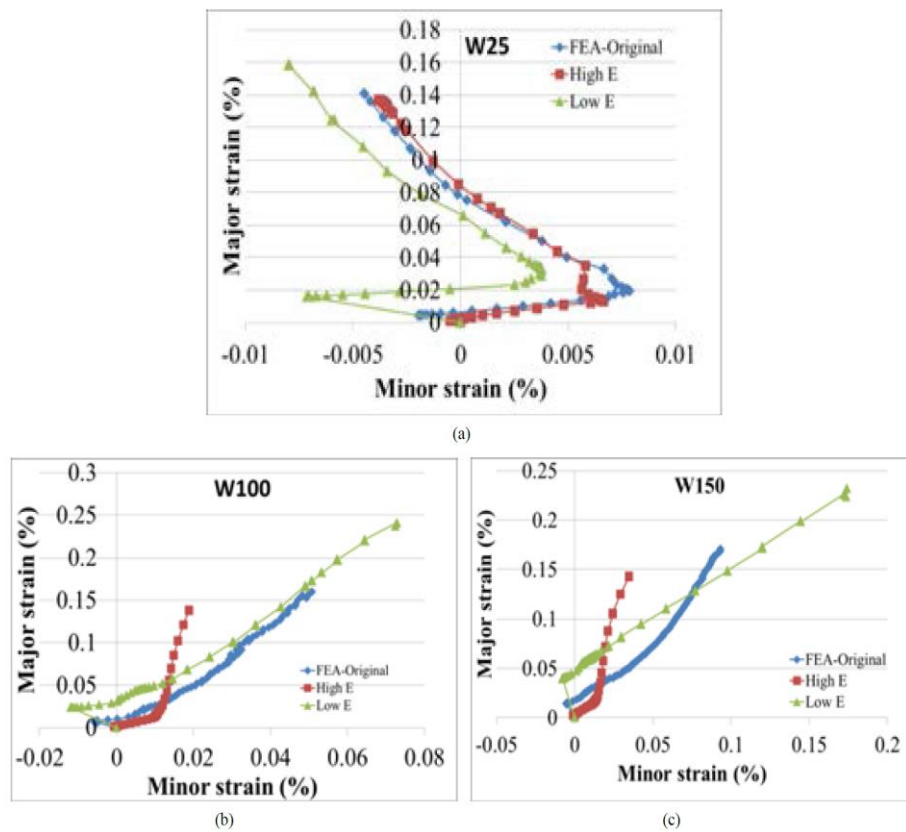


Figure 6. Effect of changing Young's modulus on strain path at the pole.

material differs by 30% compared to the original SRPP Young's modulus. In narrow specimen, the effect of this change on the induced deformation mode is negligible. However, in wider specimens, the increase of stiffness causes a shift toward plane strain deformation mode with a decrease in principal strains for an identical forming depth. The noticeable effect of changing stiffness in different specimens is the length of pre-stretch deformation stage. This stage of forming process is a force-control process in contrast to other stages with a more displacement-control nature. Generally, changing the Young's modulus within the realistic range of SRPP elasticity modulus does not show a prominent effect on the strain path of specimens, specifically in narrower specimens. Increasing the stiffness in wide specimens shows some local effects on the strain path, although the final gradient of the strain path seems to be identical.

Figure 7 elucidates the effect of PR on the strain path of different samples possessing different aspect ratios. The high and low PRs are different by 50% compared to original values. In narrow specimens, variations of PR cause a noticeable shift of the strain path. Decrease of the PR results in a more plane strain deformation mode, while increase of PR causes a shift toward more negative minor strains, e.g. shear deformation mode. However, in wider specimens the contact area along both longitudinal and transverse axes, e.g. warp and weft orientations, increases significantly. The change of contact area diminishes the effect of PR on the strain path due to the synergy between friction force and PR. Higher PR shifts the strain path of wider specimens toward negative minor strain or plane strain deformation mode, while lower PR shifts it toward biaxial stretch mode. These results reveal the complex effect of changing PR in the forming behaviour of a woven composite and its sensitivity to size effect.

Effect of shear stiffness on the strain path of woven composites, as shown in Figure 8, is probably the most

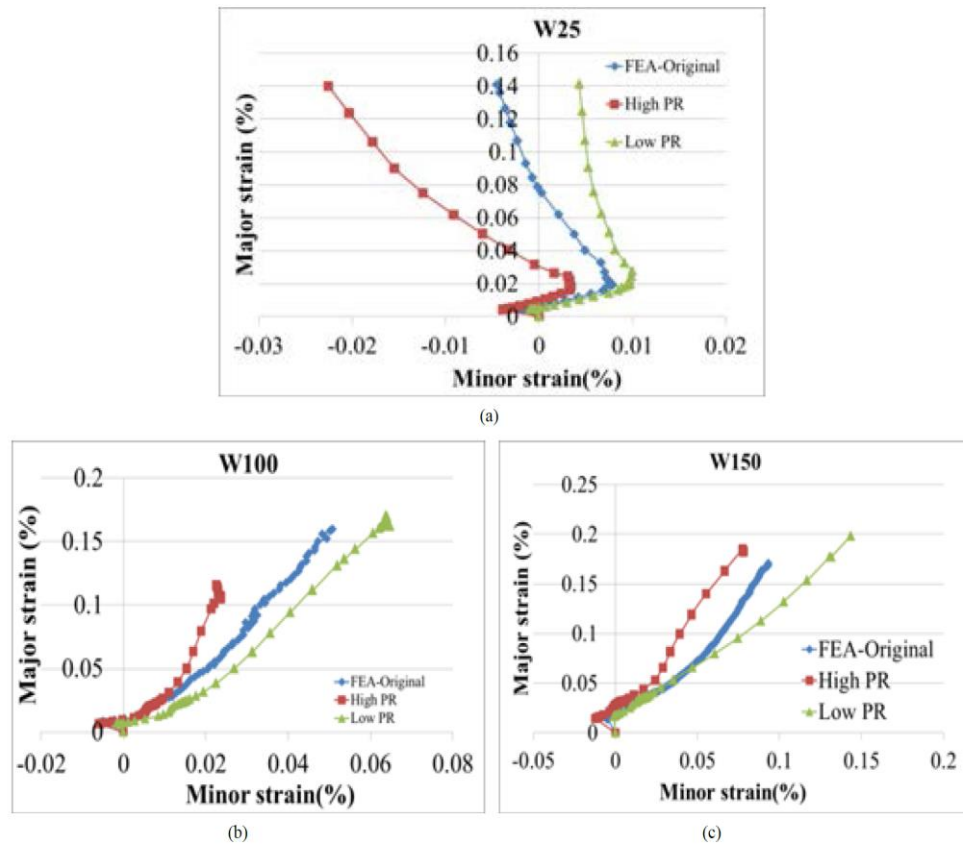


Figure 7. Effect of changing Poisson's ratio on strain path at the pole.

noticeable, yet non-intuitive phenomenon during stretch forming of a woven composite with $[0^\circ, 90^\circ]$ fibre orientations. Intuitively, the shear stiffness should not have a remarkable impact on the deformation of a $[0^\circ, 90^\circ]$ specimen during stretch forming, due to the fact that shear strain in these specimens should be very low. The numerical results show the validity of this hypothesis in narrow specimens. However, the forming results on wider specimens elucidate the significant impact of shear stiffness on the strain history. Decrease of shear strain shifts the strain path toward plane strain deformation mode, while increase of shear stiffness results in a more biaxial stretch deformation mode. Decreasing the shear stiffness causes a more uniform strain distribution on the surface of specimens in lower forming depths:

For the same forming depth, the maximum principal strain at the pole decreases, delaying onset of failure in the woven composite.

Figure 9 more clearly reveals the dependency of fibres' strains at the pole of a typical specimen (W100) to the shear stiffness of the specimen which can be correlated to the shear strain evolution at regions located along $+45^\circ$ and -45° orientations. The numerical results clearly show that once shear strain at $\pm 45^\circ$ locations starts to rise, the major strain at the pole decreases and the regions possessing maximum major strain spreads over a larger surface area around the pole. These observations lead to a more profound understanding of forming of a woven composite: Initially, the punch contacts the blank at the pole and deformations occur locally, affecting a very small region around the pole (Figure 9(a)). Other areas on the blank move downward with the punch following a rigid body motion, without experiencing noticeable normal strains. At a specific forming depth, determined by the shear stiffness of the woven composite, regions located along $\pm 45^\circ$ directions experience high shear strains and less localised maximum strain at the pole (Figure 9(b)). The contact surface between the blank

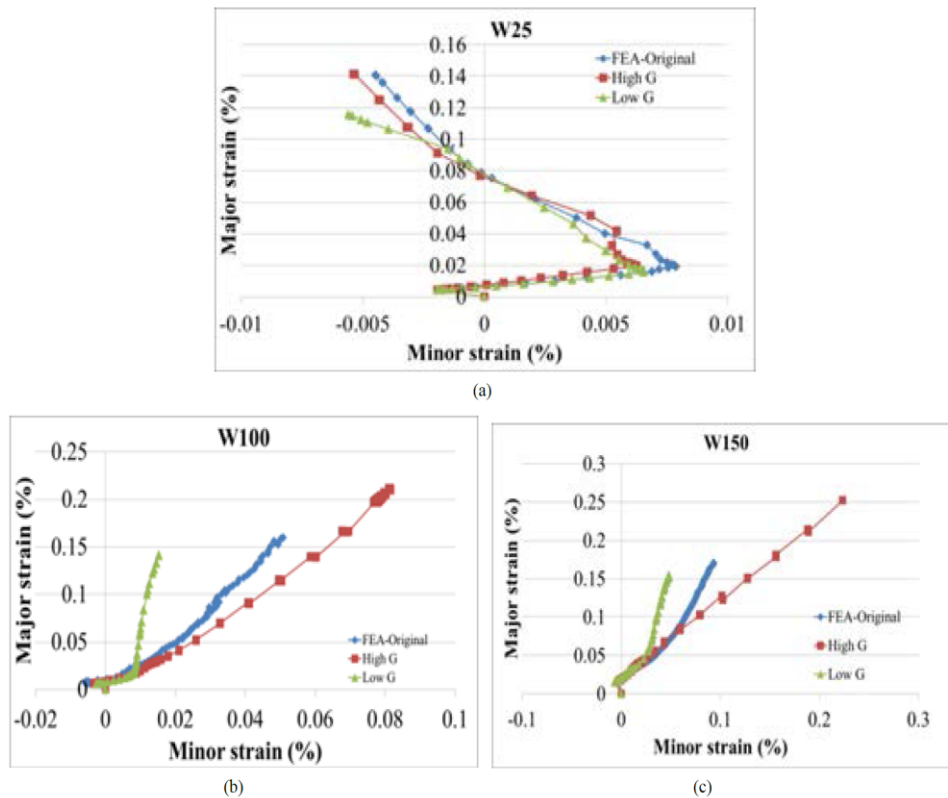


Figure 8. Effect of changing shear stiffness on strain path at the pole.

and the punch increases simultaneously. The blank starts to conform to the punch geometry further once the shear strains at $\pm 45^\circ$ areas increases. This is highlighted by a change in the strain path of the sample. During the final stages of deformation, the maximum strain moves completely from the pole to ward areas located along $\pm 45^\circ$ directions, the shear strain increases significantly and the blank conforms completely to the punch surface (Figures 9(c-c) & 9(c-d)).

4. Conclusion

Characterisation experiments were conducted on a pre-consolidated woven self-reinforced polypropylene composite (SRPP) to elucidate in-plane material properties including Young's modulus, Poisson's ratio and shear stiffness. These data were employed to construct an asymmetric orthotropic material model employed in a numerical simulation to predict stretch forming behaviour of the composite. Subsequently, stretch forming experiments were conducted on different SRPP specimens by a hemispherical punch. The induced strains during forming were continuously measured to elucidate forming behaviour of the SRPP under different forming modes. The match between the numerical simulation results and the experimental outcomes on the strain path at the pole of specimens were satisfactory. Then, the developed finite element model was employed to investigate the effect of different parameters on the forming behaviour of woven composites. All major variables showed sensitivity to the aspect ratio of the samples in changing strain path at the pole. These variables included material properties and friction condition. It was elucidated that in narrow specimens, the Poisson's ratio and friction coefficient are the most influential parameters on the strain path and therefore on the formability of the woven composites. In wide specimens, the shear stiffness and Young's modulus are more effective parameters in the formability of the composite than others. It was revealed that the shear stiffness of a $[0^\circ, 90^\circ]$ woven composite

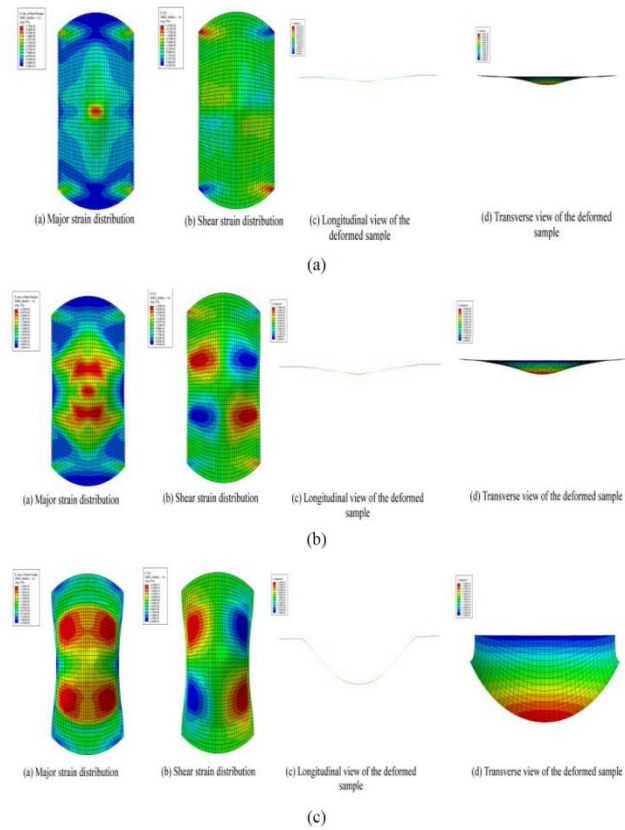


Figure 9. Effect of shear strain on the evolution of major strain and forming profile of W100.

has a significant effect on developing a more uniform surface strain and therefore the enhanced formability of the woven composite.

References

- [1] Environmental Protection Agency Website: <http://epa.gov>
- [2] Helms, H. and Lambrecht, U. (2003) Energy Savings by Light Weighting. IFEU-Institut für Energie- und Umweltforschung Heidelberg GmbH.
- [3] National Research Council. Technologies and Approaches to Reducing the Fuel Consumption of Medium- and Heavy-Duty Vehicles. National Academies Press.
- [4] Kohler, J., Schade, W., Leduc, G., Wiesenthal, T., Schade, B. and Espinoza, L.T. (2013) Leaving Fossil Fuels Behind? An Innovation System Analysis of Low Carbon Cars. *Journal of Cleaner Production*, **48**, 176-186. <http://dx.doi.org/10.1016/j.jclepro.2012.09.042>
- [5] Lewis, A.M., Kelly, J.C. and Keoleian, G.A. (2014) Vehicle Light Weighting vs. Electrification: Life Cycle Energy and GHG Emissions Results for Diverse Powertrain Vehicles. *Journal of Applied Energy*, **126**, 13-20. <http://dx.doi.org/10.1016/j.apenergy.2014.03.023>
- [6] Scida, D., Aboura, Z., Benzeggagh, M.L. and Bocherens, E. (1999) A Micromechanics Model for 3D Elasticity and Failure of Woven-Fibre Composite Materials. *Composite Science and Technology*, **59**, 505-517. [http://dx.doi.org/10.1016/S0266-3538\(98\)00096-7](http://dx.doi.org/10.1016/S0266-3538(98)00096-7)
- [7] Cousigné, O., Moncayo, D., Coutellier, D., Camanho, P., Naceur, H. and Hampel, S. (2013) Development of a New Nonlinear Numerical Material Model for Woven Composite Materials Accounting for Permanent Deformation and

- Damage. *Composite Structures*, **106**, 601-614. <http://dx.doi.org/10.1016/j.compstruct.2013.07.026>
- [8] Compston, P., Cantwell, W.J., Cardew-Hall, M.J., Kalyanasundaram, S. and Mosse, L. (2004) Comparison of Surface Strain for Stamp Formed Aluminium and Aluminium-Propylene Laminate. *Journal of Material Science*, **39**, 6087-6088. <http://dx.doi.org/10.1023/B:JMSC.0000041707.68685.72>
- [9] Davey, S., Das, R., Cantwell, W.J. and Kalyanasundaram, S. (2013) Forming Studies of Carbon Fibre Composite Sheets in Dome Forming Processes. *Journal of Composite Structures*, **97**, 310-316. <http://dx.doi.org/10.1016/j.compstruct.2012.10.026>
- [10] Kalyanasundaram, S., Dhar Malingam, S., Venkatesan, S. and Sexton, A. (2012) Effect of Process Parameters during Forming of Self-Reinforced PP-Based Fibre Metal Laminates. *Composite Structures*, **97**, 332-337. <http://dx.doi.org/10.1016/j.compstruct.2012.08.053>
- [11] Zanjani, N.A. and Kalyanasundaram, S. (2015) Induced Forming Modes in a Self-Reinforced Polypropylene Sheet during Stretch Forming Process at Room Temperature: I-Experimental Studies. *Composites Part A*, **68**, 251-263. <http://dx.doi.org/10.1016/j.compositesa.2014.09.023>
- [12] Zanjani, N.A., Wang, W. and Kalyanasundaram, S. (2015) The Effect of Fibre Orientation on the Formability and Failure Behaviour of a Woven Self-Reinforced Composite during Stamp Forming. *ASME Journal of Manufacturing Science and Engineering*, in Press.
- [13] Mosse, L., Compston, P., Cantwell, W.J., Cardew-Hall, M.J. and Kalyanasundaram, S. (2006) Stamp Forming of Polypropylene Based Fibre-Metal Laminates: The Effect of Process Variables on Formability. *Journal of Materials Processing Technology*, **172**, 163-168. <http://dx.doi.org/10.1016/j.jmatprotec.2005.09.002>
- [14] Harrison, P., Gomes, R. and Correia, N.C. (2013) Press Forming a 0/90 Cross-Ply Advanced Thermoplastic Composite Using the Double-Dome Benchmark Geometry. *Composites Part A*, **54**, 56-69. <http://dx.doi.org/10.1016/j.compositesa.2013.06.014>
- [15] Haanappel, S.P., ten Thije, R.H.W., Sachs, U., Rietman, B. and Akkerman, R. (2014) Formability Analyses of Uni-Directional and Textile Reinforced Thermoplastics. *Composites Part A*, **56**, 80-92. <http://dx.doi.org/10.1016/j.compositesa.2013.09.009>
- [16] Gohari, S., Sharifi, S., Vrcelj, Z. and Yahya, M.Y. (2015) First-Ply Failure Prediction of an Unsymmetrical Laminated Ellipsoidal Woven GFRP Composite Shell with Incorporated Surface-Bounded Sensors and Internally Pressurized. *Composites Part B: Engineering*, **77**, 502-518. <http://dx.doi.org/10.1016/j.compositesb.2015.03.058>
- [17] Derakhshan, D., Komeili, M. and Milani, A.S. (2011) An Analytical Approach to the Deflection Analysis of Woven Preforms and Composites under Tensile Loading Using the Winkler Theory of Curved Beams. *Computational Materials Science*, **96**, 403-410. <http://dx.doi.org/10.1016/j.commatsci.2014.08.044>
- [18] OCV Reinforcement Co.: www.ocvreinforcements.com
- [19] The GOM mbH. www.GOM.com

FEA predictions on forming and failure behaviours of a woven composite

In previous chapters, a path-dependant strain-based failure model based on stretch forming studies on a woven SRPP composite was proposed and a non-linear material model based on mechanical characterisation tests was constructed. In this chapter, material and failure models are implemented into a finite element simulation to predict: (1) strain path and evolution of surface strains at different locations on samples during different stages of deformation, and (2) failure depths and loci in SRPP composite under a wide range of deformation modes. Predictions made by the numerical model are compared to experimentally measured strains and loci of failure in specimens with different aspect ratios. Finally, the effect of different parameters on the strain path of a woven composite is investigated. The numerical simulation results demonstrate the potential of the finite element model in predicting failure of SRPP under complex boundary and loading conditions.

In this chapter, a homogenised macro-mechanical scheme is adopted to incorporate material and failure models into a finite element analysis. These models are implemented into Abaqus/implicit software using a user-defined material subroutine (UMAT). Specimens were modelled using a thin shell element (S4R5) capable of capturing bending effects on thin elements during forming. Hemispherical punch, open die and blank holder system were modelled using analytical rigid elements. Depending on the size of specimens, a total of 5000 to 10,000 shell elements were used to discretise blanks of SRPP composite. The contact between contact pairs, e.g. blank holder-blank and punch-blank, was established using a master-slave approach while enforcing surface-to-surface contact conditions. A linear penalty approach was adopted to prevent punch from penetrating into

the blanks during forming. A contact stabilisation procedure was adopted to resolve contact convergence problem. The ratio of dissipated energy to energy required for forming of samples was set to a minimum to ensure the numerical errors are within acceptable range. The friction coefficient between contact pairs varied from 0.3 to 0.5 to ensure having consistent results with experiments.

Finite Element Analysis (FEA) results are benchmarked against experimental outcomes and the evolution of minor and major strains at the pole of specimens is studied. Minor discrepancies between experiments and simulations are associated with heterogeneous properties of the composite and manufacturing flaws caused by high viscosity of the polypropylene polymer and the existence of resin rich regions. The reasons behind sudden change of strain gradient are discussed in terms of process parameters including aspect ratio, boundary condition and fibre orientation. Furthermore, a comparison of analytical equations for predicting mechanical properties of SRPP in FEA with experimental characterisation test results is shown in Appendix A (after bibliography section, page 154). These graphs include stress-strain curves obtained through uniaxial and bias extension tests (depicting Young's modulus and shear stiffness of the composite) and transverse vs longitudinal strains (depicting conventional definition of the Poisson's ratio) of the SRPP composite.

Evolution of surface strains on a typical SRPP sample at different depth of deformation is illustrated. Outcomes of the analysis elucidate the evolution of contact between punch and blank and its effect on development of surface strain in a SRPP. Finally, onset of failure under different deformation modes are predicted and compared with photographs of fractured samples. In thinner samples, the failure was predicted to start at a distance of 1/3 of sample's length from the edge perpendicular to the warp direction. In wider samples, two orthogonal paths of failure making 45° with fibre direction were observed.

High correlation between FEA results and experimental measurements validates high accuracy of the proposed numerical model in predicting failure of woven thermoplastic composites under complex loading conditions. The numerical model has the potential to predict formability and failure behaviour of consolidated woven thermoplastic composites during manufacturing. This numerical model facilitates manufacturing of components from woven thermoplastic composites by reducing the time and cost required to conduct trial and error experiments.

Experimental and numerical studies on forming and failure behaviours of a woven self-reinforced polypropylene composite

N. A. Zanjani¹, S. Kalyanasundaram¹

¹ Research School of Engineering
Australian National University
Acton, ACT 2601
AUSTRALIA

E-mail: nima.akhavan@anu.edu.au

Abstract: *This paper investigates forming and failure behaviours of a consolidated woven self-reinforced polypropylene (SRPP) composite through combined stamp forming experiment and finite element analysis. Mechanical properties of a woven SRPP composite were characterised using a universal testing machine and a non-contact photogrammetry system. Constitutive equations were derived as functions of strains using a homogenised orthotropic material model. Consolidated SRPP specimens with novel geometries, different aspect ratios and fibre orientations, were stretch formed in a custom built press until catastrophic failure. Evolution of principal strains was captured using a real time Digital Image Correlation (DIC) system. A path dependant failure criterion was developed as a function of deformation modes and invariants of strain tensor at the vicinity of fractured region. Material and failure models were implemented into a finite element analysis using Abaqus/implicit. Strain path at the pole of specimens, evolution of surface strains, and onset of failure were predicted using a homogenised numerical scheme. Comparison with experimental outcomes demonstrated high accuracy of the developed numerical model in predicting deformation and failure behaviours of a thermoplastic composite under a wide range of deformation modes. The model demonstrated its potential to predict formability and failure behaviour of woven thermoplastic composites during manufacturing by eliminating the need to conduct expensive, time consuming trial and error procedures.*

Keywords: *woven thermoplastic composite, real time strain measurement, finite element analysis, constitutive model, failure*

1. Introduction

Woven polymer composites have attracted worldwide attentions owing to their advantages over fibre reinforced composites including balanced thermomechanical properties, enhanced resistance to crack propagation and higher fatigue strength. Improved mechanical properties of this class of composite materials present an opportunity for their wide spread application in defence, automotive, and aerospace industries. Studies have shown that substituting metallic parts with composite materials has the potential to provide a weight reduction of 10% to 50% and a cost reduction of 10% to 20% while maintaining similar mechanical properties [1]. However, these targets can be achieved only if a more effective manufacturing process is adopted to produce components from composites. This necessitates development of a reliable failure model to predict strength of polymer composites under different loading conditions.

Polymer composites are generally made of two different polymer resins: thermosets and thermoplastics. Thermoset composite materials are currently manufactured by labour-intensive, time consuming and expensive processes including moulding and autoclaving techniques. These processes generally involve draping the reinforcement fabric into the mould, impregnation of the fabric with a resin, and curing both components under controlled pressure and temperature conditions to consolidate the composite. Prolonged processing time is required for cross linking

thermoset polymer chains to provide strength and rigidity in the final manufactured component. Thermoset composites exhibit brittle behaviour and cannot be recycled and reshaped after curing. Shortcomings of thermoset-based composites have raised worldwide interest toward adopting thermoplastic-based composites in industrial applications. Thermoplastic polymers possess a semi-crystalline structure that eliminates the necessity of cross linking during consolidation process. Thermoplastic composites can be reshaped after initial consolidation. Parts can be made of thermoplastic composites using multi-stage forming procedures such as initial consolidation followed by post forming of blanks.

Design and manufacturing parts from thermoplastic composites requires fundamental understanding of their failure behaviours. There are countless failure theories that were basically developed on thermoset polymer composites. To evaluate the accuracy of these myriad of failure theories, an international “World Wide Failure Exercise” (WWFE) was established by the science and engineering council of UK. One of the main objectives of this exercise was to benchmark and compare the predictability of failure theories based on a consistent experimental framework. The results of these exercises were collected and published in a series of publications [2-6]. Outcomes of these studies have demonstrated that “contrary to widely held misconceptions, much still remains to be done in order to ensure that reliable and accurate predictive tools are readily available for general use in design” [5]. Organisers of WWFE observed that the divergence between prediction of failure and experiments were increased with complicated loading cases. They attributed these discrepancies to the absence of standard experimental procedures to characterise these loading conditions. It was concluded the predictability of some failure criteria were more promising than others but none of these theories were capable of accurate failure predictions in composites experiencing high strains.

Thermoset-based composites are brittle and exhibit very low strain to failure. Mismatch between fibre and matrix properties results in strain concentration at their interface, leading to transverse cracking, de-bonding, and delamination in the composite. On the other hand, Failure behaviour of woven thermoplastic composites differs significantly as a result of two specific mechanisms: 1) interaction effects of interlacing yarns in woven reinforcements, and 2) much higher strain to failure of thermoplastic compared to thermoset resins. There is an ongoing research studies undertaken to understand failure mechanisms and develop failure theories for thermoplastic composites [7-20]. Current study is undertaken to develop a failure criterion for woven thermoplastic composites and demonstrate its accuracy by benchmarking results of a numerical simulation with experiments through a wide range of deformation modes.

The current paper is an extension of previous experimental studies conducted on forming and failure of a woven self-reinforced polypropylene composite. In [24], foundations of an experimental failure frameworks for self-reinforced composites have been established to identify failure limits of a SRPP at different strain ratios. Based on an experimental strain measurement technique, a relation between deformation mode and failure mode of the composite was established and a failure envelope in a principal strain space was defined. In [25], different failure morphologies of the composite observed under fracture in different deformation modes was studied using an optical microscopy system and the role of shear deformation mode in extending forming capabilities of a consolidated woven composite was investigated. In [26], mechanical characterisation experiments were conducted to develop a constitutive stress-strain relation for the composite as a function of fibre strain. It was found out that Poisson’s ratio is highly nonlinear and as such the dependency of lateral to longitudinal strains in the composite was re-defined using an incremental deformation framework. In the current study, material and failure models developed in previous papers were incorporated into a numerical simulation to predict strain path at the pole, evolution of surface strains, and onset and shape of fractured region in composite specimens. Comparison with experimental outcomes showed high accuracy of FEA predictions on deformation and failure behaviours of the consolidated woven composite during stamp forming process. Outcome of the combined experimental-numerical analysis demonstrated the potential of the present model in predicting failure of woven thermoplastic composites under complex loading conditions.

2. Material, testing method and finite element analysis

2.1 Material system

The pre-consolidated sheets of a multilayered 2/2 twill weave self-reinforced composite (SRPP), manufactured by OCV reinforcements Company [21], were used to conduct mechanical characterisation and forming tests. SRPP composite is a self-reinforced composite in which both reinforcements and matrix are made from semi-crystalline polypropylene material. The woven fabric is manufactured from PolyPropylene (PP) copolymer fibres, made of two structurally different concentric cylinders of PP: a core made of α -PP polymer covered by β -PP polymer as the skin, in which the former has significantly higher melting temperature than the latter. During manufacturing process, high pressure and temperature are applied to the composite prepregs to melt the β -PP skin and construct matrix to embed woven reinforcement. After cooling, the consolidated SRPP composite sheets are produced in which fibres and matrix are made of α and β PP polymers, respectively.

2.2 Characterisation experiments

Uniaxial and bias extension tests were conducted on rectangular SRPP specimens to extract mechanical properties of the composite as functions of strain. Details of characterisation tests are specified in [20]. Modulus of elasticity (E), Poisson's ratio (ν), and shear stiffness (G) of the SRPP are curve fitted with experimental data using exponential functions:

$$E_i(\varepsilon_i) = m \cdot \exp\left(-\frac{\varepsilon_i}{a}\right) + n \cdot \exp\left(-\frac{\varepsilon_i}{b}\right), \quad i=1,2 \quad (1)$$

$$\nu_{ij}(\varepsilon_i) = r \cdot \left[\exp\left(-\frac{\varepsilon_i}{c}\right) + \exp\left(-\frac{\varepsilon_i}{d}\right) \right], \quad i=1,2 \text{ and } j=1,2 (i \neq j) \quad (2)$$

$$G_{12} = p + s \cdot \exp(-q \cdot \gamma_{12}) \quad (3)$$

Values of constants used in equations (1) to (3) are as follows:

$$a = 14188.75, b = 841.00e^{-5}, c = 1.08, d = 9.00e^{-3}, m = 1300.00, n = 2997.00, r = -0.05, p = 117.80, q = 28.35, s = 328.70 \quad (4)$$

Indices i and j depict longitudinal and transverse directions of specimens which correspond to warp and weft directions in the woven composite. An interesting finding of characterisation experiments on SRPP composite was the high variations of transverse to longitudinal strains during uniaxial extension. Highly nonlinear dependency of transverse to longitudinal strains necessitated adopting an incremental approach to re-define Poisson's ratio of the composite. Poisson's ratio, in the current study, is defined as the instantaneous gradient of lateral strain to longitudinal strain at each stage of deformation. Based on this new definition, Poisson's ratio of SRPP at the very beginning of uniaxial extension is close to 0.45 but reduces abruptly to 0.1 after around 5% strain. Adopting conventional definition of Poisson's ratio, as the ratio of lateral to longitudinal strain at any stage of deformation, yields unrealistic predictions of deformation and failure in SRPP composite during stamp forming simulations. From the above analytical expression depicted by equations (1) to (4) an important conclusion can be made on the woven composite mechanical properties: when induced strains are low (less than 5%), the mechanical properties varies significantly. In other words, the gradient of material properties is very high at low strains. However, as the strain value increases (between 5 to 10%), the variation of material properties reduces gradually. At strains above 10%, the material constants converge toward fixed values (E becomes around 1.5 GPa and ν becomes 0.1). The effect of this phenomenon on forming and failure behaviours of composite as predicted by FEA simulations will be discussed later.

An orthotropic material model, assuming no coupling between normal and shear components of

stress and strain tensors, is adopted to construct constitutive equation of the composite:

$$\begin{pmatrix} \sigma_1 \\ \sigma_2 \\ \tau_{12} \end{pmatrix} = \begin{pmatrix} \frac{E_1}{1-\nu_{12}\cdot\nu_{21}} & \frac{E_1\cdot\nu_{21}}{1-\nu_{12}\cdot\nu_{21}} & 0 \\ \frac{E_2\cdot\nu_{12}}{1-\nu_{12}\cdot\nu_{21}} & \frac{E_2}{1-\nu_{12}\cdot\nu_{21}} & 0 \\ 0 & 0 & G_{12} \end{pmatrix} \cdot \begin{pmatrix} \varepsilon_1 \\ \varepsilon_2 \\ \gamma_{12} \end{pmatrix} \quad (5)$$

σ_1 , σ_2 , and τ_{12} depict different components of the Cauchy's stress tensor including normal stress along 1 and 2 axes and in-plane shear stress. ε_1 , ε_2 , and γ_{12} represent normal strains along 1, 2 axes and shear strain, respectively. E_1 and E_2 depict Young's modulus along 1 and 2 axes, while ν_{12} and ν_{21} are Poisson's ratios of the material which are defined as the effect of extension along the first axis depicted by the first subscript on the induced strain along the transverse axis, shown by the second subscript. G_{12} and γ_{12} depict shear stiffness and shear strain of the composite, respectively. The first four material properties (E, ν) were extracted from uniaxial extension of on-axis composite specimens and the fifth material property was obtained from bias extension test on off-axis ($\pm 45^\circ$) samples.

Measurement and calculating of shear stiffness of SRPP was done on off-axis ($\pm 45^\circ$) samples. No pre-assumption such as frictionless pin-joint between warp and weft yarns was made to calculate shear stress-strain relation. A shear stress-strain analysis was made based on experimental readings of force and strain using INSTRON and ARAMIS equipment. Off axis samples were stretched longitudinally so that the force exerted to the samples made a $\pm 45^\circ$ with fibre orientation at the start of the experiment. Once specimens were stretched, warp and weft fibres started to spin around their crossover joints and the associated rotation angle and shear strain were measured incrementally by the ARAMIS. Variations of longitudinal force vs strain were plotted using INSTRON readings. Strains were calculated using photogrammetry technique and were averaged across the mid cross section of specimen where both warp and weft were yarns were free to rotate. Then a plot of longitudinal strain vs shear strain were constructed using ARAMIS readings. Finally, these data was employed to plot uniaxial strain vs shear strain. Using all these three graphs, an analytical expression for the dependency of longitudinal strain to shear strain was constructed. Shear stiffness was calculated at each increment using instantaneous slope of this graph.

2.3 Stamp forming tests

Geometries with specific geometries as shown in Figure 1 were used to conduct forming tests on SRPP composite. It should be emphasized that the Pole is located at the intersection of longitudinal and transverse symmetry axes of specimen (centre of specimen). Underlying reason for adopting these geometries was to induce failure in the composite under a wide range of deformation modes. Experiments have shown that deformation mode at failure is a function of two variables: width-to-length ratio and fibre orientation. Specimens were cut out from full circular blanks with 200mm diameter (ϕ) into semi-rectangular shapes with width (W) ranging from 12.5 to 150mm. A full circular sample with diameter of 200mm was used to capture deformation behaviour of SRPP under biaxial extension mode. SRPP specimens with different aspect ratios and fibre orientations ($[0^\circ, 90^\circ]$ and $[-45^\circ, +45^\circ]$) were stamp formed until fracture. Forming experiments were conducted using a 300kN custom-built press with a hemispherical punch head and an open die configuration with a blank holder and built-in lock ring system (Figure 2). Specimens were fixed in the lock ring of the blank holder system along their perimeters. Therefore, Variations of aspect ratio (W/D) changed the ratio of fixed to the total perimeter of specimens and therefore resulted in failure under different deformation modes.

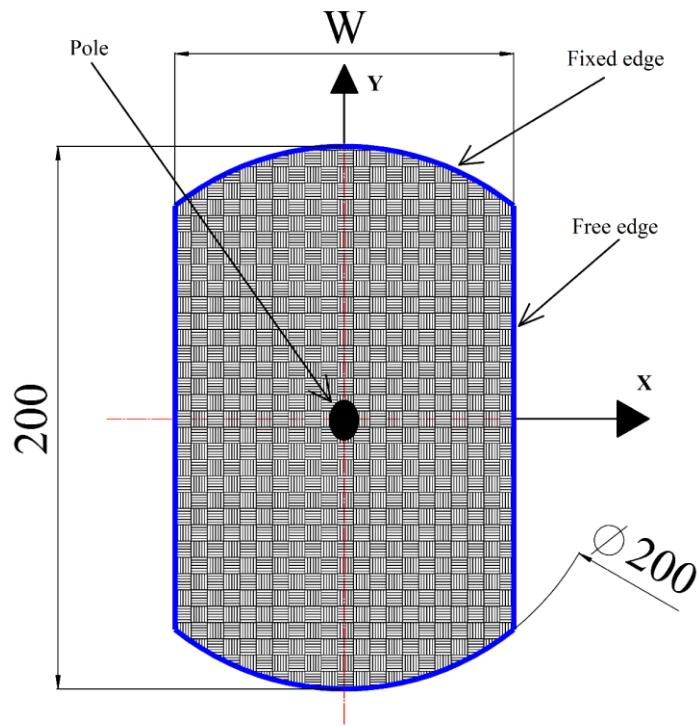
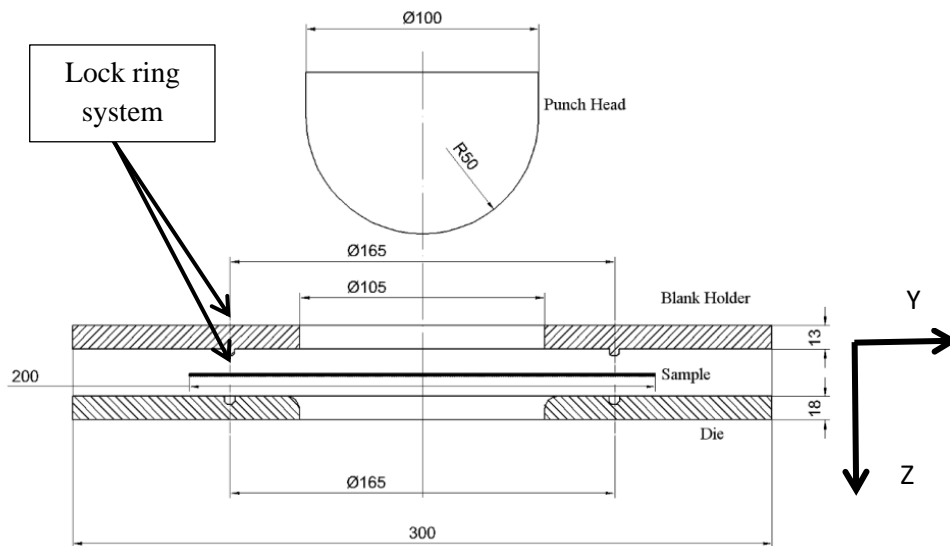
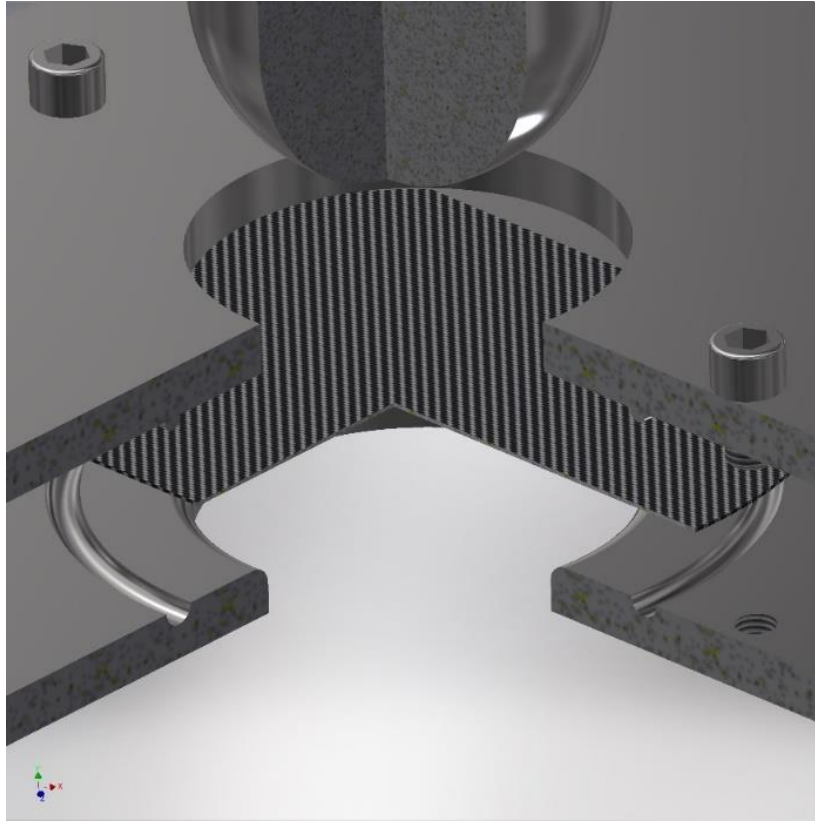


Figure 1: SRPP specimens used in forming experiments



(a) Two dimensional drawing of the stamping set-up



(b) A close up section view of the stamping set-up

Fig 2: Experimental set-up of stamp forming on SRPP composite

Surface strains were recorded using a real time photogrammetry measurement system. Details of experiments are specified in [18-20]. Stamp forming experiments were conducted due to following reasons: **1)** providing a benchmark for finite element analysis results including strain path at the pole (midpoint or intersection of the two orthogonal axes (X and Y) of specimens as shown in Figure 1), evolution of surface strains, and site of fracture; **2)** define a failure envelope for a woven thermoplastic composite as a function of strain invariants and their ratios. Each deformation mode was characterised by the ratio of two principal strains ($SR = \epsilon_{\text{minor}} / \epsilon_{\text{major}}$) ranging from $SR = +1$ for biaxial extension mode to $SR = -1$ for shear deformation mode. Other deformation modes were specified by $SR = 0$ for plane strain and $SR = -0.5$ for uniaxial extension modes. Details of constructing a failure envelope for SRPP composite, as implemented in FEA simulation through a user defined material subroutine (UMAT), is expressed by the following two equations:

$$((-0.5 \leq SR \leq +1) \text{ and } (\epsilon_{\text{minor}} \geq -8\%)) \Rightarrow \epsilon_{\text{major}}^{\text{failure}} = 0.16 \quad (6)$$

$$((-1 \leq SR \leq -0.5) \text{ and } (\epsilon_{\text{minor}} \leq -8\%)) \Rightarrow \epsilon_{\text{major}}^{\text{failure}} = -1.6 * \epsilon_{\text{minor}} + 0.032 \quad (7)$$

Failure criteria, as defined by Eq. (6) and (7), depends on the value of minor strain and strain ratio: If strain ratio (SR) is between -0.5 and +1 (deformation modes between uniaxial extension and biaxial stretch), then major strain larger than 16% results in failure of SRPP composite. Second failure region covers strain ratios less than -0.5 (deformation modes between uniaxial extension and shear deformation modes). In this region, the value of failure strain makes an inverse linear dependency to the minor strain. Equation (7), obtained from experimental forming tests on SRPP samples, reveals another interesting behavior of SRPP woven composite: failure starts at higher major strains as compressive minor strain increases. In other words, failure onset can be delayed if high compressive forces are applied along the transverse direction of the composite. This shows a coupling between failure along 1st direction and the applied stress in the 2nd direction due to interwoven structure of reinforcements.

It should be noted that both failure criteria specified by equations 6 and 7 are continuous at the strain ratio of -0.5. In addition to that, the failure envelope defined by these equations is based on principal strains and as such ignores the fiber direction. The reason behind the treatment of failure in a SRPP composite lies in its microstructure. Both constituents of the composite are made from similar material system and as such fiber directionality has least impact on failure of the composite as compared to composites made of very stiff fibers such as carbon fiber and glass fiber polymer composites.

2.4 Finite element model

Stretch forming simulations was conducted using ABAQUS-implicit solver. The orthotropic material model and failure criteria developed for the woven composite were implemented into the ABAQUS. The stamping process was modelled as a plane stress problem due to very low thickness-to-width ratio and negligible through-thickness stress in semi-rectangular specimens caused by the punch. Hemispherical punch and die system were modelled as rigid bodies. Blanks were discretised using thin shell plane stress elements from Abaqus library. These elements have 5 degrees of freedom and impose Kirchhoff-love bending conditions on thin shells using numerical constraints to capture bending deformations accurately. In this study, the largest specimen (a full circle with 200 mm diameter) was discretised by 10000 elements while the smallest sample (a semi rectangular specimen with 200 mm length and 25mm width) was discretised by 3000 elements. Stamp forming experiment was simulated as a quasi-static process using implicit technique.

The contact between contact pairs, e.g. blank holder-blank and punch-blank, was established using a master-slave approach while enforcing surface-to-surface contact conditions. A linear penalty approach was adopted to prevent punch from penetrating into the blanks during forming. A contact stabilisation procedure was adopted to resolve contact convergence problem. The ratio of dissipated energy to energy required for forming of samples was set to a minimum to ensure the numerical errors are within acceptable range. The friction coefficient between contact pairs varied from 0.3 to 0.5 to ensure having consistent results with experiments.

3. Results and discussions

In this section, outcome of stamp forming tests on SRPP specimens having novel geometries and different aspect ratios are presented and compared with numerical simulation results. First, evolution of minor and major strains at the pole of specimens leading to fracture is studied. FEA results are benchmarked against experimental outcomes and small discrepancies are associated with heterogeneous properties of the composite and manufacturing flaws. Reasons behind sudden change of strain gradient are discussed including aspect ratio of samples, enforced boundary conditions and fibre orientation. Second, evolution of surface strains on a typical SRPP sample at different depth of deformation is illustrated. This section elucidates the evolution of contact between punch and blank and its effect on development of surface strain in SRPP composite. Finally, onset of failure under a wide range of deformation modes are predicted by FEA and compared with fractured site of

composite samples in experiments. High correlation between FEA results and experimental measurements validates high accuracy of the numerical model in predicting failure of woven thermoplastic composites under a wide range of deformation modes and its potential application in composites under complex loading conditions.

3.1 Strain path

The experimental deformation modes for specimens with $[0^\circ, 90^\circ]$ and $[-45^\circ, +45^\circ]$ fibre orientations are shown in Figures 3 and 4. It is observed that $[0^\circ, 90^\circ]$ specimens experience forming modes from $SR = -0.1$ to $SR = +1$. SRPP specimens with $[-45^\circ, +45^\circ]$ fibre orientations mainly experience deformation modes between uniaxial extension to shear deformation ($SR = -0.5$ to $SR = -1$). The W150 $[-45^\circ, +45^\circ]$ specimen was an exception as it exhibited a near to biaxial stretch deformation mode due to the imposed boundary condition that prevented trrellising and caused near equibiaxial stretch in the sample. It should be emphasized that the SR values indicated in figures 3 and 4 are approximate. They are just indicated to specify the deformation mode of each specimen in the last stages of deformation prior to fracture. Experimental outcomes reveal a competition among shear deformation, draw of material, and fiber extension. An increase of width allows more material to deform into the die cavity, resulting in higher forming depths and increased major strains before failure. However, in larger specimens, with a width larger than 75mm, shearing is restricted by the lock ring. In the current study, specimen with 75mm width achieves maximum forming depth. Experimental forming results demonstrate an increase of 350% in major strains in $[-45^\circ, +45^\circ]$ samples compared to $[0^\circ, 90^\circ]$ SRPP specimens.

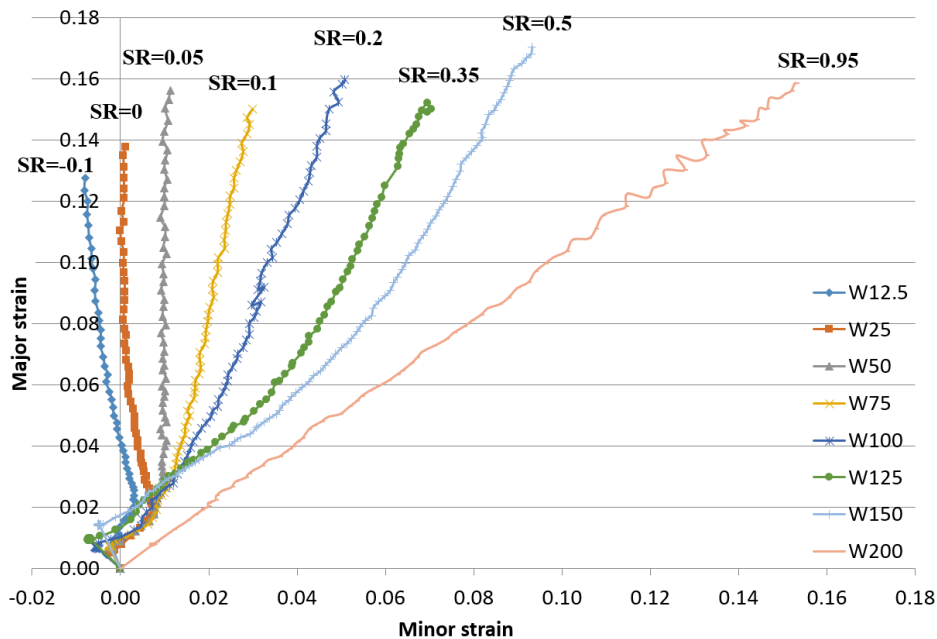


Figure 3. Strain path in $[0^\circ, 90^\circ]$ SRPP specimens

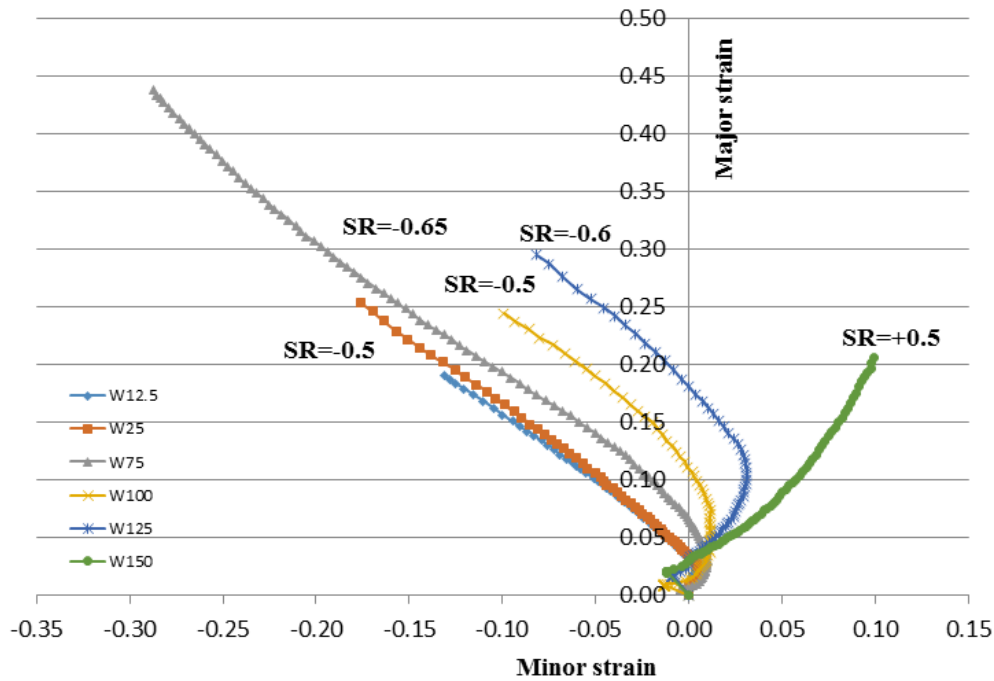


Figure 4. Strain path in $[-45^\circ, +45^\circ]$ SRPP specimens

Stamp forming of $[-45^\circ, +45^\circ]$ composite specimens fixed in the lock ring facilitates deformation through shear mode which results in higher forming depths as the composite does not prematurely fail due to fiber fracture. The outcomes of stretch forming experiments reveal the importance of shear deformation mode as the key factor in forming of woven composites in consolidated state.

Evolution of strain path at different stages of deformation is demonstrated in Figure 5. The strain path evolves at different stages of deformation indicated by different forming depths: **stage 1** or pre-stretch caused by the lock ring, **stage 2** or establishment of initial contact between punch and samples, and **stage 3** or development of contact between punch and samples. During stage 1, samples are fixed in the lock ring and extended along Y direction (Figure 1). Poisson's effect causes a contraction along X direction and therefore strain path of all specimens initiates in the second quadrant of strain space (minor strain is negative). At this stage, punch has not yet started to deform the specimen and therefore deformation along Z axis is zero. In stage 2, Punch starts its downward movement and deforms specimen in Z direction. However, deformation is localised and specimen does not conform to the punch geometry in full. In stage 3, a full contact is established and specimen completely conforms to the punch geometry along Y direction. However, specimens with less than 150mm width do not completely conform to the die geometry in X direction and therefore contact pressure is decreased. Heterogeneous contact pressure caused by fixed ends along Y direction and unconstrained edges along X direction clearly explains effect of material and contact properties on strain path at the pole, as discussed in [20].

Figure 5 compares experimental outcomes and numerical predictions on strain path at the pole in SRPP specimens having different aspect ratios. Numerical results accurately predict changes in the strain path gradient at the three specific stages of deformation (pre-stretch, initial contact, and full contact until failure). In all samples, strain path and maximum strain limit is very well predicted through the simulations.

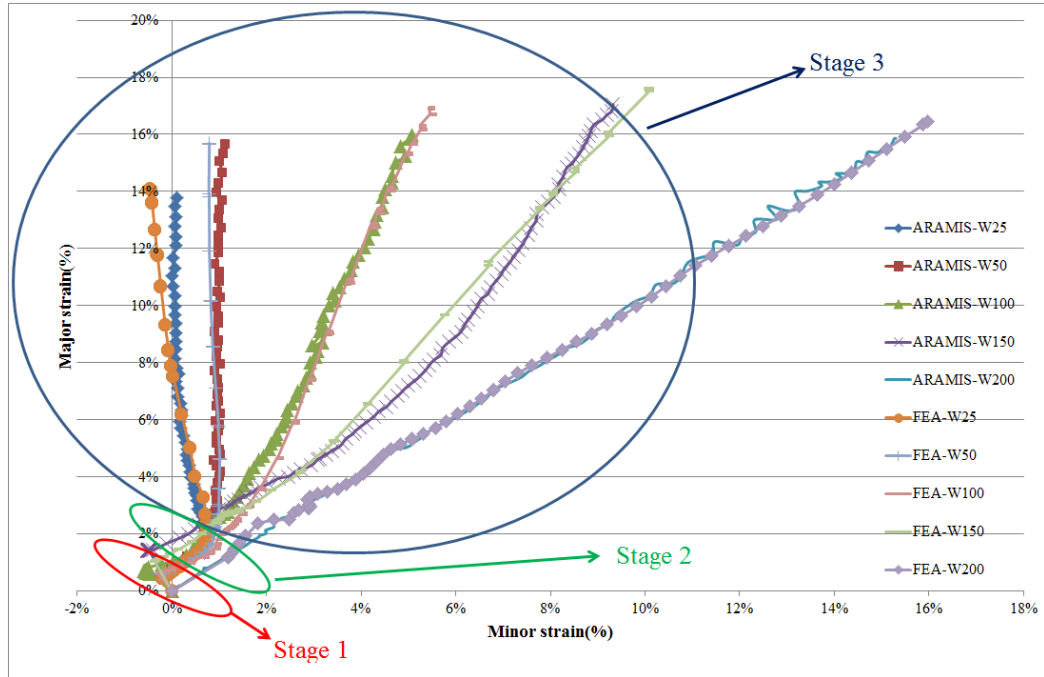


Figure 5: Comparison between strain path at the pole as measured experimentally and predicted by FEA

The observed differences between experimental and numerical results are caused by the homogeneity assumption in the modelling of the composite, which neglects highly heterogeneous behavior of woven composites and ignores localised defects due to manufacturing flaws and imperfections. Another reason for discrepancies between simulation and experimental results is due to interactions between warp and weft yarn bundles, which can only be captured by conducting extensive characterisation tests using a biaxial stretch testing machine. However, the material model developed in this study proves to be cost effective and reliable in predicting forming and failure behaviours of woven composites; the number of required characterization experiments is at a minimum and computational cost is reduced as compared to micromechanical or highly complex models considering interaction effects.

3.2 Evolution of surface strains

The failure model described by equations 6 and 7 were implemented into a finite element simulation. Failure strain has been determined by the value of major strain: for strain ratios larger than -0.5, failure occurs once the major strain exceeds 16%, under the condition that minor strain is larger than -8%. If strain ratio is less than -0.5 and minor strain is less than -8% simultaneously, composite fails if major strain exceeds the orthogonal line described by equation 7. The results of implementing the aforementioned failure criteria into the FEA are shown in Fig. 7.

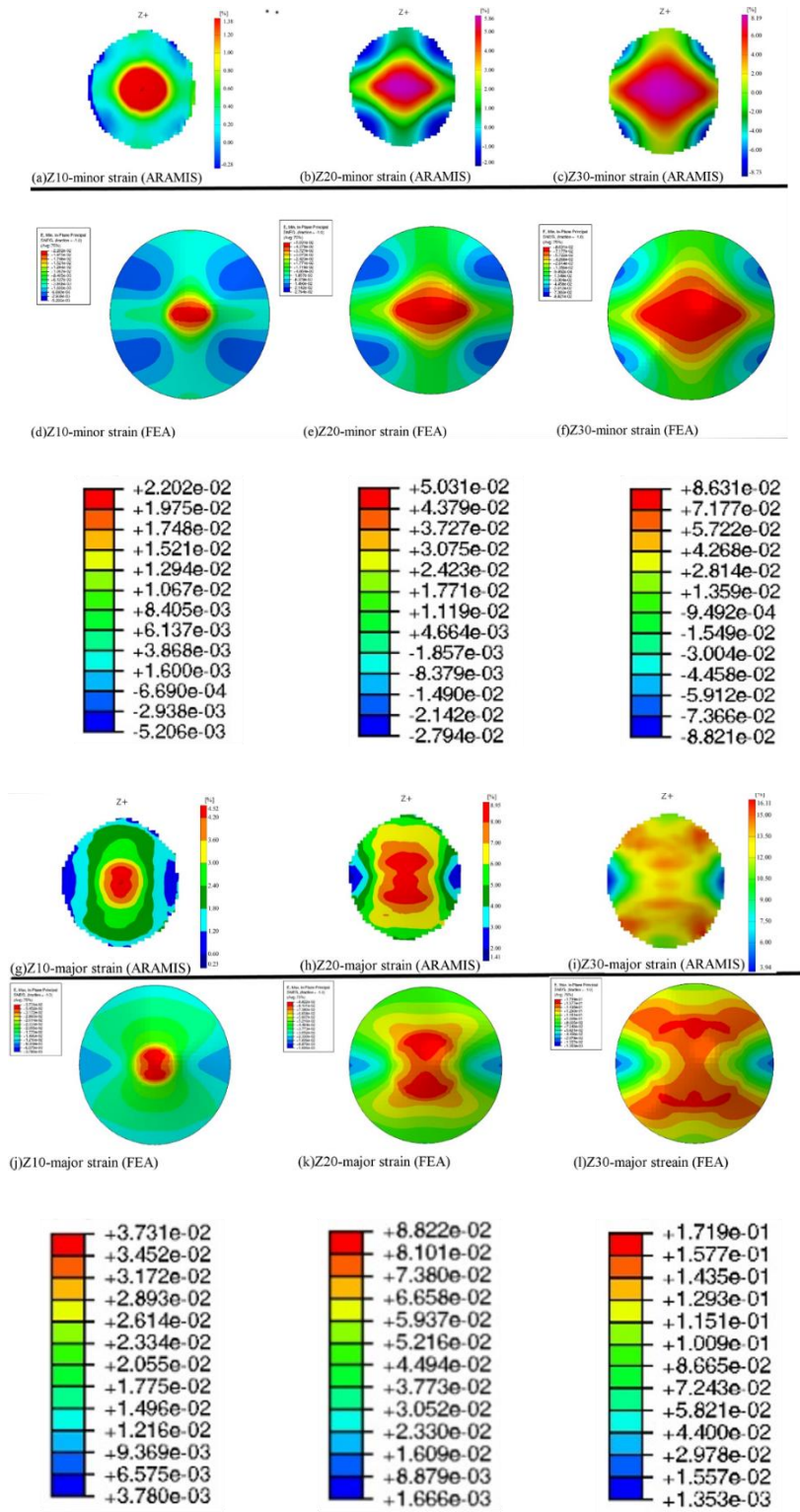


Figure 6: Evolution of surface strains as measured experimentally and predicted by FEA

The distribution of major and minor strains of a typical sample (*W150*) at different depth of deformation is shown in Figure 6. This Figure compares experimental measurements of strain conducted by DIC system with predicted values obtained from numerical simulations. These results demonstrate high correlation between experimentally measured principal strains by the ARAMIS and FEA predictions at the same depths of deformation (10mm, 20mm, and 30mm). At the very low forming depth ($Z = 10$ mm), the maximum major and minor strains cover a small region at the center of the specimen, as observed in both experimental and FEA results. The increase of forming depths expands this region, forcing it to grow toward side walls. However, the two principal strains evolve differently during deformation. The major strain stretches more along the warp fibre direction (*Y* axis) than the minor strain, indicating that the maximum strain occurs along the warp fibres due to the imposed boundary condition by the lock ring. This behaviour results in the growth of the initially circular iso-major strain envelope into an ellipsoid shape.

On the other hand, the maximum minor strain envelope grows homogenously in both the warp (*Y*) and weft (*X*) directions, making a diamond-like boundary. The predicted principal strain distribution by the FEA is very close to the pattern captured by the ARAMIS. A further increase of forming depth causes both regions to expand; however, the maximum minor strain remains in the central region of the specimen while the maximum major strain moves from the pole toward the sidewalls of the specimen along $\pm 45^\circ$ directions. This behaviour is caused by two phenomena: **1)** the maximum contact pressure loci between punch and blank, **2)** the increase of shear strain along $\pm 45^\circ$ directions. The trend and distribution of both principal strains becomes more obvious when forming depth increases. The increase in forming depth causes higher strain in specimens which, as discussed before, results in a more homogenous behaviour of the woven composite. Therefore, at higher forming depths, the surface strains become more homogenous across the surface of samples.

3.3 Failure prediction

The results of implementing strain based failure criteria into the FEA are shown in Fig. 7. The top images show photographs of fractured specimens after removal from lock ring, and the bottom images show the predicted sites of failure onset as predicted by numerical simulations. The correlations between predicted fracture loci and experimental observations are very high. In *W25* and *W100* samples, the failure initiates at a distance of 1/3 of sample's length from the lock ring and then propagates across the width of specimens to form a transverse crack. In *W150*, the failure site forms a V-shaped opening on the surface of the specimen. In *W200*, the failure initiates along 45° fibres from the pole, and then propagates to make an X-shaped crack. It is noteworthy to mention that two failure loci are predicted by FEA simulations, while the fracture started from one side of specimens during experiments. This is due to the fact that failure initiates where there is a flaw in the composite. However, in FEA simulation, no localized defect was implemented and therefore major strain pattern is completely symmetrical. The benefit of the developed numerical model lies in its ability to reveal the exact loci of failure initiation, which cannot be clearly captured by the DIC system. The results of FEA prediction on the site of fracture facilitate investigating initiation, accumulation and growth of fractures in composite specimens prior to catastrophic failure using optical microscopy systems.

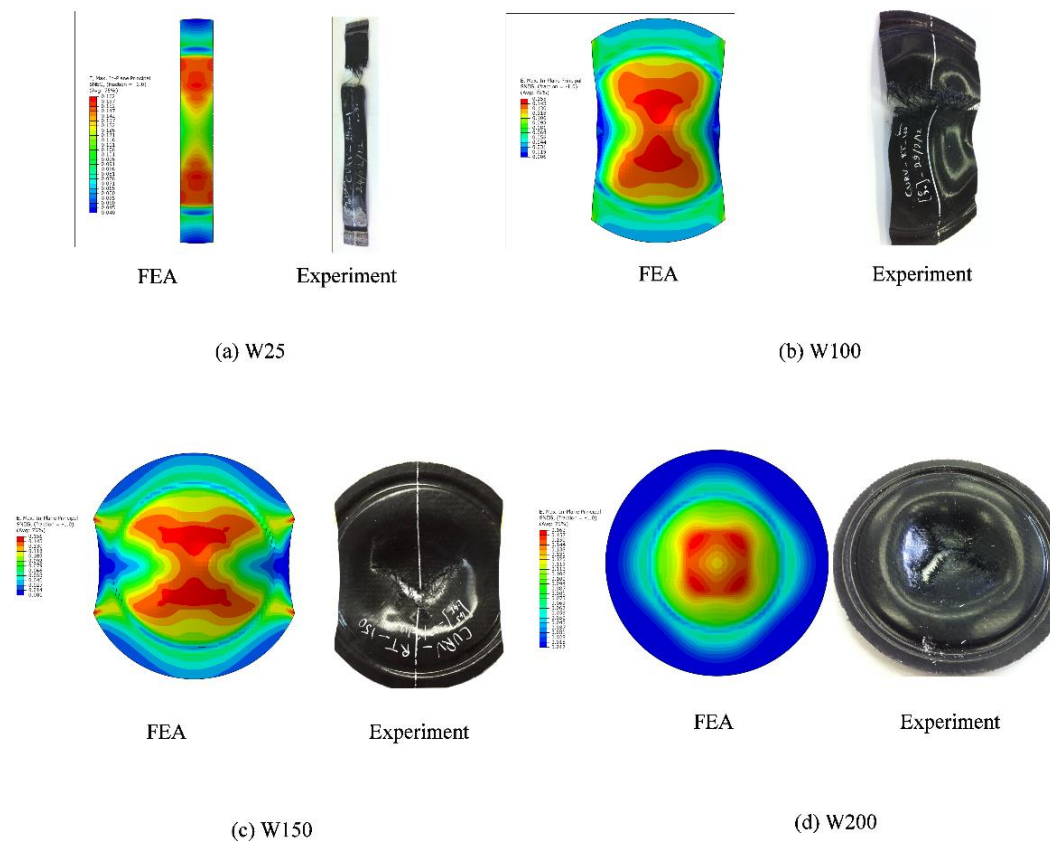


Figure 7: Comparison of predicted failure loci and fractured specimens

4. Conclusion

Characterisation experiments were conducted on a woven thermoplastic composite (SRPP) to extract material properties as functions of strains. A nonlinear orthotropic constitutive relation was adopted to develop a user defined material subroutine for the composite. Highly nonlinear behavior of the composite necessitated adopting instantaneous gradient of lateral to longitudinal strains as Poisson's ratio of SRPP, defying conventional definition used for metals. Consolidated specimens of SRPP with different aspect ratio and fibre orientation were stamp formed in a custom built press with a lock ring to experience a wide range of deformation modes prior to failure. The forming strains were continuously measured through a real time 3D photogrammetry system to capture forming and failure behaviors of the composite. Results of stamp forming experiments were used to define failure criteria of the woven composite as a function of principal strains and deformation mode. Material and failure models were implemented into a FEA simulation. The numerical predictions showed a high correlation with experiments, demonstrating its potential to accurately predict failure initiation in composite which cannot be captured using photogrammetry system. The developed failure model has the potential to predict failure of composites for complex loading conditions. This numerical model facilitates manufacturing of components from woven thermoplastic composites by eliminating the need to conduct expensive and time consuming trial and error experiments.

5. References

1. Suong D.G., Stephen V.H., Tsai W. *Composite Materials Design and Application*. Florida: CRC Press, 2003.
2. Hinton, M.J., Soden, P.D. *Predicting failure in composite laminates: the background to the exercise*. Composites Science and Technology. 1998; 58(7): 1001-10.
3. Hinton, M. J., Kaddour, A.S., Soden, P.D. *A comparison of the predictive capabilities of current failure theories for composite laminates, judged against experimental evidence*. Composites Science and Technology. 2002; 62(12): 1725-97.
4. Soden, P.D., Kaddour, A.S., Hinton, M. J. *Recommendations for designers and researchers resulting from the world-wide failure exercise*. Composites Science and Technology. 2004; 64(3): 589-604.
5. Kaddour, A.S., Hinton, M.J. *Maturity of 3D failure criteria for fibre-reinforced composites: Comparison between theories and experiments: Part B of WWFE-II*. Journal of Composite Materials. 2013; 47(6-7): 925-66.
6. Hinton, M.J., Kaddour, A.S., Soden, P.D. *Failure criteria in fibre reinforced polymer composites: the world-wide failure exercise*. Elsevier, 2004.
7. Zhou, W., et al. *Failure behavior and damage visualization of thick carbon/aramid hybrid woven composites under flexural loading conditions*, Nondestructive Testing and Evaluation, 2019; DOI: 10.1080/10589759.2019.1662902.
8. Kintada, M., Singh, A. *Progressive failure analysis of laminated composite with hole under flexural loading*. International Journal for Computational Methods in Engineering Science and Mechanics, 2018; 19(6): 419-424, DOI: 10.1080/15502287.2018.1534156.
9. Lingxiao, J., et al. *Fatigue failure characterization of multi-axial warp-knitted composites under cyclic uniaxial tensile loading*. The Journal of The Textile Institute, 2019; 110(5), 700-706, DOI: 10.1080/00405000.2018.1511230.
10. Bowkett, M., Thanapalan, K. *Comparative analysis of failure detection methods of composites materials' systems*. Systems Science & Control Engineering, 2017; 5(1), 168-177, DOI: 10.1080/21642583.2017.1311240
11. Gadade, A. M., Lal, A., Singh, B.N. *Stochastic progressive failure analysis of laminated composite plates using Puck's failure criteria*, Mechanics of Advanced Materials and Structures, 2016; 23(7), 739-757, DOI: 10.1080/15376494.2015.1029163.
12. Chelliah, S.K., Kannivel, S.K., Vellayaraj, A. *Characterization of failure mechanism in glass, carbon and their hybrid composite laminates in epoxy resin by acoustic emission monitoring*, Nondestructive Testing and Evaluation, 2019; 34(3), 254-266, DOI: 10.1080/10589759.2019.1590829.
13. Ramirez-Jimenez, C.R., et al. *Identification of Failure Modes in Glass/Polypropylene Composites by Means of the Primary Frequency Content of the Acoustic Emission Event*. Composites Science and Technology. 2004; 64(12): 1819-27.
14. Fritzsche, P., et al. *A Procedure for the Simulation of Failure in Thermoplastic Composites*. Composite Structures. 2008; 85(4): 337-49.
15. Izer, A., et al. *Effect of the Consolidation Degree on the Fracture and Failure Behavior of Self-Reinforced Polypropylene Composites as Assessed by Acoustic Emission*. Polymer Engineering & Science. 2010; 50(11): 2106-113.
16. Reyes, G., Sharma, U. *Modeling and Damage Repair of Woven Thermoplastic Composites Subjected to Low Velocity Impact*. Composite Structures. 2010; 92(2): 523-31.
17. Böhm, R., et al. *A Phenomenologically Based Damage Model for Textile Composites with Crimped Reinforcement*. Composites Science and Technology. 2010; 70(1): 81-7.
18. Hufenbach, W., et al. *The Effect of Temperature on Mechanical Properties and Failure Behaviour of Hybrid Yarn Textile-Reinforced Thermoplastics*. Materials & Design. 2011; 32(8-9): 4278-88.

19. Tsai, S.W. and Melo, J.D.D. *A Unit Circle Failure Criterion for Carbon Fiber Reinforced Polymer Composites*. Composites Science and Technology, 2016; 123: 71-78.
20. Tsai, S.W. and Melo, J.D.D. *An Invariant-Based Theory of Composites*. Composites Science and Technology, 2014; 100: 237-243.
21. Izer, A., et al. *Effect of the Consolidation Degree on the Fracture and Failure Behavior of Self-Reinforced Polypropylene Composites as Assessed by Acoustic Emission*. Polymer Engineering & Science, 2010; 50(11): 2106-2113.
22. Wang, W., Adrian L., Kalyanasundaram, S. *Effect of chemical treatments on flax fibre reinforced polypropylene composites on tensile and dome forming behaviour*. International journal of molecular sciences. 2015; 16(3): 6202-16.
23. Wang, W., et al. *Establishing a New Forming Limit Curve for a Flax Fibre Reinforced Polypropylene Composite through Stretch Forming Experiments*. Composites Part A: Applied Science and Manufacturing. 2015; 77: 114-23.
24. Zanjani, N.A., Sexton A., Kalyanasundaram S. *Induced forming modes in a pre-consolidated woven polypropylene composite during stretch forming process at room temperature: I. Experimental studies*. Composites Part A: Applied Science and Manufacturing. 2015; 68: 251-63.
25. Zanjani, N.A., Wang W., Kalyanasundaram S. *The effect of fibre orientation on the formability and failure behaviour of a woven self-reinforced composite*. Journal of Manufacturing Science and Engineering. 2015; 137(5): 0510121-9.
26. Zanjani, N.A., Kalyanasundaram, S. *Stretch Forming Simulation of Woven Composites Based on an Orthotropic Non-Linear Material Model*. Journal of Materials Science and Chemical Engineering. 2015; 3(7): 168-79.
27. <http://www.ocvreinforcements.com>

Wrinkling behaviour of a woven composite

In previous chapters, semi-rectangular specimens with different aspect ratios and fibre orientations were stretch formed to study failure of SRPP composite under tension. In this chapter, failure of SRPP composite under compressive deformation mode is investigated. Specimens with novel geometry were uniaxially extended. The distinct geometrical feature of specimens forced them to experience wrinkling during uniaxial extension, as indicated by a strain ratio of -2 . Experimental results were used to construct a wrinkling limit diagram for the composite. It was shown that wrinkling initiation cannot be predicted using conventional measures applied on metals.

In this chapter, a preliminary study on wrinkling behaviour of consolidated SRPP composite has been conducted through a modified Yoshida buckling test. Innovative geometries consisting of a main rectangular body and two lateral wings were subjected to uniaxial extension by a universal testing machine. Tensile strain in longitudinal direction caused transverse compression in samples due to Poisson's effect. Accumulation of compressive stress caused specimen to experience out-of-plane bending at some stage of deformation. Deformations and strains were recorded by a 3D optical photogrammetry system. Change in geometry of specimens after wrinkling onset was studied through the evolution of their transverse cross section.

Effect of specimens' aspect ratio on onset of wrinkling was studied. It was shown that severity and height of wrinkling are dependent to dimensions (e.g. length and width) of specimen. Evolution of principal strains before and after wrinkling initiation was investigated. It was proved that conventional wrinkling indicators, such as wrinkling limit diagram, cannot effectively predict wrinkling onset in composites. A more reliable

measure, based on evolution of local strains and their instantaneous gradients, should be developed to predict wrinkling formation during forming of woven composite specimens.

WRINKLING PHENOMENON DURING UNIAXIAL EXTENSION OF A WOVEN THERMOPLASTIC COMPOSITE

Nima A. Zanjani^{1*}, Shankar Kalyanasundaram²

^{1,2}Research School of Engineering, Australian National University, North Road, Canberra 0200, Australia

*Author to whom correspondence should be addressed
E-mail: nima.akhavan@anu.edu.au

Received 22 August 2014; accepted 7 July 2015

ABSTRACT

In the current research, wrinkling behaviour of a pre-consolidated woven self-reinforced polypropylene (SRPP) composite is investigated. Specimens possessing different aspect ratios were uniaxially extended at room temperature. Principal strains were recorded by a 3D optical photogrammetric system. Continuous measurement of out-of-plane displacements and induced in-plane strains elucidated the effect of specimens' aspect ratios on wrinkling behaviour of SRPP composite. Investigating the evolution of meridian strains offered a valuable insight into development of principal strains before and after wrinkling onset. Plotting major and minor strains in a 2D strain space clarified the role of different deformation modes in the evolution of wrinkles. It was shown that common wrinkling predictors used on metals cannot effectively predict wrinkling initiation in this class of composites and a more reliable measure, based on evolution of local strains, should be employed. The current study investigates the wrinkling behaviour of a woven thermoplastic composite for the first time through a modified Yoshida buckling experiment. The outcomes illustrated effective parameters on the wrinkling evolution in SRPP specimens.

Keywords: Principal strains, Yoshida buckling test, Wrinkling, Woven thermoplastic composites.

1. INTRODUCTION

Woven Thermoplastic Composite Materials (WTPCMs) offer attractive advantages, including excellent specific strength, improved fatigue endurance and high impact energy absorption capacity. They offer additional benefits over fibre reinforced thermosetting composites including recyclability, balanced thermo-mechanical properties and superior resistance to crack propagation [1]. However, common production methods adapted for this class of composite materials often involve labour-intensive, complex manufacturing techniques such as moulding and hand lay-up. These manufacturing processes, resulting in expensive final products, are not competitive in mass production industries. Therefore, their applications have been restricted to low volume productions such as in aerospace. To benefit from attractive properties of woven composites in a wide range of applications, new manufacturing techniques should be adopted to mass produce components from this class of composites.

Stamp forming, as a rapid production technique, have been investigated and applied extensively

on metals [2,3]. Several researchers have studied applicability of this forming process on thermoplastic composites and hybrid structures recently [4-10]. This technique consists of forming blanks rapidly by a punch and its conforming die to obtain desired geometries. The manufacturing process benefits from low manufacturing cycle time, resulting in high-quality and cost-effective final products. Stampforming of WTPCMs seems to be a promising alternative to the current manufacturing techniques of composites capable of producing hundreds of parts per hour. However, to achieve flawless products, forming and failure behaviours of WTPCMs should be studied thoroughly. Two main failure mechanisms suppressing a successful manufacturing process are fracture and wrinkling. This article investigates wrinkling behaviour of a pre-consolidated woven composite at room temperature.

Wrinkling is considered as a common type of instability when compressive stresses and strains are involved. Wrinkling is manifested through low wavelength waves in comparison with dimensions of a specimen. Wrinkling is

regarded as one of the most frequent types of instabilities in a forming process, especially as the major industrial trend is moving toward employing sheets possessing very low thickness-to-length (width) ratios. Wrinkling is not acceptable as it decreases the strength and stiffness of the manufactured parts and makes the assembly of parts difficult. Different methods have been applied to investigate wrinkling. These investigations include identifying the onset of flange wrinkling by applying Swift Cup Test [11-13], application of axial compression loads to induce buckling in specimens [14,15], employing Yoshida and modified Yoshida buckling tests in specimens with different geometries [16-19], wedge strip test method [20-22] and employing conical tapered dies [23,24].

To predict wrinkling effectively and to design flawless products with high safety factors, a concept known as Wrinkling Limit Diagram (WLD), is utilized extensively in different industries. This diagram, originally developed by Keeler, Hecker and Goodwin [2,3], comprises of principal strains induced on the surface of sheets during a manufacturing process. This diagram distinguishes between safe and failed regions in a forming practice resulted from compressive instabilities. Manufacturing components from WTPCMs is accomplished by following two different methodologies: First, Draping and subsequent consolidation of composite fabric prepregs by applying controlled pressure and temperature over sufficient period of time. Second, stamping of pre-consolidated sheets made of WTPCM. These techniques are both susceptible to the appearance of the surface wrinkles. Therefore, it is essential to evaluate the efficiency of the WLD in predicting wrinkling in a woven composite.

In the current investigation, specimens possessing specific geometries made from woven pre-consolidated SRPP were uniaxially extended at room temperature to induce wrinkling. Principal strains were recorded by a real time strain measurement system and plotted in a strain space. The effect of specimens' dimensions on the wrinkles' heights was investigated. Evolution and distribution of principal strains along longitudinal and transverse sections were investigated. The experimental outcomes were employed to

establish a Wrinkling Limit Diagram (WLD) for a woven thermoplastic composite and to investigate the effect of wrinkling onset on the evolution of WLD. It was found out that the common wrinkling predictors applied to metals could not effectively predict wrinkling onset in this class of composites. Therefore, establishing a novel indicator for predicting wrinkling initiation is necessitated if widespread application of woven composite is required.

2. EXPERIMENTAL PROCEDURE

2.1 Specimens

Specimens were made of woven self-reinforced polypropylene (SRPP) composite, CURV™, produced by Propex Fabrics of Germany. Balanced woven prepreg fabric made of highly drawn polypropylene fibres was processed through a hot compaction technique, developed at Leeds University, possessing 0.9 g/cm^3 density. Geometries utilized to investigate wrinkling behaviour of SRPP specimens were based on specimens introduced in [25]. To investigate the effect of different parameters on wrinkling initiation and to investigate WLD evolution and distribution, several geometries possessing different aspect ratios were used. The schematic of specimens and the associated dimensions are depicted in Fig. 1 and Table 1, respectively. Each sample could be virtually considered as a main rectangular part with two side wings attached to it. The total length and the thickness of all the specimens were 200mm and 1mm, respectively.

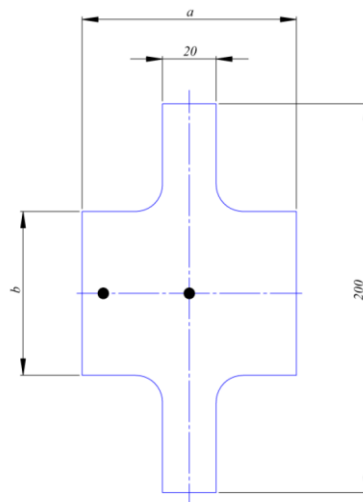


Fig. 1: Dimensions of wrinkling specimens

Table 1: Wing section variations in different specimens (Dimensions are in millimetre)

Specimen	a	b	Specimen	a	b	Specimen	a	b	Specimen	a	b
4540	45	40	5540	55	40	6540	65	40	7540	75	40
4560	45	60	5560	55	60	6560	65	60	7560	75	60
4580	45	80	5580	55	80	6580	65	80	7580	75	80

2.2 Specimens preparation and experimental setup

All specimens were cut from consolidated SRPP sheet by water jet method to decrease the amount of damage and delamination at the edge of samples. Top surface of specimens was cleaned by an isopropanol solution, followed by applying a white paint as the surface coating to provide sufficient contrast against stochastic black dot pattern applied later. The main equipment employed consisted of an INSTRON machine and an in-situ 3D-photogrammetric optical measurement system (the ARAMIS). The ARAMIS contained of two high speed CCD cameras installed on a tripod and faced toward the specimens to record deformations and their evolutions during uniaxial extension of samples. The extension rate was set to 10 mm/min and the shutter speed of cameras was selected as 2 fps (frame per second). Painted specimens were clamped between grippers of the INSTRON machine to be extended until failure. The captured images were employed to measure and calculate displacements and strains by kinematics of deformation. The outcomes of the current investigations were adopted to elucidate the effect of different parameters on wrinkling initiation and evolution in pre-consolidated SRPP specimens for the first time.

3 Results and discussions

3.1 Evolution of out-of-plane displacements

During uniaxial extension of semi-rectangular specimens, each sample elongated in vertical direction (Y) and tended to compress in horizontal direction (X) due to Poisson's effect. This generally caused positive major strain along Y-direction and negative minor strain along X-direction in samples. The excess material on the wing of specimens tended to draw inside the main rectangular region generating high compressive stresses. In-plane stiffness of specimens caused a resistance against flow of material from wings to the main part, causing a bending moment around longitudinal symmetry axis of the sample.

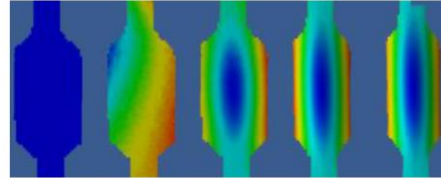


Fig. 2: Evolution of out-of-plane displacement in 4560 sample (From left to right: Y=0 mm, 0.1 mm, 5 mm, 10, 12 mm)

The evolution of out-of-plane displacements in 4560 specimen at different stages of deformation is shown in Fig. 2. First image on the left shows displacements in the fixed specimen before being clamped by the upper gripper. This indicates a strain-free condition in the specimen as it is not subjected to any external loading yet. The second image represents induced Z displacements in the sample after being fixed between both upper and lower grippers. This is called the gripper's effect, as friction between gripper and specimen caused a small amount of out-of-plane displacement in the specimen due to inducing small compressive strains in longitudinal direction. The next three images depict induced Z displacements at extensions of 5mm, 10mm and 12 mm respectively, all signifying post wrinkling behaviour of the specimen. Acute observations revealed specific behaviour of SRPP specimens before and after wrinkling onset:

- Out-of-plane displacements initiate in two regions: edges of the sample in wing areas and centre of specimen. However, the directions of induced out-of-plane displacements in these two areas are opposite to each other. Edges tend to buckle in positive direction (outward) while pole exhibited negative displacement (inward), or vice versa. The directions of Z-displacements in these two regions were completely unpredictable as they were dependent to the inherit asymmetry of the material caused by imperfections. However, the induced principal

strains in concave and convex surfaces were completely different due to through-thickness effects commonly observed during bending of plates and shells.

- Wrinkling waves in the rectangular section were manifested around the middle of the specimen or pole. However, by an increase in Y extension, the highly buckled area extended more toward both fixed ends of the specimen along longitudinal direction, depicted by the dark blue central region. In other words, the width of the buckled region remained constant during the experiment, while its length increased as the applied extension increased. The transverse buckling waves could be better visualised in Fig. 3, representing the evolution of the transverse section in 4560 specimen during experiment at extensions of 0 , 5 , 10 and 12 mm. These images reveal the shape of specimen at different stages of deformation by the amount of induced out-of-plane displacements across the transverse section passing through the middle of the specimen (the pole).

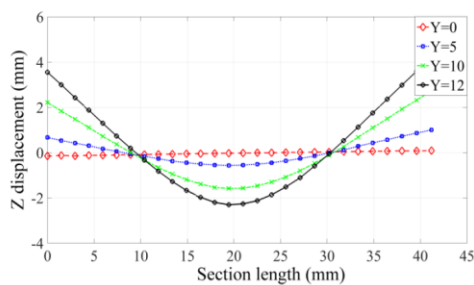


Fig. 3: Evolution of transverse section in 4560 specimen (Y is in mm)

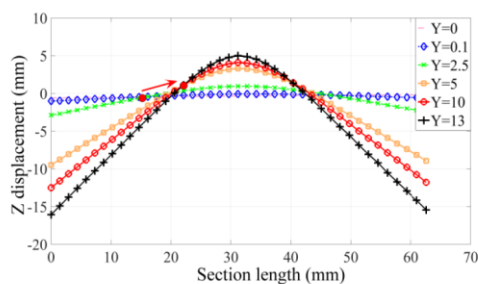


Fig. 4: Evolution of transverse section in 6580 specimen (Y is in mm)

- The evolution of neutral point (surface) during wrinkling could be observed in Figs. 3 and 4. In Fig. 3 the neutral point moves on a

straight horizontal line, while in Fig. 4 it moves on a curved path. Initially, the neutral surface is located toward the outer edges of the wing area. However, as extension increases, this neutral surface moves toward the centre of specimen on a curved path indicated by the arrow. The observed differences between the evolutions of spatial coordinates of neutral points during wrinkling demonstrate dependency of wrinkling phenomenon to the aspect ratio of SRPP samples.

- Resultant transverse sections of different specimens at the last stage of deformation are depicted in Fig. 5. The identical cross section of different specimens suggests that the developed wrinkling wave is dependent to the materials property such as in-plane components of stiffness and bending stiffness, or E , G and EI , respectively (E and G depicts young and shear moduli, while I represents moment of inertia of the section). Therefore, it is reasonable to conclude that coefficients of the parametric equation describing quadratic shape of the curved sections are dependent to the material property which could be obtained by characteristic experiments such as uniaxial extension and bias tests. However, the induced out-of-plane displacements in different specimens, represented in Fig. 6, elucidate the dependency of buckles height to dimensions of the specimen. Therefore, it is reasonable to conclude that wrinkling initiation and evolution and deformed cross-section of SRPP specimens due to buckling are all functions of both material properties and specimen geometries.

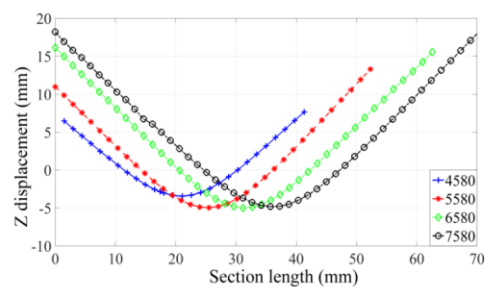


Fig. 5: Final cross-section of different specimens prior to failure

- Fig. 6 reveals the dependency of wrinkling height to both width and length of the wing area or to the aspect ratio of specimens. Each series represent a unique width of the wing area (depicted by parameter a). Horizontal axis exhibits the length of the wing (parameter

b) and vertical axis represents final Z displacements calculated by adding the heights of induced wrinkles at both the edge and the pole locations. The gradient of curves in different regions is identical. This suggests the similar effect of width variation in each group of specimens. However, the overall variations in the wrinkling heights are not proportional to these parameters, as the gradients of curves between 45 to 55 and 55 to 65 series are not identical. This suggests a complicated correlation between out-of-plane deformation and aspect ratio of SRPP specimens during wrinkling.

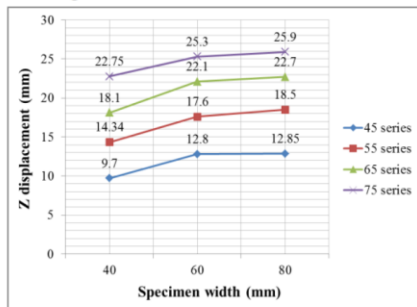


Fig. 6: Evolution of Z-displacement in different specimens

3.2 Evolution and distribution of principal strains

Major and minor strains distributions and their evolutions along longitudinal and transverse cross sections of a typical specimen are represented in Fig. 7. Strain distributions along these two axes are represented during different stages of deformation up to failure. These evolutions are depicted in terms of induced out-of-plane displacements. A meticulous observation reveals fundamental behaviour of pre-consolidated woven SRPP during wrinkling in terms of principal strains' evolutions:

- Major and minor strains distributions along transverse section are influenced by wrinkling behaviour. In pre-buckling stage of deformation, the distribution of principal strains is uniform along this section. However, after 5mm of Y-displacement (depicting wrinkling onset), the major strains are localised more in the centre of specimen than wings region. This could be interpreted as the effect of out-of-plane displacement in reducing the induced principal strains in wing areas. This is caused by decreasing wings' contributions in overall in-plane stiffness of the specimen after onset of

buckling. The 'edge effect' could also be observed in principal strains' evolution as their magnitudes tend to zero near the edges.

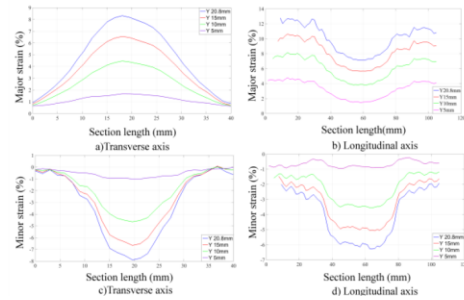


Fig. 7: Evolution of major and minor strains along longitudinal and transverse axes of 4560 specimen

- Evolution of principal strains along longitudinal axis is less affected by wrinkling phenomenon, as the difference between major and minor strain values at different stages of buckling is proportional to the buckling height. In other words, initiation of buckling does not affect the trend of evolution of principal strains. Interestingly, the value of major strain in the middle of the specimen tends to decrease as the cross section of the specimen becomes larger. This represents the heterogeneous nature of strain distribution in the specimen. In other words, strains in specimens possessing variable width could not simply be depicted by an average value, yet its dependency to the location should also be considered if an accurate distribution of strains is required. Moreover, the amount of fluctuations and spiky behaviour in longitudinal axis is more significant than transverse section exhibiting a more uniform and homogenous behaviour in the distribution of principals trains. The underlying reason for this behaviour is the angle between fibre orientation in the specimens and applied loads. Another effective parameter in wrinkling is the imposed boundary conditions. All specimens possessed $[0^\circ, 90^\circ]$ fibre orientations and there were clamped and loaded along their longitudinal fibre axes. Therefore, initial clamping and loading of the specimen caused high amount of pre-tension in these direction and therefore influencing the friction condition between warp (longitudinal) fibres. These conditions resulted in spiky and non-uniform behaviour of major and minor strains along warp (longitudinal) direction caused by the

change in friction condition between interlacing yarns.

- Another significant difference between longitudinal and transverse principal strains evolution is observed through a more uniform, less abrupt variations in transverse direction compared to a rapid variation along longitudinal axis, between 40mm to 80mm distance along this axis. The difference between major and minor strains behaviours in these two orthogonal directions highlights the effect of applied boundary conditions and variations of sample's width on principal strains' evolution. Warp fibres are clamped by the upper and lower grippers and therefore the induced deformations are restricted by the enforced boundary conditions and high pre-tension prior to the start of experiments. This specific forming condition results in a more heterogeneous behaviour of warp compared to weft fibres.

- The difference between major and minor strains along longitudinal axis at different buckling heights remains identical. This means that major and minor strains along longitudinal axis proportionally vary with wrinkles height. However, along transverse direction, the change in principal strains is disproportional to the induced wrinkles height. This is due to different response of specimen to uniaxial extension in wing and rectangular areas, specifically after onset of buckling. These behaviours are caused by different boundary and load conditions and the contact between interlacing yarns.

3.3 Evolution of Wrinkling Limit Diagram

A Wrinkling Limit Diagram (WLD) is a graphical representation of induced strains in different regions of a sample before and after onset of wrinkling. Its significance in industrial application is manifested through its capability to distinguish between wrinkled and unwrinkled regions in strain space and therefore it is widely employed by product engineers and designers to determine safe deformation margins. Generally, in a strain space, different ratios of minor to major strains exhibit different deformation modes. These modes include biaxial stretch, plane strain, uniaxial extension, shear and wrinkling modes. The attributed strain ratios depicting these deformation modes are +1, 0, -0.5, -1 and -2, respectively (as depicted by parameter SR in Fig. 8). Therefore, a line drawn in strain space, depicting minor to major strains of -2, is generally used to differentiate between wrinkled and unwrinkled areas.

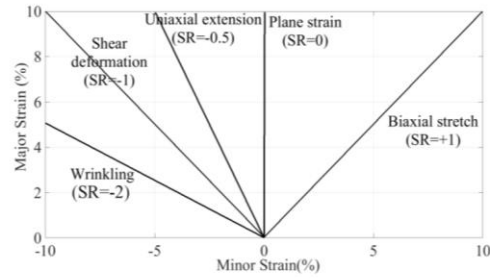


Fig. 8: Incorporated deformation modes in a forming practice

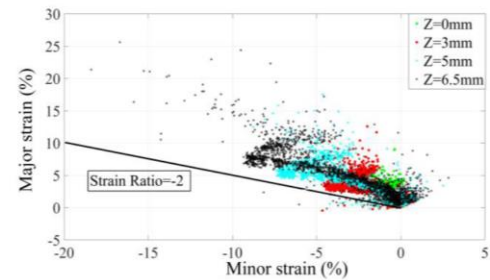


Fig. 9: Wrinkling Limit Diagram of 5580 specimen at different stages of deformation

To investigate the validity and applicability of this wrinkling measure on woven thermoplastic composites, the evolution of surface strains in a pre-consolidated woven SRPP is investigated. This measure was used to clarify the evolution of principal strains prior and after buckling onset in specimens. Fig. 9 represents WLD of a typical SRPP specimen during various stages of a modified Yoshida buckling test. These stages include one stage prior to buckling initiation, and post-buckling stages including Z displacements of 3mm, 5mm and 6.5 mm. It is noticeable that wrinkles heights were measured on a point near the edge of the wing and they do not depict total wrinkling height in 5580 specimen measured by the difference between displacements at the pole and the edge.

Prior to buckling initiation, the strain distributions in 5580 specimen were located between uniaxial extension and plane strain modes. The surface of specimen did not experience out-of-plane displacements and therefore wrinkling predictions based on outcomes of the wrinkling limit diagram deemed to be reliable. However, after onset of buckling, signified by Z of 3mm, the surface strains distribution evolved in strain space, occupying a region between uniaxial extension

and shear deformation mode. Small amount of surface strains were positioned under wrinkling limit line, predicting a small region on the specimen experiencing wrinkling. This prediction could be justified by observing a very small area in the centre of specimen experiencing negative minor strain or compressive strain (Fig. 10). However, the points located below the wrinkling limit curve do not contain all points experiencing wrinkling including wing areas. The increase in extension caused a significant growth in both the magnitude of compressive strains developed in the specimen and the area experiencing negative minor strain (Fig. 9 and 10). However, by increasing the value of Z-displacement and enlarging the affected area, the wrinkling limit diagram moved away from strain ratio of -2 toward uniaxial extension mode. It can be observed from Fig. 10 that although the maximum minor strain has increased from -5% in Z=3mm to minor strains of -8% and -15% in Z=5 and 6.5mm respectively, disproportional increase in major strain caused strain distribution to deviate from wrinkling limit diagram toward higher strain ratios.

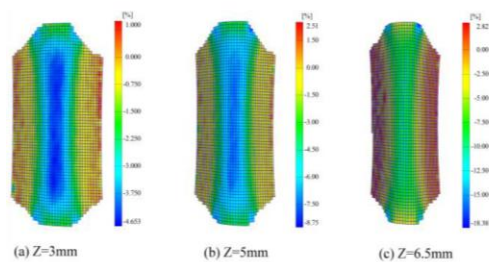


Fig. 10: Distribution of minor strains at different stages of deformation in 5580 specimen: a) Z=3 mm b)Z=5 mm c)Z=6.5 mm

These observations are contradictory to the common behaviour of metals representing strain ratio of -2 during wrinkling. The experimental outcomes reveal woven thermoplastic composite materials do not necessarily follow common wrinkling path in a strain space and the evolution of strains in SRPP specimens does not necessarily intersect with wrinkling limit curve during wrinkling. The underlying reason is probably different mechanisms triggering onset of buckling in metals and woven composites. This suggests that wrinkling initiation in a woven thermoplastic composite cannot be accurately predicted by merely using a wrinkling limit diagram. Therefore a more

effective wrinkling predictor is required if wrinkling should be avoided during manufacturing of components made of woven composite materials. Applying an efficient, reliable and convenient wrinkling predictor is necessitated in high-volume industries where a combination of rapid production methodology and low-cost manufacturing is desirable. Widespread application of woven thermoplastic materials in industries demanding low-weight, high strength and environmental friendly materials, requires application of an effective method to predict and to hamper wrinkling. This would be the subject of future research on wrinkling of woven composites.

4. CONCLUSIONS

Wrinkling is a common instability observed during manufacturing components made of thin sheets. This is an undesirable phenomenon as it affects both functionality and appearance of products. Wide spread application of light-weight, high strength components made of woven thermoplastic composite materials necessitates a systematic approach in studying of the response of these materials when subjected to compressive strain and stress states. This facilitates finding proper measures to predict and hamper wrinkling during manufacturing components made of woven composites. To investigate the wrinkling behaviour of a woven pre-consolidated self-reinforced polypropylene, twelve samples possessing specific geometries were subjected to uniaxial extension via a modified Yoshida buckling test. The specific geometry of these specimens caused high compressive stresses in the material leading to onset of out-of-plane deformations during some stages of uniaxial deformation. Results of an optical photogrammetry measurement elucidated distribution and evolution of displacements and strains in different regions of specimens before and after wrinkling onset. It was found out that wrinkling was initiated from the wing and central areas of the specimens as a result of Poisson's effect, although directions of induced out-of-plane displacements in these two regions were opposite to each other. The similarity in deformed cross sections of specimens due to buckling, suggested the dependency of out-of-plane deformations on material properties. However, variations in specimens' aspect ratios affected the height of wrinkles. Therefore, it was concluded that wrinkling deformation in

woven SRPP was not only a function of material properties, but also was affected by specimen geometry. Evolution of principal strains along transverse and longitudinal axes of specimens revealed the effect of width variations, boundary conditions and load orientation on major and minor strains. Due to these effective parameters, the fluctuations and spiky behaviour in induced strains was more pronounced in longitudinal than transverse directions. The distribution of principal strains revealed the heterogeneous behaviour of SRPP during wrinkling and therefore revealed the unsuitability of employing an average strain

measure to predict and prevent wrinkling. Examination of common wrinkling predictors on pre-consolidated SRPP specimens, such as a wrinkling limit diagram, elucidated their inefficiency on predicting wrinkling in this class of composite materials. This study revealed the importance of considering the wrinkling mechanism associated with wrinkling onset in a woven composite. Therefore it is suggested that a novel predictor based on local strains should be sought if a more accurate wrinkling predictor is required for this class of composites.

References:

1. **Suppakul P., Bandyopadhyay S.**, "The effect of weave pattern on the mode-I interlaminar fracture energy of E-glass/vinyl ester composites", *Composites Science and Technology*, **62** (2002), 709–717.
2. **Goodwin G.M.**, "Application of strain analysis to sheet metal forming problems in the press shop", *Metallurgia Italiana*, **60** (1968), 764-774.
3. **Hecker S.S.**, "Simple technique for determining forming limit curves", *Sheet metal industries*, **53** (1975), 671-675.
4. **Sexton A., Cantwell W.J., Kalyanasundaram S.**, "Stretch forming studies on a fibre metal laminate based on a self-reinforcing polypropylene composite", *Journal of Composite Structures*, **94** (2012), 431-437.
5. **Mosse L., Cantwell W.J., Cardew-Hall M.J., Compston P., Kalyanasundaram S.** "The Effect of process temperature on the formability of fibre-metal laminates", *Composites Part A*, **36** (2005), 158-166.
6. **Mosse L., Compston P., Cantwell W.J., Cardew-Hall M.J., Kalyanasundaram S.** "Stamp forming of polypropylene based fibre-metal laminates: The effect of process variables on formability", *Journal of materials processing technology*, **172** (2006), 163-168.
7. **Kalyanasundaram S., DharMalingam S., Venkatesan S., Sexton A.**, "Effect of process parameters during forming of self-reinforced PP-based fibre metal laminates", *Composite structures*, **97** (2012), 332-337.
8. **A. Zanjani N., Kalyanasundaram S.**, "Induced forming modes in a self-reinforced polypropylene sheet during stretch forming process at room temperature: I-Experimental Studies", *Composites Part A: Applied Science and Manufacturing*, **68** (2015), 251-263.
9. **A. Zanjani N., Wang W., alyanasundaram S.**, "The effect of fibre orientation on the formability and failure behaviour of a woven self-reinforced composite during stamp forming", *ASME – J. Manuf. Sci. Eng* (2015). (in press) (doi:10.1115/1.4030894)
10. **Wang W., Lowe A., Davey S., A. Zanjani N., Kalyanasundaram S.**, "Establishing a new forming limit curve for a flax fibre reinforced polypropylene composite through stretch forming experiments", *Composites Part A: Applied Science and Manufacturing*, **77** (2015), 114-123.
11. **Thirumarudchelvan S., Loh N.H.**, "Deep drawing of cylindrical cups with friction-actuated blank holding", *Journal of Materials Processing Technology*, **40** (1994), 343-358.
12. **Triantafyllidis N., Needleman A.**, "An analysis of wrinkling in the Swift cup test", *Journal of Engineering Materials and technology*, **102/3** (1980), 241-248.
13. **Samanta S.K., Mitra A., Maity A.K.**, "3D finite element analysis of wrinkling in the swift-cup test: Onset and growth", *Publication of American Society of Mechanical Engineers*, **39** (1992), 75-86.
14. **Lee L.H.N.**, "Inelastic buckling of cylindrical shells under axial compression and internal pressure", *Proceedings of the Seventh Midwestern Mechanics Conference*, **1**(1961), 190–202.
15. **Paquette J.A., Kyriakides S.**, "Plastic buckling of tubes under axial compression and internal pressure", *International Journal of Mechanical Sciences*, **48** (2006), 855-867.
16. **Cheng H.S.**, "Experimental and numerical analysis of the buckling and post-buckling phenomenon in the Yoshida test", *Proceedings of the International*

- Conference on Manufacturing Science and Engineering, 2006.
- Wan M.**, “Wrinkle behaviour of automobile thin sheet metals by modified Yoshida buckling test”, *Material science and technology*, **12** (2004), 442-445.
- Kim J.B.**, “Wrinkling initiation and growth in modified Yoshida buckling test: finite element analysis and experimental comparison”, *International Journal of Mechanical Sciences*, **42** (2000), 1683-1714.
- Wang X., Cao J.**, “On the prediction of side-wall wrinkling in sheet metal forming processes”, *International Journal of Mechanical Sciences*, **42** (2000), 2369–2394.
- Lu H., Cheng H.S., Cao J., Liu W.K.** “Adaptive enrichment meshfree simulation and experiment on buckling and post-buckling analysis in sheet metal forming”, *Computer Methods in Applied Mechanics and Engineering*, **194** (2005), 2569–2590.
- Cheng H.S., Cao J., Yaob H., Liu S.D., Kinsey B.**, “Wrinkling behaviour of laminated steel sheets”, *Journal of Materials Processing Technology*, **151** (2004), 133–140.
22. **Cao J., Wang X., Mills F.A.**, “Characterization of sheet buckling phenomenon subjected to controlled boundary constraints”, *ASME J. Manuf. Sci. Eng.*, **124** (2002), 493–501.
23. **Narayanasamy R., Loganathan C.**, “Some studies on wrinkling limit of commercially purealuminium sheet metals of different grades when drawn through Conical and Tractrix dies”, *International Journal of Mechanics and Materials in Design*, **3** (2006), 129–144.
24. **Narayanasamy R., Sathiya Narayanan C.**, “Wrinkling behaviour of interstitial free steel sheetswhen drawn through tapered dies”, *Materials and Design*, Vol. **28** (2007), 254–259.
25. **Schleich R., Albiez C., Papaioanu A., MBA M.L.**, ‘Investigation on simulation of buckling of aluminium sheet alloys’, 7th European LS-DYNA Conference, 2009.

Summary and future work

9.1 Introduction

Currently, there is a major concern regarding application of composites in high volume industries to address energy consumption and sustainability issues. Woven thermoplastic composites have shown potential to be used in a wide range of applications owing to their full recyclability, balanced thermomechanical properties, and ease of processing compared to thermosets. However, forming and failure behaviours of thermoplastic composites are different from their thermoset counterparts as a result of their dissimilar microstructure and polymeric bonds. As such, conventional failure models developed for thermoset composites are not suitable for predicting failure in woven thermoplastic composites made by high volume manufacturing processes. According to a recent survey on performance and accuracy of existing failure theories (WWFE), existing models are incapable of accurately predicting failure in composites under complicated loading conditions.

The current research aims at developing a fundamental understanding of the formability and failure behaviour of woven thermoplastic composites. This project targets studying forming, failure, and wrinkling behaviours of woven thermoplastic composites through combined experimental and numerical analyses. A custom-built press with a hemispherical punch was used to form specimens into an open die until failure. A three-dimensional real time photogrammetry system was used to capture deformations and strains on the surface of samples during all stages of deformation. A failure limit diagram was constructed to capture failure of the composite under a wide range of deformation modes. Characterisation experiments were conducted to develop a constitutive material model for the woven composite. Material and failure models were implemented into a finite element simulation

to predict formability and failure of a woven thermoplastic composite and assess its reliability and accuracy by benchmarking against experiments. In the last part of this thesis, an innovative modified Yoshida buckling test was designed and for the first time wrinkling behaviour of a woven composite using a wrinkling limit diagram was studied. Evolution of strains before and after wrinkling initiation was captured and it was concluded that an indicator based on instantaneous gradient of the strain ratio could effectively capture wrinkling initiation in composites.

9.2 Contributions

- A novel experimental set-up was designed to study forming and failure of pre-consolidated woven thermoplastic composites including a self-reinforced polypropylene composite (SRPP) and a glass fibre reinforced polypropylene composite (GRPP).
- Specimens having semi-rectangular geometries, with different aspect ratios and fibre orientations, were stretch formed by a hemispherical punch in an open die equipped with a built-in lock ring system. Surface strains were measured using an in-situ photogrammetry measurement system and a digital image correlation technique.
- Principal strains were captured during forming and plotted in a two-dimensional space to construct a path dependent failure envelope for the SRPP composite.
- The failure envelope was used to develop an analytical failure model for the SRPP composite based on induced deformation modes and principal strains.

- The effect of fibre orientation, specimens' aspect ratio and boundary condition on formability, strain evolution, and failure mechanism of woven composites were studied.
- Consolidated composite specimens were characterised through uniaxial and bias extension tests using a universal testing machine, real time strain measurement system and dynamic extensometers.
- Characterisation experiment results demonstrated a highly nonlinear dependency between longitudinal and transverse strains of SRPP composite during deformation. This behaviour necessitated adopting an incremental approach to re-define Poisson's ratio of the composite.
- Constitutive equations were used to develop a nonlinear orthotropic material model. This model was implemented into a user defined material system (UMAT) using FORTRAN.
- Stretch forming of a woven composite was modelled in a finite element simulation software (Abaqus/implicit). UMAT was incorporated into the analysis to predict and benchmark formability and failure of the SRPP composite against experimental results.
- Strain path at the pole of specimens, strain distribution and evolution at different depths of forming, and failure onset and loci were used as measures to evaluate accuracy and reliability of the numerical model. FEA results showed a very good agreement with experiments.
- A novel modified Yoshida buckling test was designed to study failure of the consolidated SRPP composite under compressive state of stress.
- Specimens with different fibre orientations and aspect ratios were tested using a universal testing machine and a real time strain measurement system.

- Distribution and evolution of strains before and after wrinkling onset were examined using a photogrammetry strain measurement system.

9.3 Summary of findings

1. Stretch forming studies have been conducted on a woven self-reinforced composite to investigate the formability of the composite and develop a strain-based failure criteria for predicting failure under a wide range of deformation modes.
2. Specimens with different aspect ratios were stretch formed to induce failure under a wide range of deformation modes.
3. Outcomes of these experiments showed that due to a uniform strain distribution and the absence of localised thinning, the woven self-reinforced composite could be formed into complex doubly-curved geometries without experiencing failure.
4. The combined effect of boundary condition, aspect ratio and fibre orientation of specimens resulted in forming and failure under a specific mode of deformation including biaxial stretch, plane strain, uniaxial extension, shear deformation and wrinkling.
5. Localised strain ratio, defined by the ration of minor to major strain, and the strain path at a specific location determined whether a composite forms or fails under a particular forming condition.
6. A change of fibre orientation in SRPP composite facilitates achieving higher forming depths in areas prone to failure due to a change in deformation mode.
7. A change in fibre orientation causes a drastic change in the observed failure mechanism during forming of SRPP composite.

8. Structural and mechanical properties of reinforcements have a noticeable impact on formability and failure behaviour of woven thermoplastic composites.
9. Results of forming tests demonstrated that the formability of a consolidated composite depends strongly on type of reinforcements and induced deformation modes.
10. Results of stamp forming on a glass-fibre reinforced (GRPP) and a self-reinforced polypropylene (SRPP) composite showed that the former mainly fails due to fibre fracture while the latter fails by a combined failure mechanisms due to identical properties of reinforcements and the matrix.
11. Forming and failure off GRPP composite are highly sensitive to the strain path while in SRPP composite deformation mode has a more pronounced impact.
12. Reinforcements used in SRPP are ductile as opposed to brittle nature of glass fibres in GRPP. Thus, SRPP can sustain large deformations before catastrophic failure while failure in GRPP initiates early during forming until total failure of the structure.
13. Poisson's ratio and coefficient of friction have a major impact on the formability of narrow SRPP samples, while in wider specimens shear stiffness and young's modulus have a more pronounced effect.
14. Shear deformation plays a major contribution in the formability of SRPP.
15. Result of wrinkling experiments showed that severity and height of wrinkles were dependent to the aspect ratio of specimens.
16. It was shown that the gradient of principal strains is a more suitable measure to predict onset of compressive instabilities than a wrinkling limit diagram. This measure can be used as a universal criterion to predict wrinkling onset in a wide range of material systems including woven thermoplastic composites.

9.4 Future work

- It is expected that high temperature forming of the composite facilitates achieving greater depth of deformation due to a reduced shear stiffness and requires further investigations.
- Material properties of woven composites should be characterised at elevated temperatures. The results can be used to study the effect of temperature on evolution of mechanical properties and develop a temperature-dependant constitutive equation for the woven SRPP composite.
- Forming studies need to be undertaken at high temperatures to determine the optimum process parameters and study failure mechanisms of the SRPP composite under different deformation modes and forming temperatures. The results would be adopted to develop a temperature dependant FLC for SRPP.
- High temperature material and failure models obtained by experimental studies could be incorporated into a coupled thermomechanical finite element analysis to predict forming and failure behaviours of woven composites under complex loading conditions.
- Using a biaxial testing machine, forming and failure behaviours of the composite under different strain paths at room and elevated temperatures can be studied. Results can be used to validate and refine the proposed failure model, if necessary.
- Using Scanning Electron Microscopy (SEM) and CT-scan techniques can reveal initiation and evolution of micro-cracks in woven composites and their relation with modes of deformation. The results can be adopted to develop a multi-scale failure model.

Bibliography

1. Shafiee, S. and E. Topal, *When will fossil fuel reserves be diminished?* Energy Policy. vol. **37**(1): pp. 181-189, 2009.
2. Abas, N., A. Kalair, and N. Khan, *Review of fossil fuels and future energy technologies.* Futures. vol. **69**: pp. 31-49, 2015.
3. Mohr, S., et al., *Projection of world fossil fuels by country.* Fuel. vol. **141**: pp. 120-135, 2015.
4. Höök, M. and X. Tang, *Depletion of fossil fuels and anthropogenic climate change—A review.* Energy Policy. vol. **52**: pp. 797-809, 2013.
5. Speirs, J., C. McGlade, and R. Slade, *Uncertainty in the availability of natural resources: Fossil fuels, critical metals and biomass.* Energy Policy. vol. **87**: pp. 654-664, 2015.
6. Le Quere, C., et al., *Trends in the sources and sinks of carbon dioxide.* Nature Geoscience. vol. **2**(12): pp. 831-836, 2009.
7. Andres, R.J., et al., *Monthly, global emissions of carbon dioxide from fossil fuel consumption.* Tellus Series B-Chemical and Physical Meteorology. vol. **63**(3): pp. 309-327, 2011.
8. Hansen, J., et al., *Global temperature change.* Proceedings of the National Academy of Sciences of the United States of America. vol. **103**(39): pp. 14288-14293, 2006.
9. Schipper, L., et al., *The evolution of carbon dioxide emissions from energy use in industrialized countries: an end-use analysis.* Energy Policy. vol. **25**(7-9): pp. 651-672, 1997.
10. Koffler, C. and K. Rohde-Brandenburger, *On the calculation of fuel savings through lightweight design in automotive life cycle assessments.* International Journal of Life Cycle Assessment. vol. **15**(1): pp. 128-135, 2010.
11. Bilgen, S., K. Kaygusuz, and A. Sari, *Renewable energy for a clean and sustainable future.* Energy Sources. vol. **26**(12): pp. 1119-1129, 2004.
12. <http://www.energy.gov/>.
13. European Commission of Energy, *Progress towards achieving the KYOTO and EU2020 objectives*, 2014.

14. Garnaut, R., *The Garnaut climate change review*. Cambridge University Press, 2008.
15. <https://www.compositesworld.com/articles/the-outlook-for-thermoplastics-in-aerospace-composites-2014-2023>.
16. http://www.engineering.lancs.ac.uk/structures/fibre_reinforced_composites.htm.
17. Khan, G.A., et al., *Studies on the mechanical properties of woven jute fabric reinforced poly (l-lactic acid) composites*. Journal of King Saud University-Engineering Sciences. vol. **28**(1): pp. 69-74, 2016.
18. Breuer, U. and M. Neitzel, *The challenge of stamp forming high-strength thermoplastic composites for transportation*. Society for the Advancement of Material and Process Engineering(USA). vol.: pp. 1508-1519, 1997.
19. Suemasu, H., K. Friedrich, and M. Hou, *On deformation of woven fabric-reinforced thermoplastic composites during stamp-forming*. Composites Manufacturing. vol. **5**(1): pp. 31-39, 1994.
20. Hou, M. and K. Friedrich, *3-D stamp forming of thermoplastic matrix composites*. Applied Composite Materials. vol. **1**(2): pp. 135-153, 1994.
21. Zhu, B., et al., *Experimental investigation of formability of commingled woven composite preform in stamping operation*. Composites Part B: Engineering. vol. **42**(2): pp. 289-295, 2011.
22. Gamstedt, K. and S.I.S. Andersen, *Fatigue degradation and failure of rotating composite structures-Materials characterisation and underlying mechanisms*. 2001.
23. Topal, S., et al., *Late-stage fatigue damage in a 3D orthogonal non-crimp woven composite: An experimental and numerical study*. Composites Part A: Applied Science and Manufacturing. vol. **79**: pp. 155-163, 2015.
24. Boniface, L., *Damage development in fibre-reinforced plastics' laminates*. University of Surrey (United Kingdom). 1989.
25. Jamison, R.D., *On the interrelationship between fiber fracture and ply cracking in graphite/epoxy laminates*, in *Composite Materials: Fatigue and Fracture*. ASTM International, 1986.
26. Tarakçioğlu, N., L. Gemi, and A. Yapici, *Fatigue failure behavior of glass/epoxy±55 filament wound pipes under internal pressure*. Composites Science and Technology. vol. **65**(3-4): pp. 703-708, 2005.
27. <http://F-16.net>.

28. Hinton, M.J., A.S. Kaddour, and P.D. Soden, *A comparison of the predictive capabilities of current failure theories for composite laminates, judged against experimental evidence*. Composites Science and Technology. vol. **62**(12): pp. 1725-1797, 2002.
29. Hinton, M.J., A.S. Kaddour, and P.D. Soden, *Evaluation of failure prediction in composite laminates: background to part C of the exercise*. Composites Science and Technology. vol. **64**(3): pp. 321-327, 2004.
30. Hart-Smith, L.J., *Should fibrous composite failure modes be interacted or superimposed?* Composites. vol. **24**(1): pp. 53-55, 1993.
31. Soden, P.D., M.J. Hinton, and A.S. Kaddour, *A comparison of the predictive capabilities of current failure theories for composite laminates*. Composites Science and Technology. vol. **58**(7): pp. 1225-1254, 1998.
32. Soden, P.D., A.S. Kaddour, and M.J. Hinton, *Recommendations for designers and researchers resulting from the world-wide failure exercise*. Composites Science and Technology. vol. **64**(3): pp. 589-604, 2004.
33. Zinoviev, P.A., et al., *The strength of multilayered composites under a plane-stress state*. Composites Science and Technology. vol. **58**(7): pp. 1209-1223, 1998.
34. Zinoviev, P.A., O.V. Lebedeva, and L.P. Tairova, *A coupled analysis of experimental and theoretical results on the deformation and failure of composite laminates under a state of plane stress*. Composites Science and Technology. vol. **62**(12): pp. 1711-1723, 2002.
35. Hart-Smith, L.J., *Predictions of a generalized maximum-shear-stress failure criterion for certain fibrous composite laminates*. Composites Science and Technology. vol. **58**(7): pp. 1179-1208, 1998.
36. Hart-Smith, L.J., *The truncated maximum strain composite failure model*. Composites. vol. **24**(7): pp. 587-591, 1993.
37. Hashin, Z. and A. Rotem, *A fatigue failure criterion for fiber reinforced materials*. Journal of composite materials. vol. **7**(4): pp. 448-464, 1973.
38. Puck, A. and H. Schürmann, *Failure analysis of FRP laminates by means of physically based phenomenological models*, in *Failure Criteria in Fibre-Reinforced-Polymer Composites*. Elsevier. pp. 832-876, 2004.
39. Edge, E., *A comparison of theory and experiment for the stress-based Grant-Sanders method*, in *Failure Criteria in Fibre-Reinforced-Polymer Composites*. Elsevier. pp. 739-769, 2004.

40. Chamis, C., *Failure criteria for filamentary composites*, in *Composite Materials: Testing and Design*. ASTM International, 1969.
41. Eckold, G., *Failure criteria for use in the design environment*. *Composites Science and Technology*. vol. **58**(7): pp. 1095-1105, 1998.
42. Wolfe, W.E. and T.S. Butalia, *A strain-energy based failure criterion for non-linear analysis of composite laminates subjected to biaxial loading*. *Composites Science and Technology*. vol. **58**(7): pp. 1107-1124, 1998.
43. Kashtalyan, M. and C. Soutis, *Predicting residual stiffness of cracked composite laminates subjected to multi-axial inplane loading*. *Journal of Composite Materials*. vol. **47**(20-21): pp. 2513-2524, 2013.
44. Pinho, S., G. Vyas, and P. Robinson, *Response and damage propagation of polymer-matrix fibre-reinforced composites: Predictions for WWFE-III Part A*. *Journal of Composite Materials*. vol.: pp. 0021998313476972, 2013.
45. Soutis, C., *Compressive strength of composite laminates with an open hole: Effect of ply blocking*. *Journal of Composite Materials*. vol.: pp. 0021998312466122, 2012.
46. Singh, C.V. and R. Talreja, *A synergistic damage mechanics approach to mechanical response of composite laminates with ply cracks*. *Journal of Composite Materials*. vol. **47**(20-21): pp. 2475-2501, 2013.
47. Cousigné, O., et al., *Development of a new nonlinear numerical material model for woven composite materials accounting for permanent deformation and damage*. *Composite Structures*. vol. **106**: pp. 601-614, 2013.
48. Chevalier, J., et al., *Micro-mechanics based pressure dependent failure model for highly cross-linked epoxy resins*. *Engineering Fracture Mechanics*. vol. **158**: pp. 1-12, 2016.
49. Barbero, E.J. and F.A. Cosso, *Determination of material parameters for discrete damage mechanics analysis of carbon-epoxy laminates*. *Composites Part B: Engineering*. vol. **56**: pp. 638-646, 2014.
50. Moure, M.M., et al., *Analysis of damage localization in composite laminates using a discrete damage model*. *Composites Part B: Engineering*. vol. **66**: pp. 224-232, 2014.
51. Tsai, S.W. and J.D.D. Melo, *A unit circle failure criterion for carbon fiber reinforced polymer composites*. *Composites Science and Technology*. vol. **123**: pp. 71-78, 2016.
52. Tsai, S.W. and J.D.D. Melo, *An invariant-based theory of composites*. *Composites Science and Technology*. vol. **100**: pp. 237-243, 2014.

53. Tsai, S.W., A. Arreiro, and J.D. Melo, *A trace-based approach to design for manufacturing of composite laminates*. Journal of Reinforced Plastics and Composites. vol., 2015.
54. De Greef, N., et al., *The effect of carbon nanotubes on the damage development in carbon fiber/epoxy composites*. Carbon. vol. **49**(14): pp. 4650-4664, 2011.
55. Bogdanovich, A.E., et al., *Quasi-static tensile behavior and damage of carbon/epoxy composite reinforced with 3D non-crimp orthogonal woven fabric*. Mechanics of Materials. vol. **62**: pp. 14-31, 2013.
56. De Greef, N., et al., *Damage development in woven carbon fiber/epoxy composites modified with carbon nanotubes under tension in the bias direction*. Composites Part A: Applied Science and Manufacturing. vol. **42**(11): pp. 1635-1644, 2011.
57. Talreja, R. and J. Varna, *Modeling Damage, Fatigue and Failure of Composite Materials*. Elsevier, 2015.
58. Ivanov, D.S., et al., *Failure analysis of triaxial braided composite*. Composites Science and Technology. vol. **69**(9): pp. 1372-1380, 2009.
59. Lomov, S.V., et al., *Full-field strain measurements for validation of meso-FE analysis of textile composites*. Composites Part A: Applied science and manufacturing. vol. **39**(8): pp. 1218-1231, 2008.
60. Daggumati, S., et al., *Fatigue and post-fatigue stress-strain analysis of a 5-harness satin weave carbon fibre reinforced composite*. Composites Science and Technology. vol. **74**: pp. 20-27, 2013.
61. Yurgartis, S.W. and S.S. Sternstein, *A micrographic study of bending failure in five thermoplastic-carbon fibre composite laminates*. Journal of Materials Science. vol. **23**(5): pp. 1861-1870, 1988.
62. Couque, H., C. Albertini, and J. Lankford, *Failure mechanisms in a unidirectional fibre-reinforced thermoplastic composite under uniaxial, in-plane biaxial and hydrostatically confined compression*. Journal of Materials Science Letters. vol. **12**(24): pp. 1953-1957, 1993.
63. Oya, N. and H. Hamada, *Mechanical properties and failure mechanisms of carbon fibre reinforced thermoplastic laminates*. Composites Part A: Applied Science and Manufacturing. vol. **28**(9-10): pp. 823-832, 1997.
64. Ramirez-Jimenez, C.R., et al., *Identification of failure modes in glass/polypropylene composites by means of the primary frequency content of the acoustic emission event*. Composites Science and Technology. vol. **64**(12): pp. 1819-1827, 2004.

65. Fritzsche, P., et al., *A procedure for the simulation of failure in thermoplastic composites*. Composite Structures. vol. **85**(4): pp. 337-349, 2008.
66. Izer, A., et al., *Effect of the consolidation degree on the fracture and failure behavior of self-reinforced polypropylene composites as assessed by acoustic emission*. Polymer Engineering & Science. vol. **50**(11): pp. 2106-2113, 2010.
67. Reyes, G. and U. Sharma, *Modeling and damage repair of woven thermoplastic composites subjected to low velocity impact*. Composite Structures. vol. **92**(2): pp. 523-531, 2010.
68. Böhm, R., M. Gude, and W. Hufenbach, *A phenomenologically based damage model for textile composites with crimped reinforcement*. Composites Science and Technology. vol. **70**(1): pp. 81-87, 2010.
69. Hufenbach, W., et al., *The effect of temperature on mechanical properties and failure behaviour of hybrid yarn textile-reinforced thermoplastics*. Materials & Design. vol. **32**(8-9): pp. 4278-4288, 2011.
70. Fedulov, B.N., et al., *Modelling of thermoplastic polymer failure in fiber reinforced composites*. Composite Structures. vol. **163**: pp. 293-301, 2017.
71. Wang, W., et al., *Establishing a new Forming Limit Curve for a flax fibre reinforced polypropylene composite through stretch forming experiments*. Composites Part A: Applied Science and Manufacturing. vol. **77**: pp. 114-123, 2015.
72. Hufenbach, W., et al., *The effect of temperature on mechanical properties and failure behaviour of hybrid yarn textile-reinforced thermoplastics*. Materials & Design. vol. **32**(8-9): pp. 4278-4288, 2011.
73. Hufenbach, W., et al. *Failure behaviour of textile reinforced thermoplastic composites made of hybrid yarns-I: Probabilistically based damage models*. in *ICF12, Ottawa 2009*. 2009.
74. Böhm, R. and W. Hufenbach, *Experimentally based strategy for damage analysis of textile-reinforced composites under static loading*. Composites Science and Technology. vol. **70**(9): pp. 1330-1337, 2010.
75. Sexton, A., W. Cantwell, and S. Kalyanasundaram, *Stretch forming studies on a fibre metal laminate based on a self-reinforcing polypropylene composite*. Composite Structures. vol. **94**(2): pp. 431-437, 2012.
76. Mosse, L., et al., *Stamp forming of polypropylene based fibre-metal laminates: the effect of process variables on formability*. Journal of Materials Processing Technology. vol. **172**(2): pp. 163-168, 2006.

77. Mosse, L., et al., *The effect of process temperature on the formability of polypropylene based fibre–metal laminates*. Composites Part A: Applied Science and Manufacturing. vol. **36**(8): pp. 1158-1166, 2005.
78. Kalyanasundaram, S., et al., *Effect of process parameters during forming of self reinforced–PP based Fiber Metal Laminate*. Composite Structures. vol. **97**: pp. 332-337, 2013.
79. Chen, B.Y., et al., *Modelling the tensile failure of composites with the floating node method*. Computer Methods in Applied Mechanics and Engineering. vol. **308**(Supplement C): pp. 414-442, 2016.
80. Paris, F., E. Correa, and V. Mantič, *Micromechanical Evidences on Interfibre Failure of Composites*, in *The Structural Integrity of Carbon Fiber Composites: Fifty Years of Progress and Achievement of the Science, Development, and Applications*, P.W.R. Beaumont, C. Soutis, and A. Hodzic, Editors., Springer International Publishing: Cham. pp. 359-390, 2017.
81. González-Cantero, J.M., et al., *Semi-analytic model to evaluate non-regularized stresses causing unfolding failure in composites*. Composite Structures. vol. **171**(Supplement C): pp. 77-91, 2017.
82. de Macedo, R.Q., et al., *Intraply failure criterion for unidirectional fiber reinforced composites by means of asymptotic homogenization*. Composite Structures. vol. **159**(Supplement C): pp. 335-349, 2017.
83. Tao, Y., et al., *Experimental and theoretical studies on inter-fiber failure of unidirectional polymer-matrix composites under different strain rates*. International Journal of Solids and Structures. vol. **113-114**(Supplement C): pp. 37-46, 2017.
84. Hart-Smith, L.J., *Is there really no need to be able to predict matrix failures in fibre-polymer composite structures? Part 2: Examples of matrix failures preceding fibre failures*. Australian Journal of Mechanical Engineering. vol. **12**(2): pp. 160-178, 2014.
85. Talreja, R., *Assessment of the fundamentals of failure theories for composite materials*. Composites Science and Technology. vol. **105**(Supplement C): pp. 190-201, 2014.
86. http://cao.mech.northwestern.edu/stress_based.html.
87. Stoughton, T.B. and J.W. Yoon, *Review of Drucker's postulate and the issue of plastic stability in metal forming*. International Journal of Plasticity. vol. **22**(3): pp. 391-433, 2006.

88. Kim, J.-B., et al., *The effect of plastic anisotropy on compressive instability in sheet metal forming*. International Journal of Plasticity. vol. **16**(6): pp. 649-676, 2000.
89. Kim, J., J. Yoon, and D. Yang, *Investigation into the wrinkling behaviour of thin sheets in the cylindrical cup deep drawing process using bifurcation theory*. International journal for numerical methods in engineering. vol. **56**(12): pp. 1673-1705, 2003.
90. Wang, X., J. Xiao, and Y.C. Zhang, *A method for solving the buckling problem of a thin-walled shell*. International Journal of Pressure Vessels and Piping. vol. **81**(12): pp. 907-912, 2004.
91. Tong, L. and T.K. Wang, *Simple solutions for buckling of laminated conical shells*. International Journal of Mechanical Sciences. vol. **34**(2): pp. 93-111, 1992.
92. Al-Hassani, S.T.S., M. Darvizeh, and H. Haftchenari, *An analytical study of buckling of composite tubes with various boundary conditions*. Composite Structures. vol. **39**(1): pp. 157-164, 1997.
93. Peek, R., *Wrinkling of tubes in bending from finite strain three-dimensional continuum theory*. International Journal of Solids and Structures. vol. **39**(3): pp. 709-723, 2002.
94. Timoshenko, S.P. and J.M. Gere, *Theory of elastic stability*. 1961. McGrawHill-Kogakusha Ltd, Tokyo. vol.: pp. 109, 1961.
95. Donnell, L. and C. Wan, *Effect of imperfections on buckling of thin cylinders and columns under axial compression*. Journal of Applied Mechanics-Transactions of the ASME. vol. **17**(1): pp. 73-83, 1950.
96. Hutchinson, J.W. and M.Y. He, *Buckling of cylindrical sandwich shells with metal foam cores*. International Journal of Solids and Structures. vol. **37**(46-47): pp. 6777-6794, 2000.
97. Pircher, M. and R. Bridge, *The influence of circumferential weld-induced imperfections on the buckling of silos and tanks*. Journal of Constructional Steel Research. vol. **57**(5): pp. 569-580, 2001.
98. Yang, G. and M.A. Bradford, *Thermal-induced buckling and postbuckling analysis of continuous railway tracks*. International Journal of Solids and Structures. vol. **97-98**: pp. 637-649, 2016.
99. Tran, D.C., et al., *Thermal buckling of thin sheet related to cold rolling: Latent flatness defects modeling*. Thin-Walled Structures. vol. **113**: pp. 129-135, 2017.

100. Harrison, B., L. Yuan, and S. Kyriakides, *Measurement of Lined Pipe Liner Imperfections and the Effect on Wrinkling and Collapse Under Bending*. (49965): pp. V005T04A036, 2016.
101. Cao, J. and M.C. Boyce, *Wrinkling behavior of rectangular plates under lateral constraint*. International Journal of Solids and Structures. vol. **34**(2): pp. 153-176, 1997.
102. Tomita, Y. and A. Shindo, *Onset and growth of wrinkles in thin square plates subjected to diagonal tension*. International Journal of Mechanical Sciences. vol. **30**(12): pp. 921-931, 1988.
103. Hutchinson, J.W., *Plastic Buckling*, in *Advances in Applied Mechanics*, Y. Chia-Shun, Editor., Elsevier. pp. 67-144, 1974.
104. Hutchinson, J.W., *Imperfection-sensitivity in the plastic range*. Journal of the Mechanics and Physics of Solids. vol. **21**(3): pp. 191-204, 1973.
105. Hutchinson, J.W., *Post-bifurcation behavior in the plastic range*. Journal of the Mechanics and Physics of Solids. vol. **21**(3): pp. 163-190, 1973.
106. Morovvati, M.R., B. Mollaei-Darjani, and M.H. Asadian-Ardakani, *A theoretical, numerical, and experimental investigation of plastic wrinkling of circular two-layer sheet metal in the deep drawing*. Journal of Materials Processing Technology. vol. **210**(13): pp. 1738-1747, 2010.
107. Shafaat, M.A., M. Abbasi, and M. Ketabchi, *Investigation into wall wrinkling in deep drawing process of conical cups*. Journal of Materials Processing Technology. vol. **211**(11): pp. 1783-1795, 2011.
108. Kowsarinia, E., Y. Alizadeh, and H.S.S. Pour, *Theoretical and experimental study on the effects of explosive forming parameters on plastic wrinkling of annular plates*. The International Journal of Advanced Manufacturing Technology. vol. **67**(1): pp. 877-885, 2013.
109. Wong, W. and S. Pellegrino, *Wrinkled membranes II: analytical models*. Journal of Mechanics of Materials and Structures. vol. **1**(1): pp. 27-61, 2006.
110. Geckeler, J., *Plastisches Knicken der Wandung von Hohlzylindern und einige andere Faltungerscheinungen an Schalen und Blechen*. ZAMM-Journal of Applied Mathematics and Mechanics/Zeitschrift für Angewandte Mathematik und Mechanik. vol. **8**(5): pp. 341-352, 1928.
111. Senior, B.W., *Flange wrinkling in deep-drawing operations*. Journal of the Mechanics and Physics of Solids. vol. **4**(4): pp. 235-246, 1956.
112. Alexander, J., *An appraisal of the theory of deep drawing*. Metallurgical Reviews. vol. **5**(1): pp. 349-411, 1960.

113. Yu, T. and W. Johnson, *The buckling of annular plates in relation to the deep-drawing process*. International Journal of Mechanical Sciences. vol. **24**(3): pp. 175-188, 1982.
114. Morovvati, M., B. Mollaei-Dariani, and M. Asadian-Ardakani, *A theoretical, numerical, and experimental investigation of plastic wrinkling of circular two-layer sheet metal in the deep drawing*. Journal of Materials Processing Technology. vol. **210**(13): pp. 1738-1747, 2010.
115. Triantafyllidis, N. and A. Needleman, *An Analysis of Wrinkling in the Swift Cup Test*. Journal of Engineering Materials and Technology. vol. **102**(3): pp. 241-248, 1980.
116. Narayanasamy, R. and C.S. Narayanan, *Forming, fracture and wrinkling limit diagram for if steel sheets of different thickness*. Materials & Design. vol. **29**(7): pp. 1467-1475, 2008.
117. Martins, P., et al., *Formability and simulative tests in modern sheet metal forming education*, in *Modern Mechanical Engineering*. Springer. pp. 411-447, 2014.
118. Ahmetoglu, M., et al., *Control of Blank Holder Force to Eliminate Wrinkling and Fracture in Deep-Drawing Rectangular Parts*. CIRP Annals - Manufacturing Technology. vol. **44**(1): pp. 247-250, 1995.
119. Abbasi, M., et al., *New attempt to wrinkling behavior analysis of tailor welded blanks during the deep drawing process*. Materials & Design. vol. **40**: pp. 407-414, 2012.
120. Narayanasamy, R. and R. Sowerby, *Forming behaviour of some sheet steel materials when drawn through a conical die*. Journal of Materials Processing Technology. vol. **39**(1): pp. 43-53, 1993.
121. Loganathan, C. and R. Narayanasamy, *Effect of mechanical properties on the wrinkling behaviour of three different commercially pure aluminium grades when drawn through conical and tractrix dies*. Materials Science and Engineering: A. vol. **406**(1-2): pp. 229-253, 2005.
122. Hezam, L.M.A., et al., *Development of a new process for producing deep square cups through conical dies*. International Journal of Machine Tools and Manufacture. vol. **49**(10): pp. 773-780, 2009.
123. Dhaiban, A.A., M.E.S. Soliman, and M.G. El-Sebaie, *Finite element modeling and experimental results of brass elliptic cups using a new deep drawing process through conical dies*. Journal of Materials Processing Technology. vol. **214**(4): pp. 828-838, 2014.

124. Bardi, F.C. and S. Kyriakides, *Plastic buckling of circular tubes under axial compression—part I: Experiments*. International Journal of Mechanical Sciences. vol. **48**(8): pp. 830-841, 2006.
125. Zeinoddini, M., M. Ezzati, and G.A.R. Parke, *Plastic buckling, wrinkling and collapse behaviour of dented X80 steel line pipes under axial compression*. Journal of Loss Prevention in the Process Industries. vol. **38**: pp. 67-78, 2015.
126. Yuan, L. and S. Kyriakides, *Wrinkling and Collapse of Girth-Welded Lined Pipe Under Bending*. (45462): pp. V06AT04A039, 2014.
127. Hu, L.L., et al., *Influence of internal pressure on the out-of-plane dynamic behavior of circular-celled honeycombs*. International Journal of Impact Engineering. vol., 2017.
128. Lu, G.Y., et al., *A study on the impact response of liquid-filled cylindrical shells*. Thin-Walled Structures. vol. **47**(12): pp. 1557-1566, 2009.
129. Rajabiehfarid, R., et al., *Experimental and numerical investigation of dynamic plastic behavior of tube with different thickness distribution under axial impact*. Thin-Walled Structures. vol. **109**: pp. 174-184, 2016.
130. Yoshida, K., et al., *Effects of Material Properties on Surface Deflection Behavior Due to Elastic Recovery in Press Forming*. Advanced Technology of Plasticity. vol. **1**: pp. 747-752, 1984.
131. Kim, J.B., J.W. Yoon, and D.Y. Yang, *Wrinkling initiation and growth in modified Yoshida buckling test: Finite element analysis and experimental comparison*. International Journal of Mechanical Sciences. vol. **42**(9): pp. 1683-1714, 2000.
132. Cheng, H.S., et al., *Wrinkling behavior of laminated steel sheets*. Journal of Materials Processing Technology. vol. **151**(1–3): pp. 133-140, 2004.
133. Schreyer, S. and W. Volk. *Optimization of the Modified Yoshida Buckling Test to Investigate the Influence of Curvature*. in *Advanced Materials Research*. 2016. Trans Tech Publ.
134. Bayraktar, E., N. Isac, and G. Arnold, *Buckling limit diagrams (BLDs) of interstitial free steels (IFS): Comparison of experimental and finite element analysis*. Journal of Materials Processing Technology. vol. **164-65**(0): pp. 1487-1494, 2005.
135. Pearce, R., *Sheet metal forming*. Springer Science & Business Media, 1991.
136. Ameziane-Hassani, H. and K. Neale, *On the analysis of sheet metal wrinkling*. International journal of mechanical sciences. vol. **33**(1): pp. 13-30, 1991.

137. Kim, Y. and Y. Son, *Study on wrinkling limit diagram of anisotropic sheet metals*. Journal of Materials Processing Technology. vol. **97**(1-3): pp. 88-94, 2000.
138. Szacinski, A. and P. Thomson, *Investigation of the existence of a wrinkling-limit curve in plastically-deforming metal sheet*. Journal of materials processing technology. vol. **25**(2): pp. 125-137, 1991.
139. Narayanasamy, R., J. Satheesh, and C.S. Narayanan, *Effect of annealing on combined forming, fracture and wrinkling limit diagram of Aluminium 5086 alloy sheets*. International Journal of Mechanics and Materials in Design. vol. **4**(1): pp. 31, 2008.
140. Li, H., et al., *A new method to accurately obtain wrinkling limit diagram in NC bending process of thin-walled tube with large diameter under different loading paths*. Journal of Materials Processing Technology. vol. **177**(1-3): pp. 192-196, 2006.
141. Djavanroodi, F. and A. Derogar, *Experimental and numerical evaluation of forming limit diagram for Ti6Al4V titanium and Al6061-T6 aluminum alloys sheets*. Materials & Design. vol. **31**(10): pp. 4866-4875, 2010.
142. Narayanasamy, R. and C. Loganathan, *Study on wrinkling limit of commercially pure aluminium sheet metals of different grades when drawn through conical and tractrix dies*. Materials Science and Engineering: A. vol. **419**(1): pp. 249-261, 2006.
143. Szacinski, A.M. and P.F. Thomson, *Investigation of the existence of a wrinkling-limit curve in plastically-deforming metal sheet*. Journal of Materials Processing Technology. vol. **25**(2): pp. 125-137, 1991.
144. Dick, R.E. and J.W. Yoon, *Wrinkling during Cup Drawing with NUMISHEET2014 Benchmark Test*. steel research international. vol. **86**(8): pp. 915-921, 2015.
145. M. Komeili and A.S. Milani, *Shear response of woven fabric composites under meso-level uncertainties*. Journal of composite materials. vol. **47**(19): pp. 2331-2441, 2013.

Appendix A

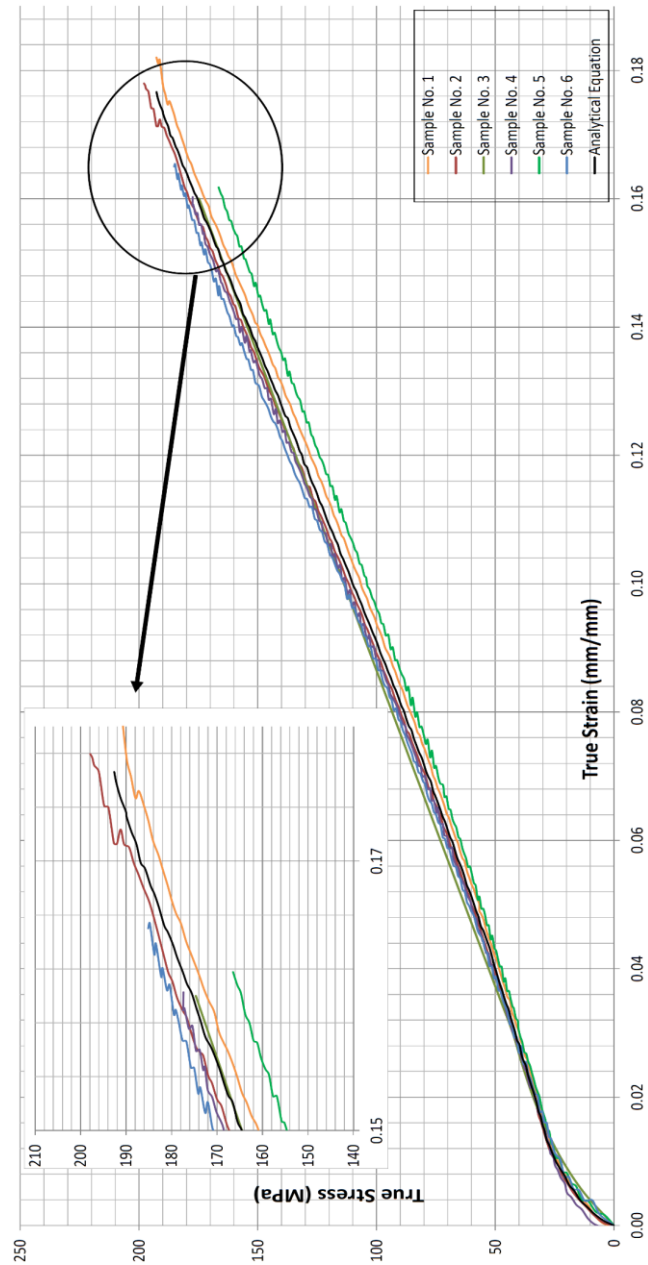


Figure A1: Stress-strain curves of SRPP obtained from uniaxial extension of six $[0^\circ, 90^\circ]$ specimens compared with the analytical curve

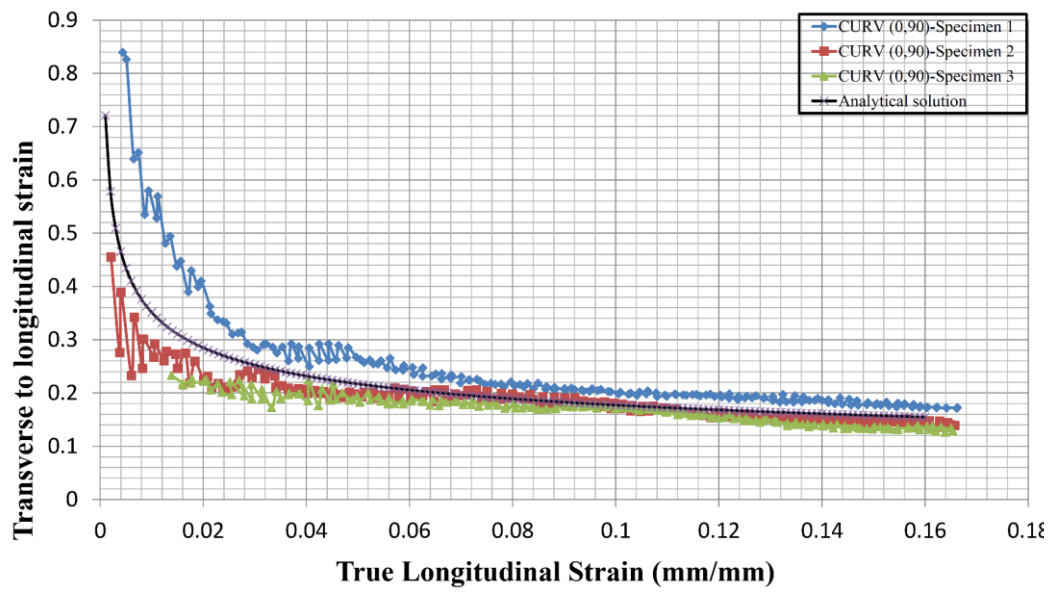


Figure A2: Conventional Poisson's ratio of SRPP obtained from uniaxial extension of three [-45,+45] specimens compared with the analytical curve

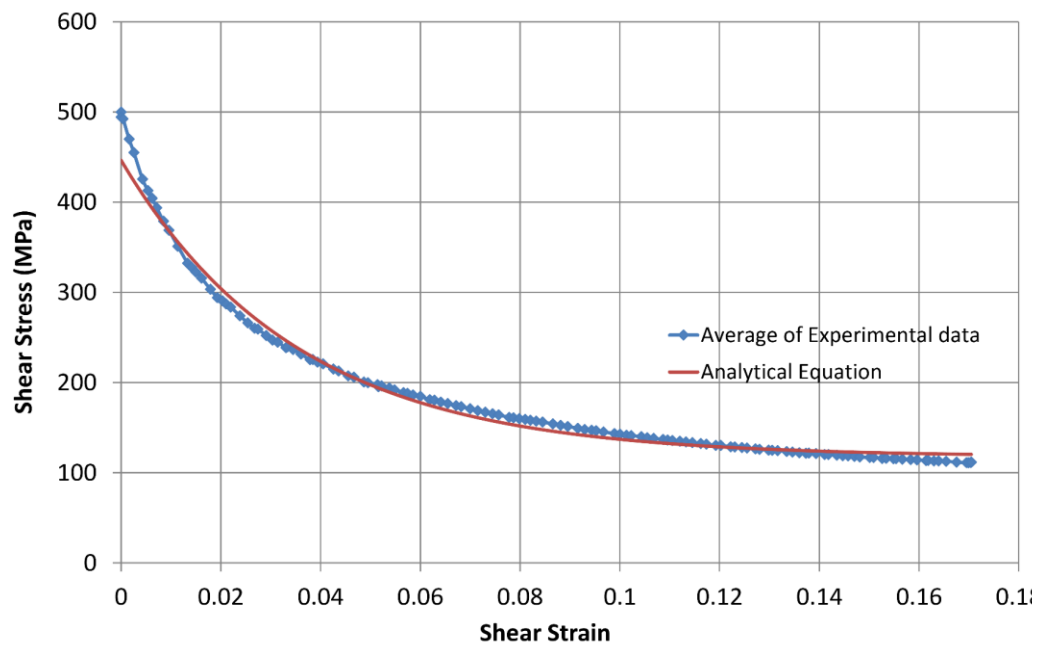


Figure A3: A comparison of analytical and experimental shear stress-strain graphs of SRPP composite obtained from bias extension test results